Universiteit Leiden

Sterrewacht Leiden

Learning Reionization History with Quasar IGM Damping Wings

Timo Kist, PhD candidate at Leiden Observatory
Supervisor: Joseph F. Hennawi

Timo Kist, Leiden Observatory, kist@strw.leidenuniv.nl

Quasars in a Reionizing Universe

Proximity Zones & IGM Damping Wings

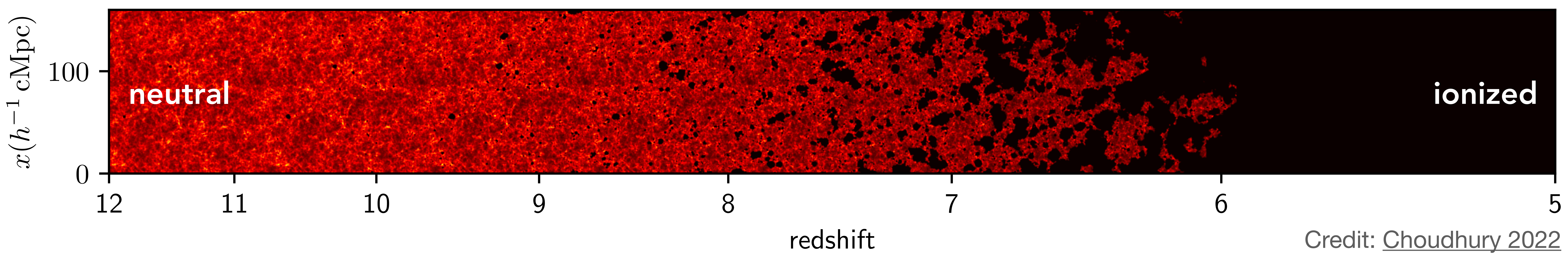

Credit: Choudhury 2022

Timo Kist, Leiden Observatory, kist@strw.leidenuniv.nl

Quasars in a Reionizing Universe

Proximity Zones & IGM Damping Wings

Lyman-α dark pixel fractions

McGreer+ 2015

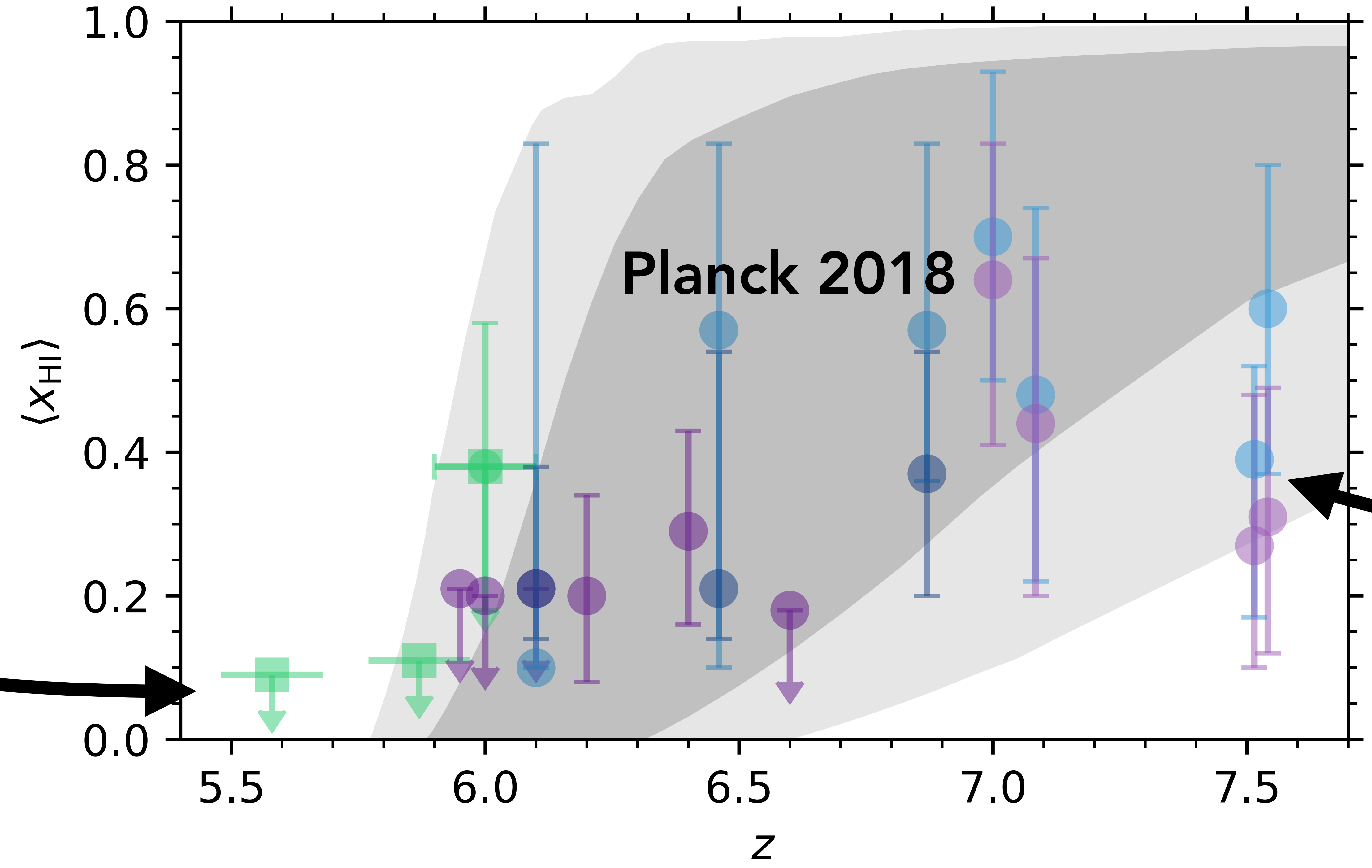

Quasar IGM damping wings

Greig+ 2017
Davies+ 2018
Ďurovčíková+ 2020

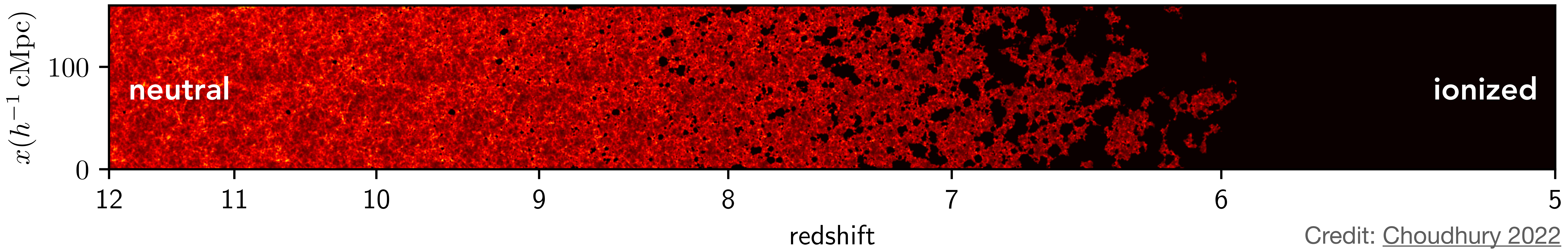

Credit: Choudhury 2022

Timo Kist, Leiden Observatory, kist@strw.leidenuniv.nl

Quasars in a Reionizing Universe

Proximity Zones & IGM Damping Wings

Timo Kist, Leiden Observatory, kist@strw.leidenuniv.nl

Quasars in a Reionizing Universe

Proximity Zones & IGM Damping Wings

Timo Kist, Leiden Observatory, kist@strw.leidenuniv.nl

Quasars in a Reionizing Universe

Proximity Zones & IGM Damping Wings

Gunn-Peterson trough:

Complete absorption in the Ly-α forest region starting at IGM neutral fractions $\langle x_{\rm HI} \rangle \gtrsim 10^{-4}$

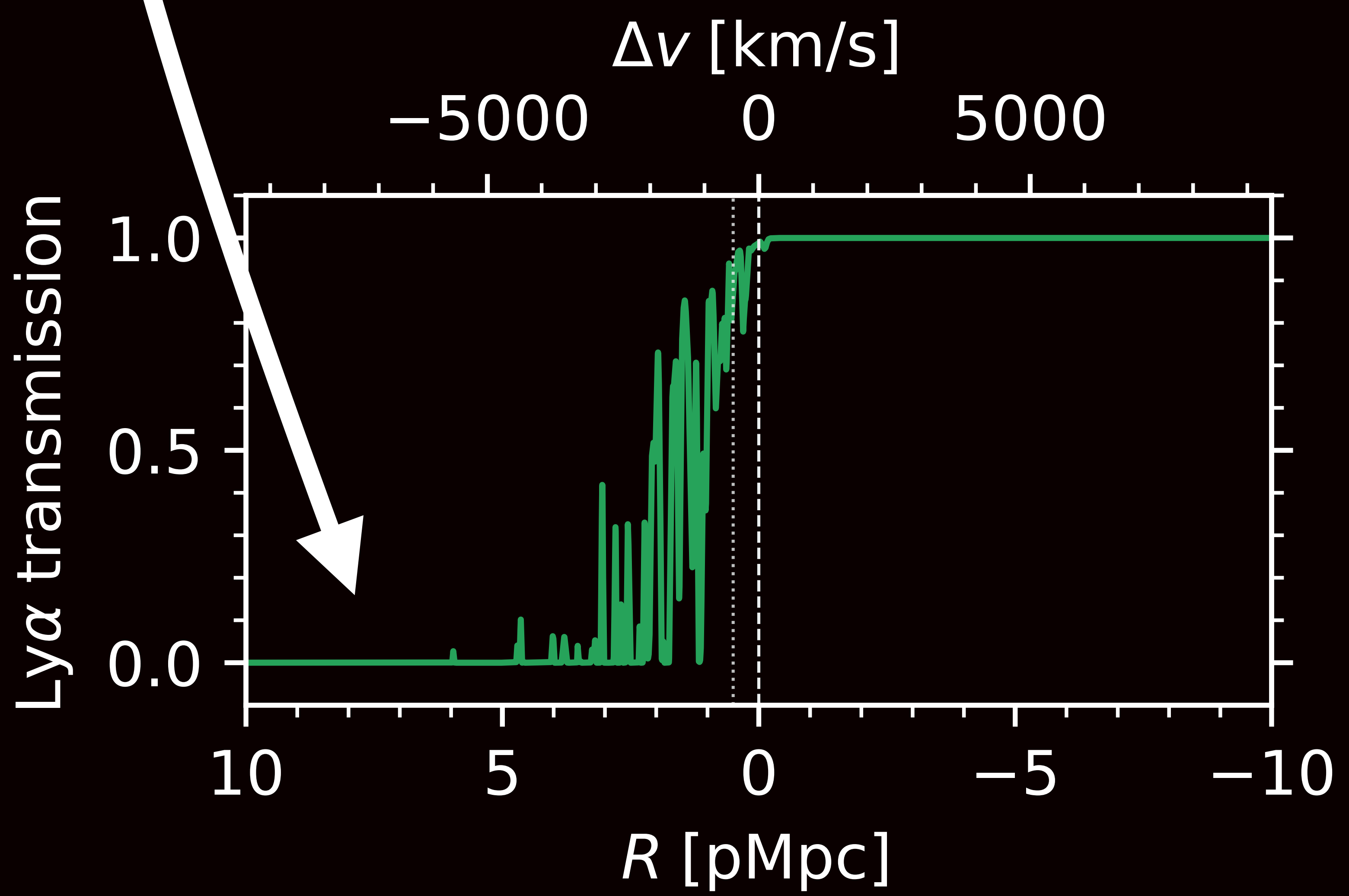

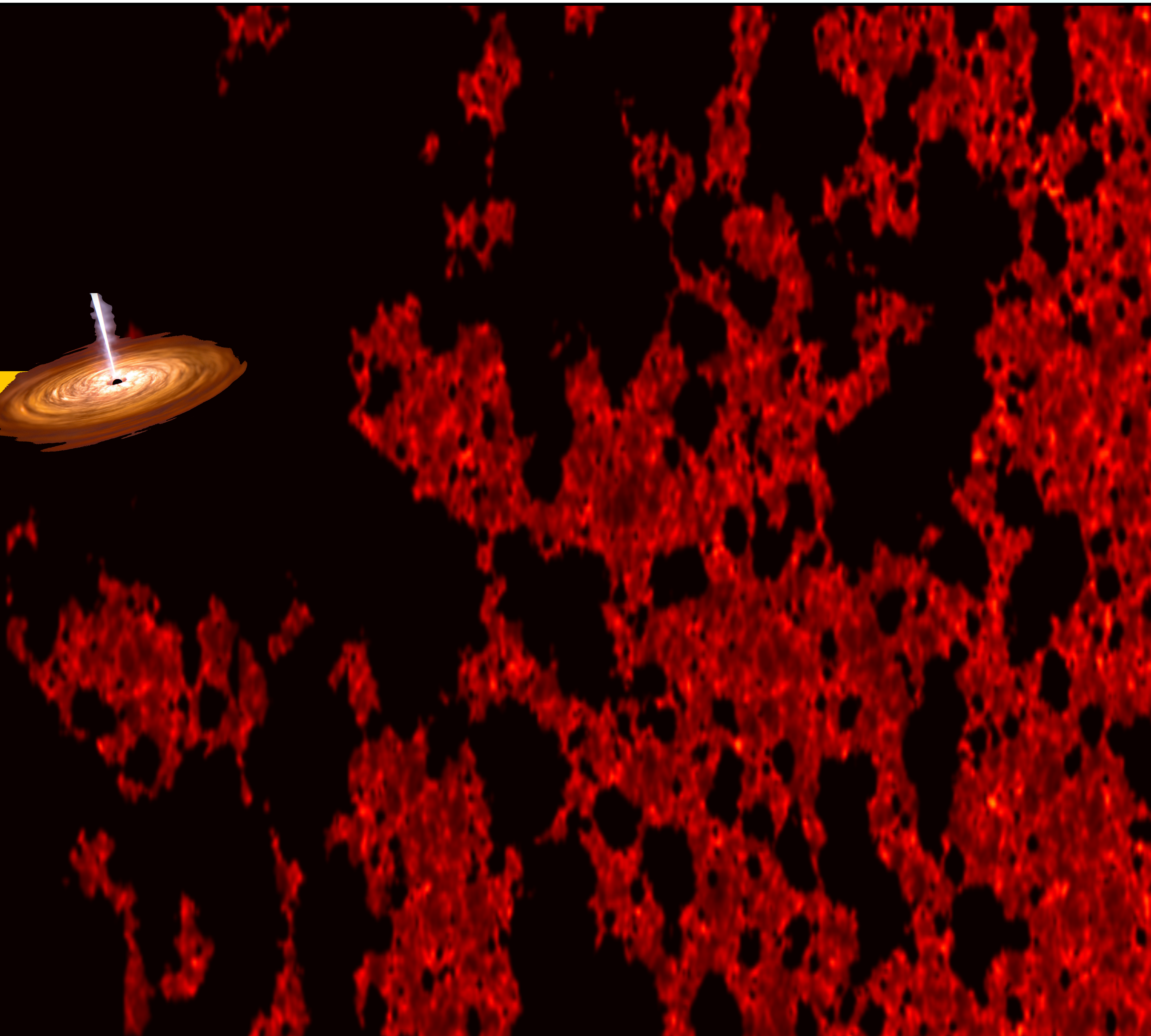

Timo Kist, Leiden Observatory, kist@strw.leidenuniv.nl

Quasars in a Reionizing Universe

Proximity Zones & IGM Damping Wings

Gunn-Peterson trough:

Complete absorption in the Ly-α forest region starting at IGM neutral fractions $\langle x_{\mathrm{HI}} \rangle \gtrsim 10^{-4}$

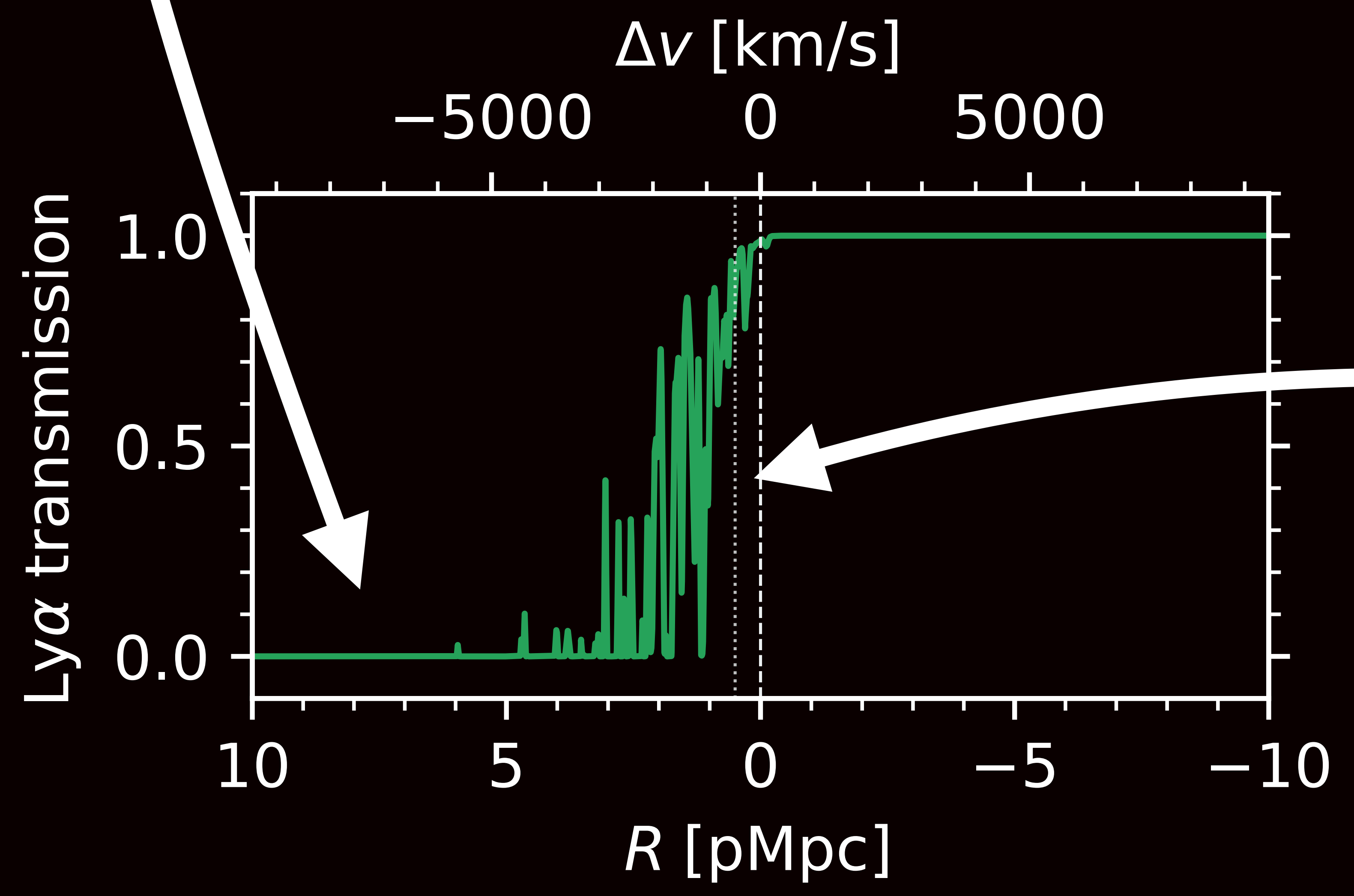

Quasar proximity zone:

The quasar carves out an ionized bubble whose size depends on its lifetime

Timo Kist, Leiden Observatory, kist@strw.leidenuniv.nl

Quasars in a Reionizing Universe

Proximity Zones & IGM Damping Wings

Timo Kist, Leiden Observatory, kist@strw.leidenuniv.nl

Quasars in a Reionizing Universe

Proximity Zones & IGM Damping Wings

Timo Kist, Leiden Observatory, kist@strw.leidenuniv.nl

Quasars in a Reionizing Universe

Proximity Zones & IGM Damping Wings

Euclid will find hundreds of QSOs at $z > 6$

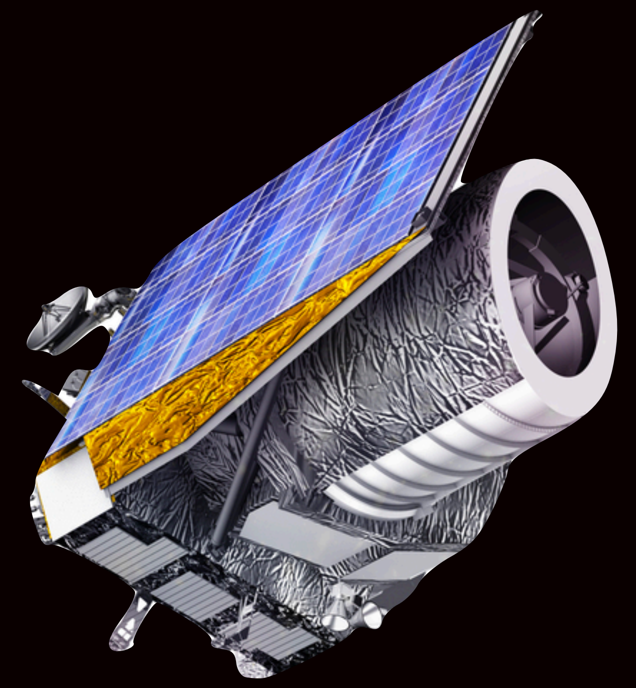

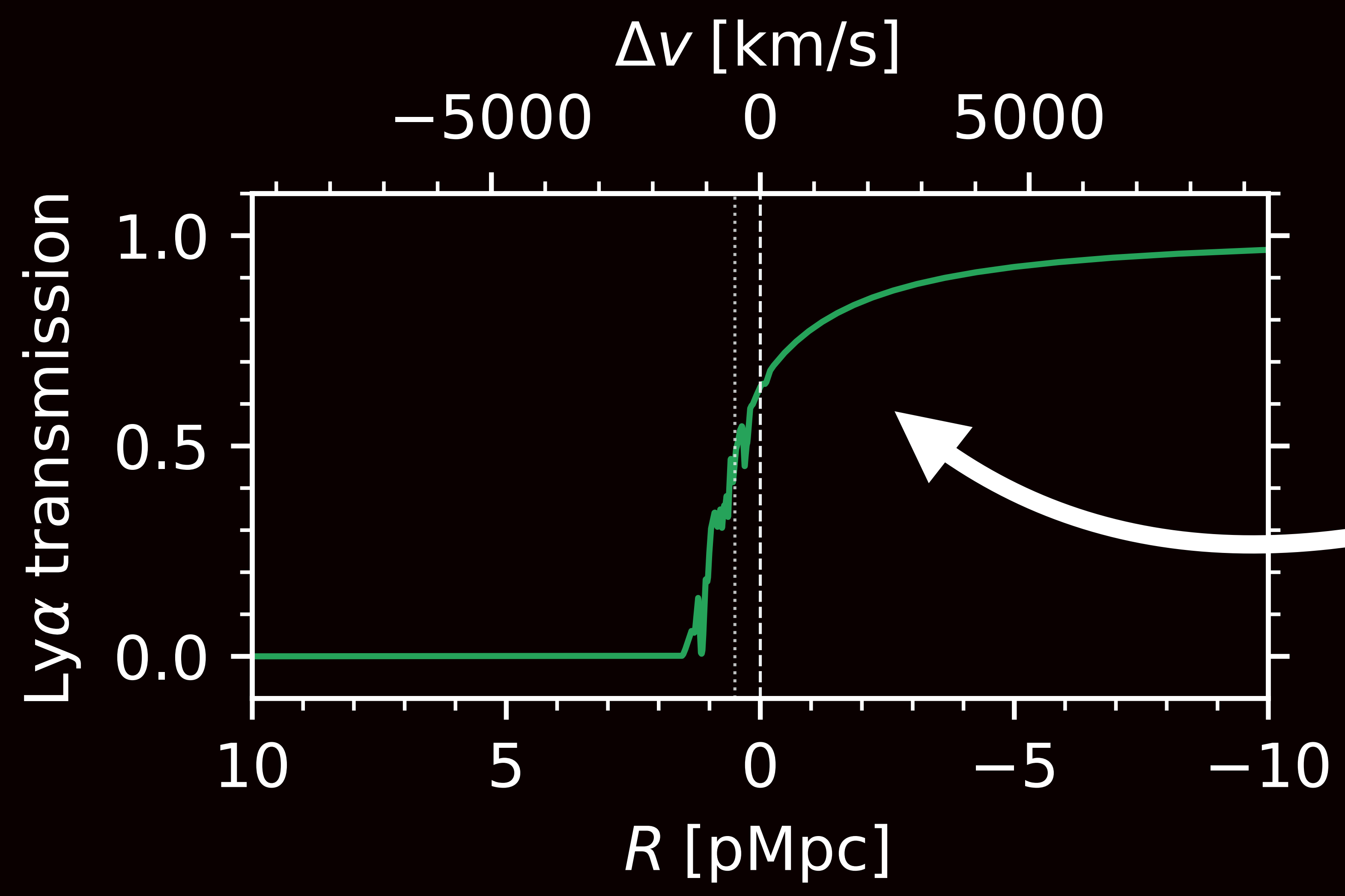

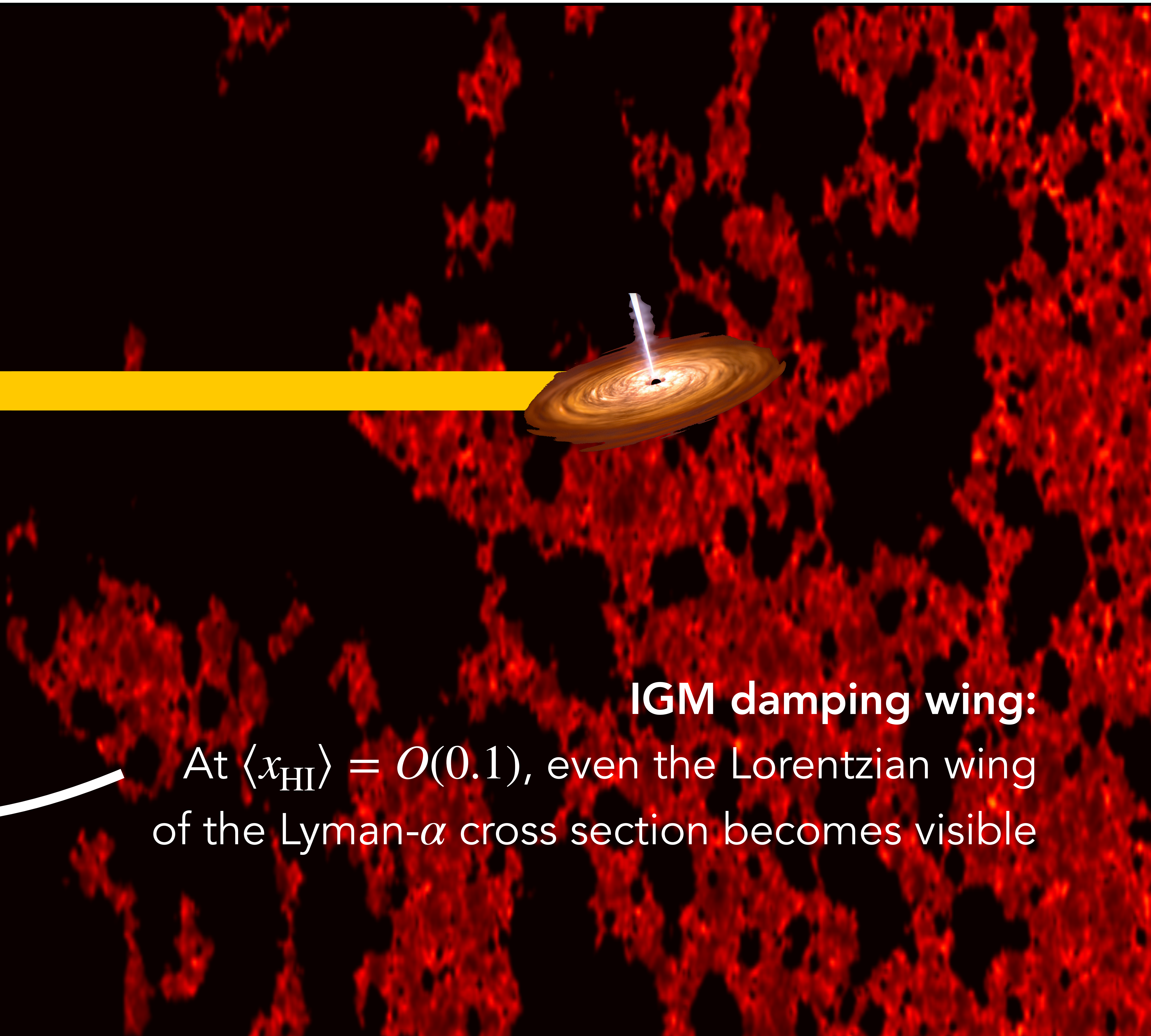

IGM damping wing:

At $\langle x_{\rm HI} \rangle = O(0.1)$, even the Lorentzian wing of the Lyman-α cross section becomes visible

Timo Kist, Leiden Observatory, kist@strw.leidenuniv.nl

Forward-Modelling Damping Wing Absorption

Constructing realistic skewers based on cosmological simulations

Nyx hydrodynamical simulations:

1200 density and temperature skewers around the most massive DM halos

`21cmFast`:

21 reionization topologies ($0 \leq \langle x_{\rm HI} \rangle \leq 1$) with 10 000 $x_{\rm HI}$ skewers each

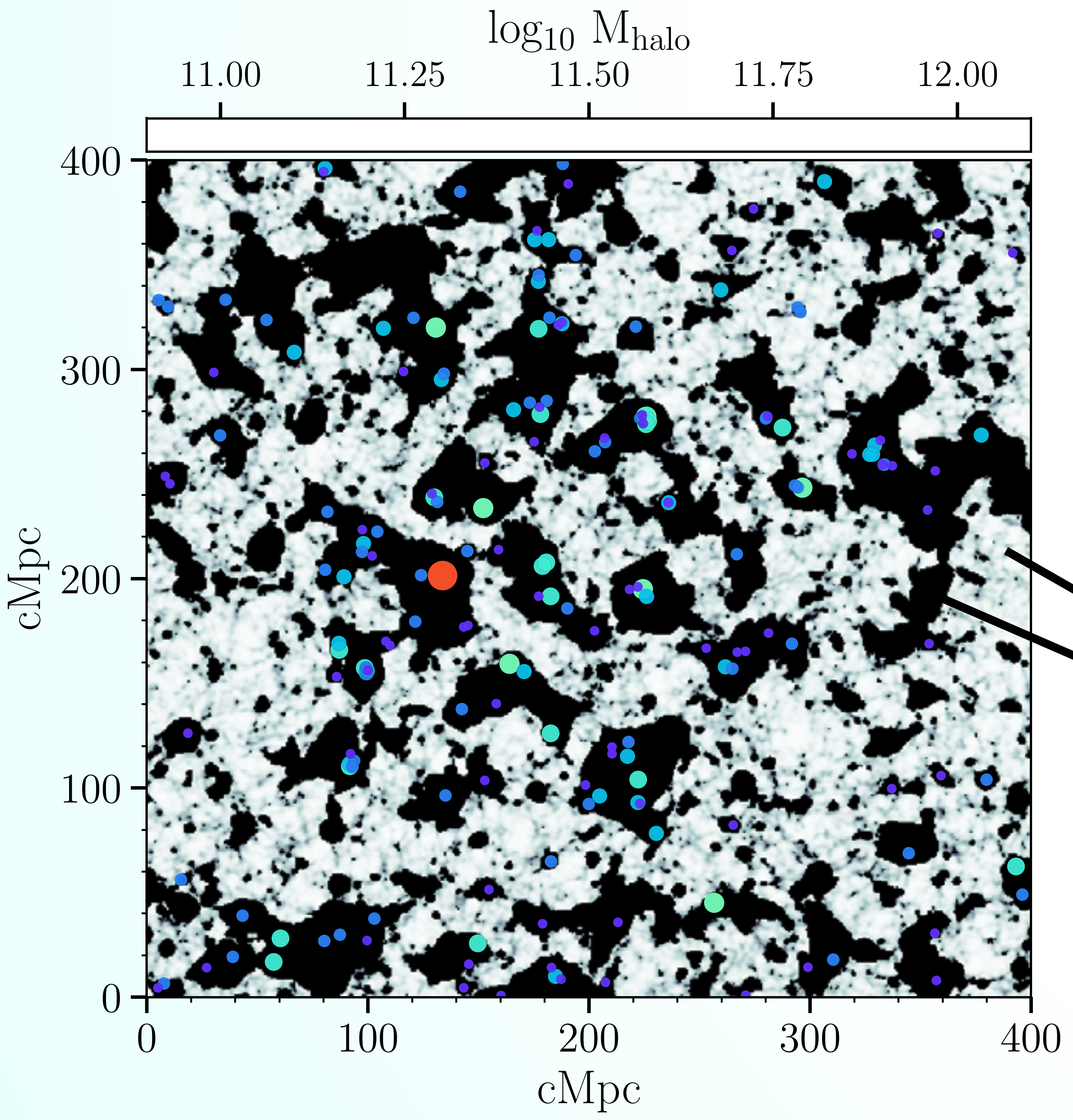

white: neutral

black: ionized

Credit: Davies+ 2018

1D Radiative Transfer

51 quasar lifetimes between $10^3\,\mathrm{yr} \leq t_{\rm Q} \leq 10^8\,\mathrm{yr}$

1200 x 21 x 51 grid of Ly-α transmission skewers

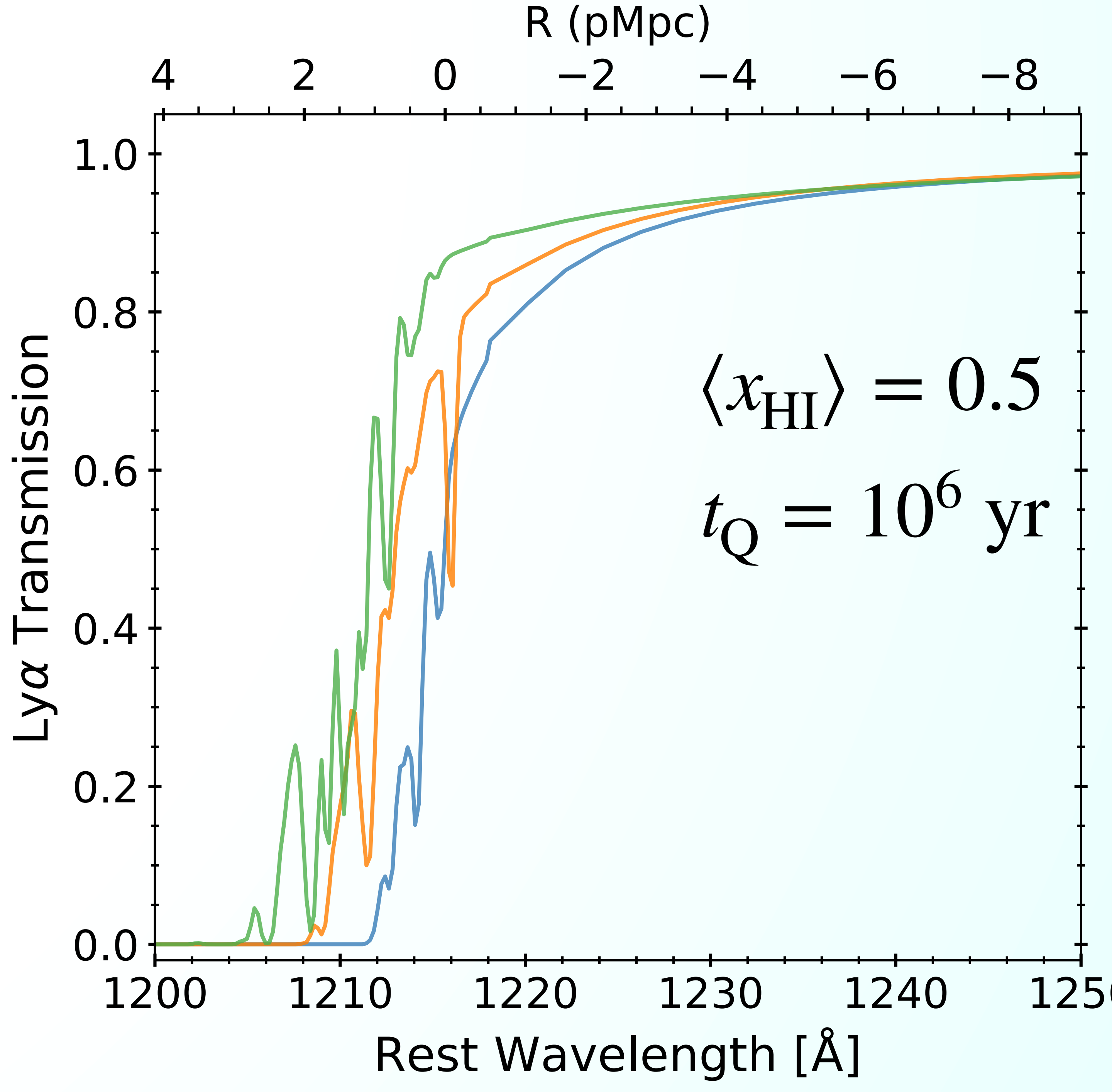

Kist, Hennawi & Davies 2024a

Timo Kist, Leiden Observatory, kist@strw.leidenuniv.nl

Forward-Modelling Damping Wing Absorption

Constructing realistic skewers based on cosmological simulations

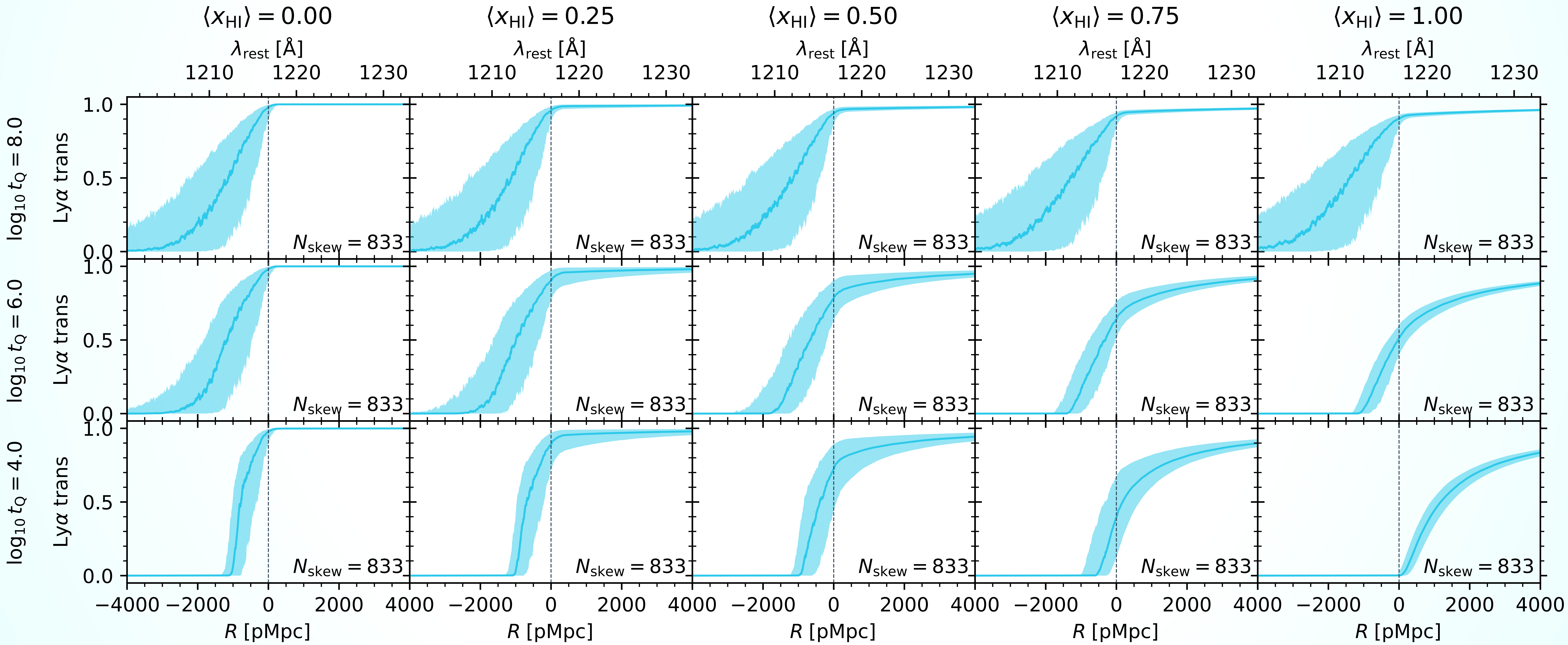

Kist, Hennawi & Davies 2024b (in prep.)

Timo Kist, Leiden Observatory, kist@strw.leidenuniv.nl

Forward-Modelling Damping Wing Absorption

Constructing realistic skewers based on cosmological simulations

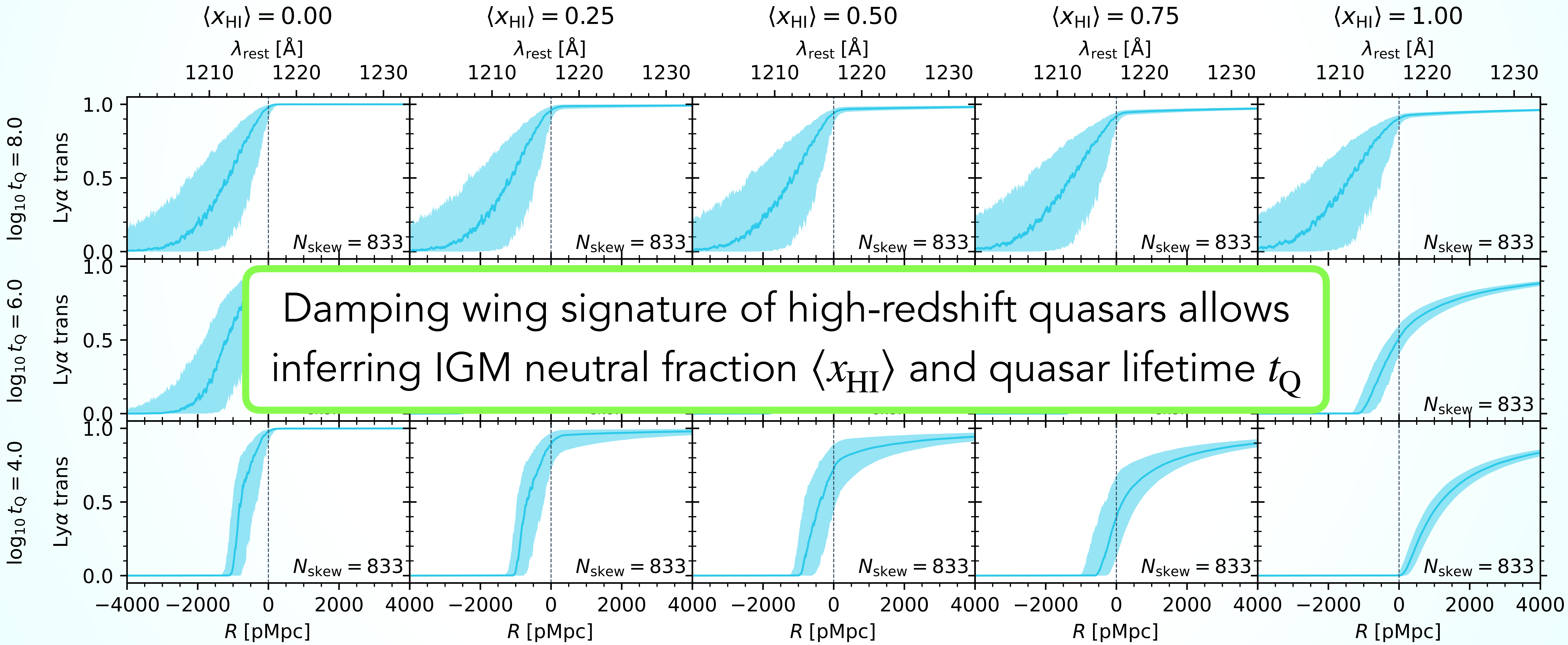

Damping wing signature of high-redshift quasars allows inferring IGM neutral fraction $\langle x_{HI} \rangle$ and quasar lifetime t_Q

Kist, Hennawi & Davies 2024b (in prep.)

Timo Kist, Leiden Observatory, kist@strw.leidenuniv.nl

Predicting the Quasar Continuum

A low-redshift PCA model

PCA decomposed continuum: $s_{\mathrm{DR}}(\boldsymbol{\xi}) = \langle s \rangle + \boldsymbol{\xi} \cdot \boldsymbol{A}$

mean spectrum $\langle s \rangle$

PCA vectors $\boldsymbol{A}_1$, $\boldsymbol{A}_2$, ⋮

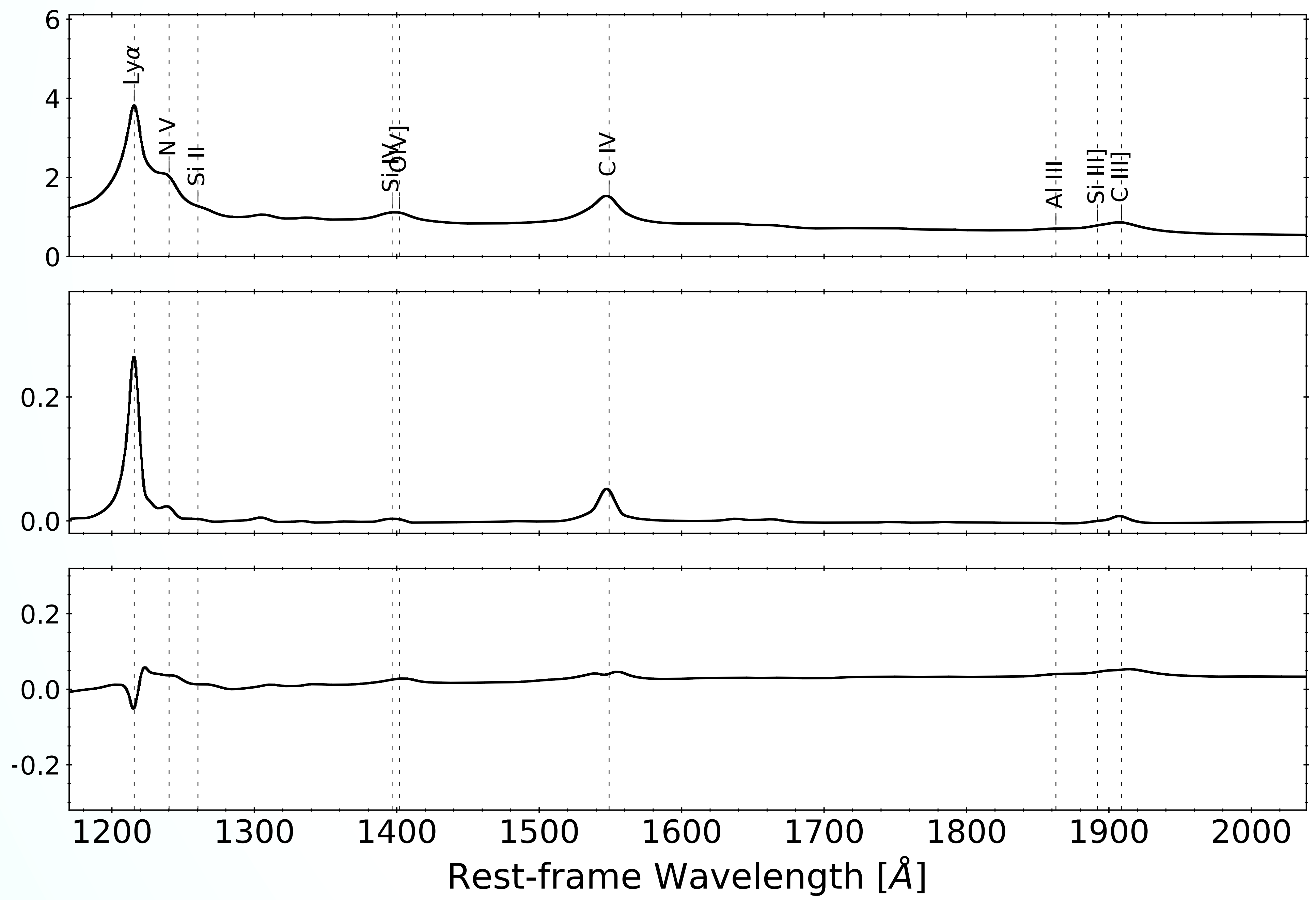

Hennawi, **Kist**, Davies & Tamanas 2024

- 15 559 SDSS-autofit spectra (2.149 < z < 4, R ~ 2000, S/N > 10)
- 95% - 5% training-test split:
  - Training set of 14 781 low-redshift spectra to build PCA model
  - Test set of 778 spectra to draw mock continua and estimate reconstruction error

Timo Kist, Leiden Observatory, kist@strw.leidenuniv.nl

From an Observed Quasar Spectrum to $\langle x_{\mathrm{HI}} \rangle$

A Quasar in a Neutral Environment

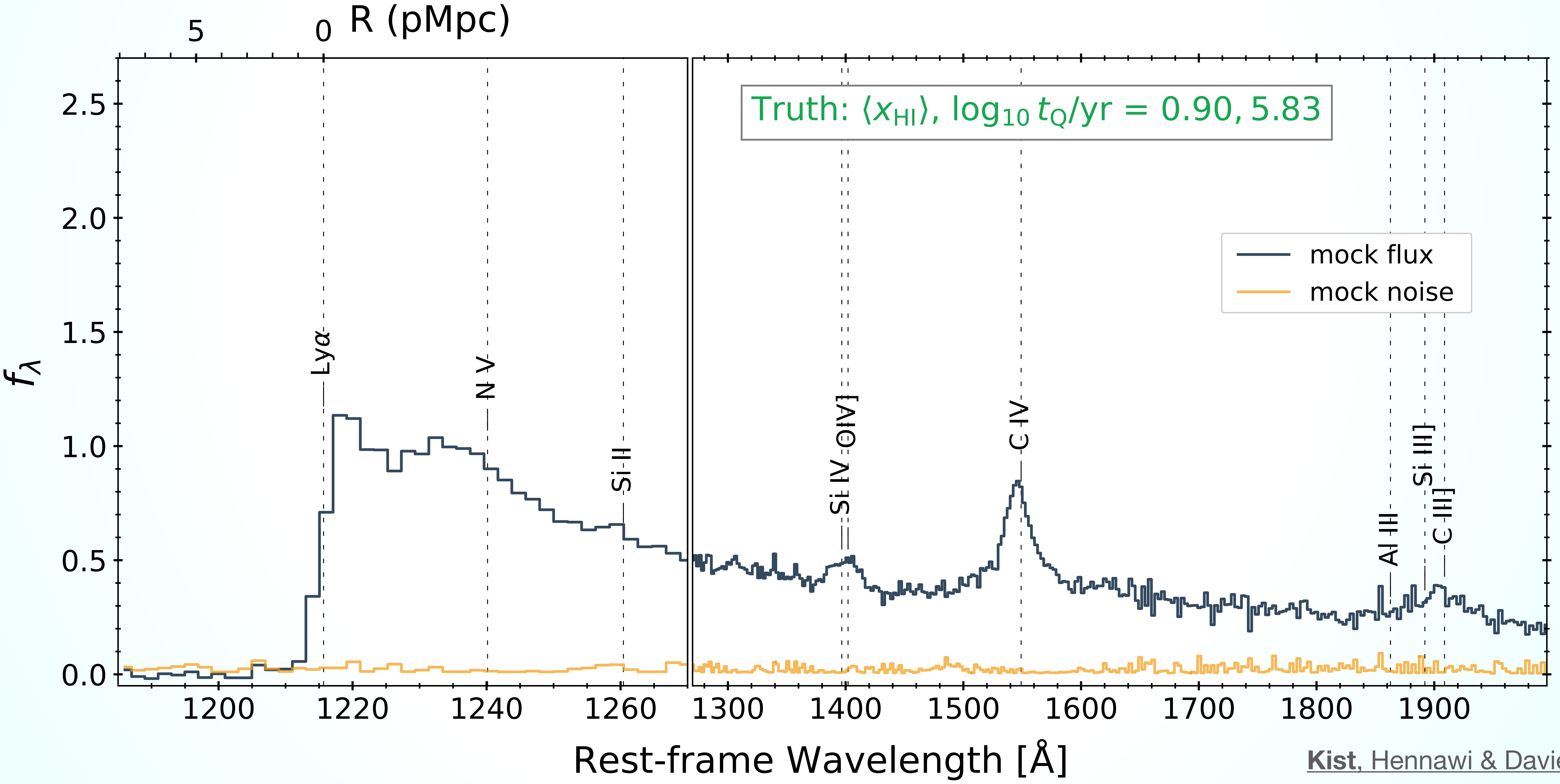

Kist, Hennawi & Davies 2024a

Timo Kist, Leiden Observatory, kist@strw.leidenuniv.nl

From an Observed Quasar Spectrum to $\langle x_{\mathrm{HI}} \rangle$

A Quasar in a Neutral Environment

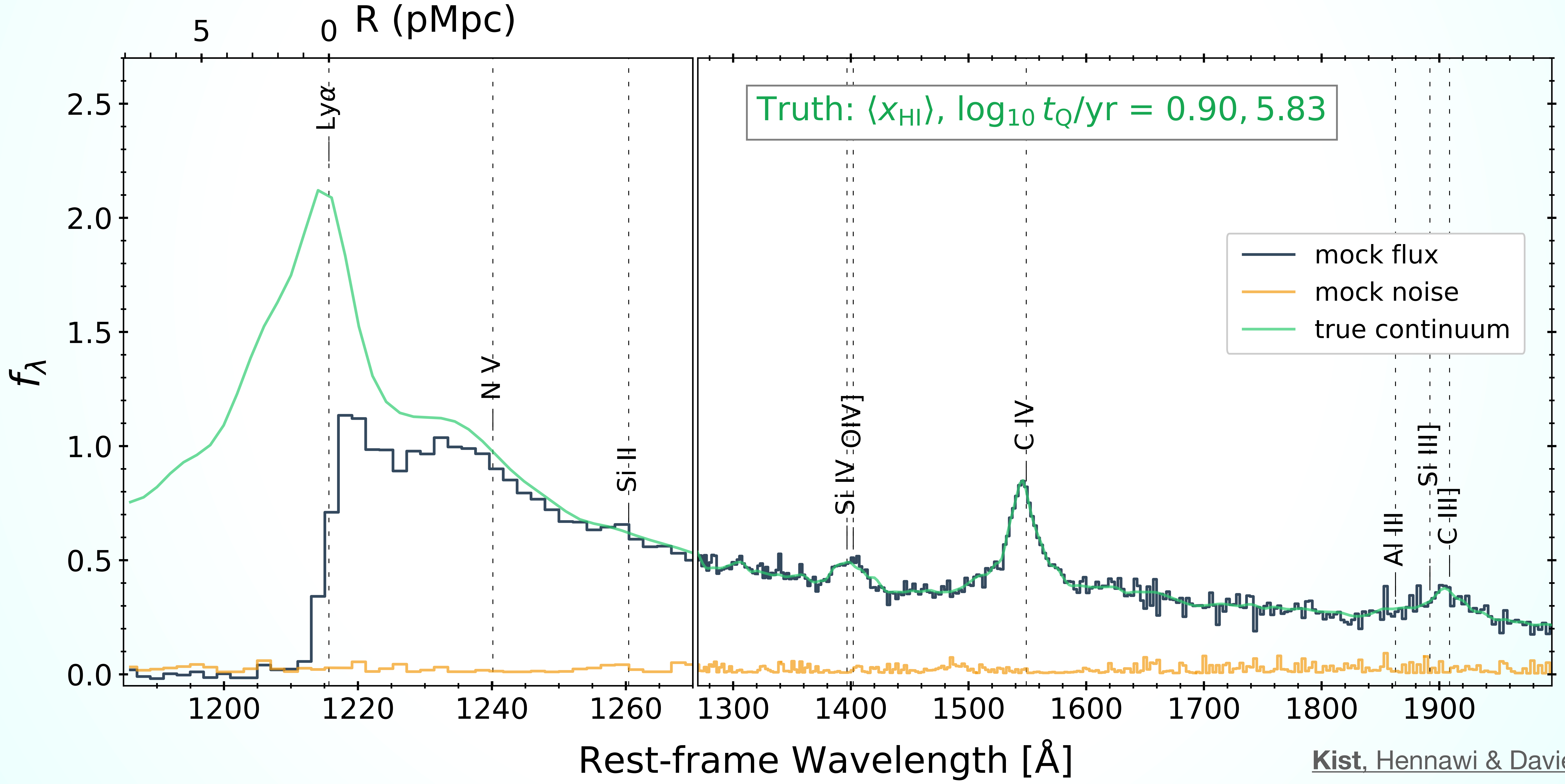

Kist, Hennawi & Davies 2024a

Timo Kist, Leiden Observatory, kist@strw.leidenuniv.nl

From an Observed Quasar Spectrum to $\langle x_{\mathrm{HI}} \rangle$

A Quasar in a Neutral Environment

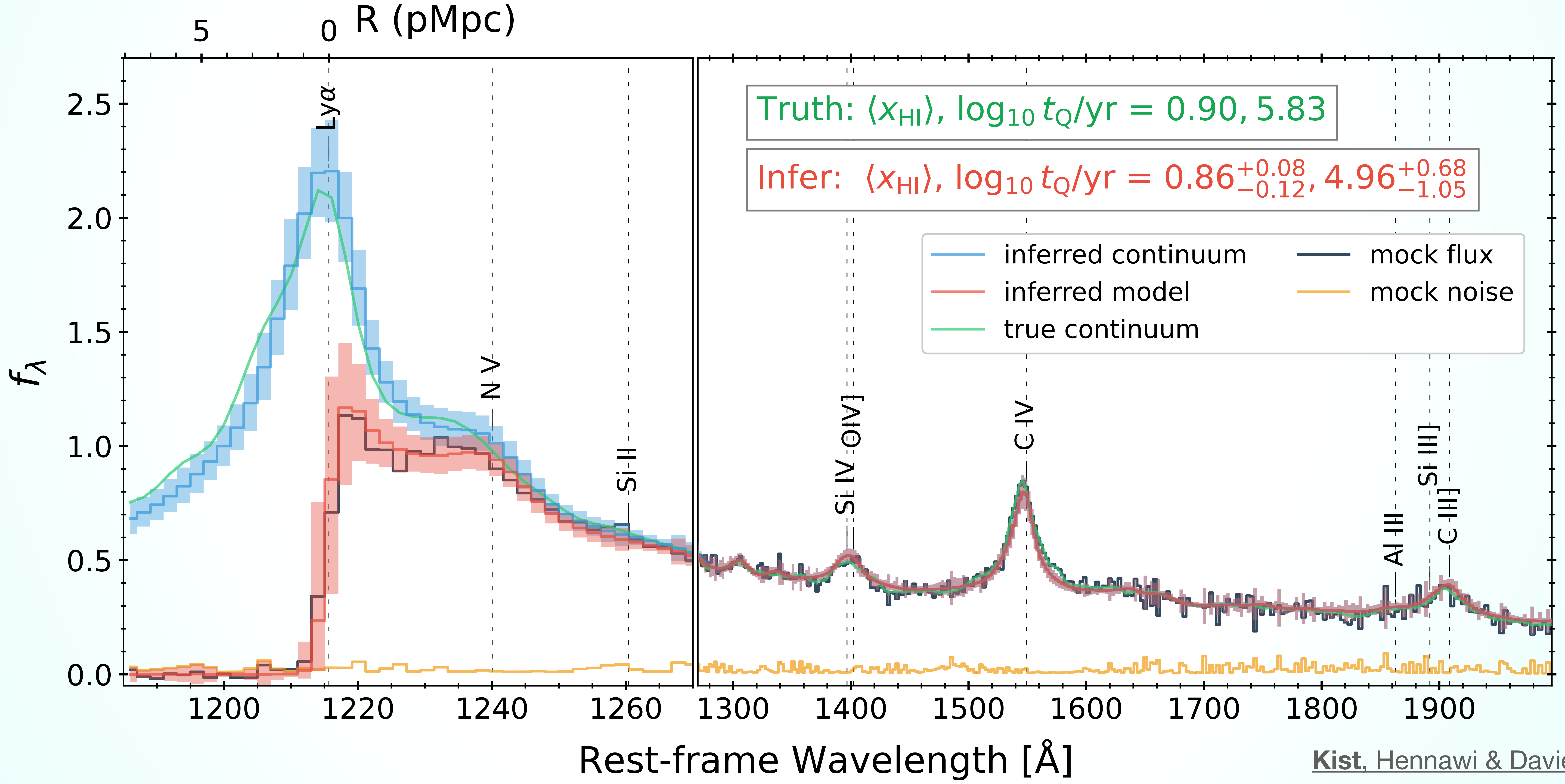

Kist, Hennawi & Davies 2024a

Timo Kist, Leiden Observatory, kist@strw.leidenuniv.nl

From an Observed Quasar Spectrum to $\langle x_{\rm HI} \rangle$

HMC Inference Pipeline

DATA

Real (or mock) quasar spectrum with observational noise

MODEL

Quasar continuum model

Reconstruction error stochastic process

+

IGM transmission field stochastic process

BAYESIAN INFERENCE

with a Gaussian likelihood approximation

- **Jointly** fitting the quasar continuum & IGM damping wing
- Likelihood operates on the **entire** spectrum (red- and blueward of Lyman-α)
- **Fast** GPU-accelerated JAX-based Hamiltonian Monte Carlo implementation (runtimes ~15 min)

POSTERIOR

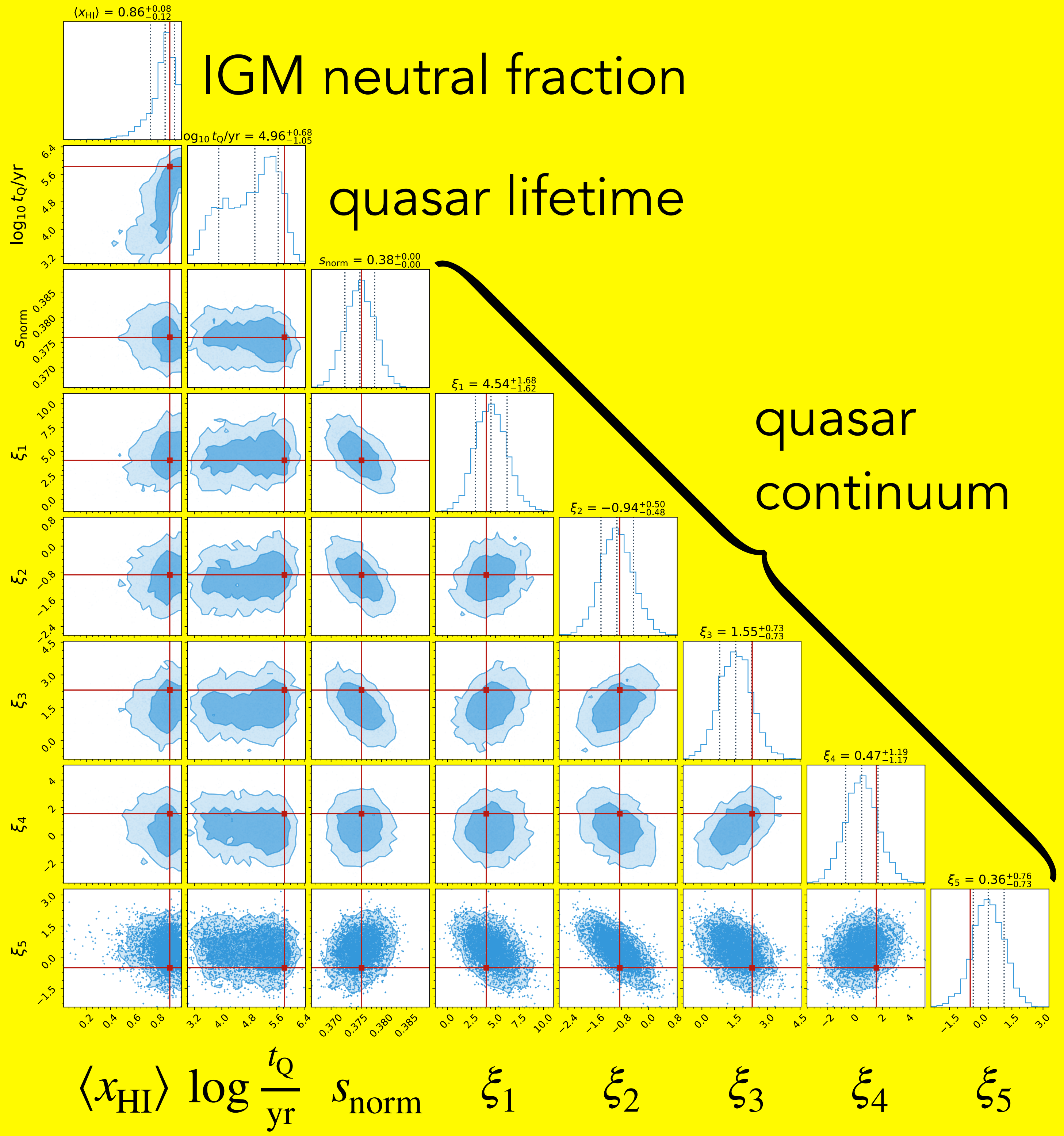

Kist, Hennawi & Davies 2024a

Timo Kist, Leiden Observatory, kist@strw.leidenuniv.nl

From an Observed Quasar Spectrum to $\langle x_{\rm HI} \rangle$

HMC Inference Pipeline

DATA

Real (or mock) quasar spectrum with observational noise

MODEL

Quasar continuum model

Reconstruction error stochastic process

+

IGM transmission field stochastic process

BAYESIAN INFERENCE

with a Gaussian likelihood approximation

- **Jointly** fitting the quasar continuum & IGM damping wing
- Likelihood operates on the **entire** spectrum (red- and blueward of Lyman-α)
- **Fast** GPU-accelerated JAX-based Hamiltonian Monte Carlo implementation (runtimes ~15 min)

POSTERIOR

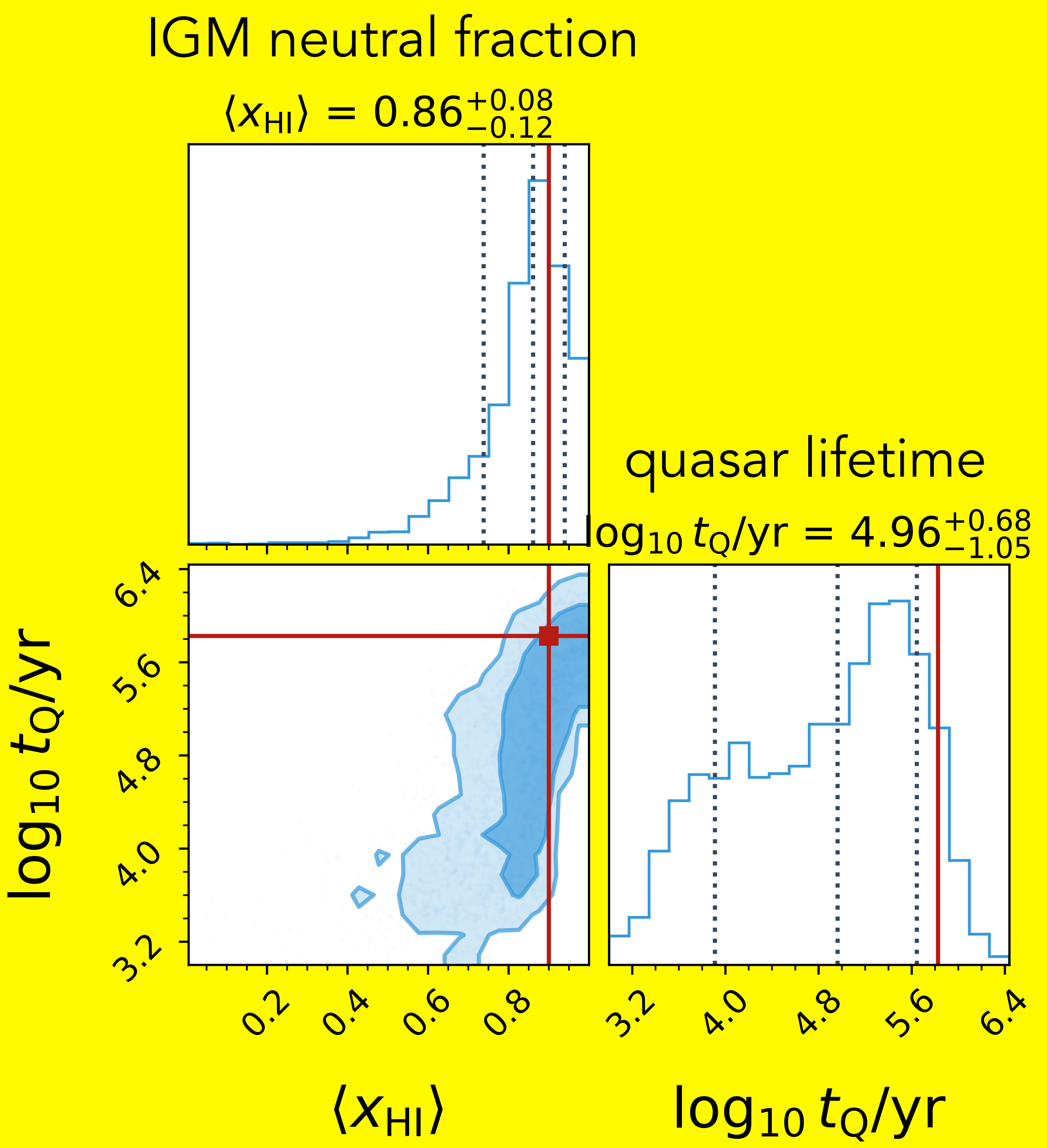

Kist, Hennawi & Davies 2024a

Timo Kist, Leiden Observatory, kist@strw.leidenuniv.nl

From an Observed Quasar Spectrum to $\langle x_{\mathrm{HI}} \rangle$

HMC Inference Pipeline

DATA

Real (or mock) quasar spectrum with observational noise

MODEL

Quasar continuum model

Reconstruction error stochastic process

+

IGM transmission field stochastic process

BAYESIAN INFERENCE

with a Gaussian likelihood approximation

- **Jointly** fitting the quasar continuum & IGM damping wing
- Likelihood operates on the **entire** spectrum (red- and blueward of Lyman-α)
- **Fast** GPU-accelerated JAX-based Hamiltonian Monte Carlo implementation (runtimes ~15 min)

POSTERIOR

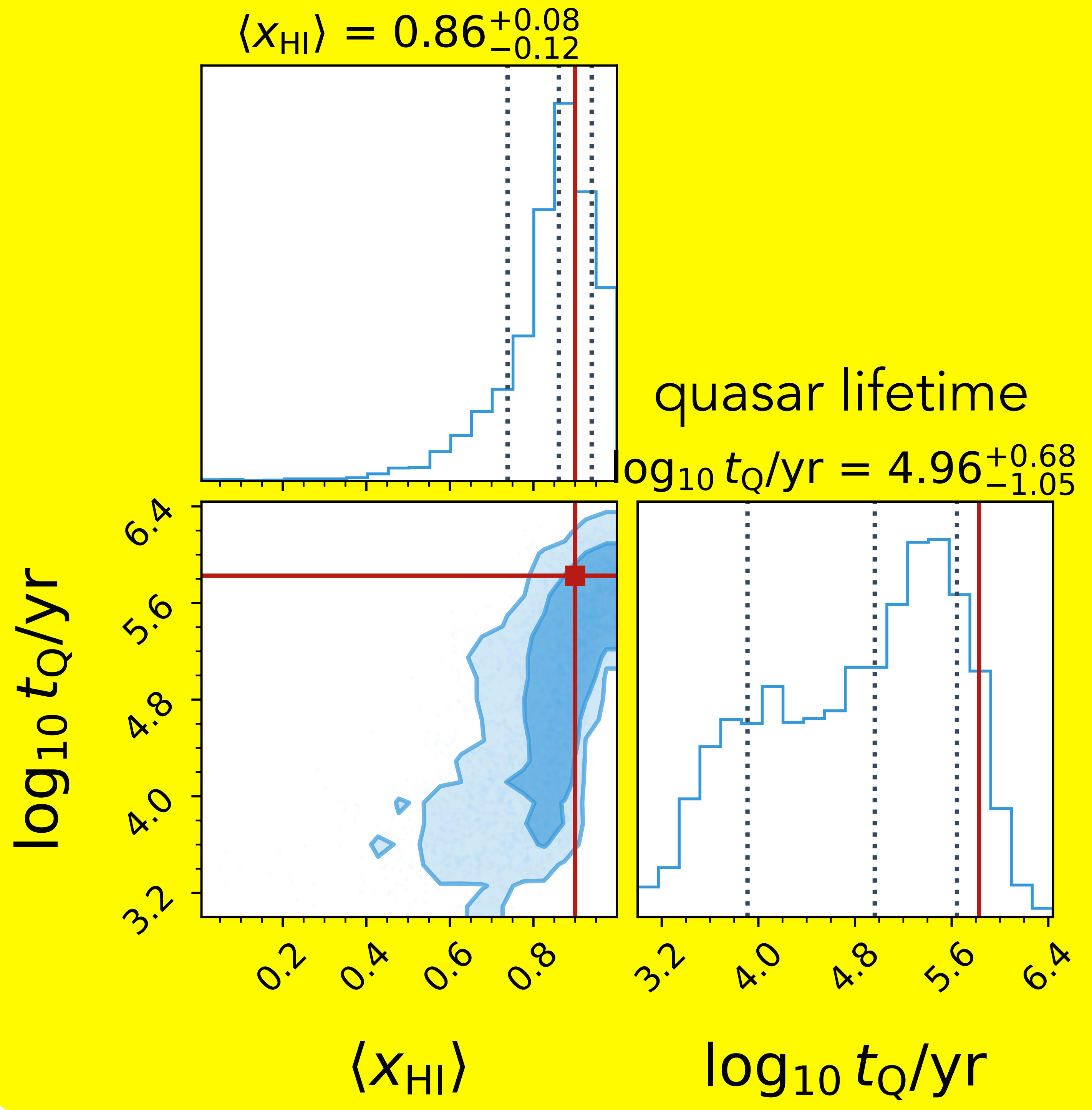

Kist, Hennawi & Davies 2024a

Timo Kist, Leiden Observatory, kist@strw.leidenuniv.nl

From an Observed Quasar Spectrum to $\langle x_{\rm HI} \rangle$

HMC Inference Pipeline

DATA

Real (or mock) quasar spectrum with observational noise

MODEL

Quasar continuum model

Reconstruction error stochastic process

+

IGM transmission field stochastic process

BAYESIAN INFERENCE

with a Gaussian likelihood approximation

- **Jointly** fitting the quasar continuum & IGM damping wing
- Likelihood operates on the **entire** spectrum (red- and blueward of Lyman-α)
- **Fast** GPU-accelerated JAX-based Hamiltonian Monte Carlo implementation (runtimes ~15 min)

POSTERIOR

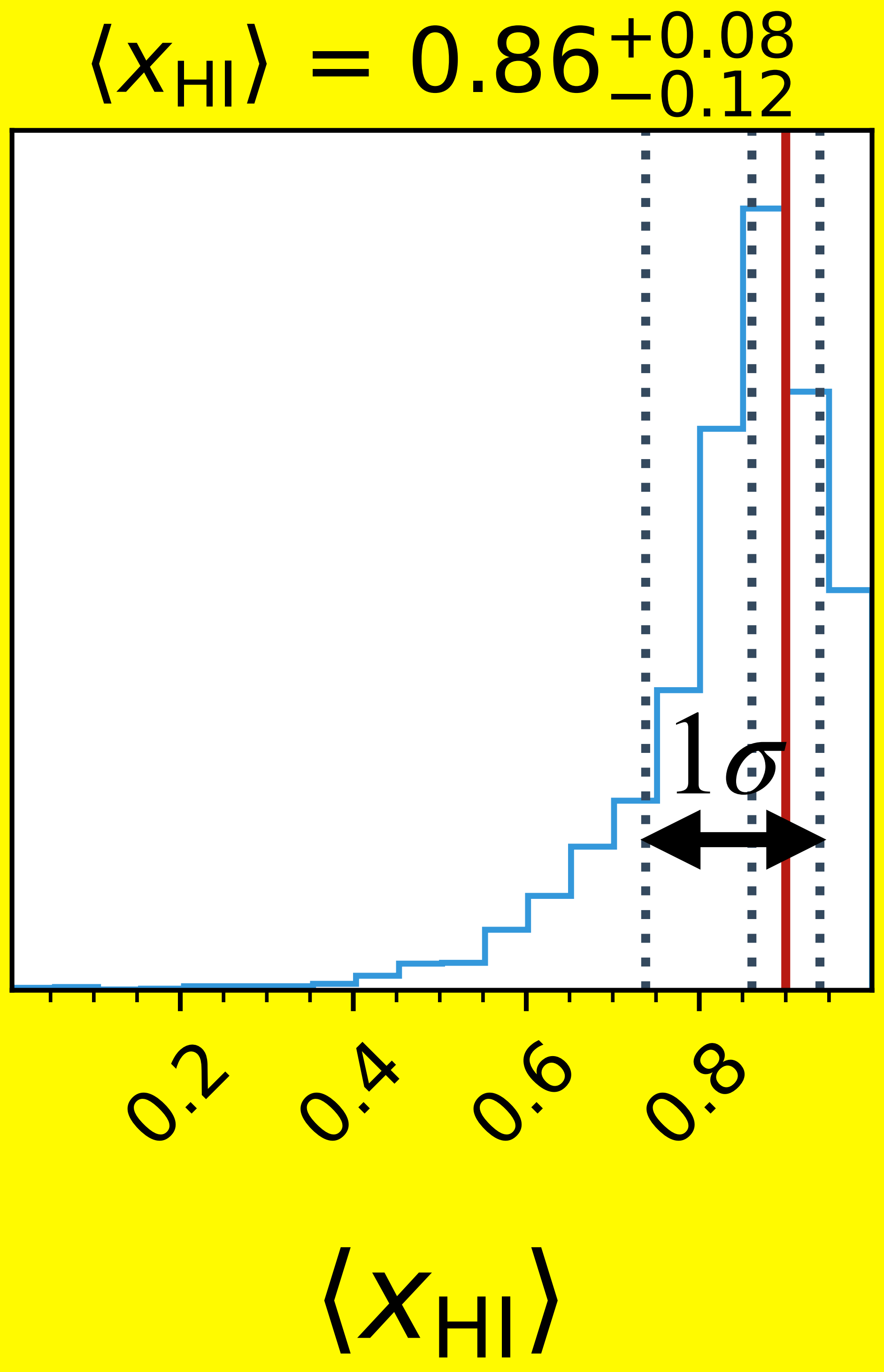

Kist, Hennawi & Davies 2024a

Timo Kist, Leiden Observatory, kist@strw.leidenuniv.nl

Quantifying $\langle x_{\mathrm{HI}} \rangle$ Inference Precision

Variation across parameter space

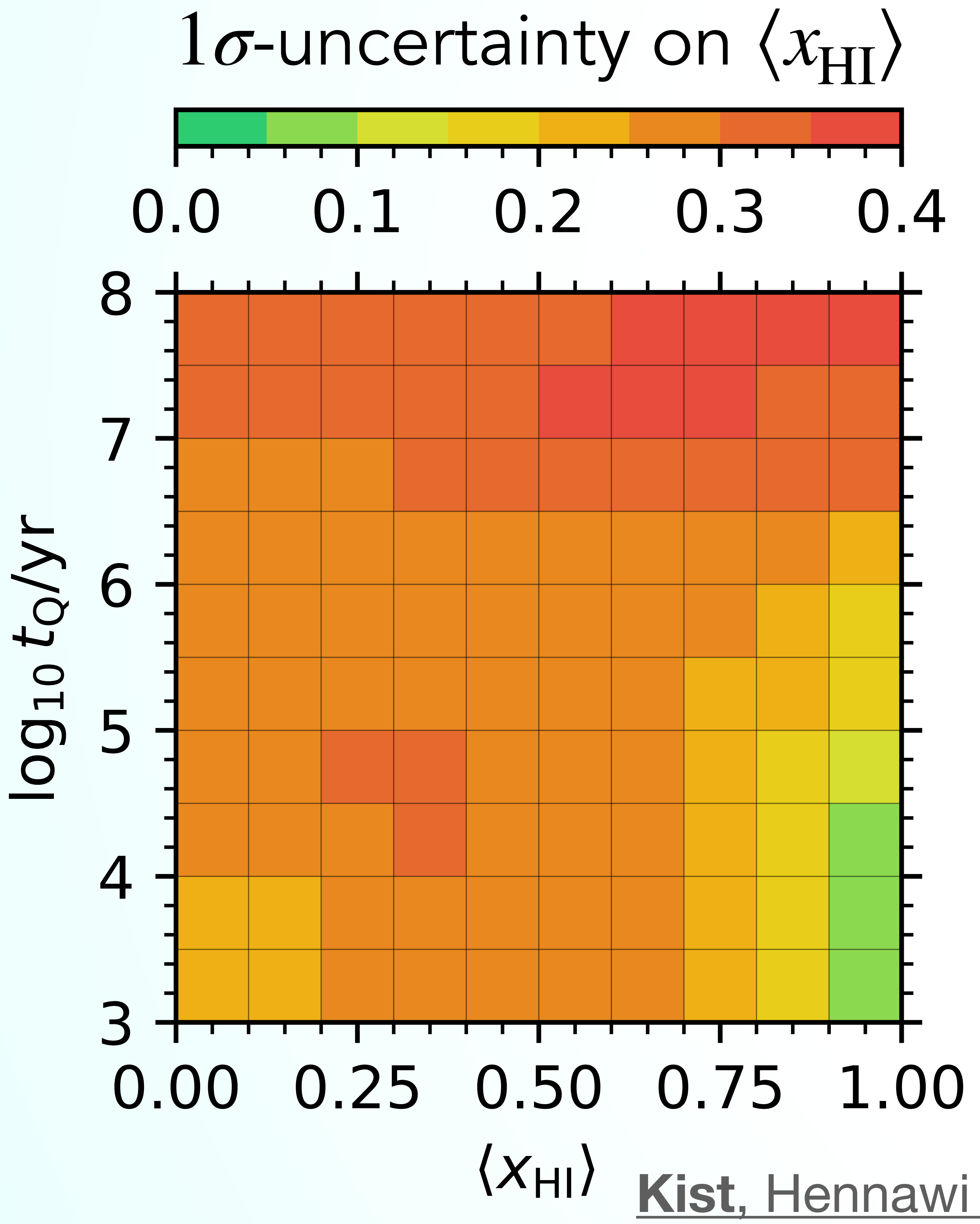

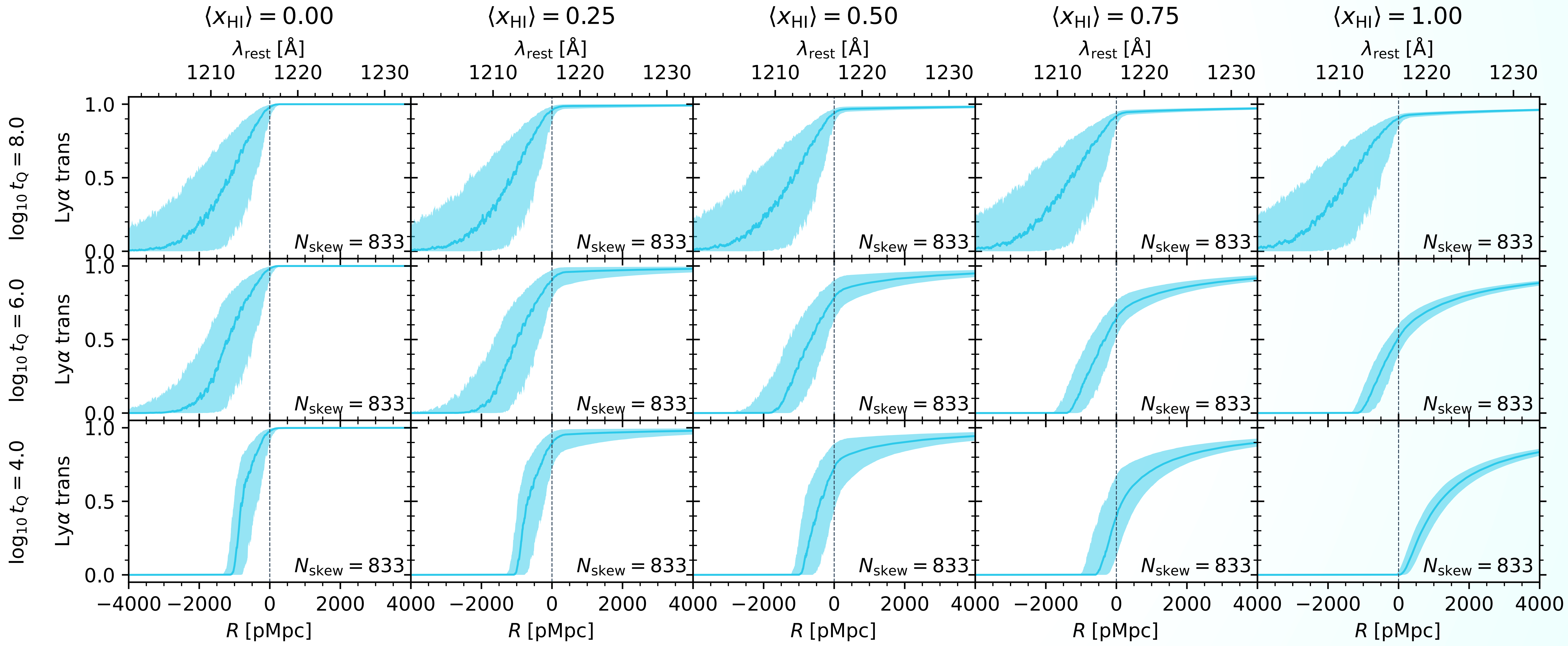

Kist, Hennawi & Davies 2024a

Kist, Hennawi & Davies 2024b (in prep.)

Timo Kist, Leiden Observatory, kist@strw.leidenuniv.nl

Quantifying $\langle x_{HI} \rangle$ Inference Precision

Variation across parameter space

1σ-uncertainty on $\langle x_{HI} \rangle$

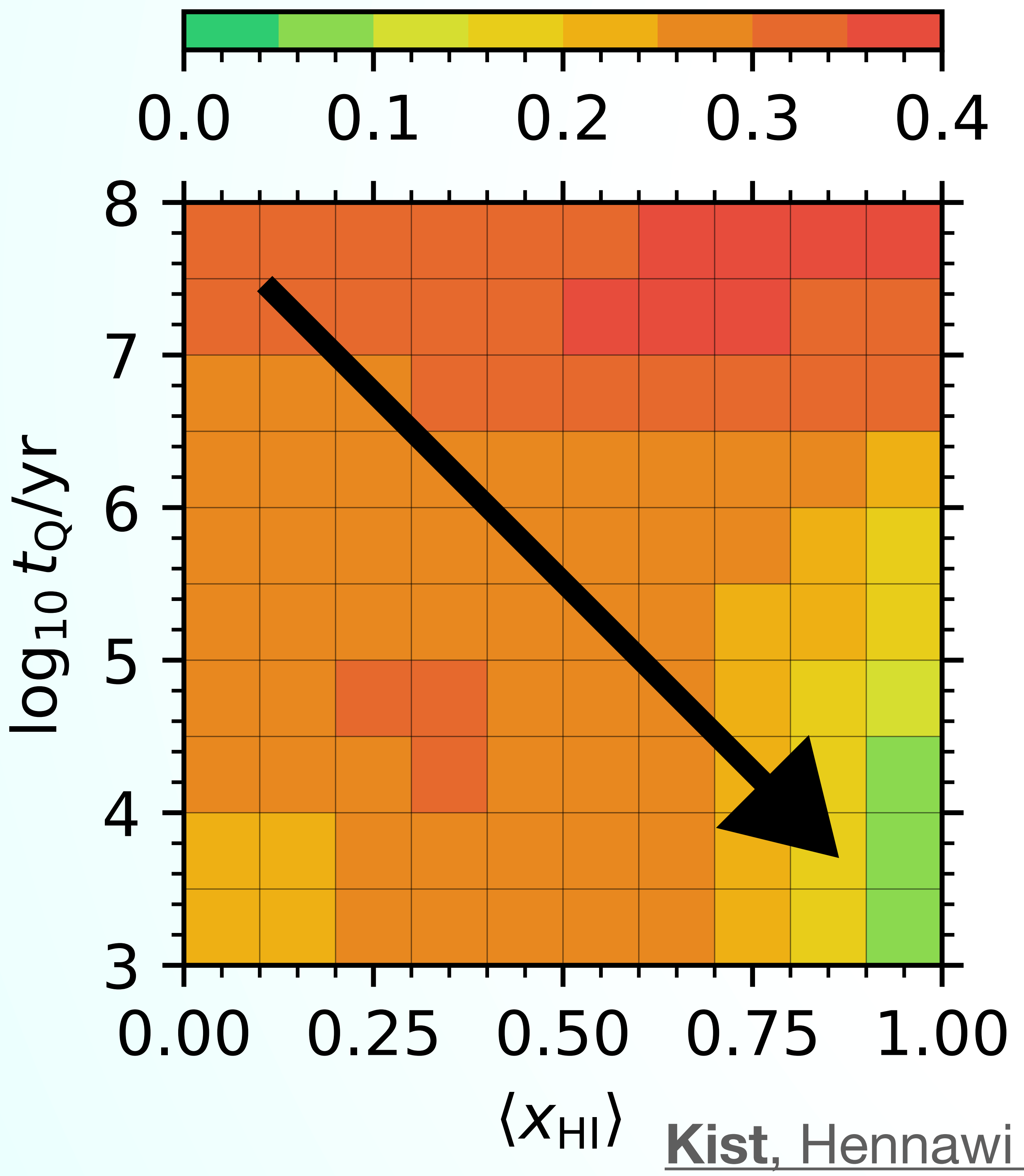

Kist, Hennawi & Davies 2024a

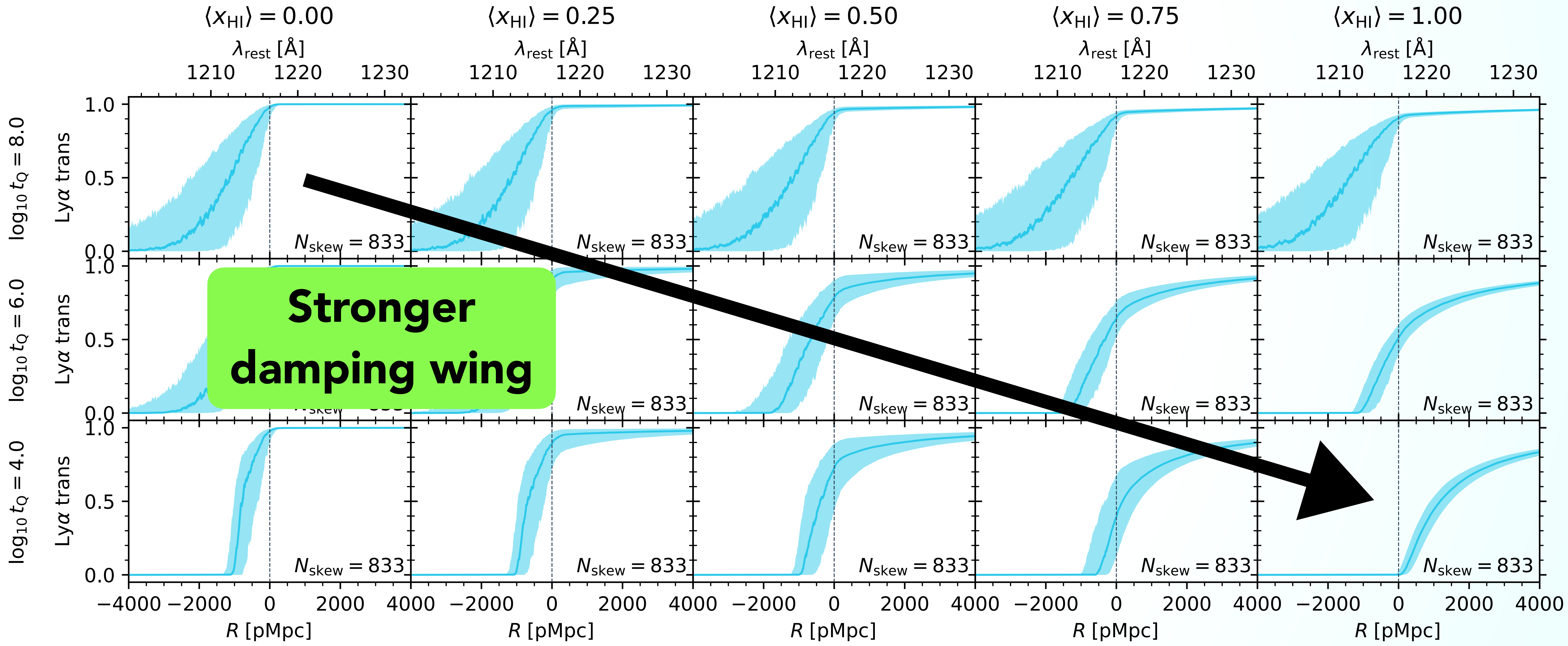

Kist, Hennawi & Davies 2024b (in prep.)

Timo Kist, Leiden Observatory, kist@strw.leidenuniv.nl

Quantifying $\langle x_{HI} \rangle$ Inference Precision

Variation across parameter space

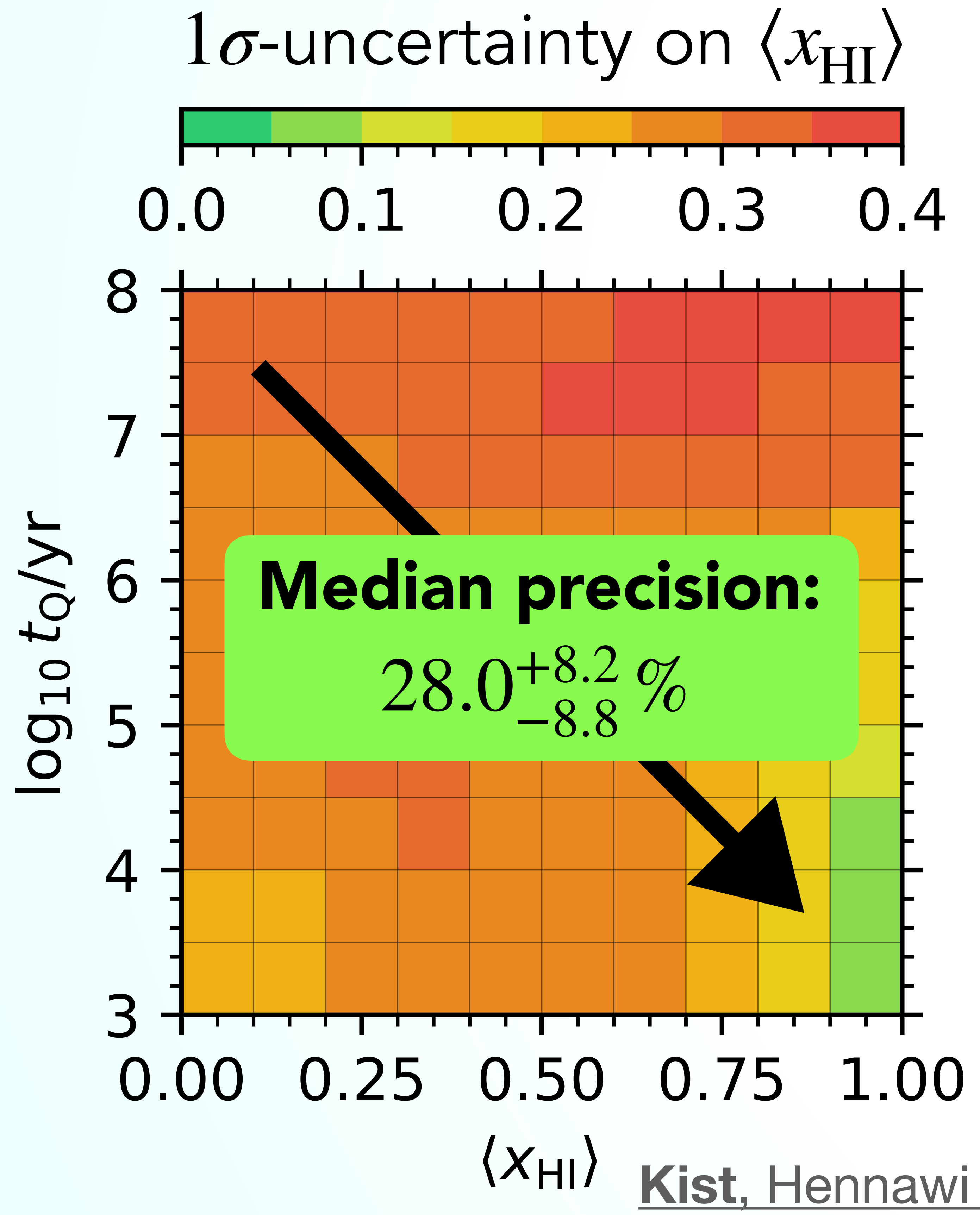

Kist, Hennawi & Davies 2024a

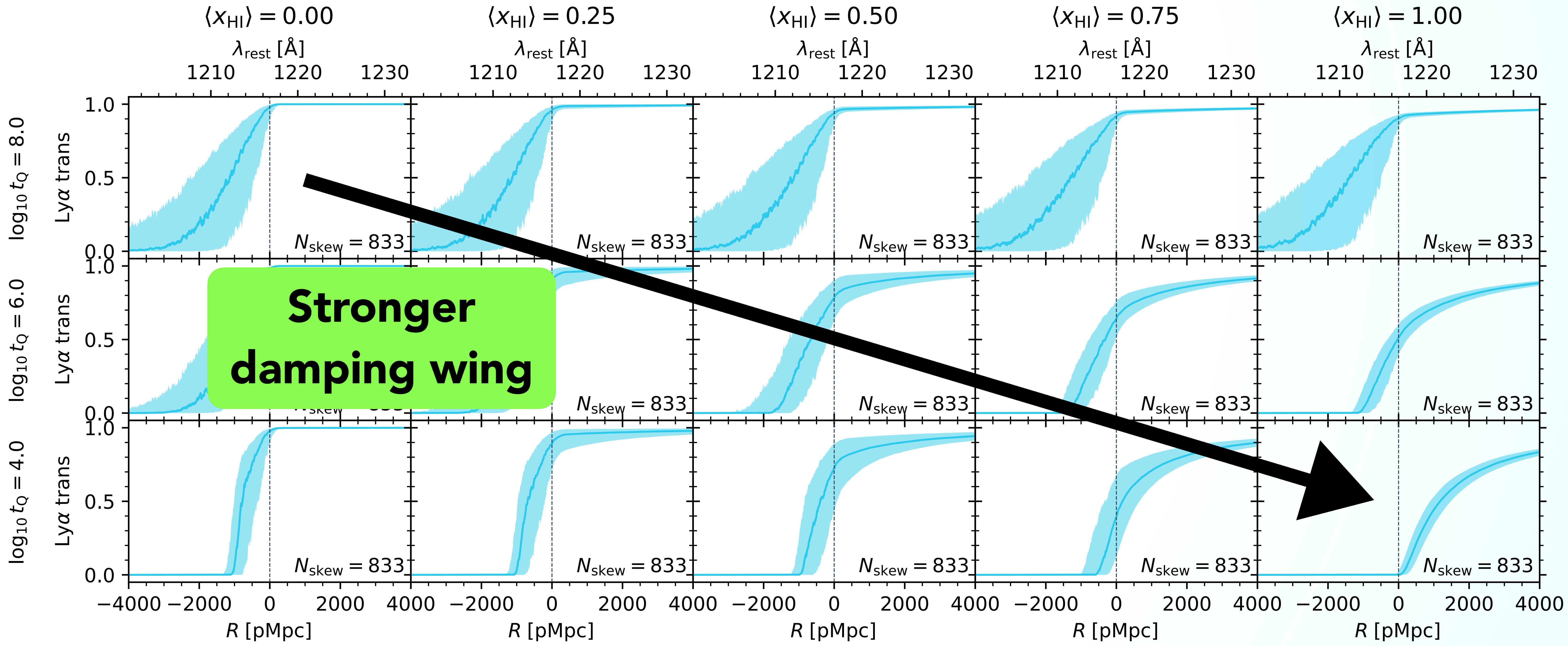

Kist, Hennawi & Davies 2024b (in prep.)

Timo Kist, Leiden Observatory, kist@strw.leidenuniv.nl

Quantifying $\langle x_{\rm HI} \rangle$ Inference Precision

Variation across parameter space

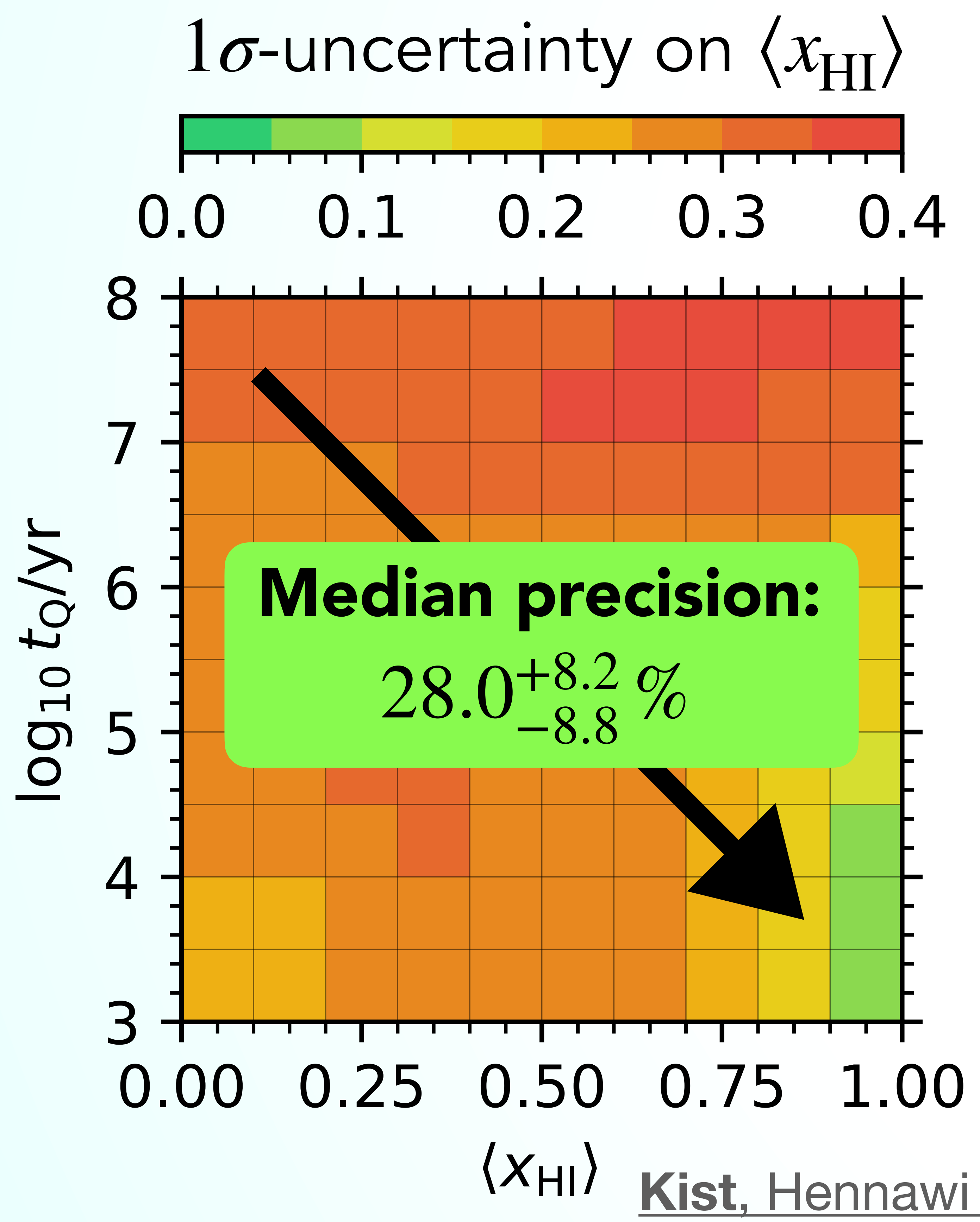

Kist, Hennawi & Davies 2024a

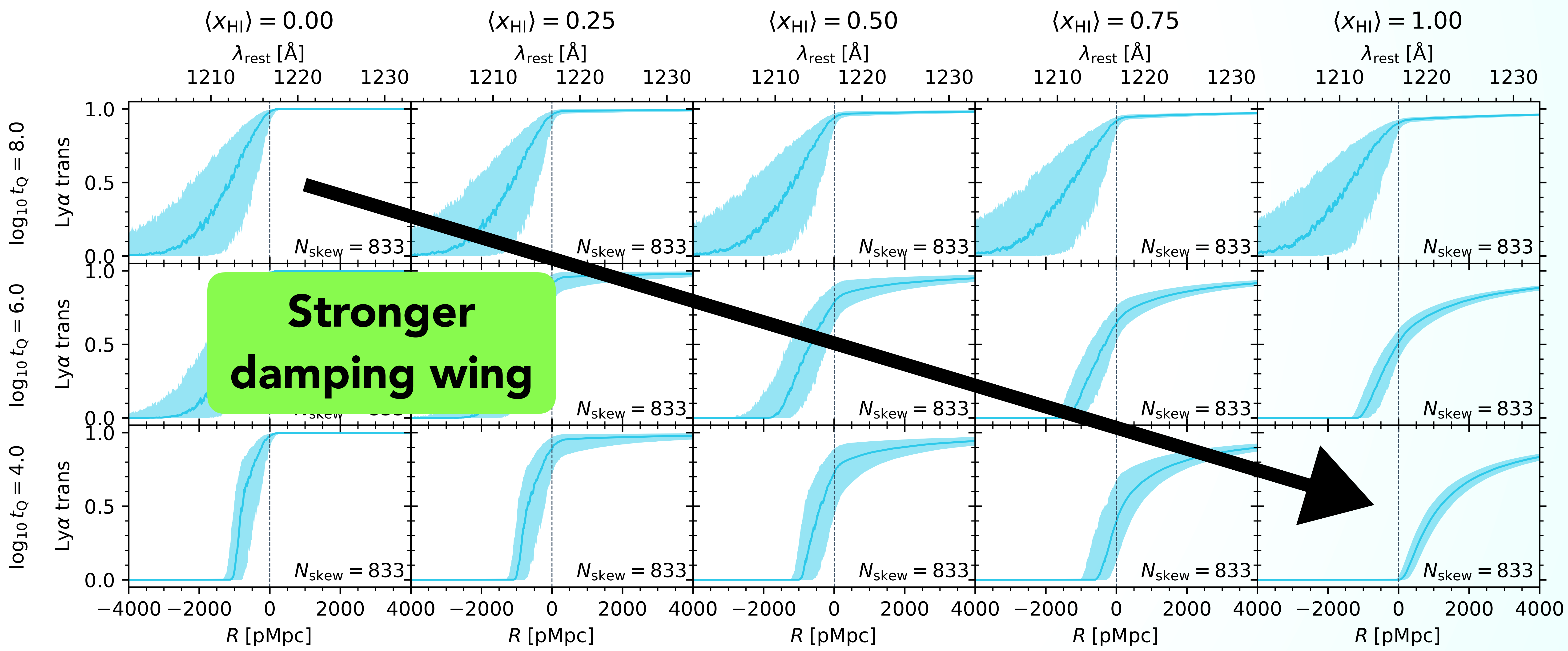

Kist, Hennawi & Davies 2024b (in prep.)

Main sources of uncertainty: continuum reconstruction and **stochasticity of ionized bubble sizes**

Timo Kist, Leiden Observatory, kist@strw.leidenuniv.nl

Quantifying $\langle x_{HI} \rangle$ Inference Precision

Variation across parameter space

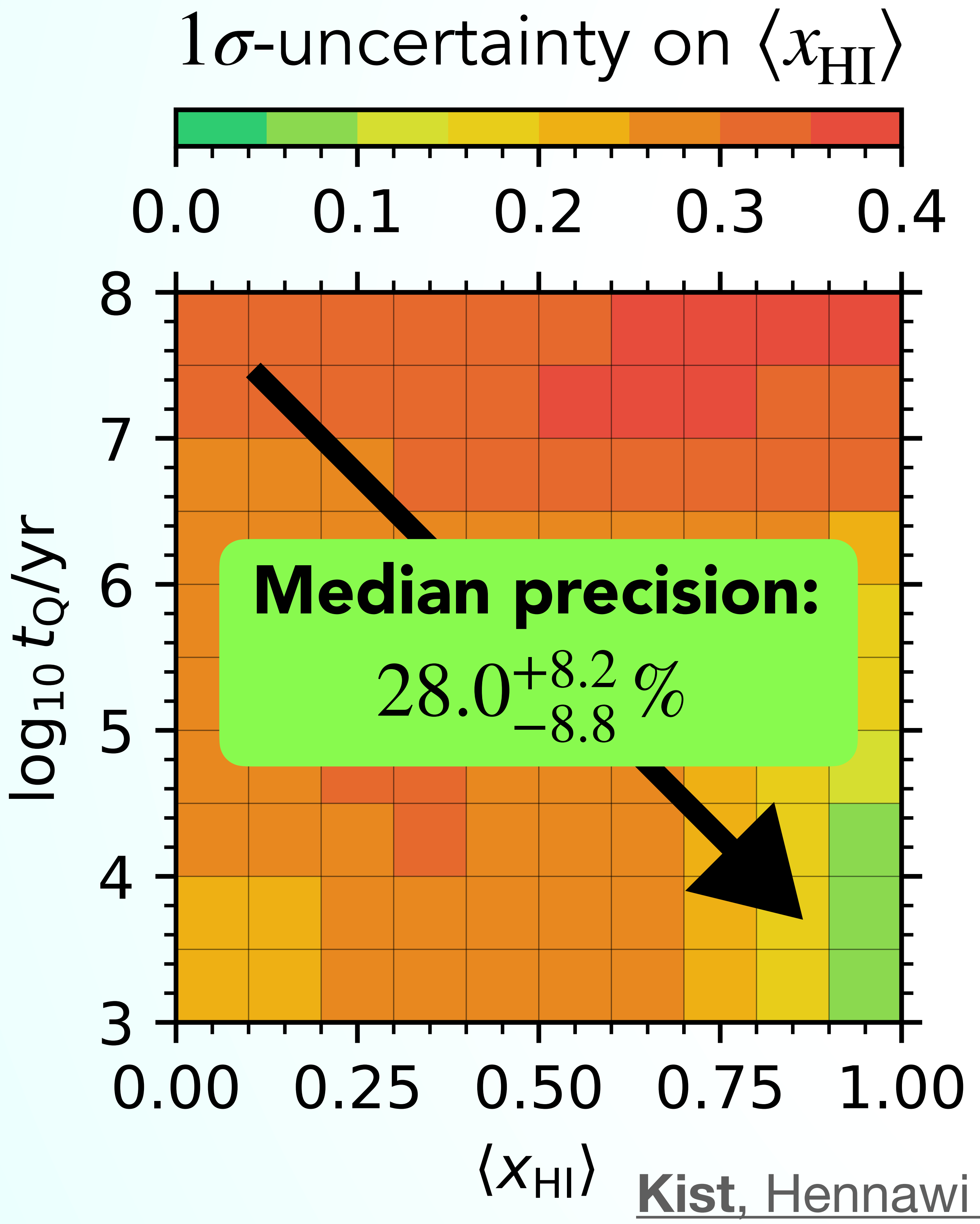

Kist, Hennawi & Davies 2024a

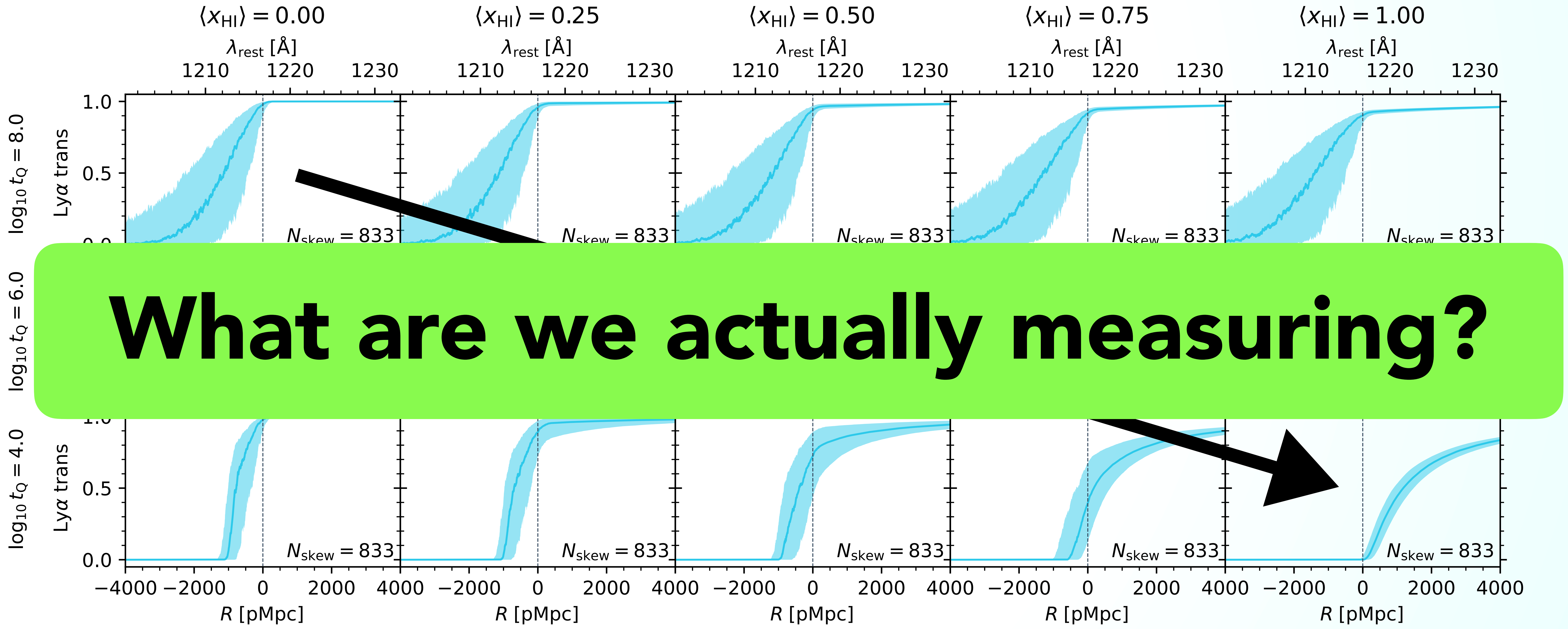

Kist, Hennawi & Davies 2024b (in prep.)

Main sources of uncertainty: continuum reconstruction and **stochasticity of ionized bubble sizes**

Timo Kist, Leiden Observatory, kist@strw.leidenuniv.nl

Measuring the local HI content in front of a quasar

Introducing a new label for the HI column density

Timo Kist, Leiden Observatory, kist@strw.leidenuniv.nl

Measuring the local HI content in front of a quasar

Introducing a new label for the HI column density

Kist, Hennawi & Davies 2024b (in prep.)

Timo Kist, Leiden Observatory, kist@strw.leidenuniv.nl

Measuring the local HI content in front of a quasar

Introducing a new label for the HI column density

Kist, Hennawi & Davies 2024b (in prep.)

Timo Kist, Leiden Observatory, kist@strw.leidenuniv.nl

Measuring the local HI content in front of a quasar

Introducing a new label for the HI column density

$\langle x_{\mathrm{HI}} \rangle = 0.5 \quad t_{\mathrm{Q}} = 10^6\ \mathrm{yr}$

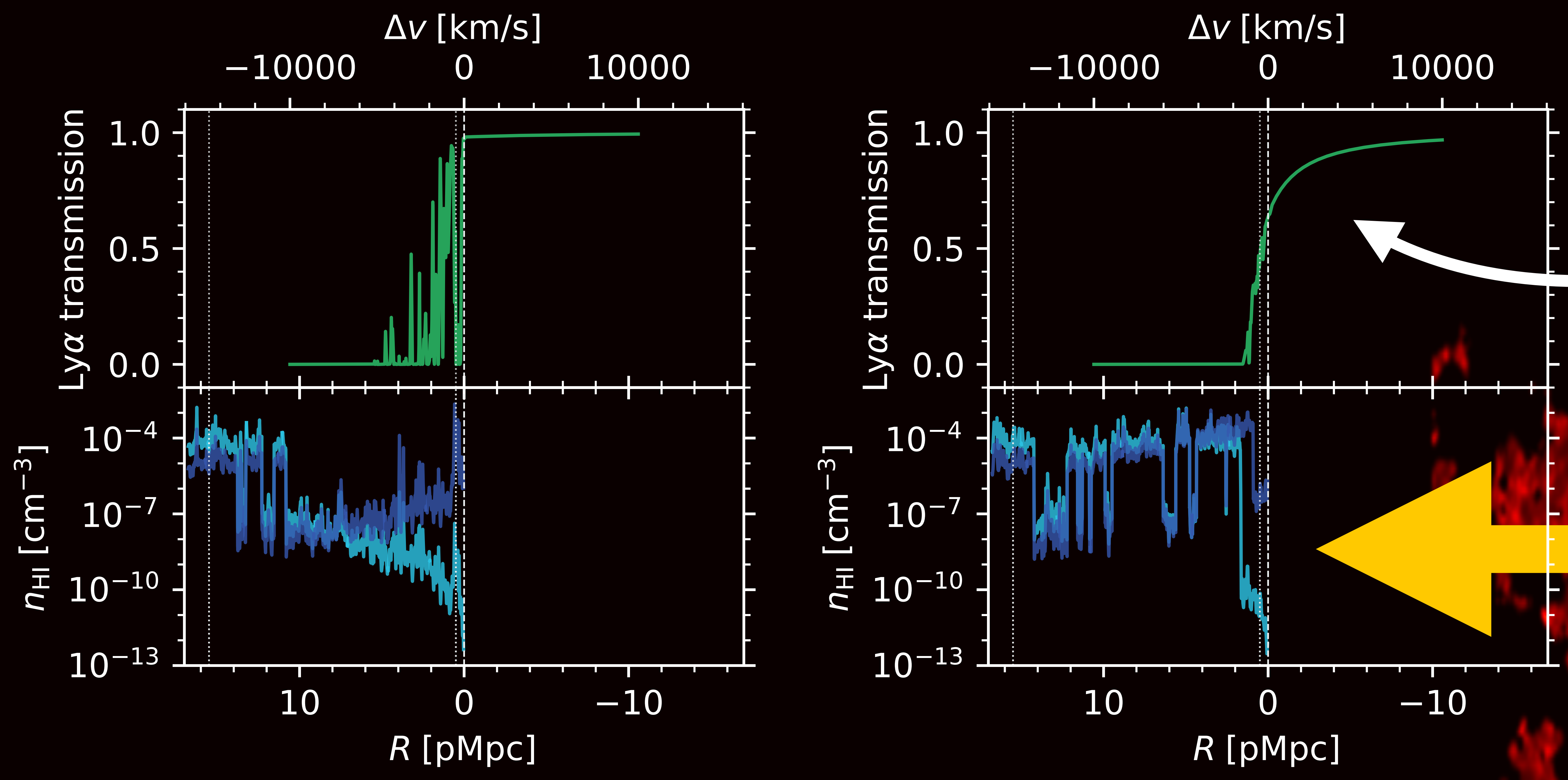

damping wing optical depth

$$\tau_{\mathrm{DW}}(\lambda_{\mathrm{obs}}) = \int_0^{R(z_{\mathrm{QSO}})} n_{\mathrm{HI}}^{\mathrm{QSO}}(R) \times \sigma_\alpha\left(\nu(R)\right)\, \mathrm{d}R$$

(velocity-weighted) HI column density

$$N_{\mathrm{HI}}^{\mathrm{DW}} = \int_{R_{\mathrm{min}}}^{R_{\mathrm{max}}} n_{\mathrm{HI}}^{\mathrm{gal}}(R) \times \frac{\mathcal{N}}{(v - v_{\mathrm{T}})^{-2}}\, \mathrm{d}R$$

Kist, Hennawi & Davies 2024b (in prep.)

Timo Kist, Leiden Observatory, kist@strw.leidenuniv.nl

Measuring the local HI content in front of a quasar

Introducing a new label for the HI column density

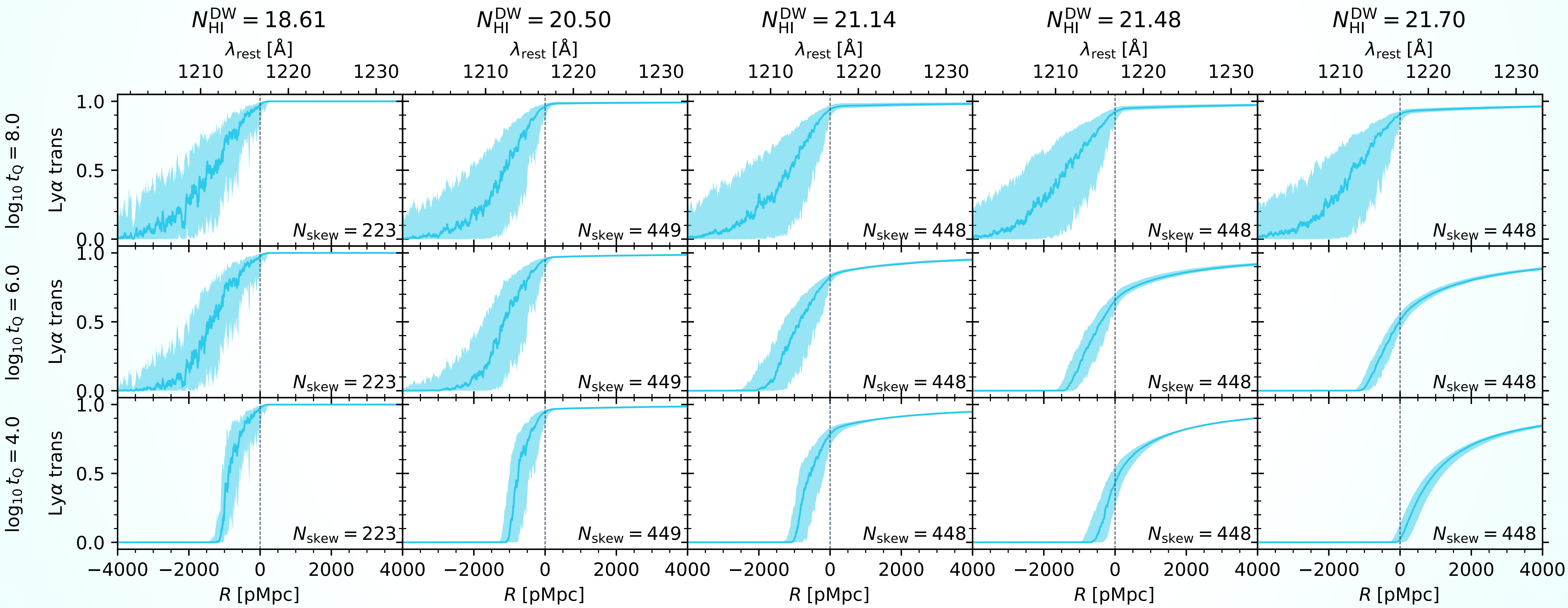

Kist, Hennawi & Davies 2024b (in prep.)

Timo Kist, Leiden Observatory, kist@strw.leidenuniv.nl

Measuring the local HI content in front of a quasar

Introducing a new label for the HI column density

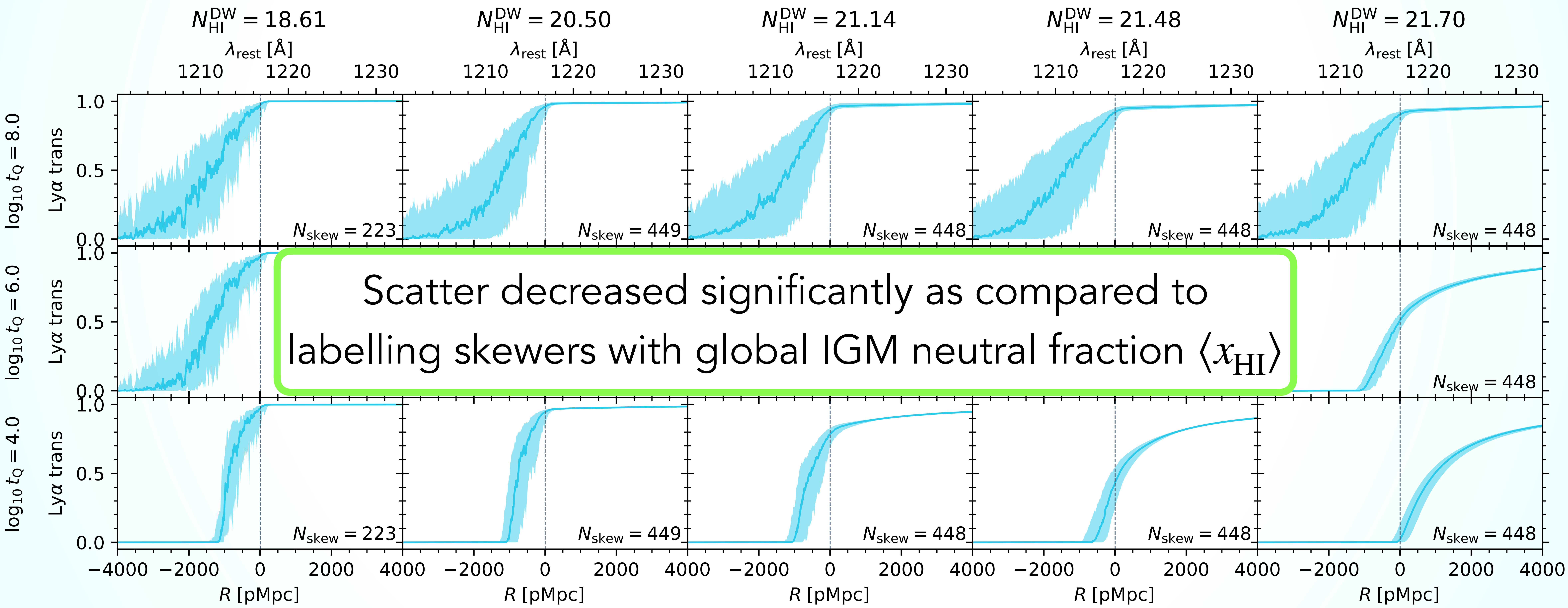

Scatter decreased significantly as compared to labelling skewers with global IGM neutral fraction $\langle x_{HI} \rangle$

Kist, Hennawi & Davies 2024b (in prep.)

Timo Kist, Leiden Observatory, kist@strw.leidenuniv.nl

Quantifying $N_{\rm HI}^{\rm DW}$ Inference Precision

Variation across parameter space

1σ-uncertainty on $\log_{10} N_{\rm HI}^{\rm DW}$

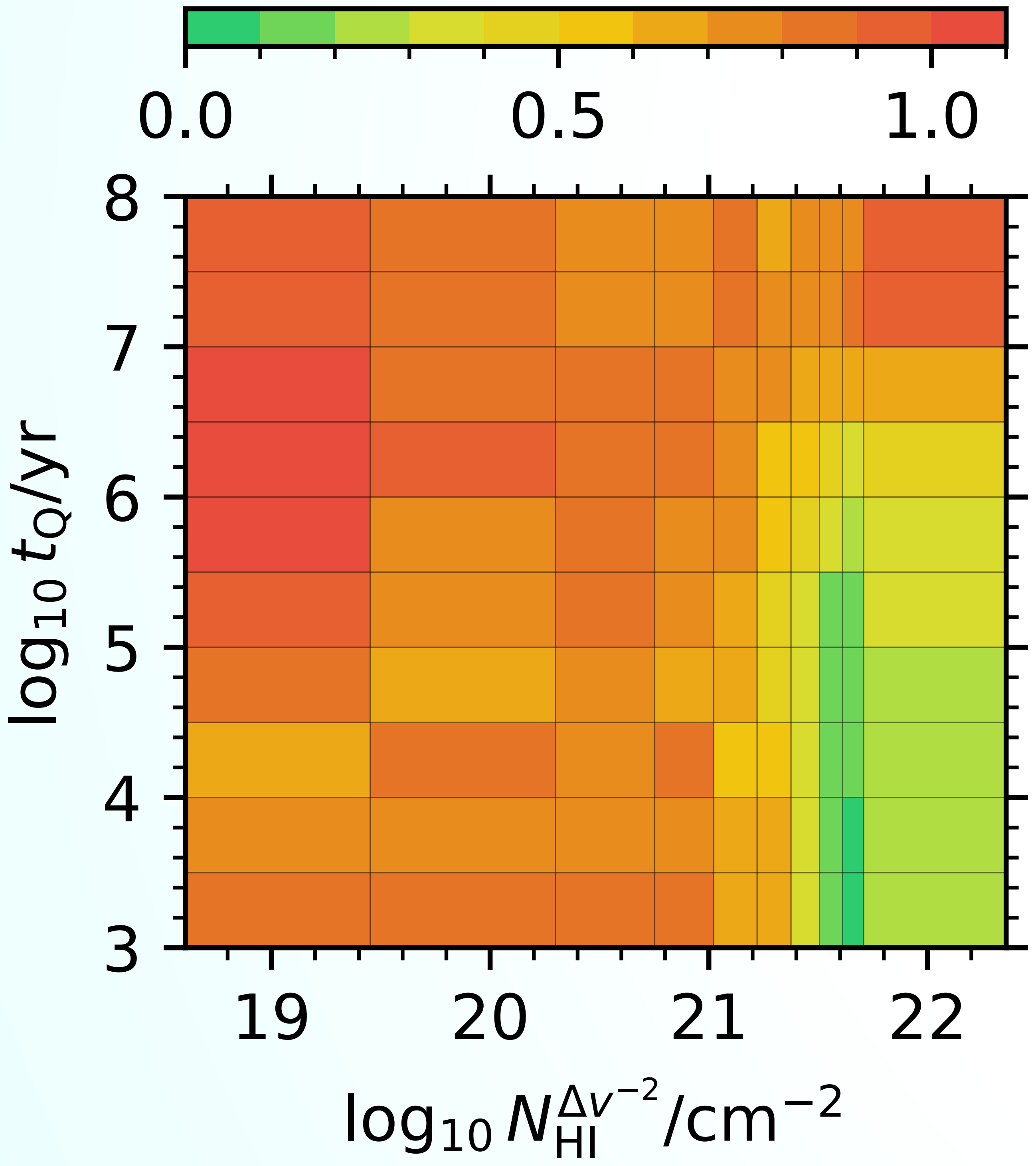

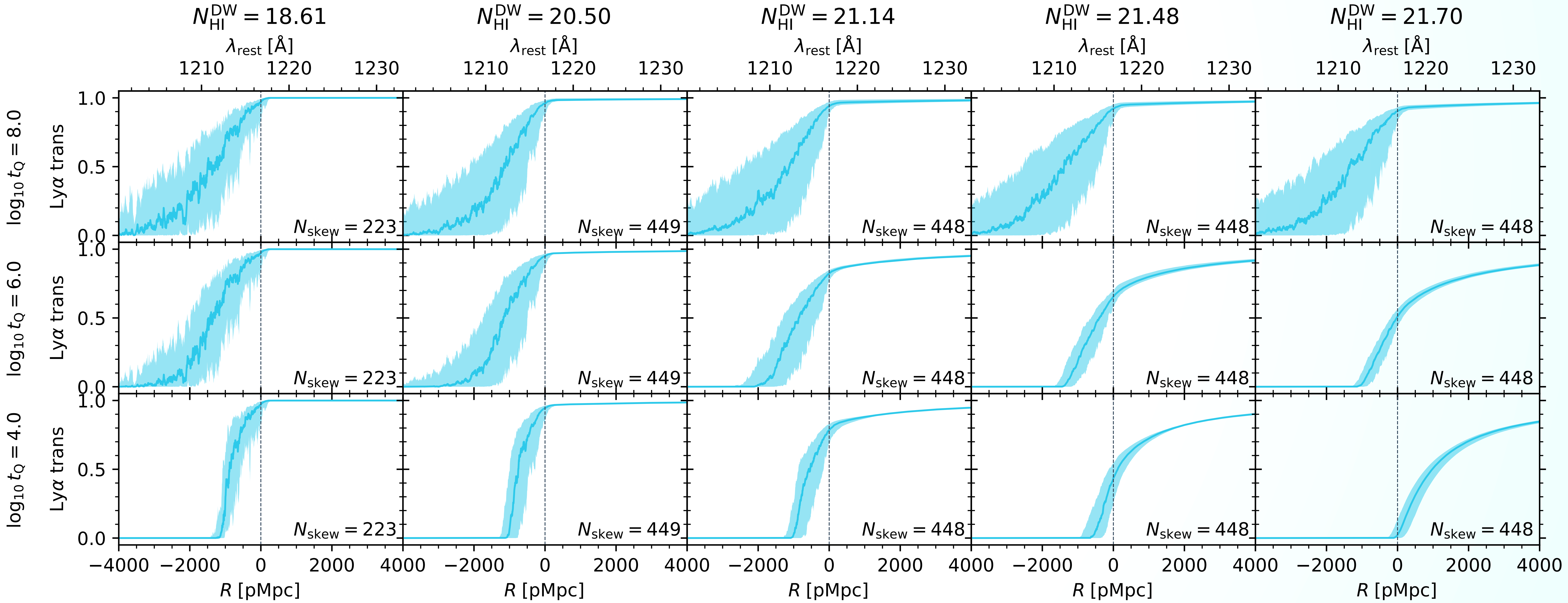

Kist, Hennawi & Davies 2024b (in prep.)

Timo Kist, Leiden Observatory, kist@strw.leidenuniv.nl

Quantifying $N_{\mathrm{HI}}^{\mathrm{DW}}$ Inference Precision

Variation across parameter space

1σ-uncertainty on $\log_{10} N_{\mathrm{HI}}^{\mathrm{DW}}$

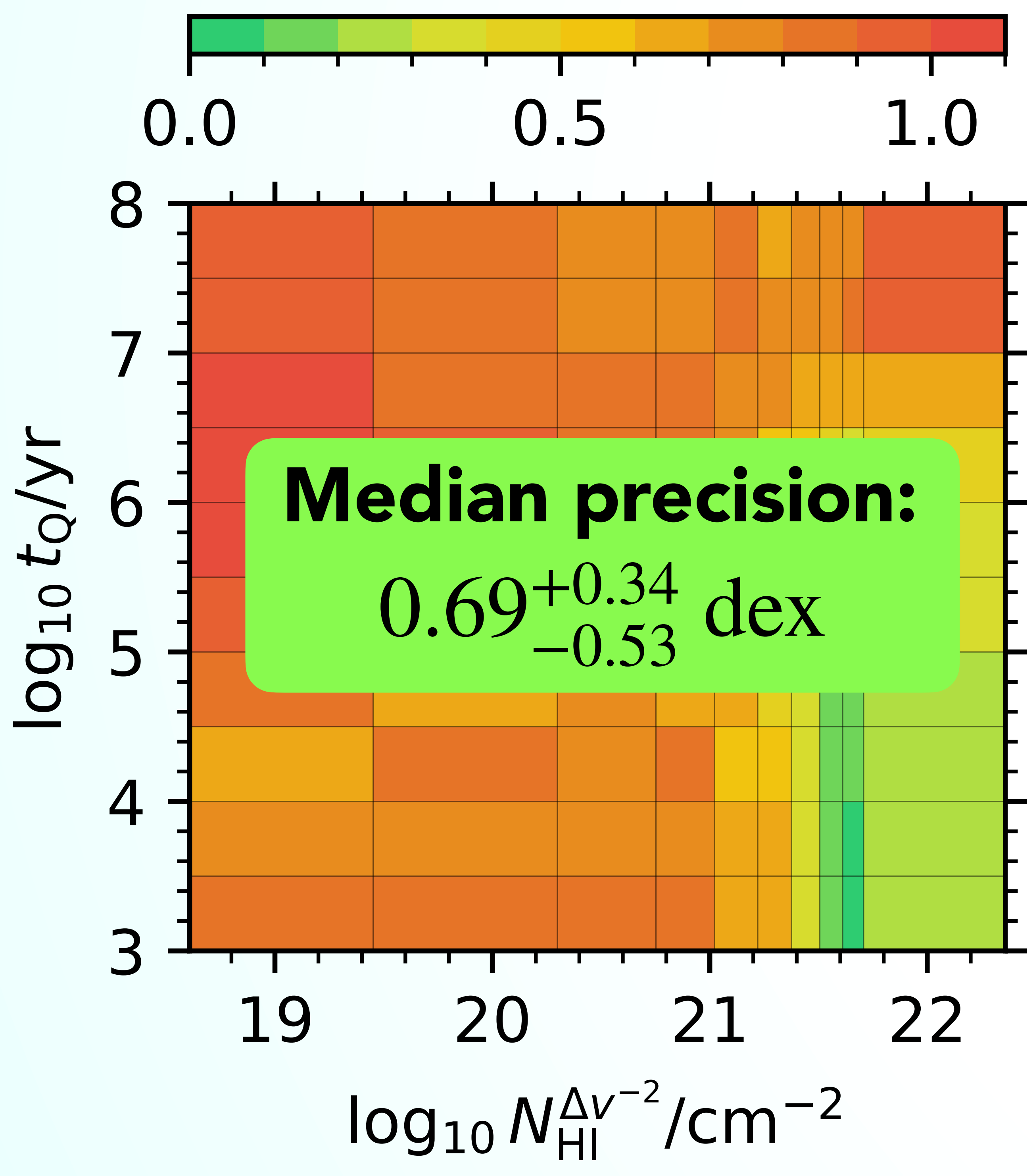

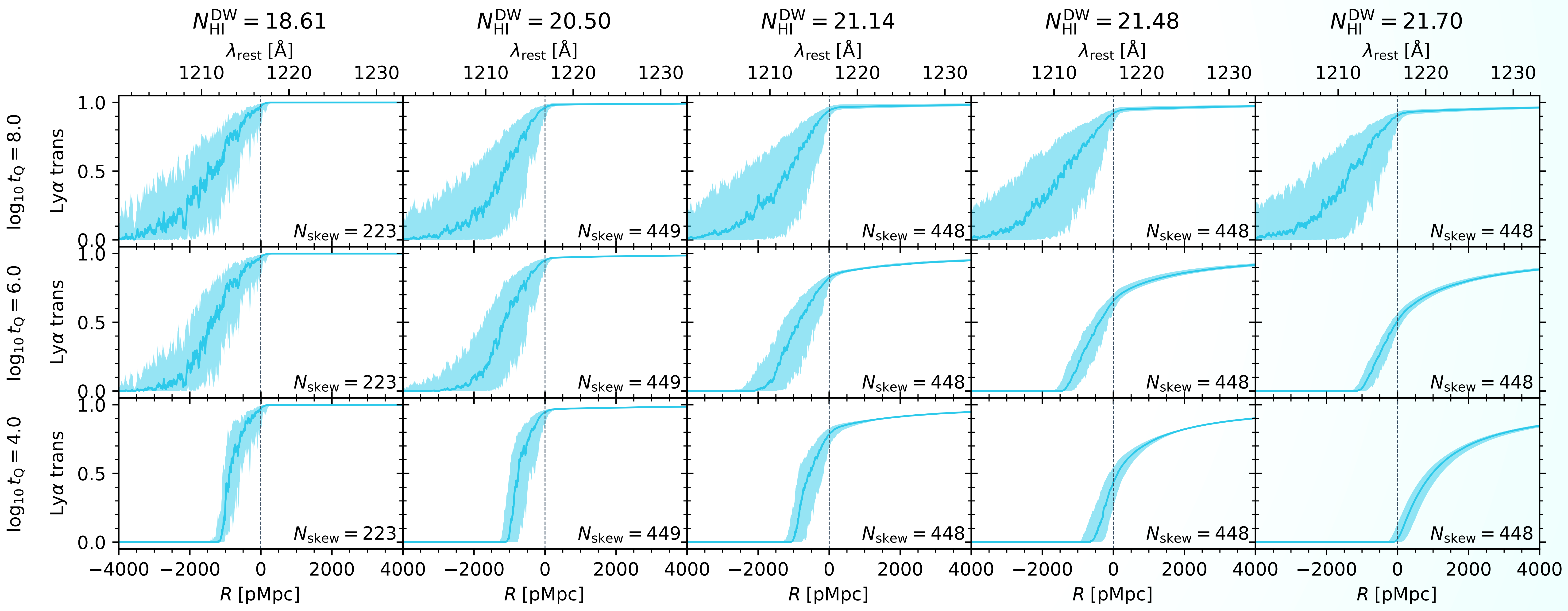

Kist, Hennawi & Davies 2024b (in prep.)

Timo Kist, Leiden Observatory, kist@strw.leidenuniv.nl

Inferring $N_{\rm HI}^{\rm DW}$ in front of a z = 6.83 quasar

A JWST spectrum of J0411-0907

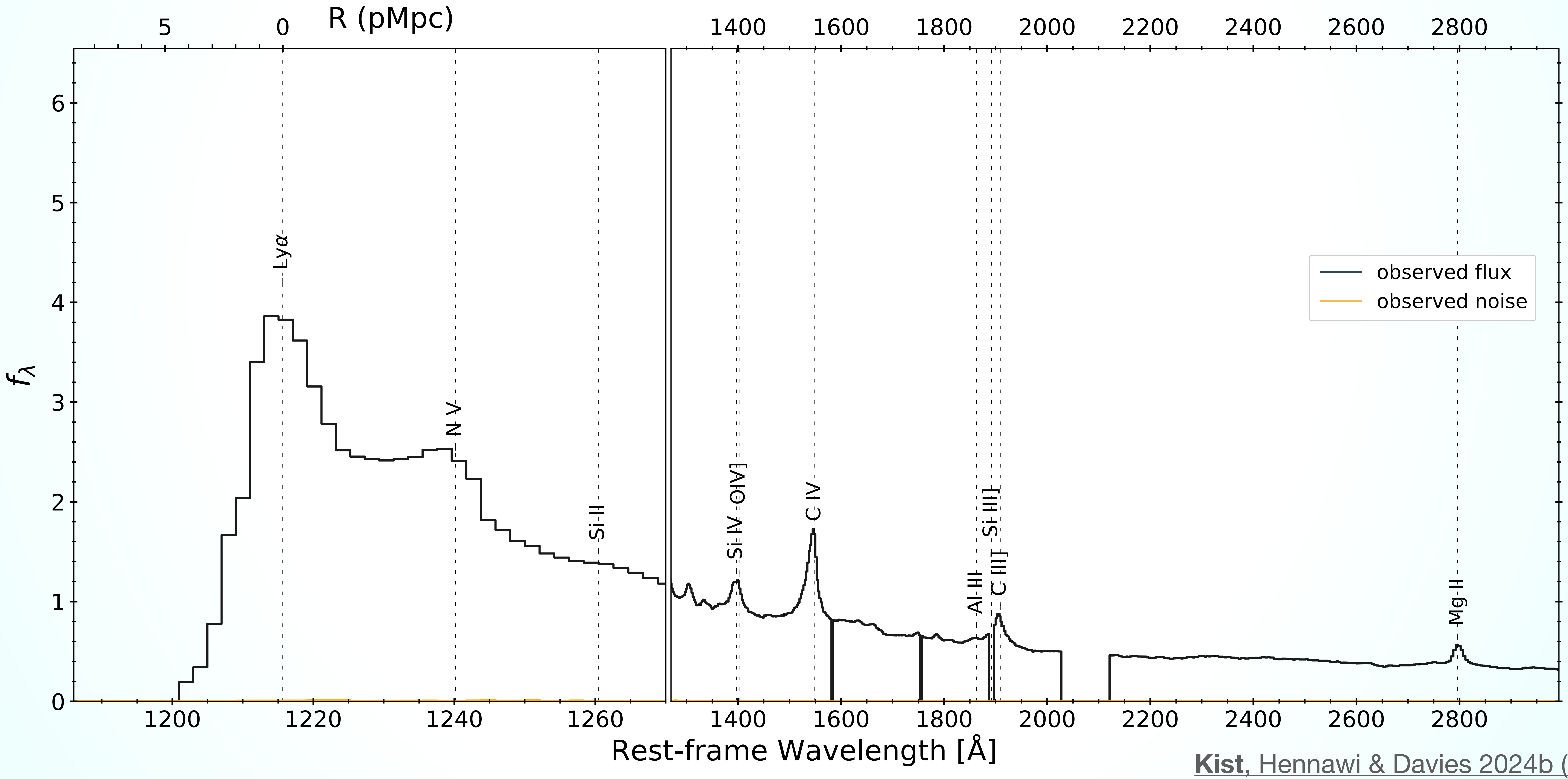

Kist, Hennawi & Davies 2024b (in prep.)

Timo Kist, Leiden Observatory, kist@strw.leidenuniv.nl

Inferring $N_{\mathrm{HI}}^{\mathrm{DW}}$ in front of a z = 6.83 quasar

A JWST spectrum of J0411-0907

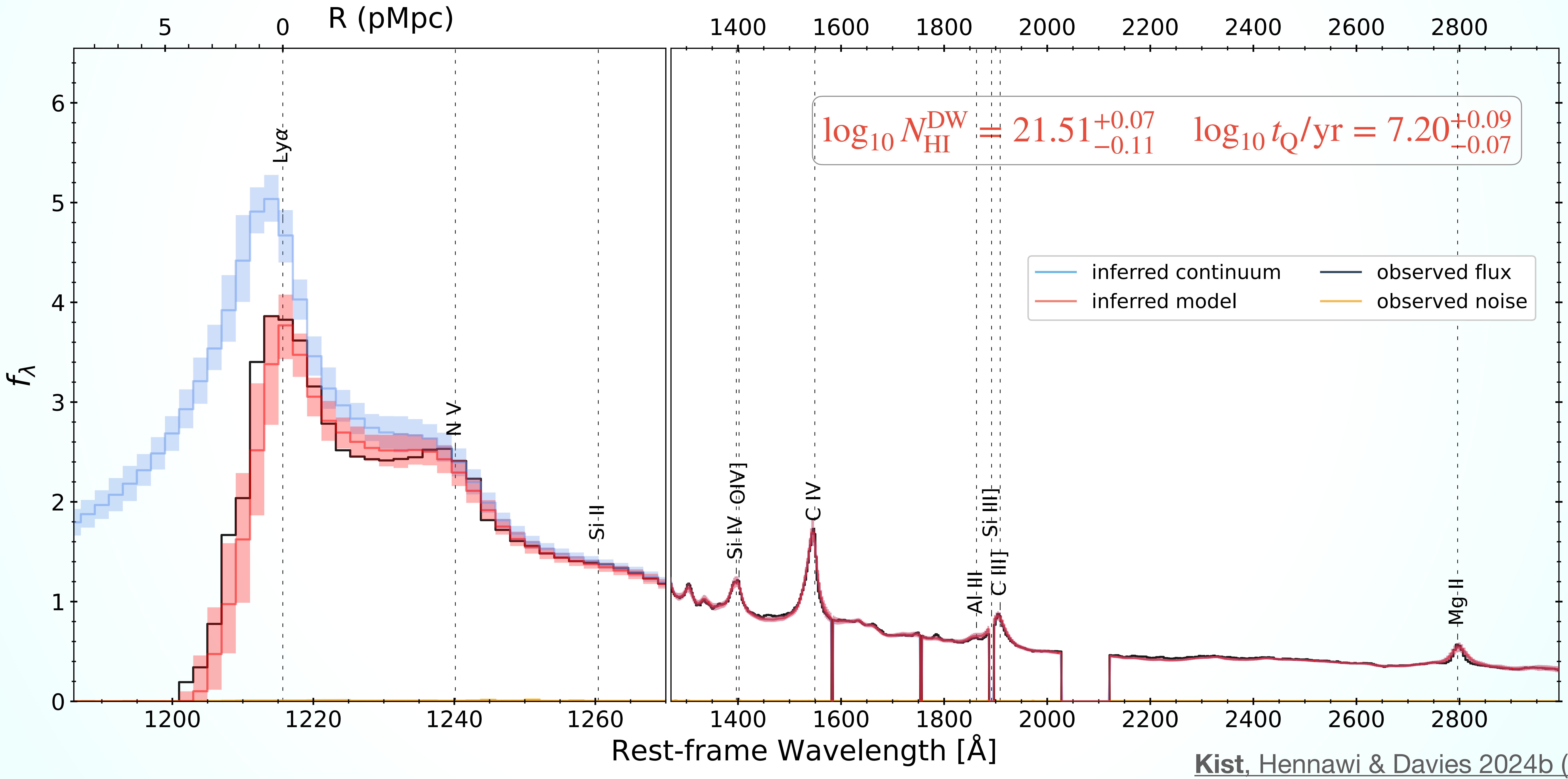

Kist, Hennawi & Davies 2024b (in prep.)

Timo Kist, Leiden Observatory, kist@strw.leidenuniv.nl

Inferring $N_{\mathrm{HI}}^{\mathrm{DW}}$ in front of a z = 6.83 quasar

A JWST spectrum of J0411-0907

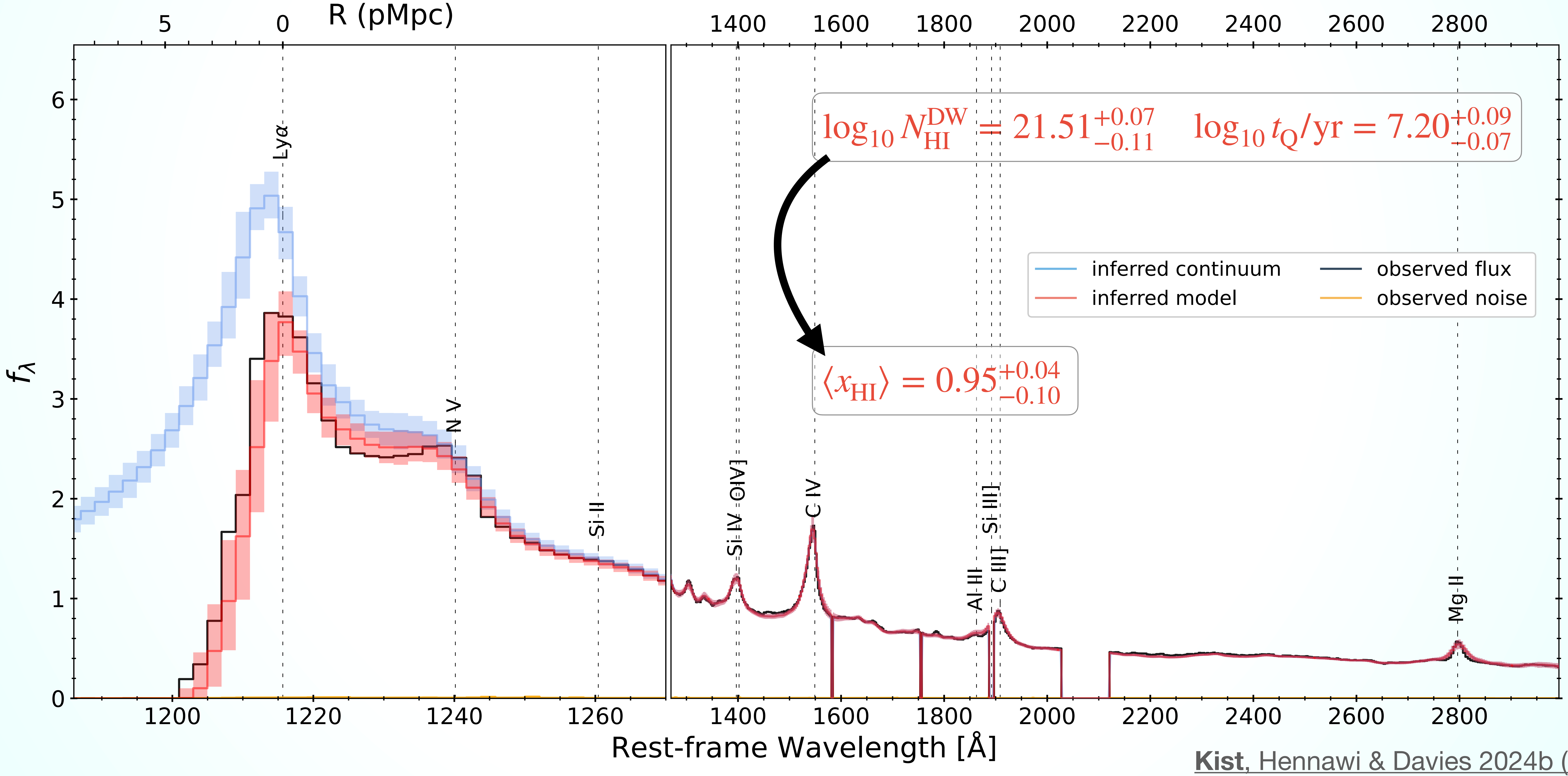

Kist, Hennawi & Davies 2024b (in prep.)

Timo Kist, Leiden Observatory, kist@strw.leidenuniv.nl

EUCLID

The Quasar Yield of the Wide-Field Survey

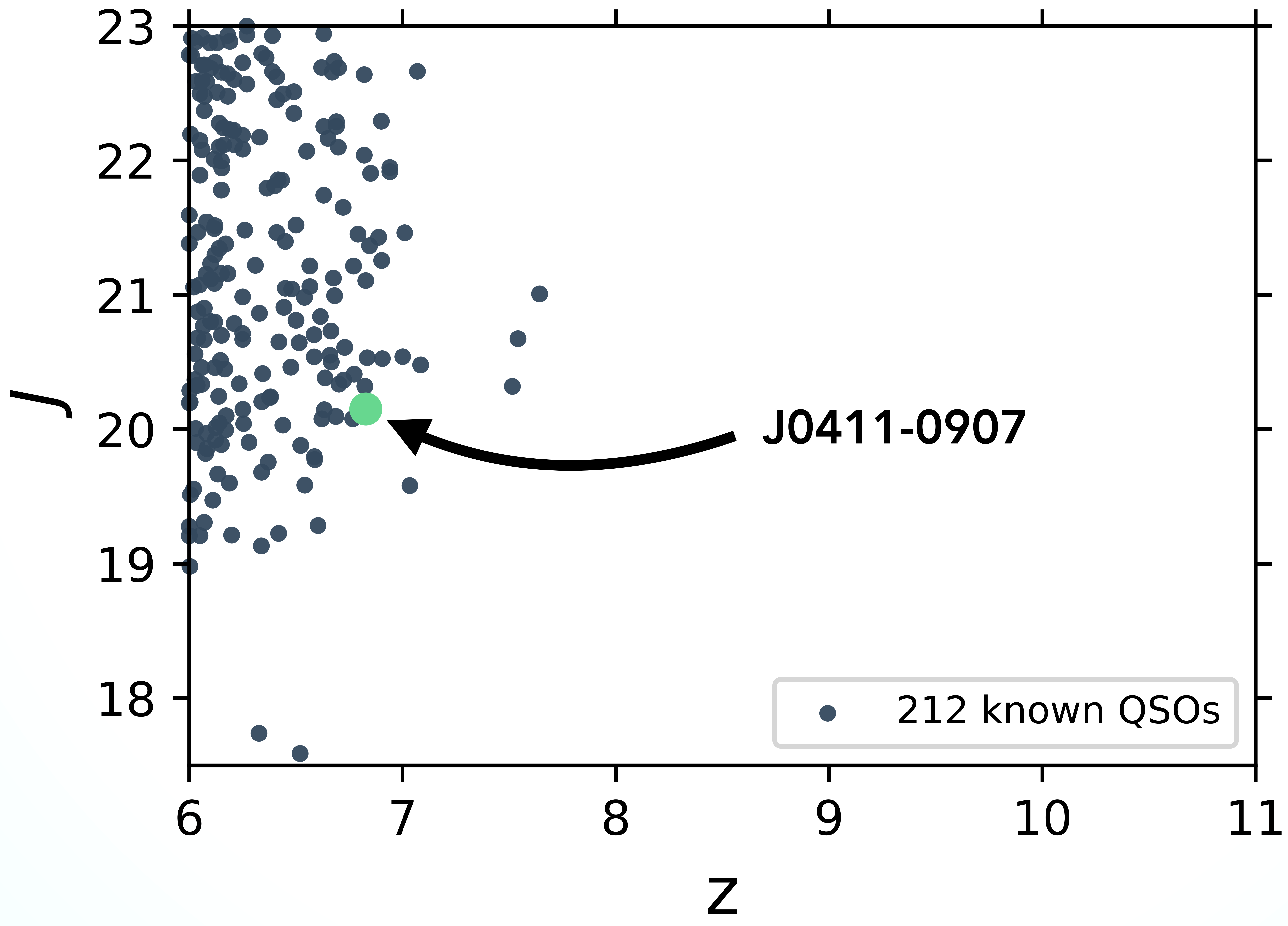

Kist, Hennawi & Davies 2024c (in prep.)

Timo Kist, Leiden Observatory, kist@strw.leidenuniv.nl

EUCLID

The Quasar Yield of the Wide-Field Survey

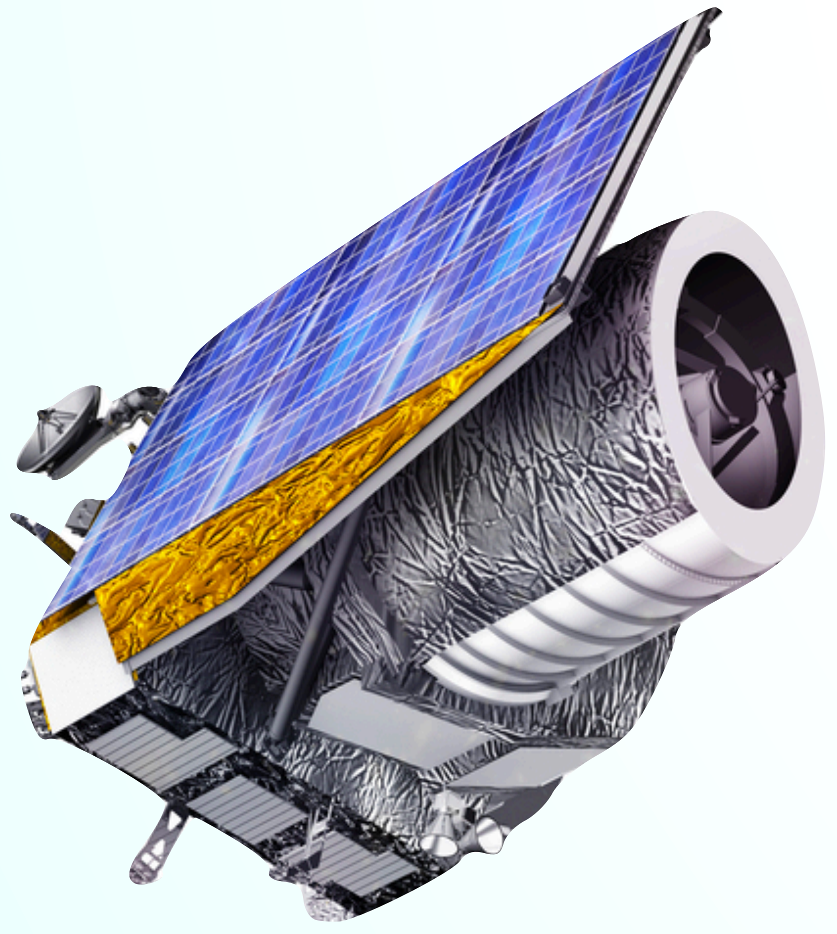

Samples from a Wang+2019 quasar luminosity function

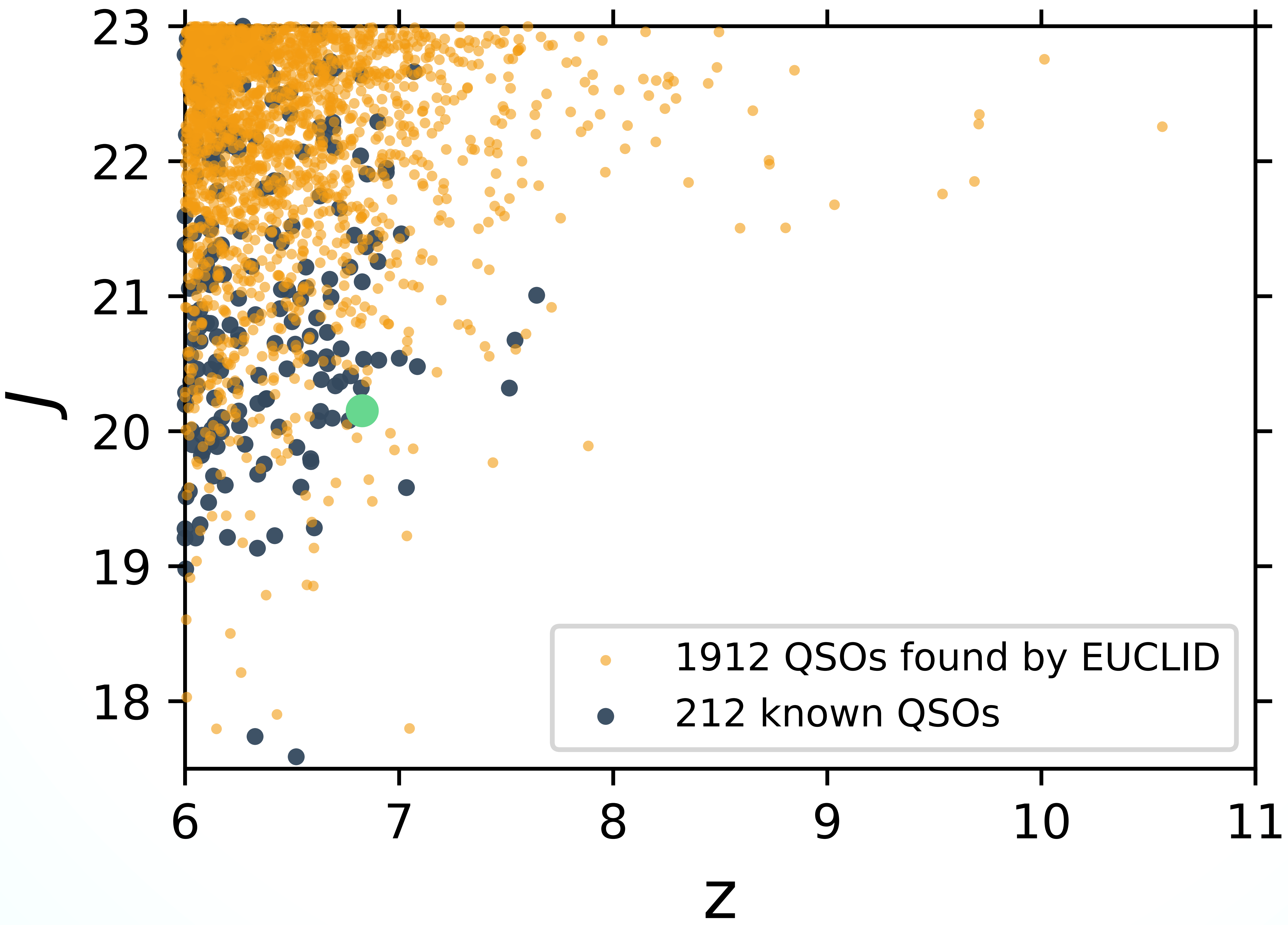

Kist, Hennawi & Davies 2024c (in prep.)

Timo Kist, Leiden Observatory, kist@strw.leidenuniv.nl

EUCLID

The Quasar Yield of the Wide-Field Survey

Samples from a Wang+2019 quasar luminosity function

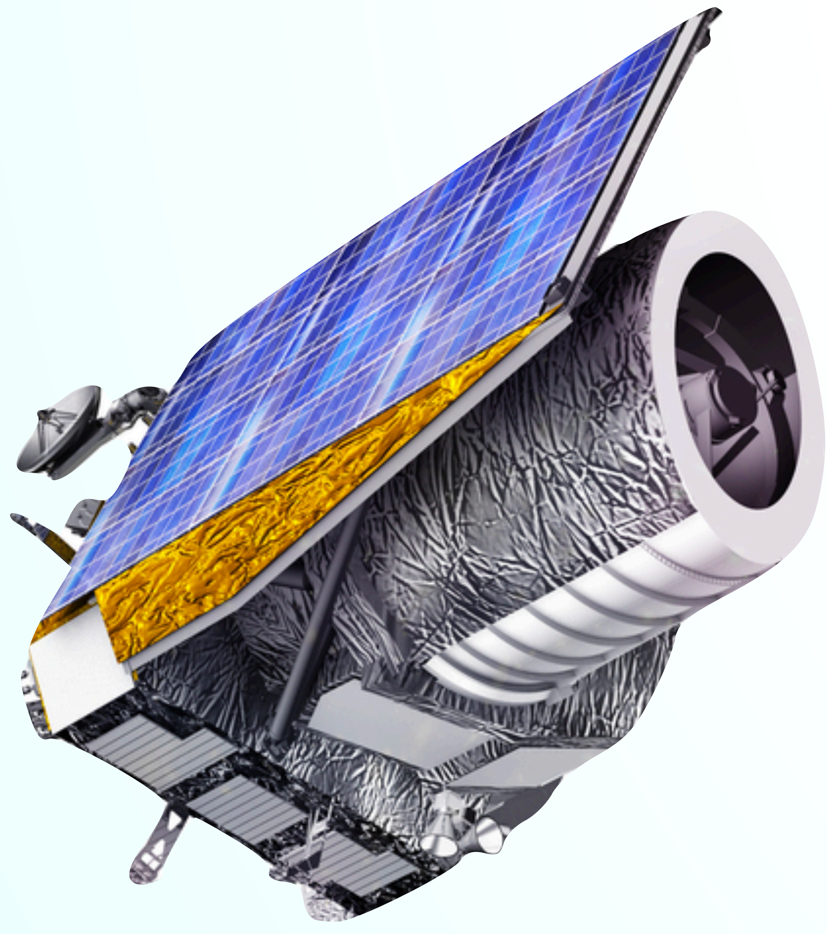

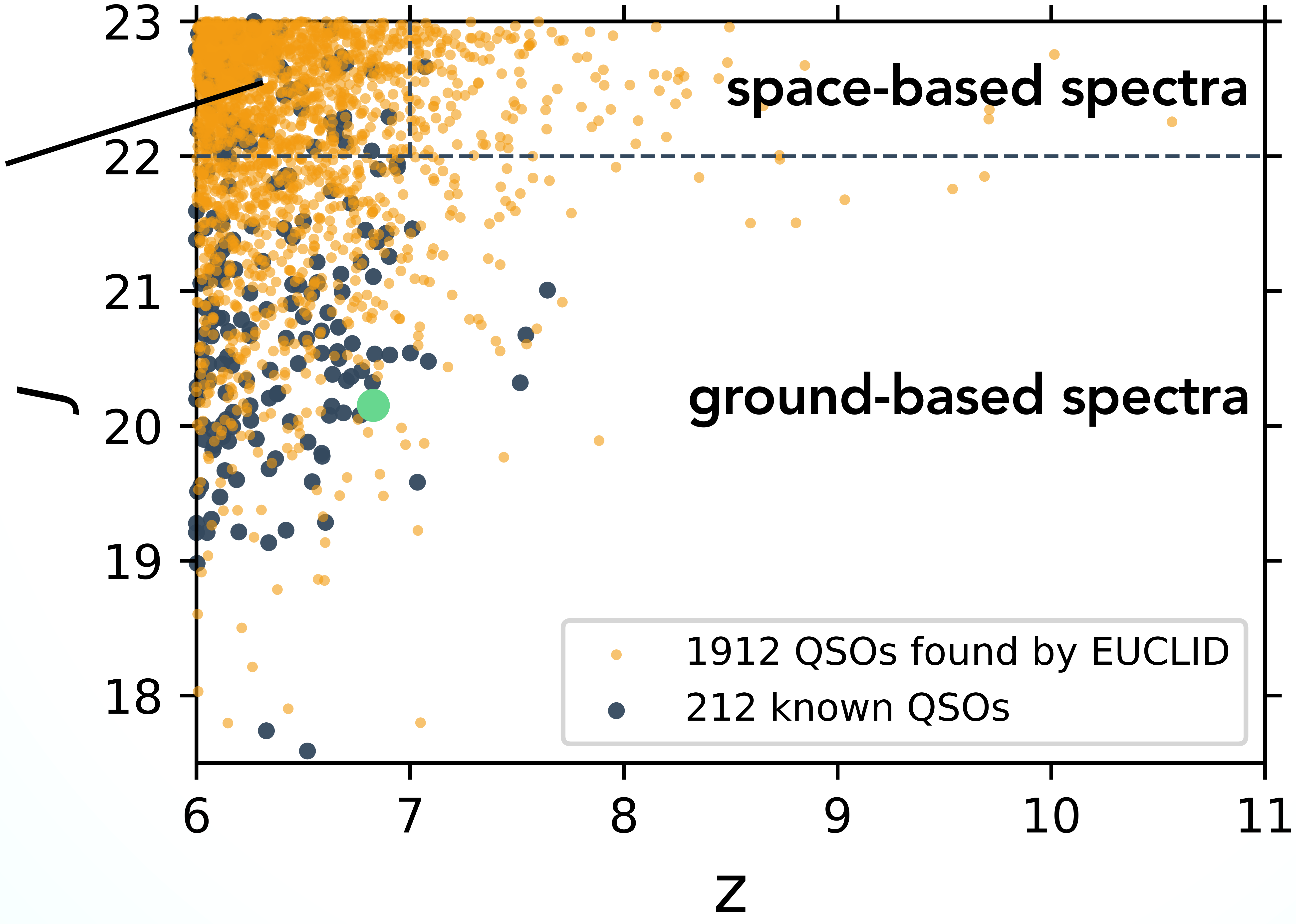

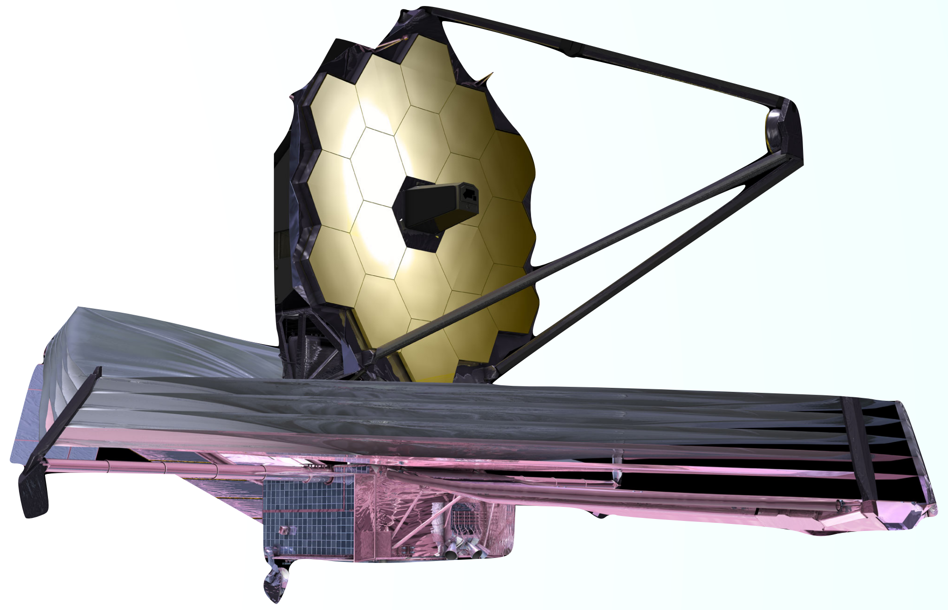

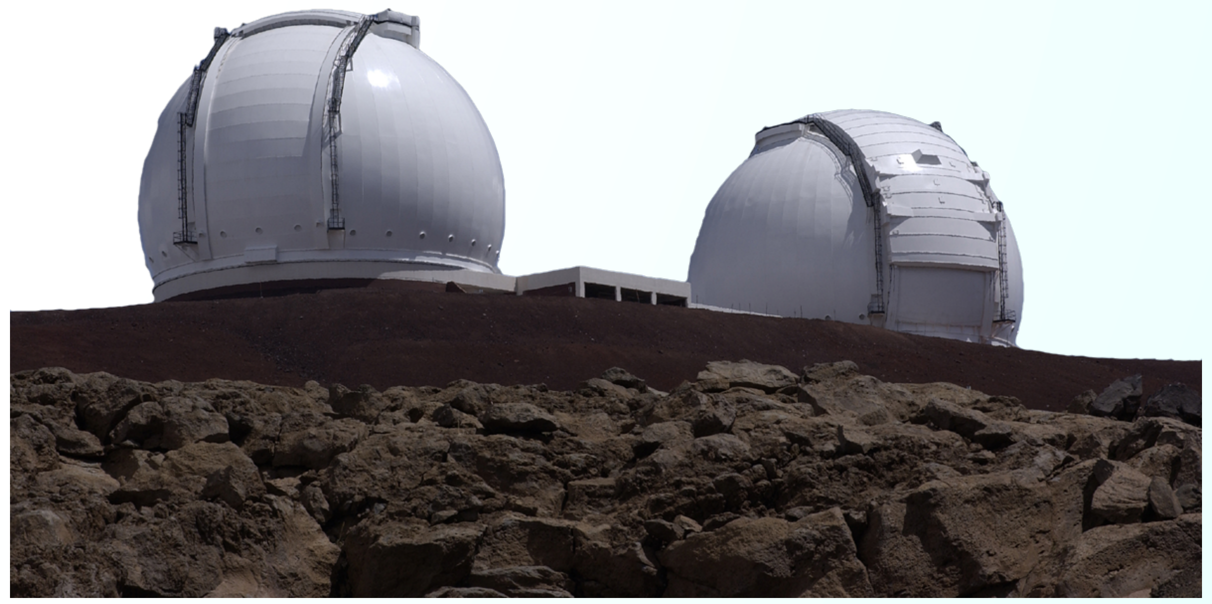

Kist, Hennawi & Davies 2024c (in prep.)

Timo Kist, Leiden Observatory, kist@strw.leidenuniv.nl

EUCLID

The Quasar Yield of the Wide-Field Survey

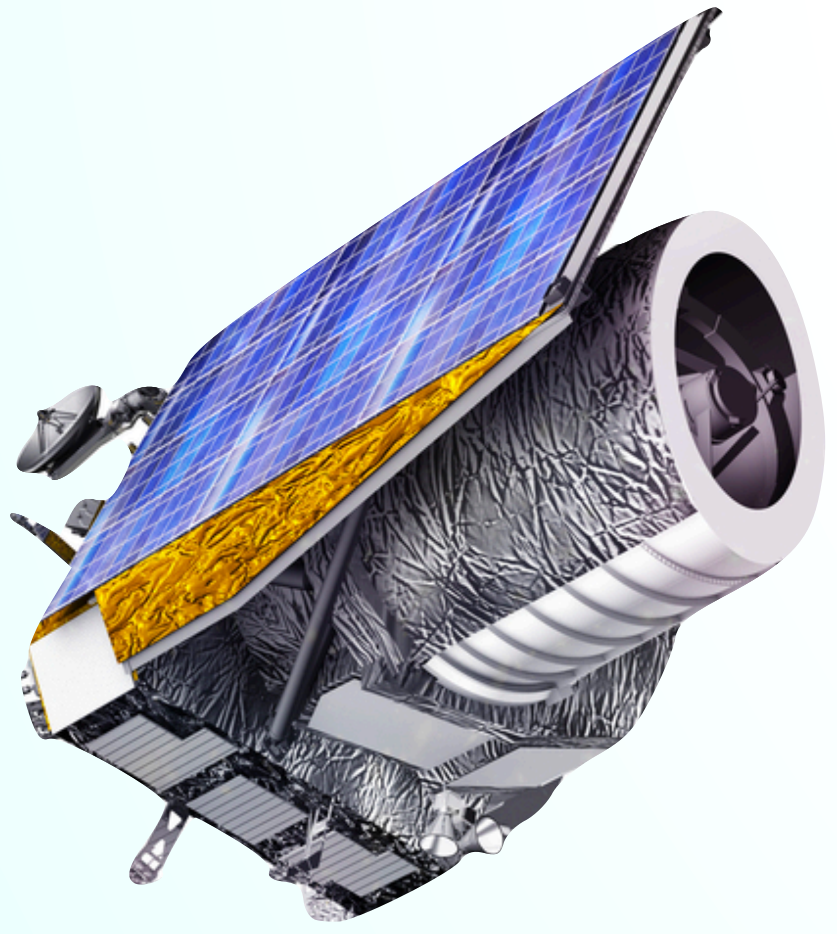

Samples from a Wang+2019 quasar luminosity function

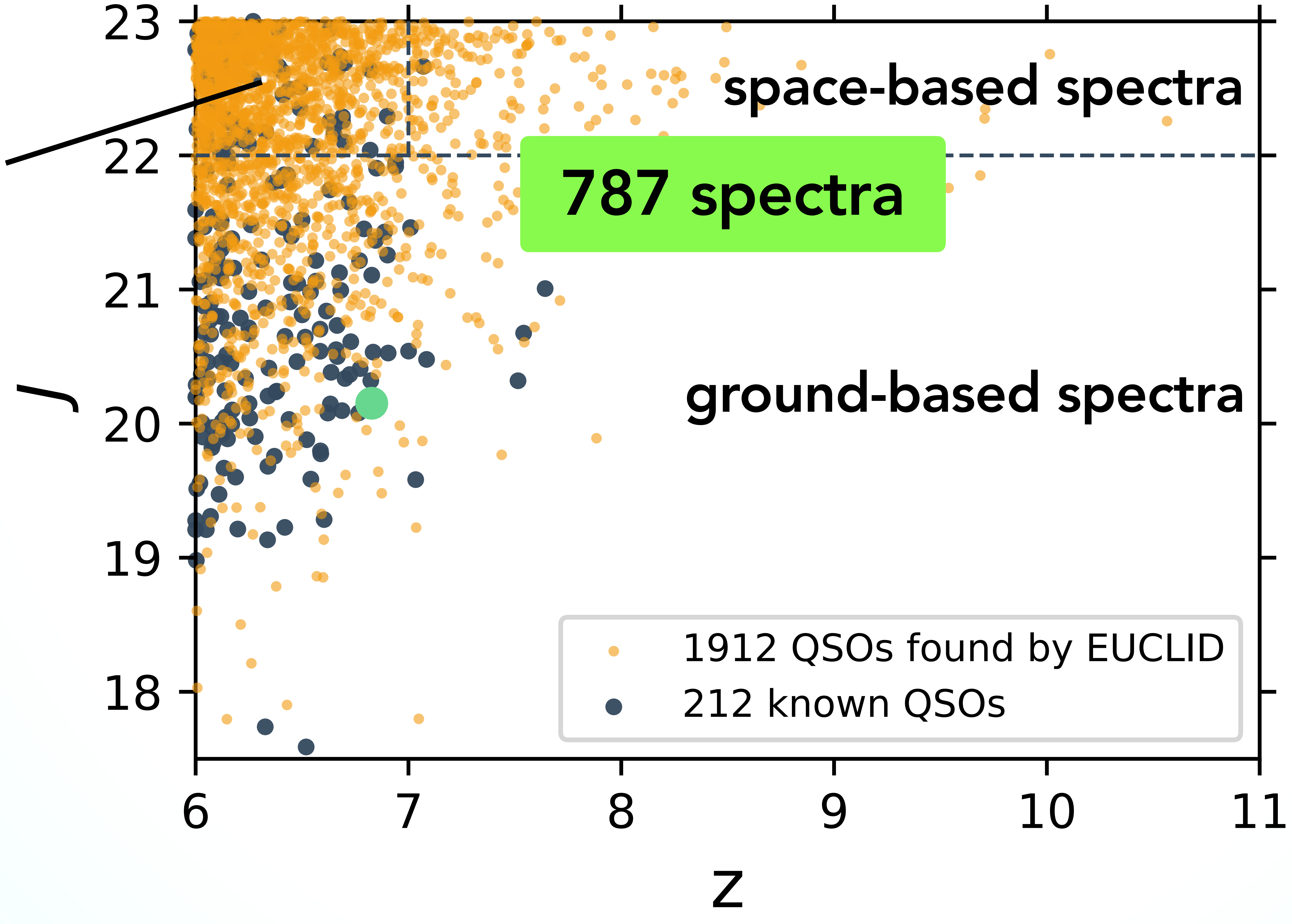

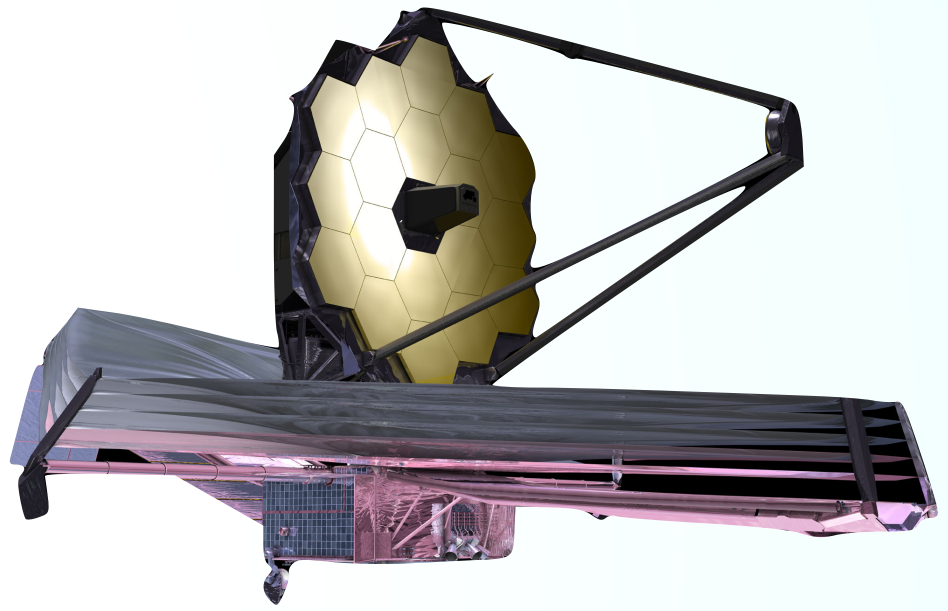

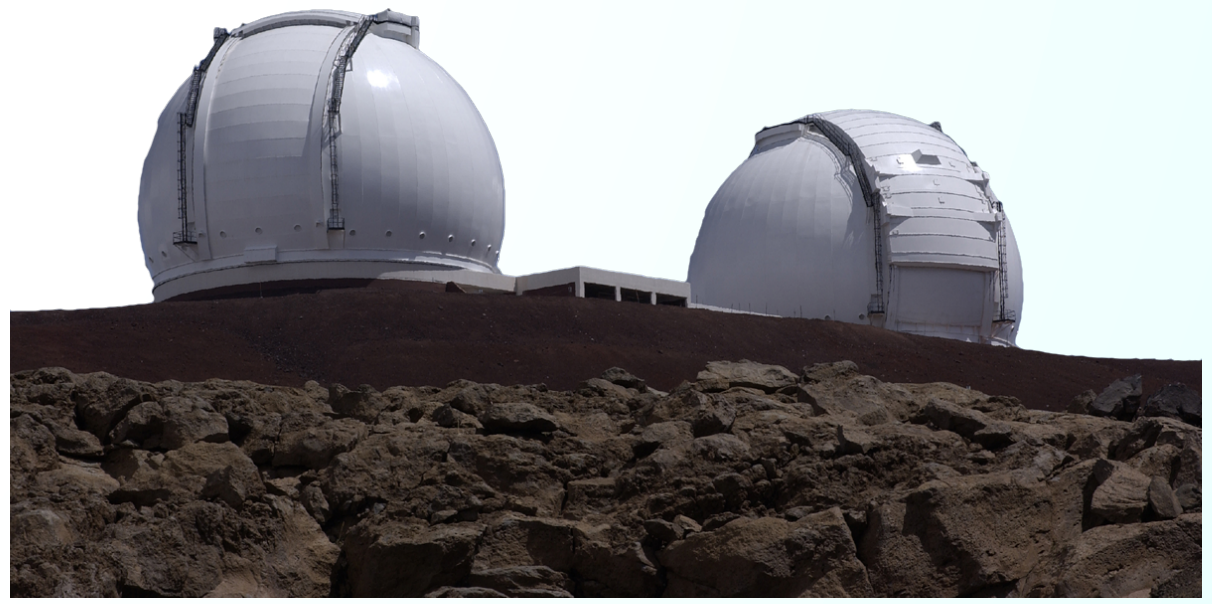

Kist, Hennawi & Davies 2024c (in prep.)

Timo Kist, Leiden Observatory, kist@strw.leidenuniv.nl

Constraining Reionization History with EUCLID & JWST

A forecast of upcoming IGM damping wing constraints

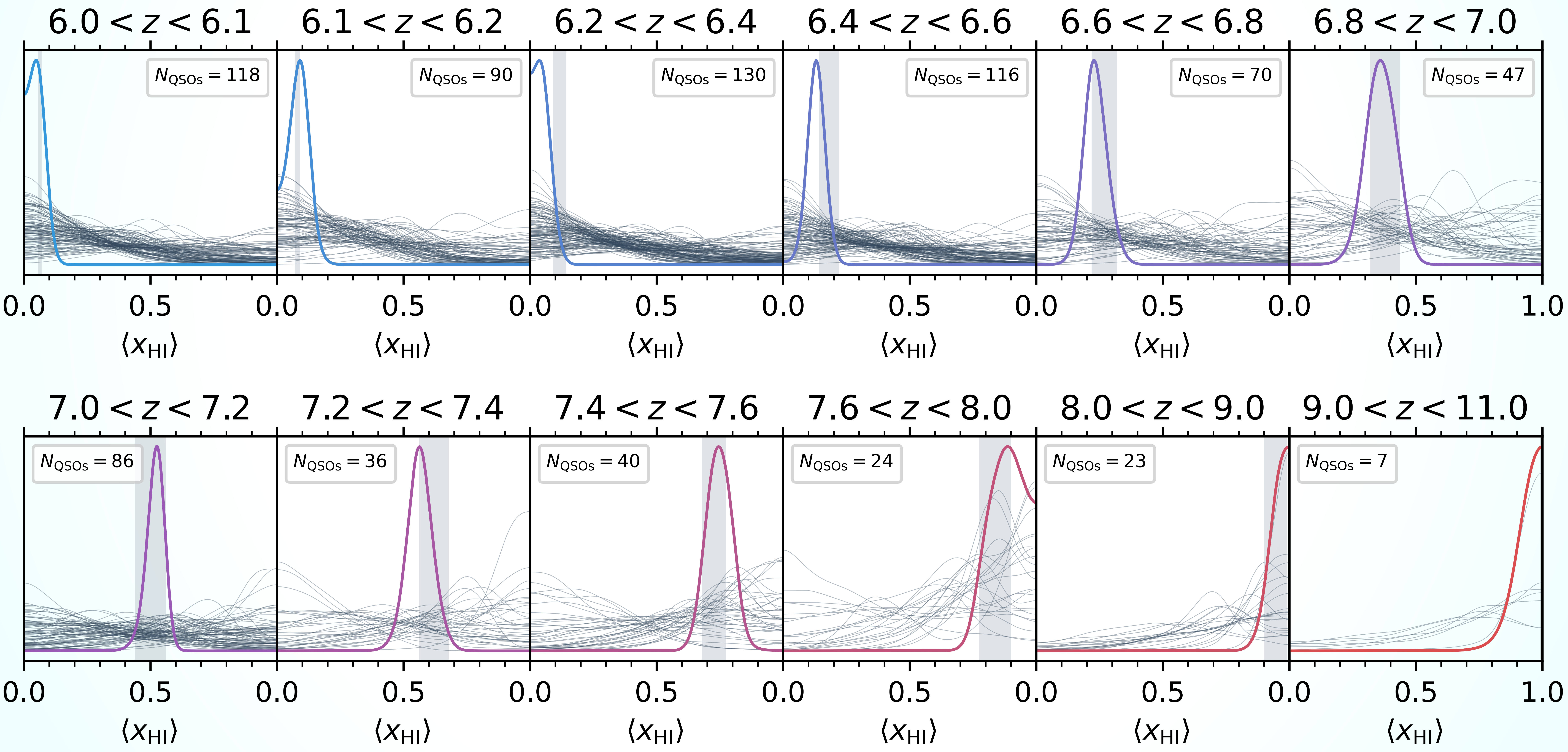

Kist, Hennawi & Davies 2024c (in prep.)

Timo Kist, Leiden Observatory, kist@strw.leidenuniv.nl

Constraining Reionization History with EUCLID & JWST

A forecast of upcoming IGM damping wing constraints

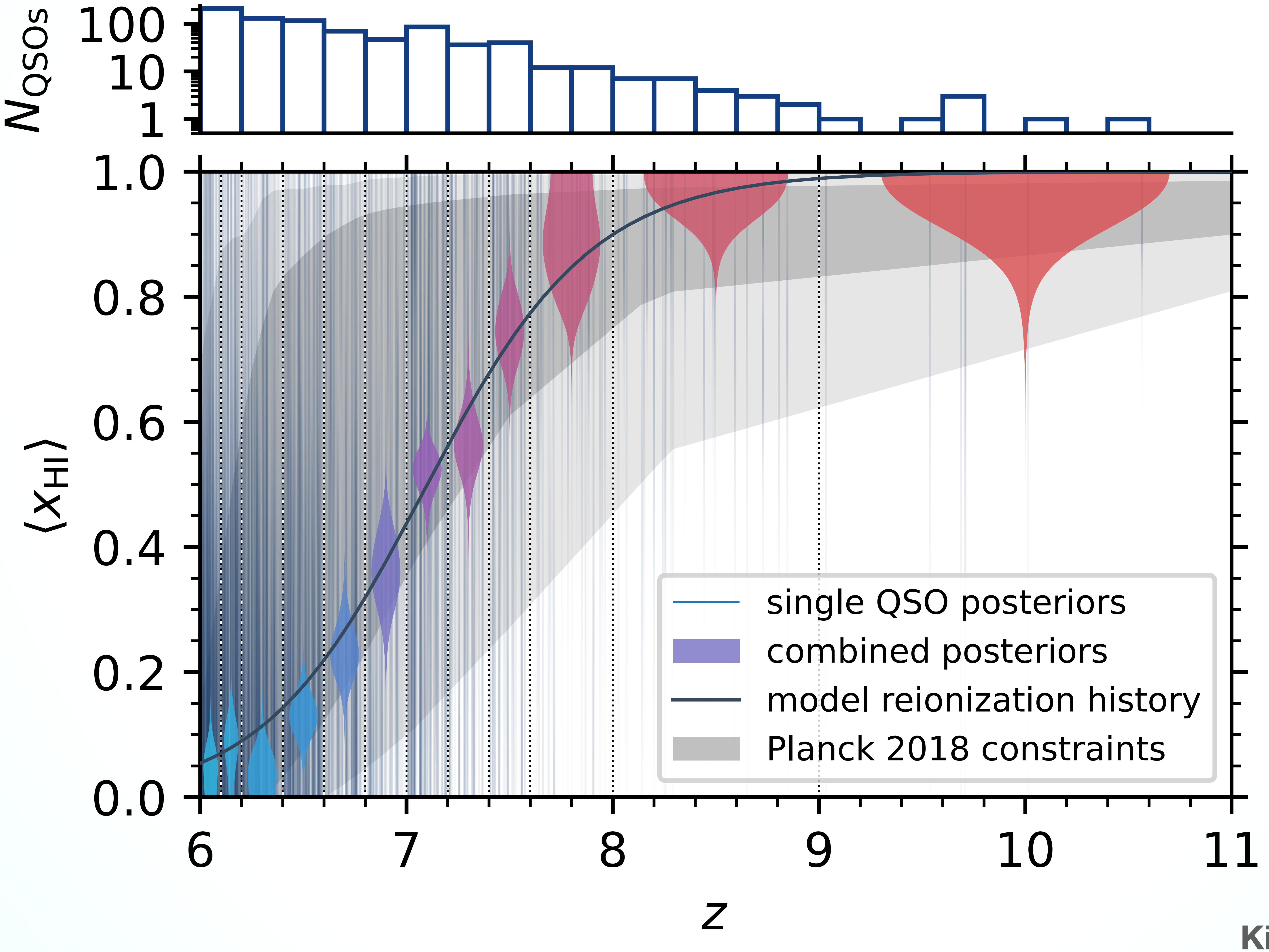

Kist, Hennawi & Davies 2024c (in prep.)

Timo Kist, Leiden Observatory, kist@strw.leidenuniv.nl

Constraining Reionization History with EUCLID & JWST

A forecast of upcoming IGM damping wing constraints

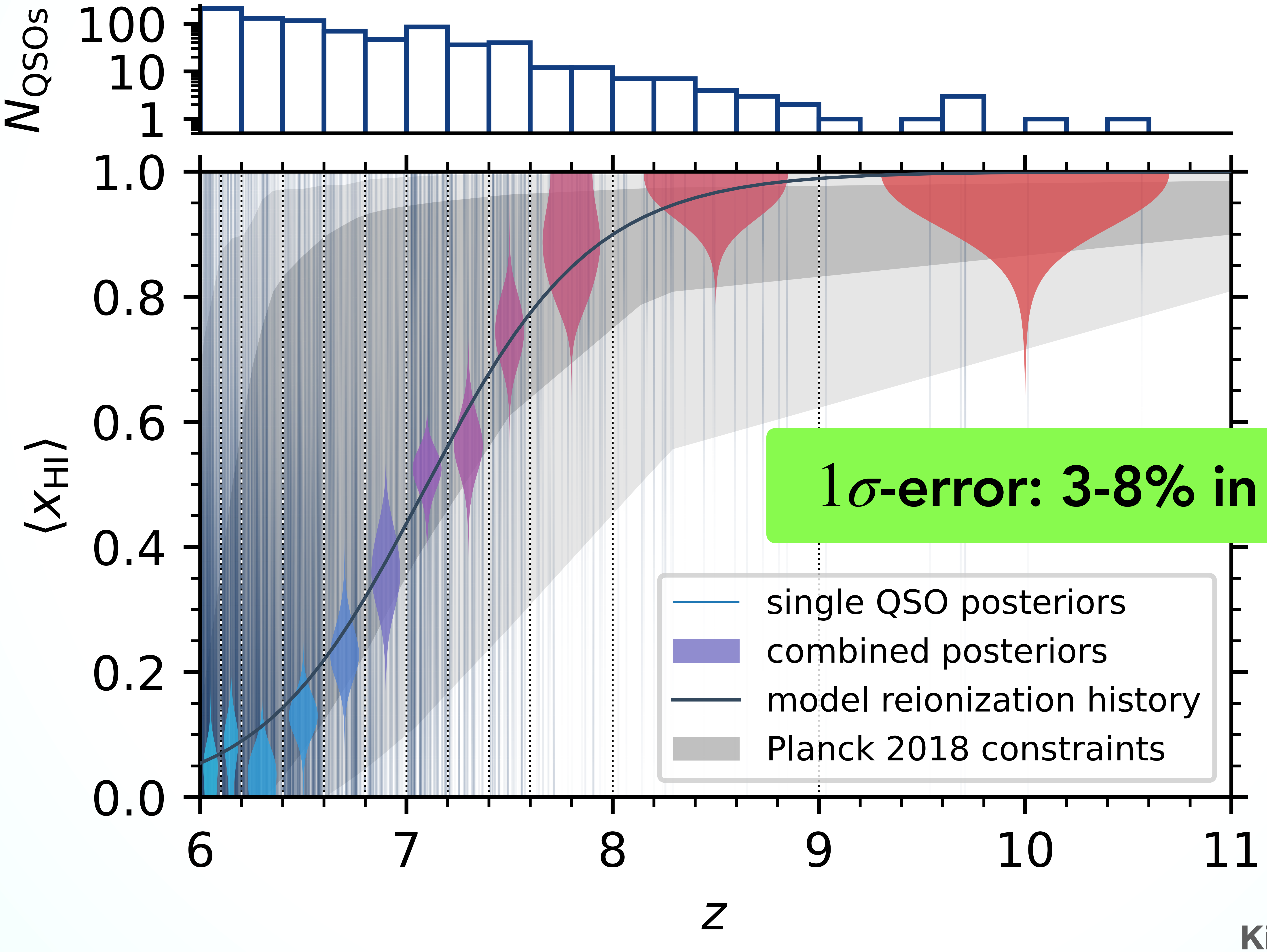

1σ-error: 3-8% in each redshift bin!

Kist, Hennawi & Davies 2024c (in prep.)

Timo Kist, Leiden Observatory, kist@strw.leidenuniv.nl

Summary

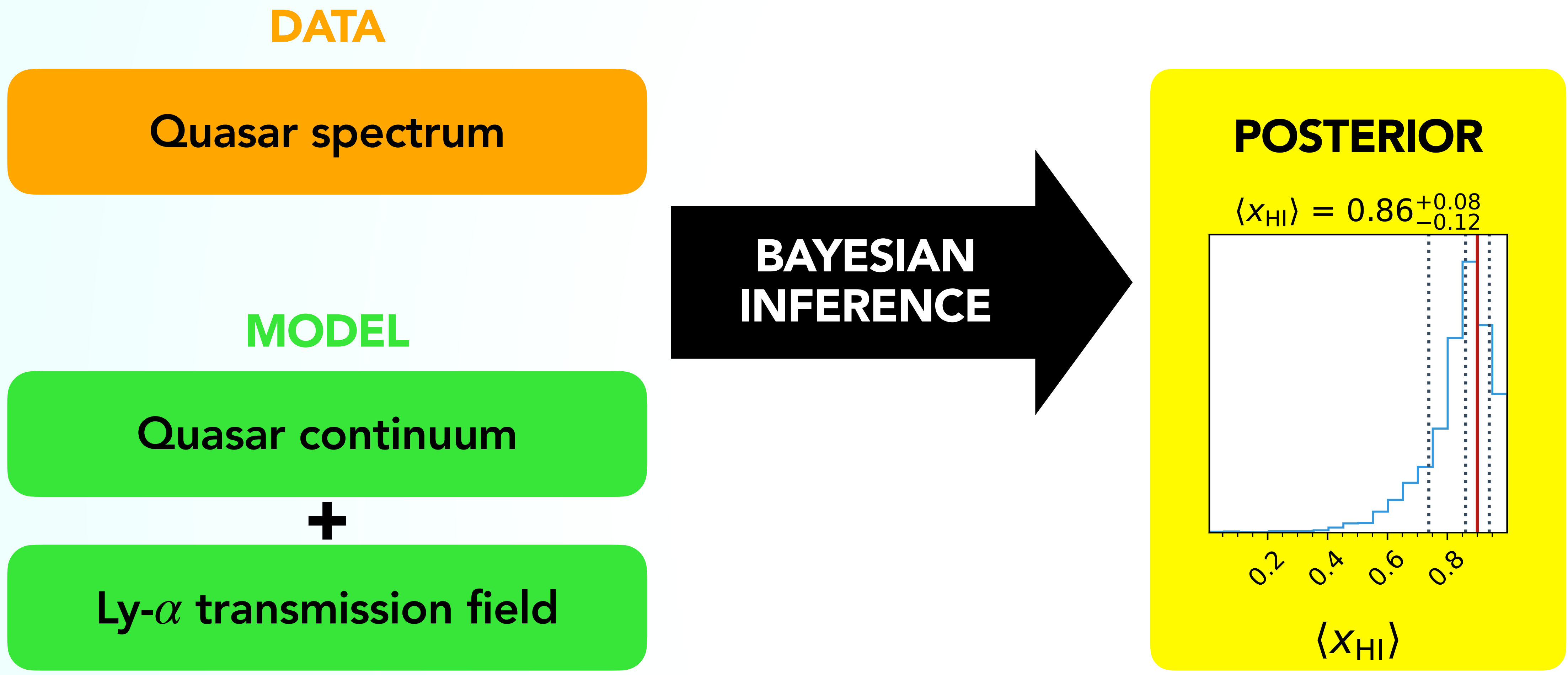

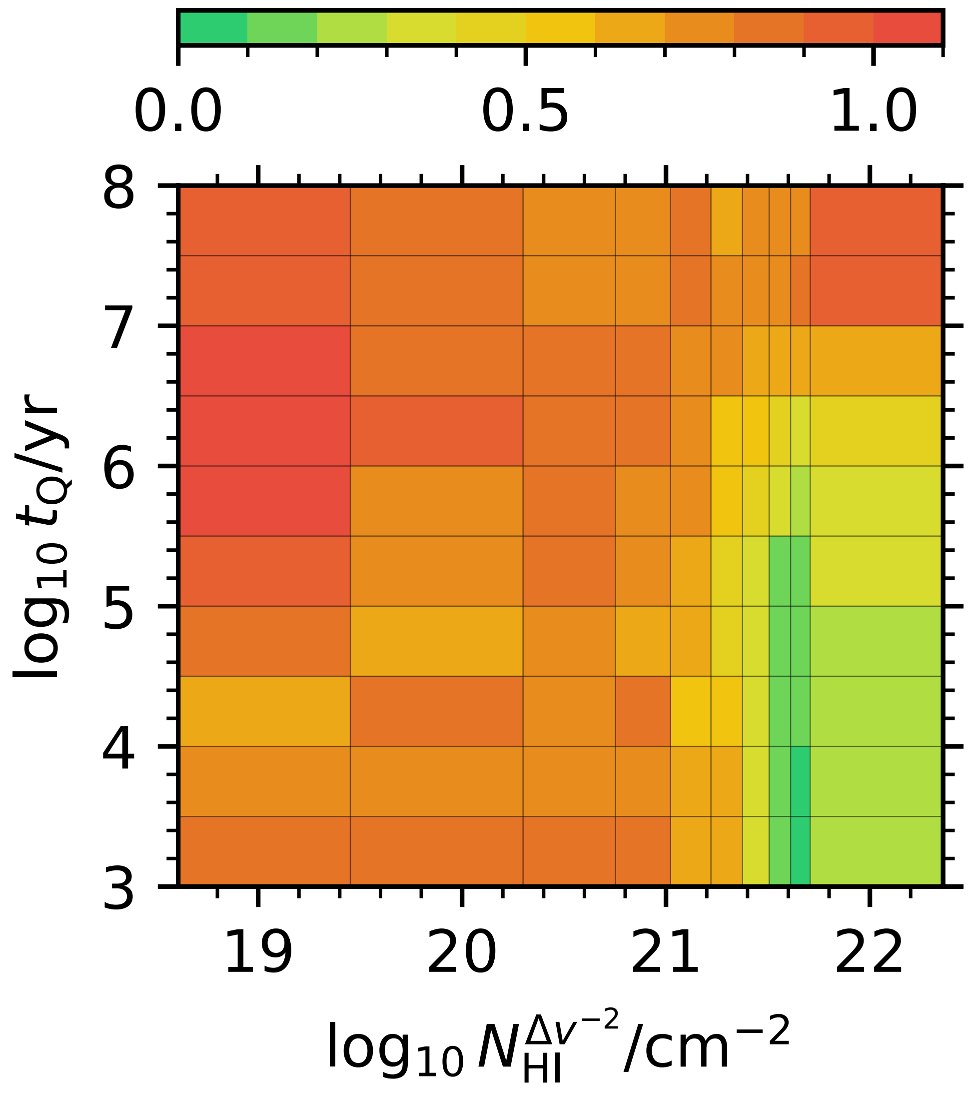

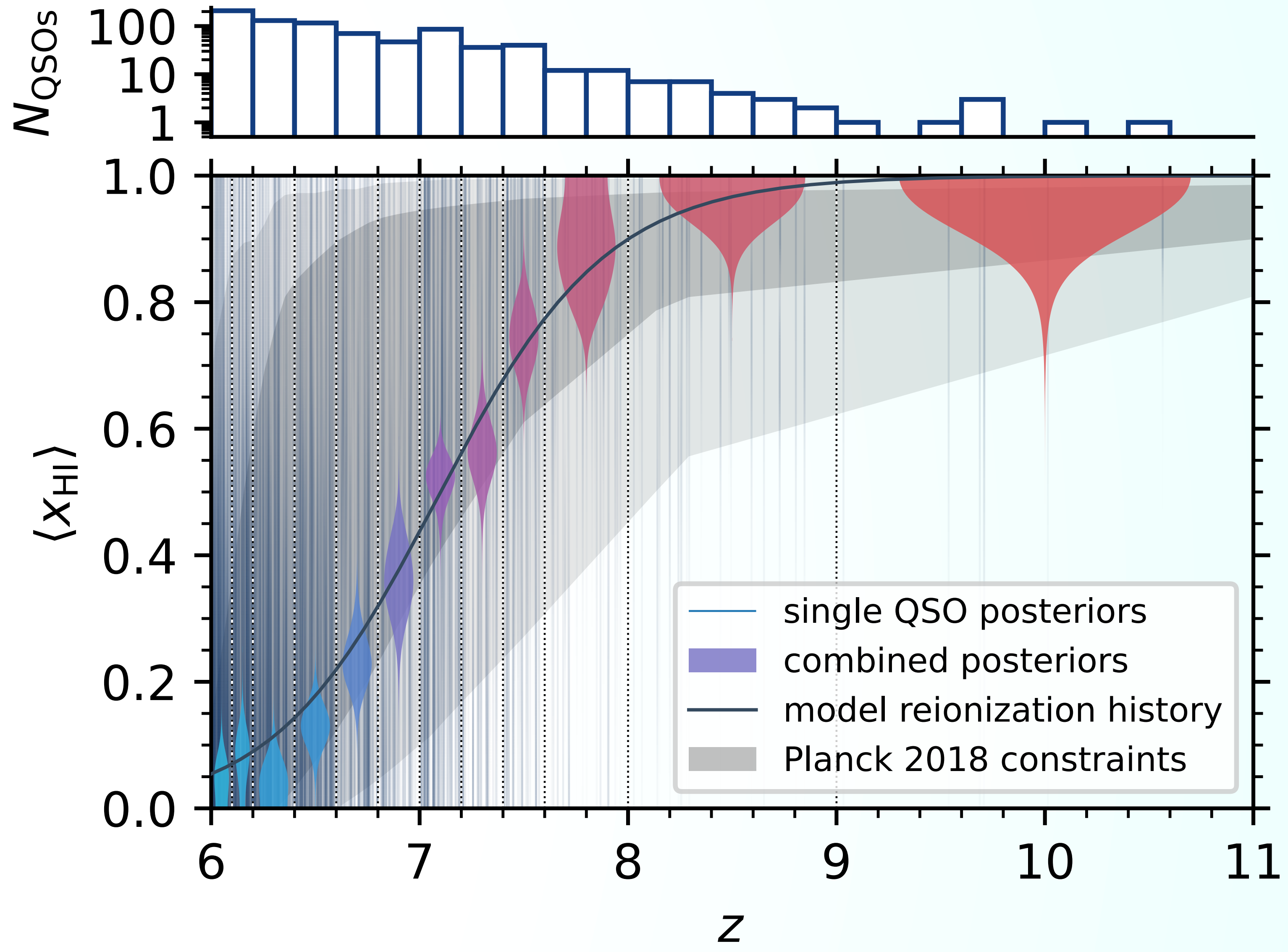

Fast HMC pipeline to infer $\langle x_{HI} \rangle$ and t_Q using the damping wing imprint of high-redshift quasars

Inferring $\langle x_{HI} \rangle$ at $28.0^{+8.2}_{-8.8}\,\%$ precision, or even the local HI column density at $0.69^{+0.34}_{-0.53}$ dex

EUCLID & JWST:
3-8% constraints on $\langle x_{HI} \rangle(z)$ between $6 \lesssim z \lesssim 11$

Timo Kist, Leiden Observatory, kist@strw.leidenuniv.nl

Timo Kist, Leiden Observatory, kist@strw.leidenuniv.nl

Backup Slides

Timo Kist, Leiden Observatory, kist@strw.leidenuniv.nl

Converting the constraints

The *global* IGM neutral fraction inferred from J0411-0907

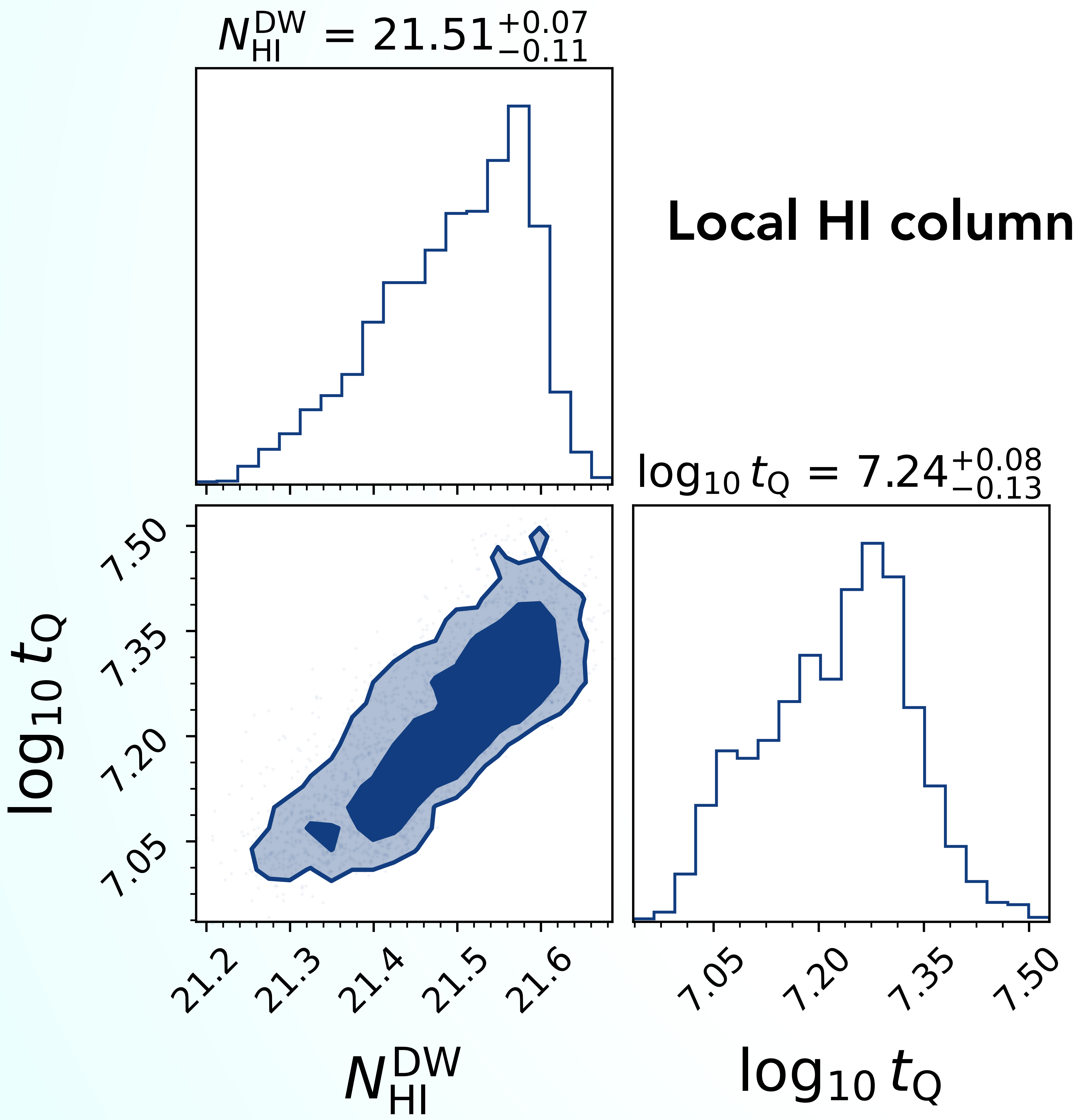

Local HI column density

Kist, Hennawi & Davies 2024b (in prep.)

Timo Kist, Leiden Observatory, kist@strw.leidenuniv.nl

Converting the constraints

The *global* IGM neutral fraction inferred from J0411-0907

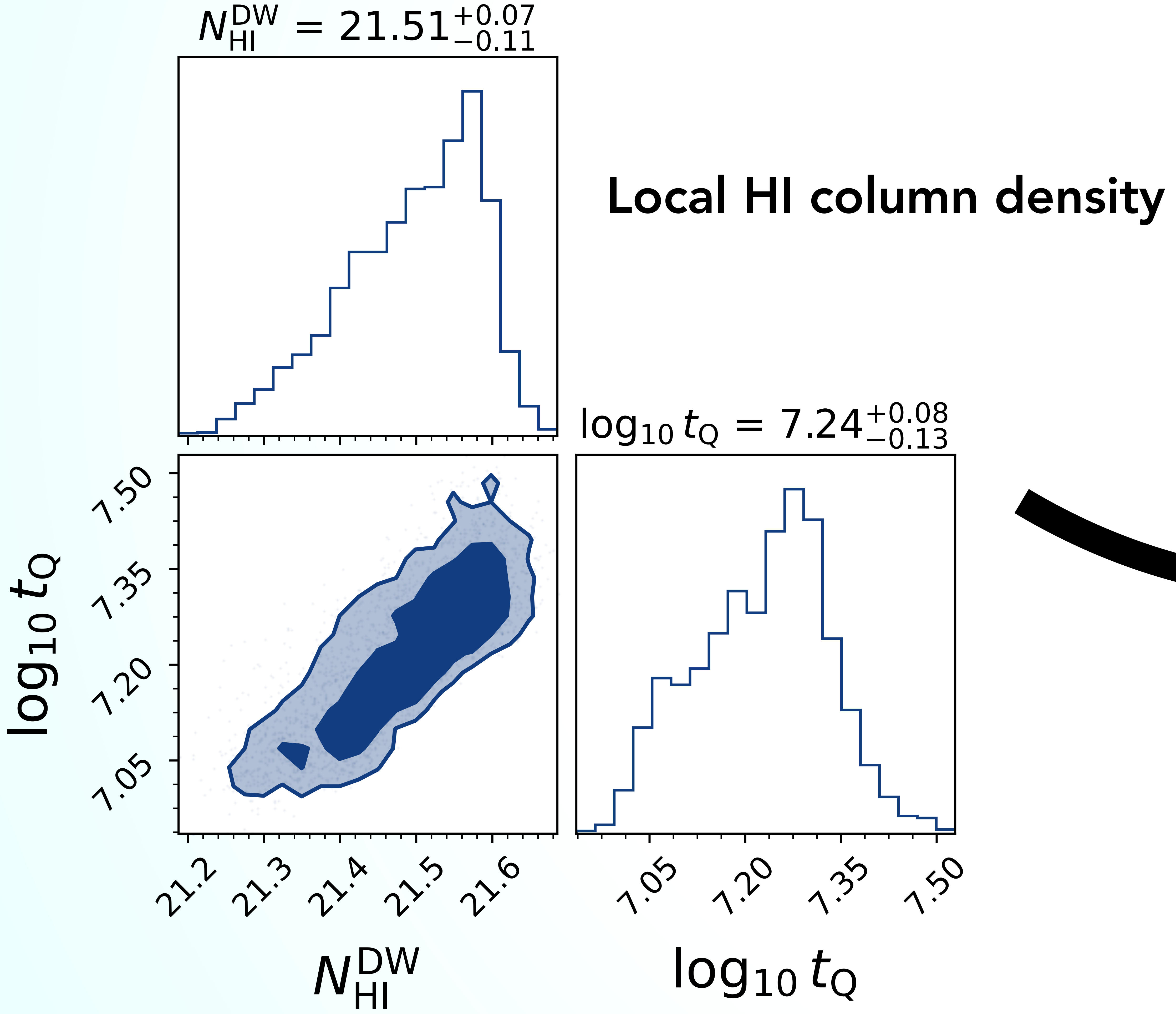

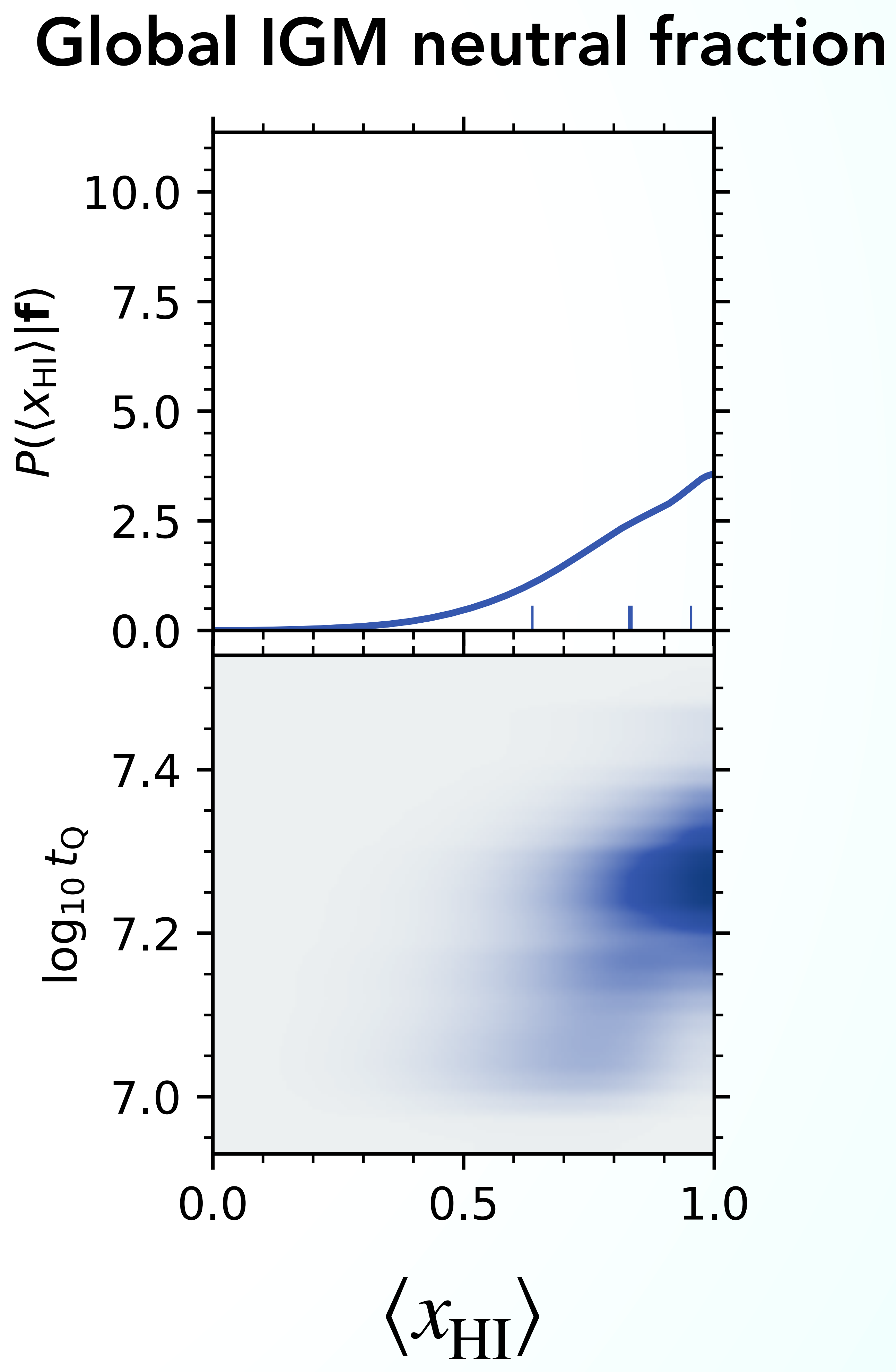

Kist, Hennawi & Davies 2024b (in prep.)

Timo Kist, Leiden Observatory, kist@strw.leidenuniv.nl

Converting the constraints

The *global* IGM neutral fraction inferred from J0411-0907

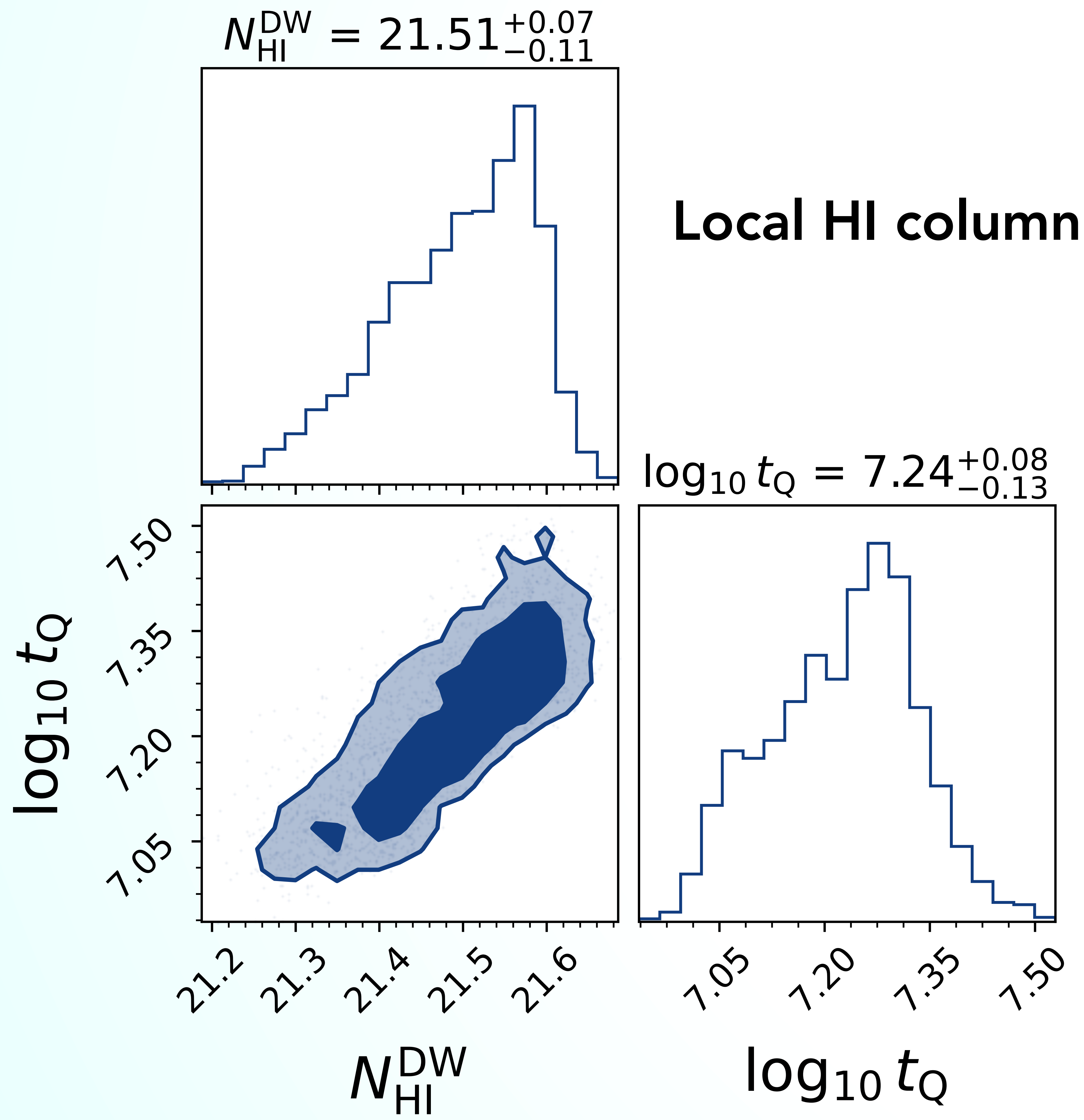

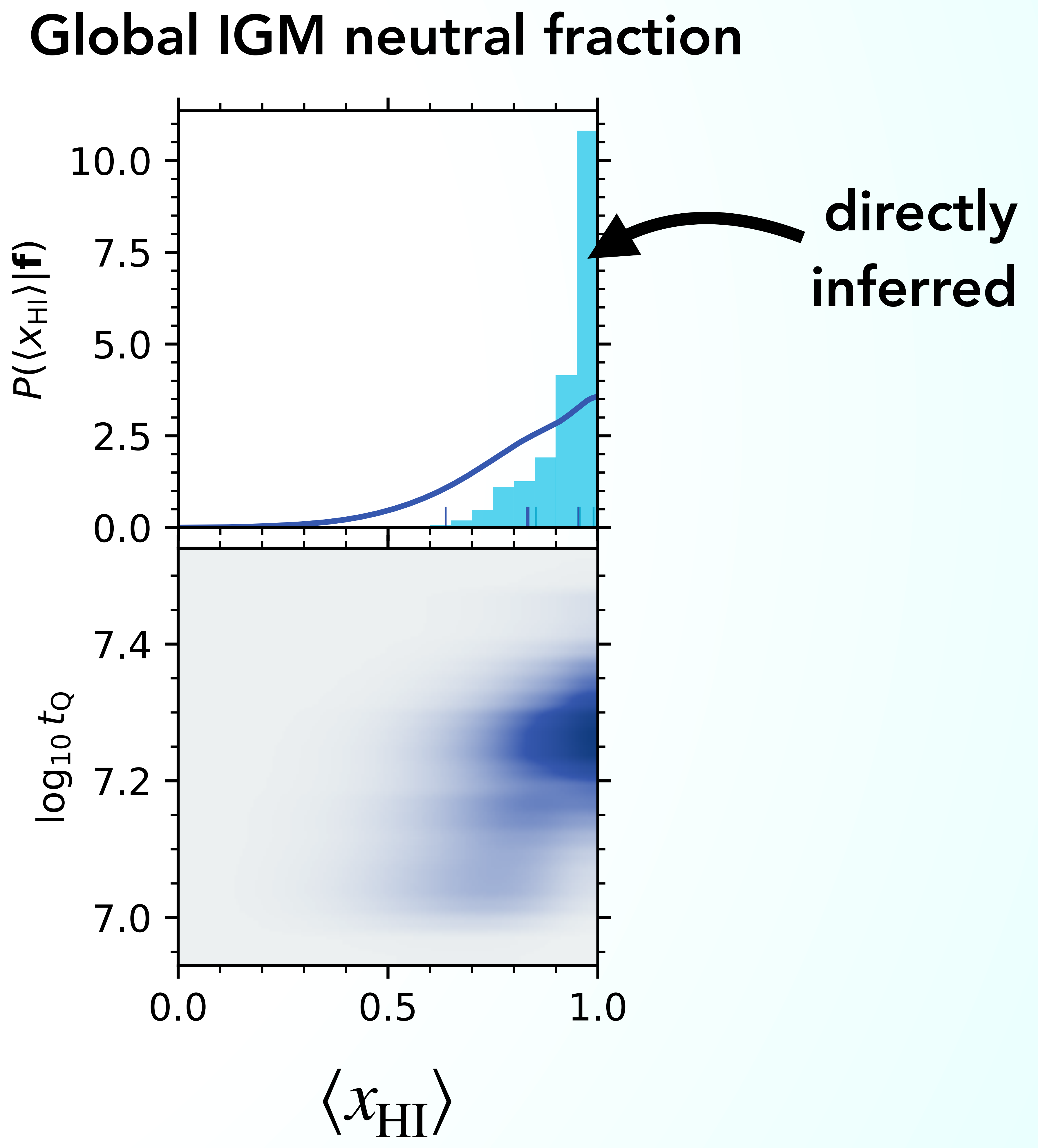

Kist, Hennawi & Davies 2024b (in prep.)

Timo Kist, Leiden Observatory, kist@strw.leidenuniv.nl

Constraining Reionization History with EUCLID & JWST

A forecast of upcoming IGM damping wing constraints

Toy model for $\langle x_{\rm HI} \rangle(z)$

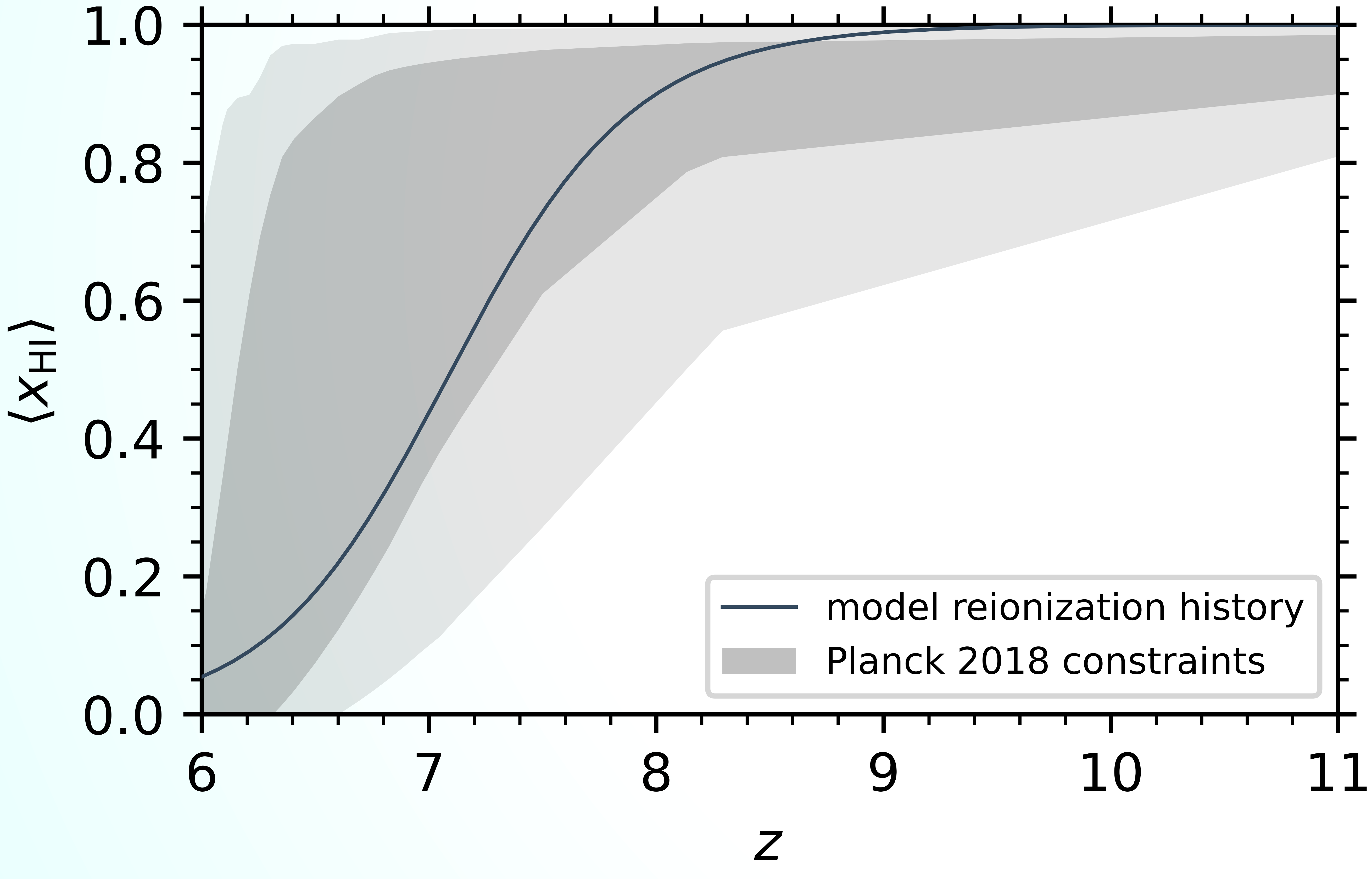

Lognormal $t_{\rm Q}$ distribution (Khrykin+ 2021)

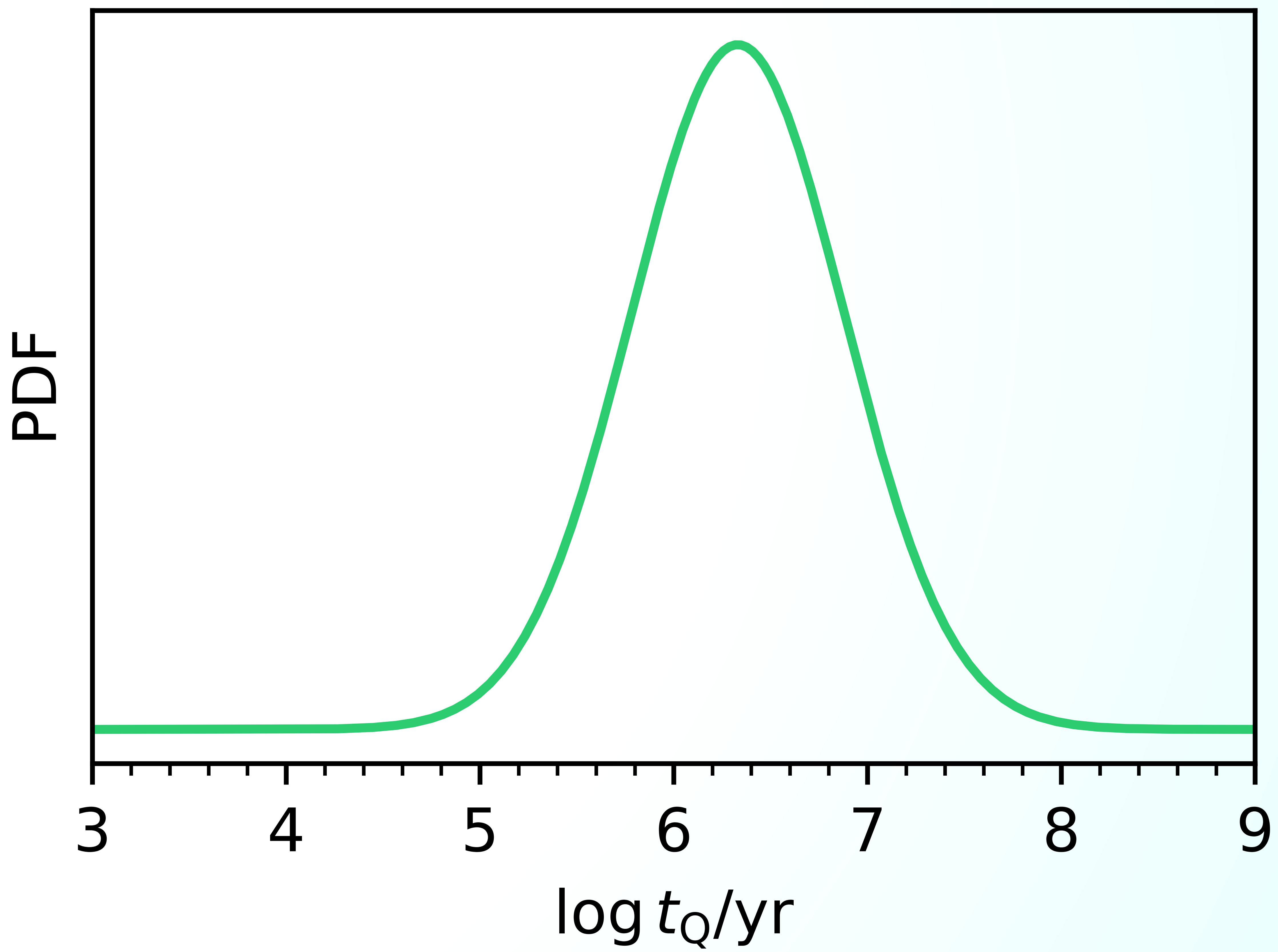

Kist, Hennawi & Davies 2024c (in prep.)

Timo Kist, Leiden Observatory, kist@strw.leidenuniv.nl

The PCA Continuum Model

Impact on Inference Precision

Continuum-normalized spectrum:

→ optimal bound on inferring $\langle x_{\rm HI} \rangle$ and $t_{\rm Q}$ without nuisance parameters

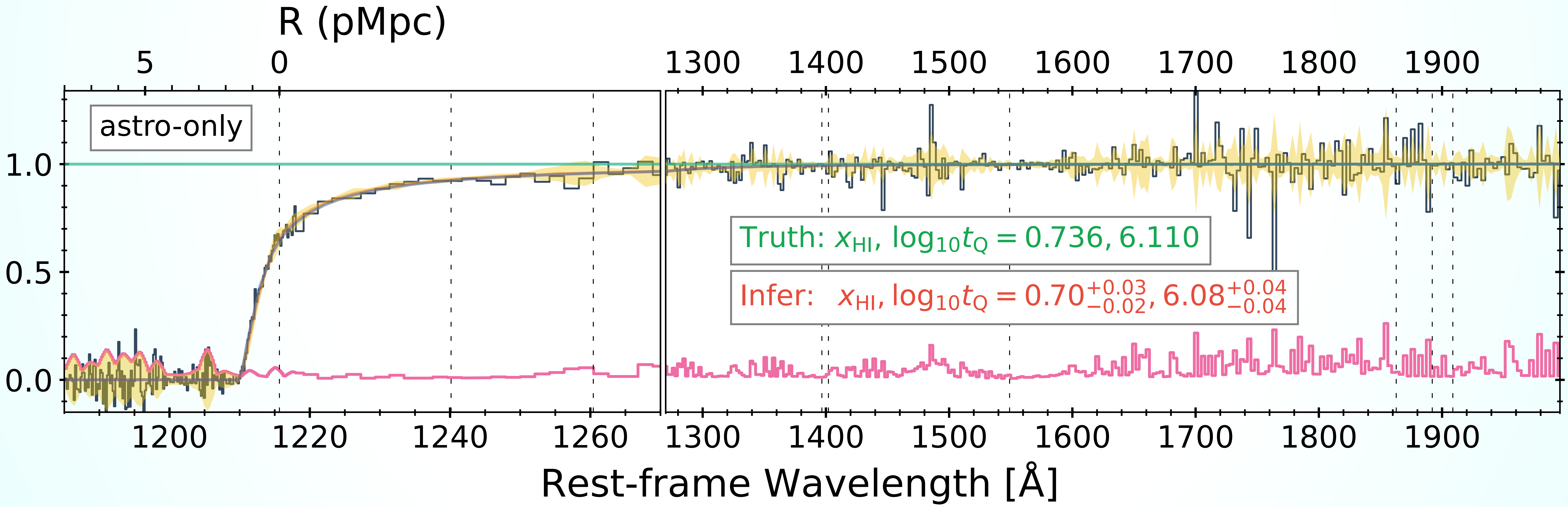

Hennawi, Kist, Davies+ 2023a (in prep.)

Timo Kist, Leiden Observatory, kist@strw.leidenuniv.nl

The PCA Continuum Model

Impact on Inference Precision

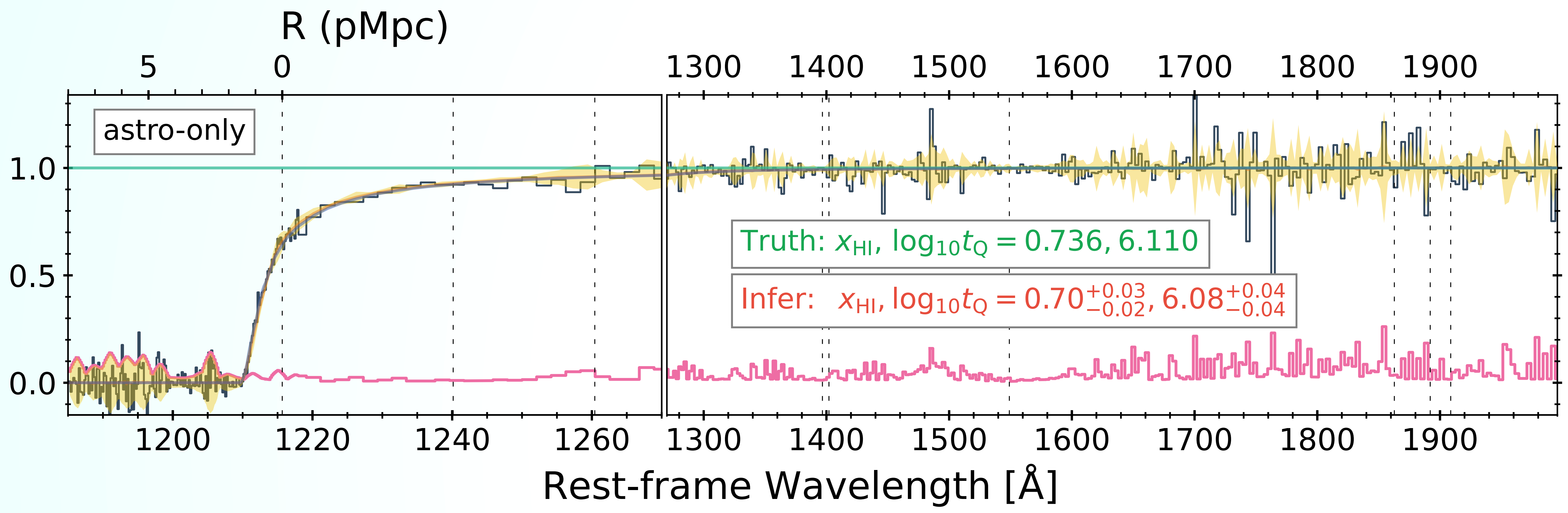

Hennawi, Kist, Davies+ 2023a (in prep.)

Timo Kist, Leiden Observatory, kist@strw.leidenuniv.nl

The PCA Continuum Model

Impact on Inference Precision

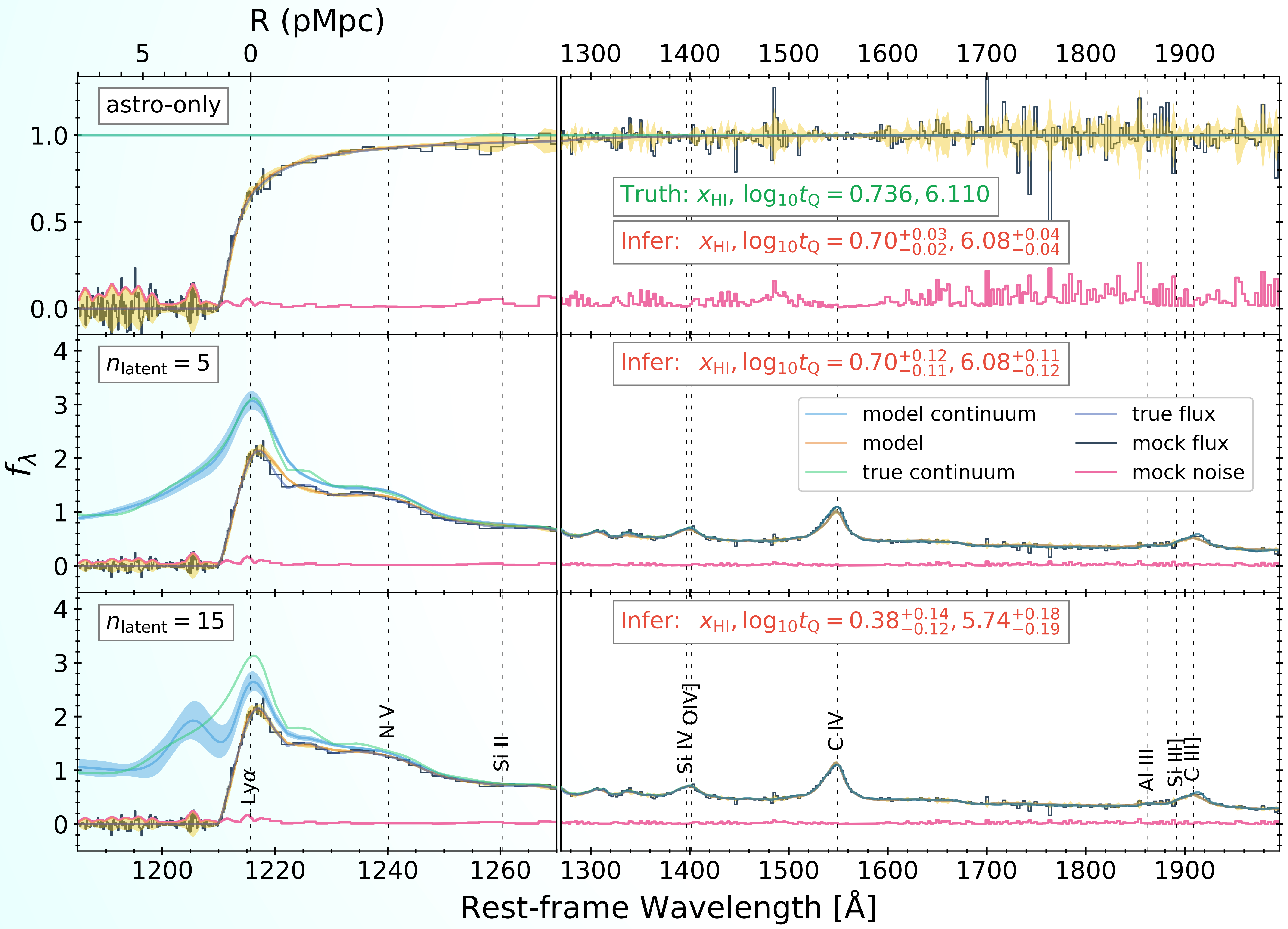

Hennawi, Kist, Davies+ 2023a (in prep.)

Timo Kist, Leiden Observatory, kist@strw.leidenuniv.nl

The PCA Continuum Model

Impact on Inference Precision

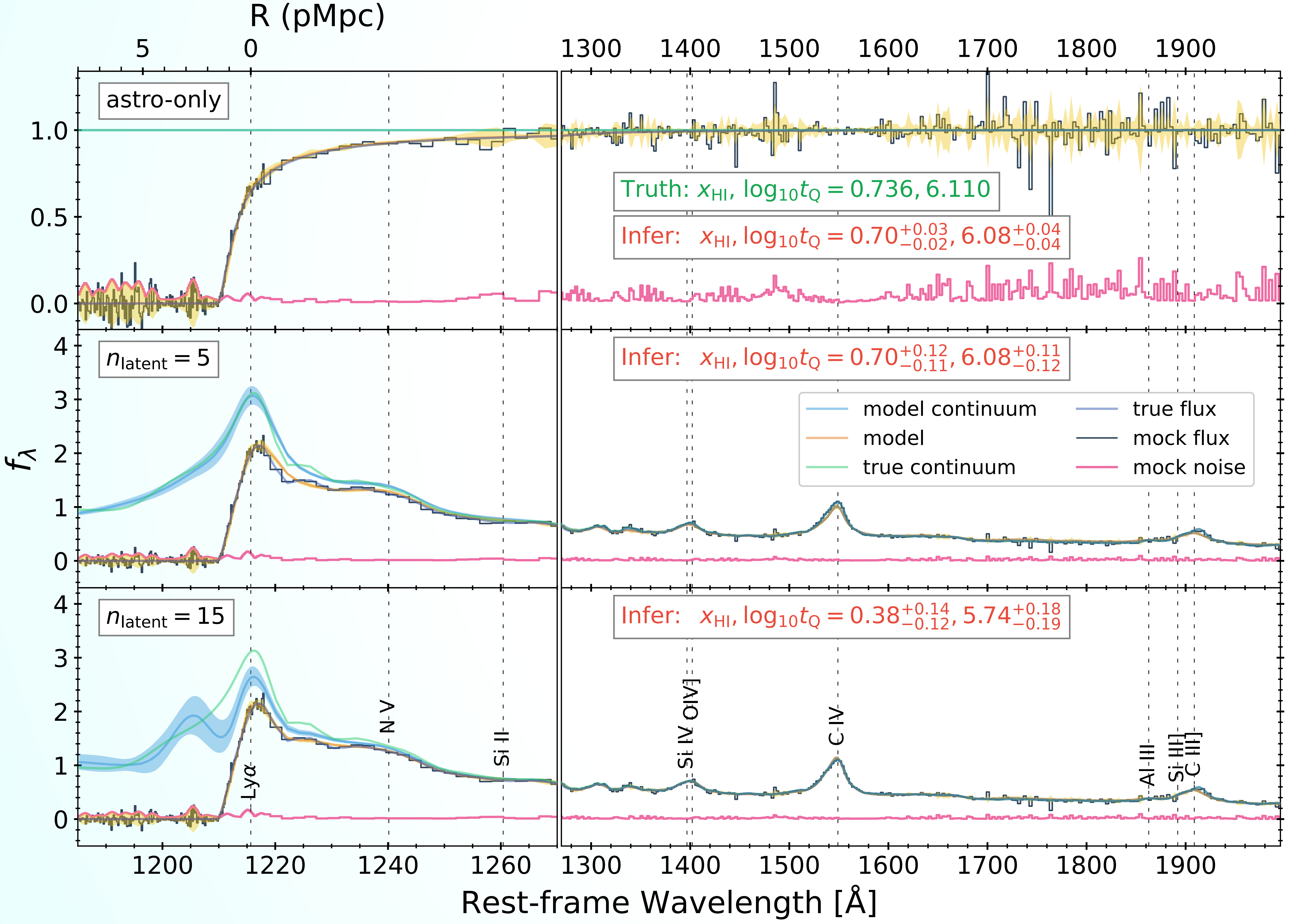

Average precision of 100 mock samples:

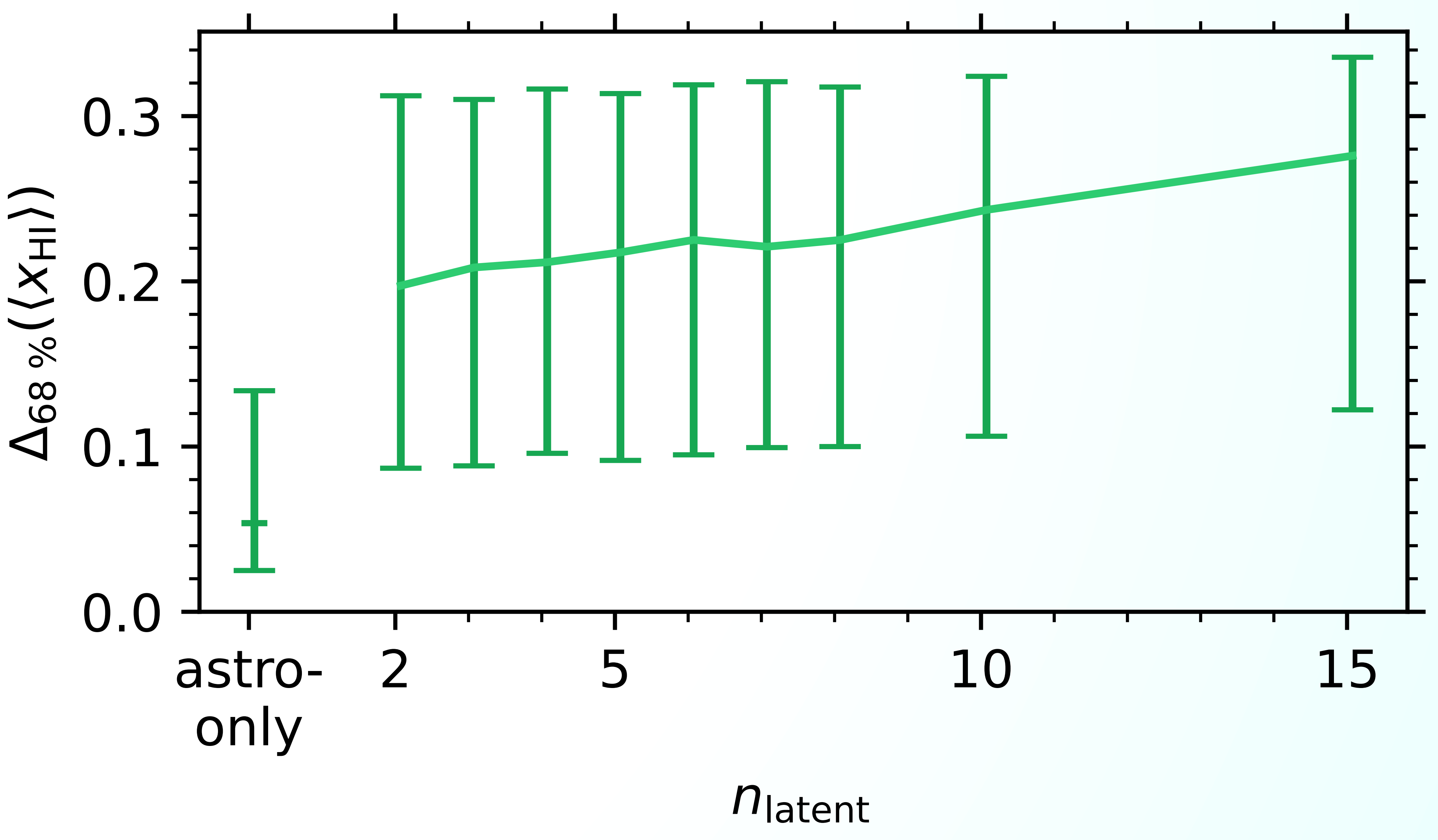

Hennawi, Kist, Davies+ 2023a (in prep.)

Timo Kist, Leiden Observatory, kist@strw.leidenuniv.nl

The PCA Continuum Model

Impact on Inference Precision

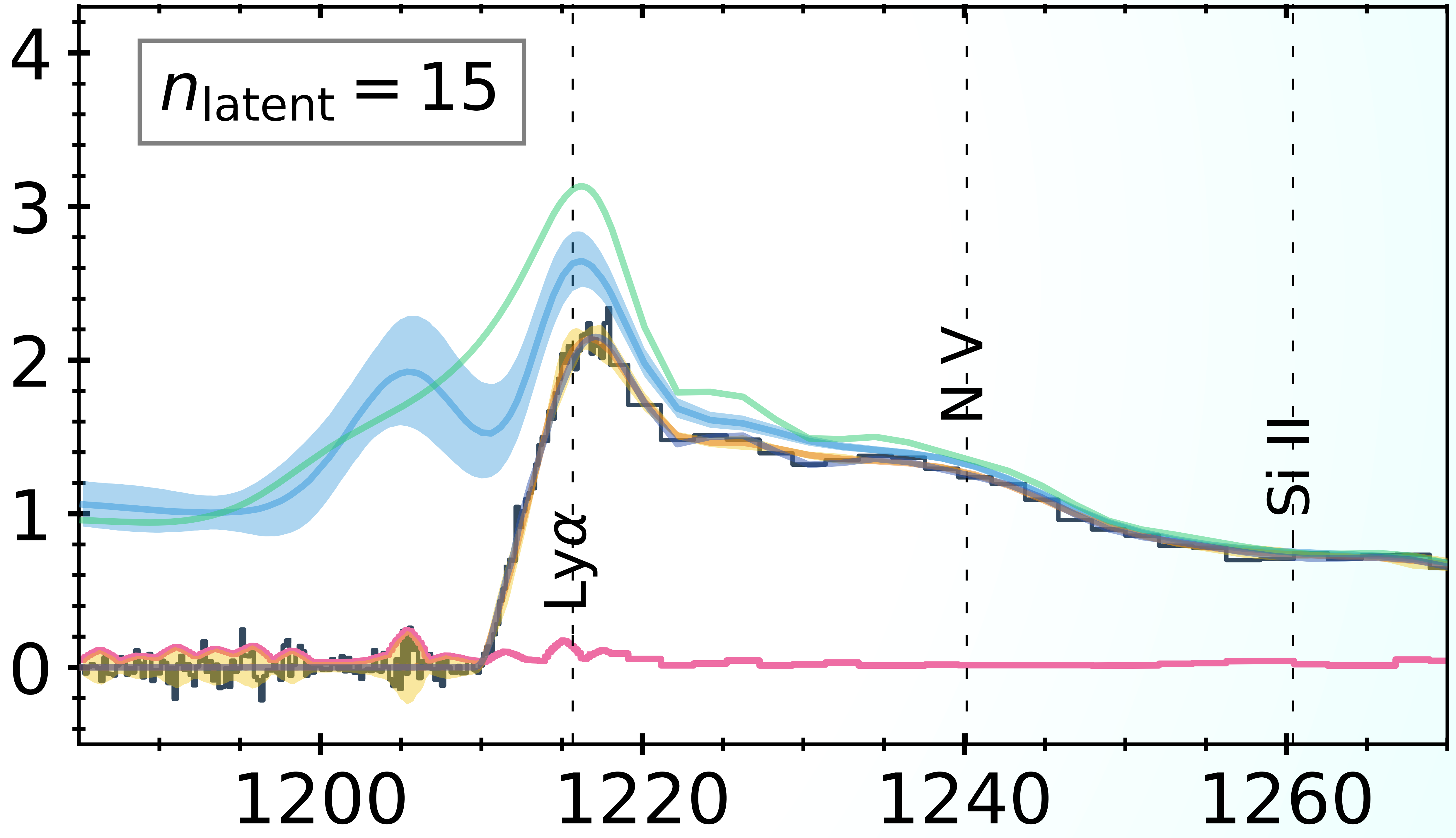

Hennawi, Kist, Davies+ 2023a (in prep.)

Timo Kist, Leiden Observatory, kist@strw.leidenuniv.nl

The PCA Continuum Model

Impact on Inference Precision

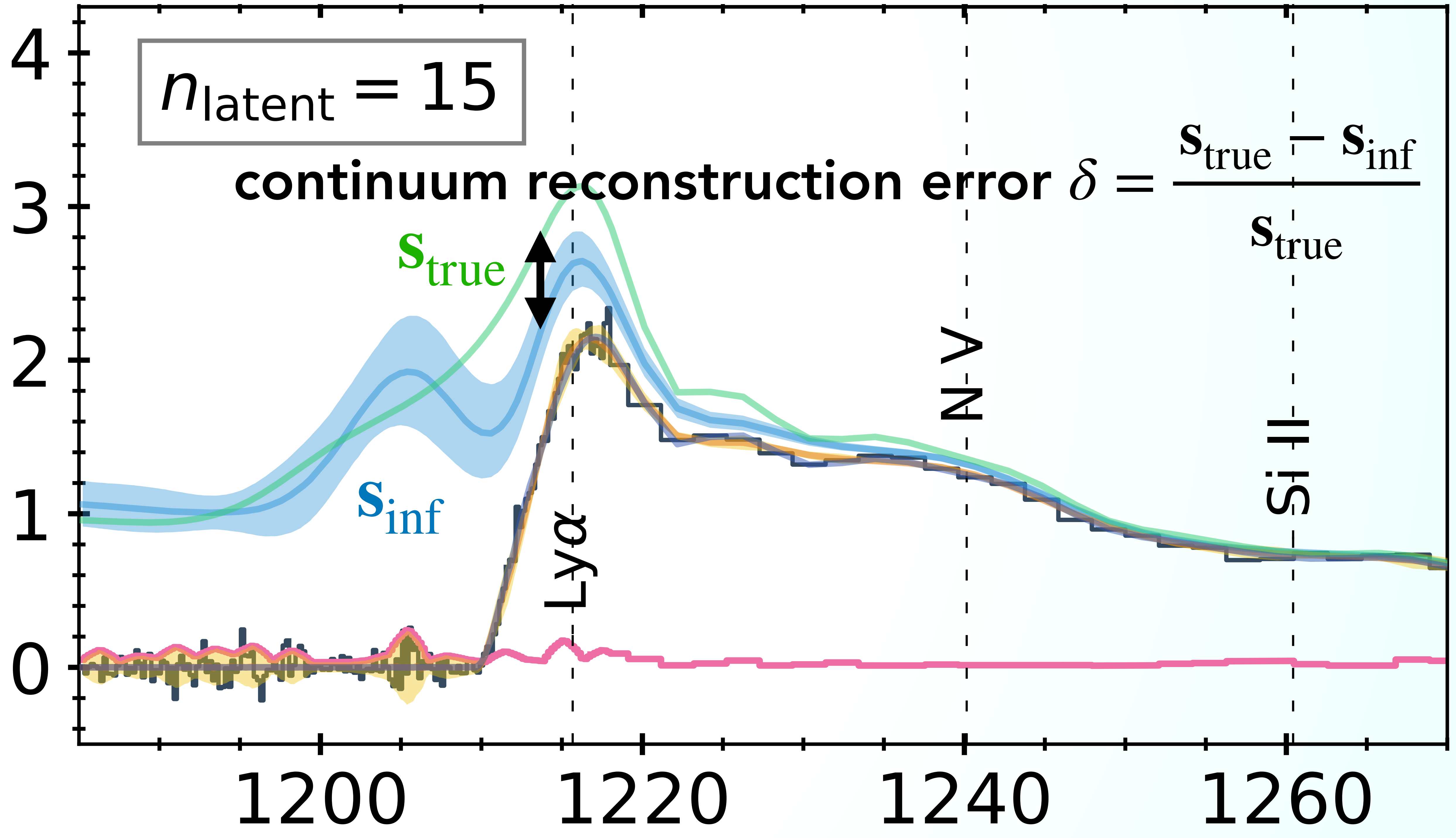

Hennawi, Kist, Davies+ 2023a (in prep.)

Timo Kist, Leiden Observatory, kist@strw.leidenuniv.nl

The PCA Continuum Model

Impact on Inference Precision

Variation of the continuum reconstruction error w.r.t. 100 mock samples

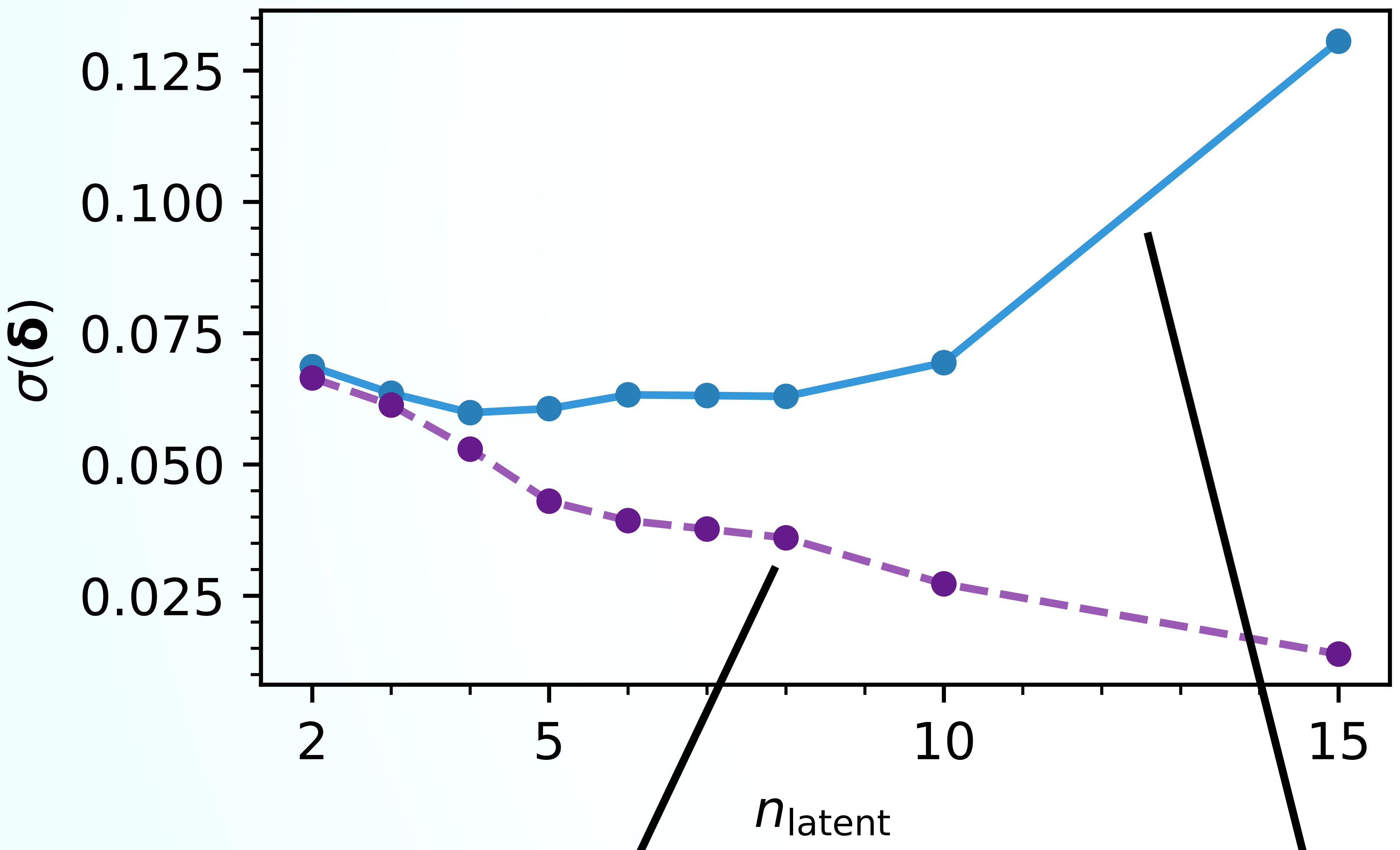

pure continuum fitting error

inferred continuum error

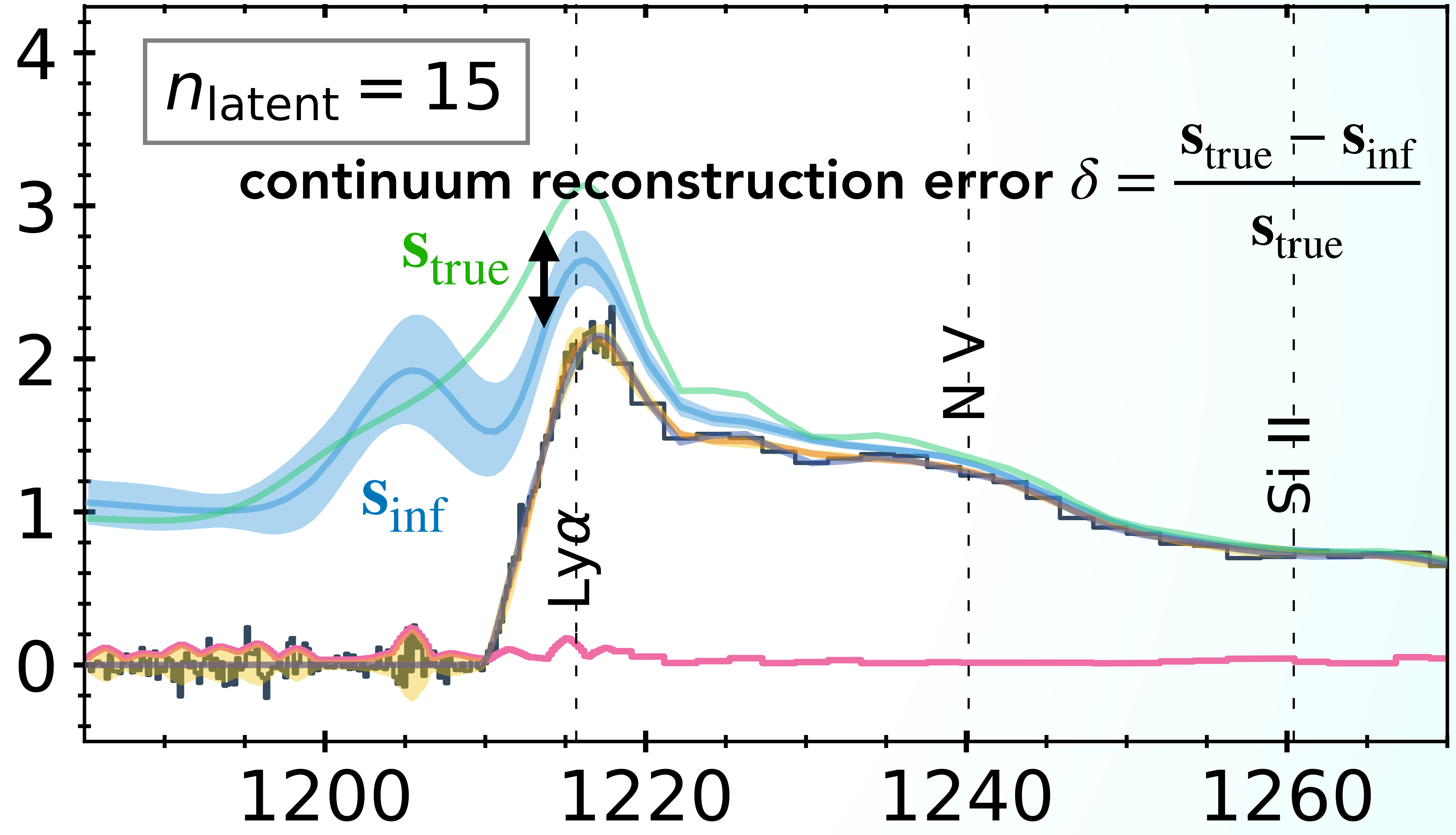

Hennawi, Kist, Davies+ 2023a (in prep.)

Timo Kist, Leiden Observatory, kist@strw.leidenuniv.nl

The PCA Continuum Model

Impact on Inference Precision

Variation of the continuum reconstruction error w.r.t. 100 mock samples

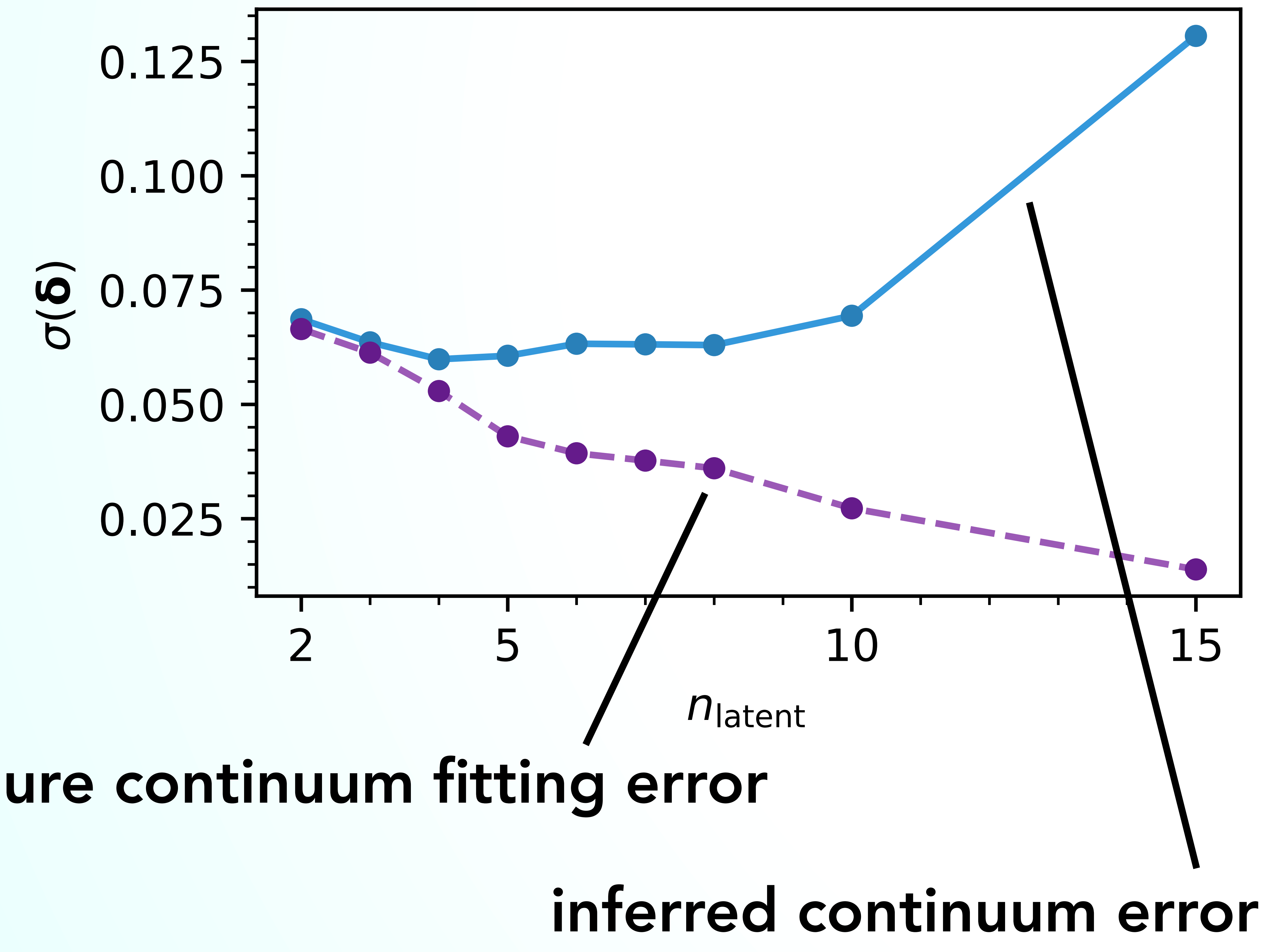

Average precision of 100 mock samples:

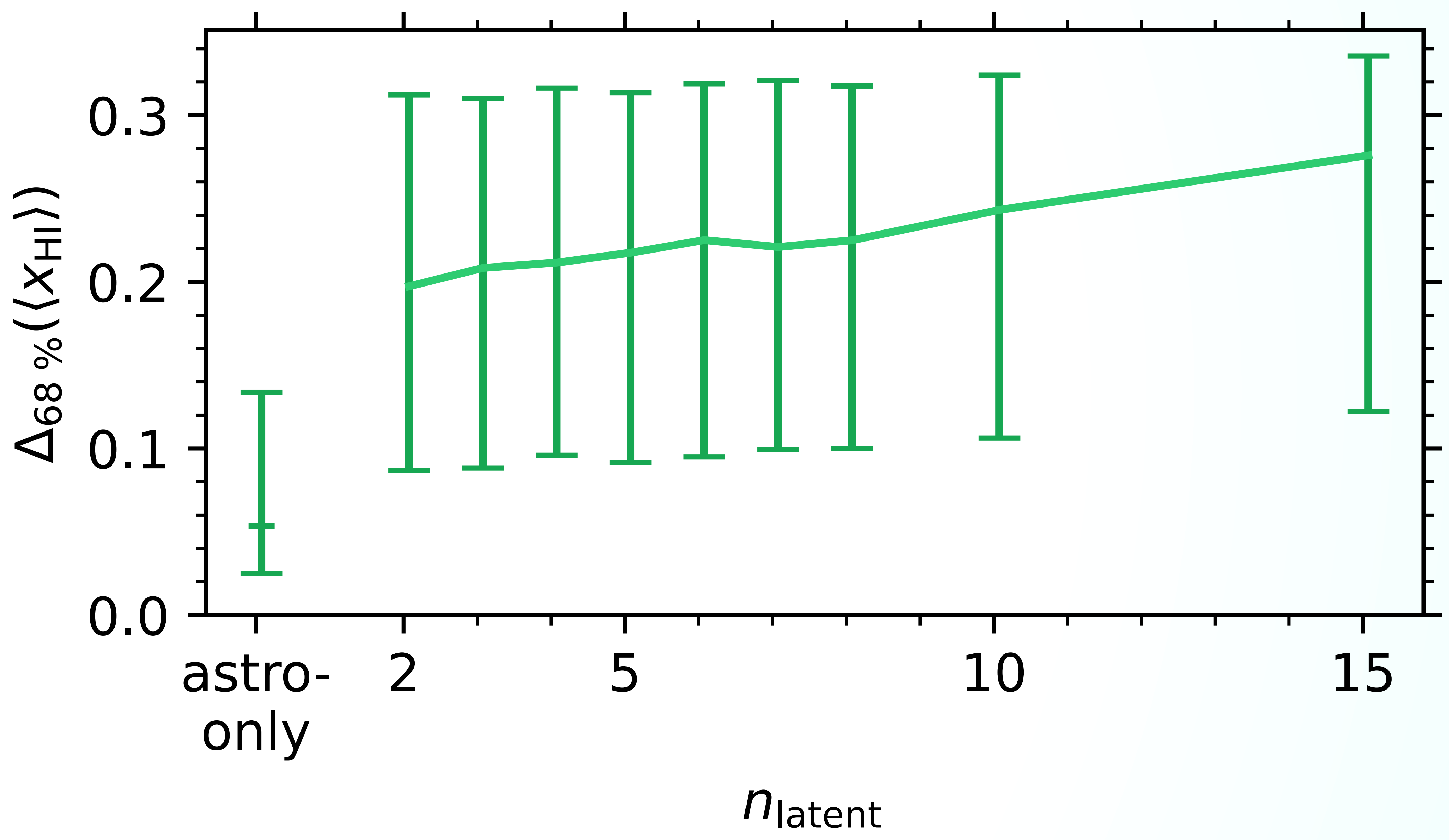

- All information about the Lyman-α forest is encoded in the first few PCA vectors

→ Additional latent dimensions improve the continuum fit but lose constraining power

Hennawi, Kist, Davies+ 2023a (in prep.)

Timo Kist, Leiden Observatory, kist@strw.leidenuniv.nl

The PCA Continuum Model

Impact on Inference Precision

Variation of the continuum reconstruction error w.r.t. 100 mock samples

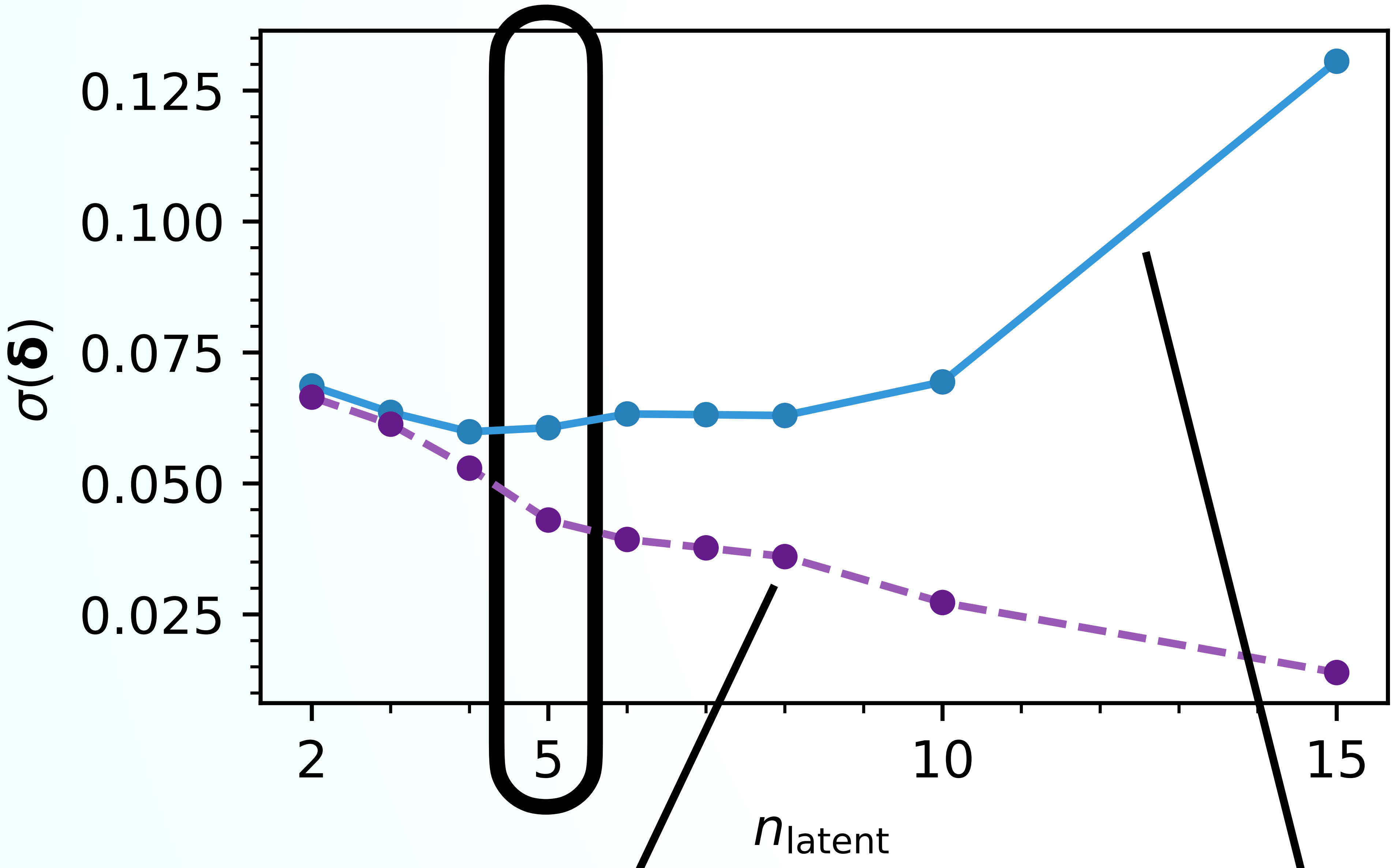

pure continuum fitting error

inferred continuum error

Average precision of 100 mock samples:

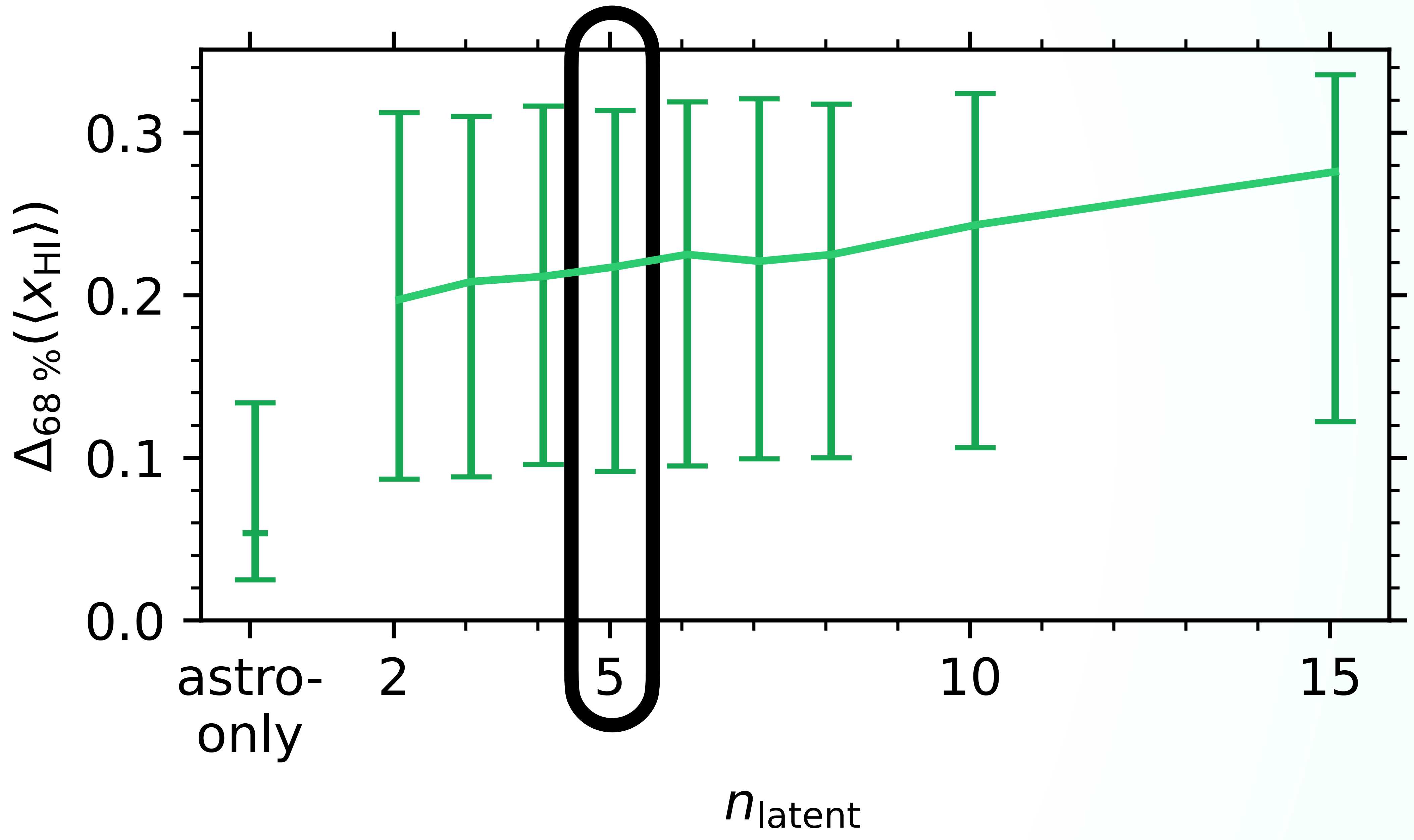

- All information about the Lyman-α forest is encoded in the first few PCA vectors

→ Additional latent dimensions improve the continuum fit but lose constraining power

Hennawi, Kist, Davies+ 2023a (in prep.)

Timo Kist, Leiden Observatory, kist@strw.leidenuniv.nl

Observational Setup

Impact on Inference Precision

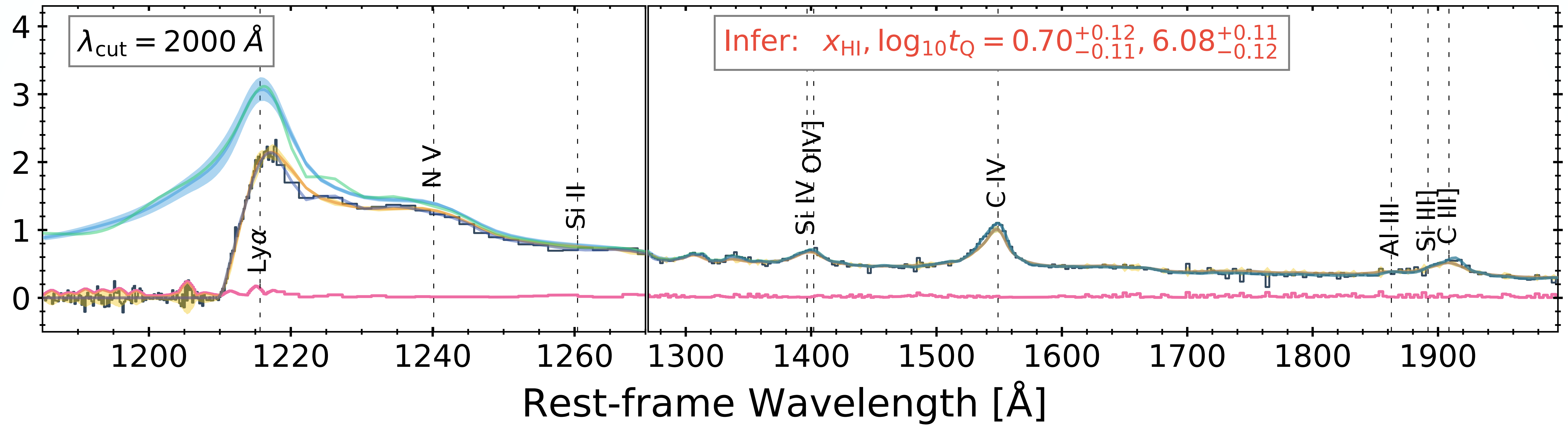

Hennawi, Kist, Davies+ 2023a (in prep.)

Spectral resolution

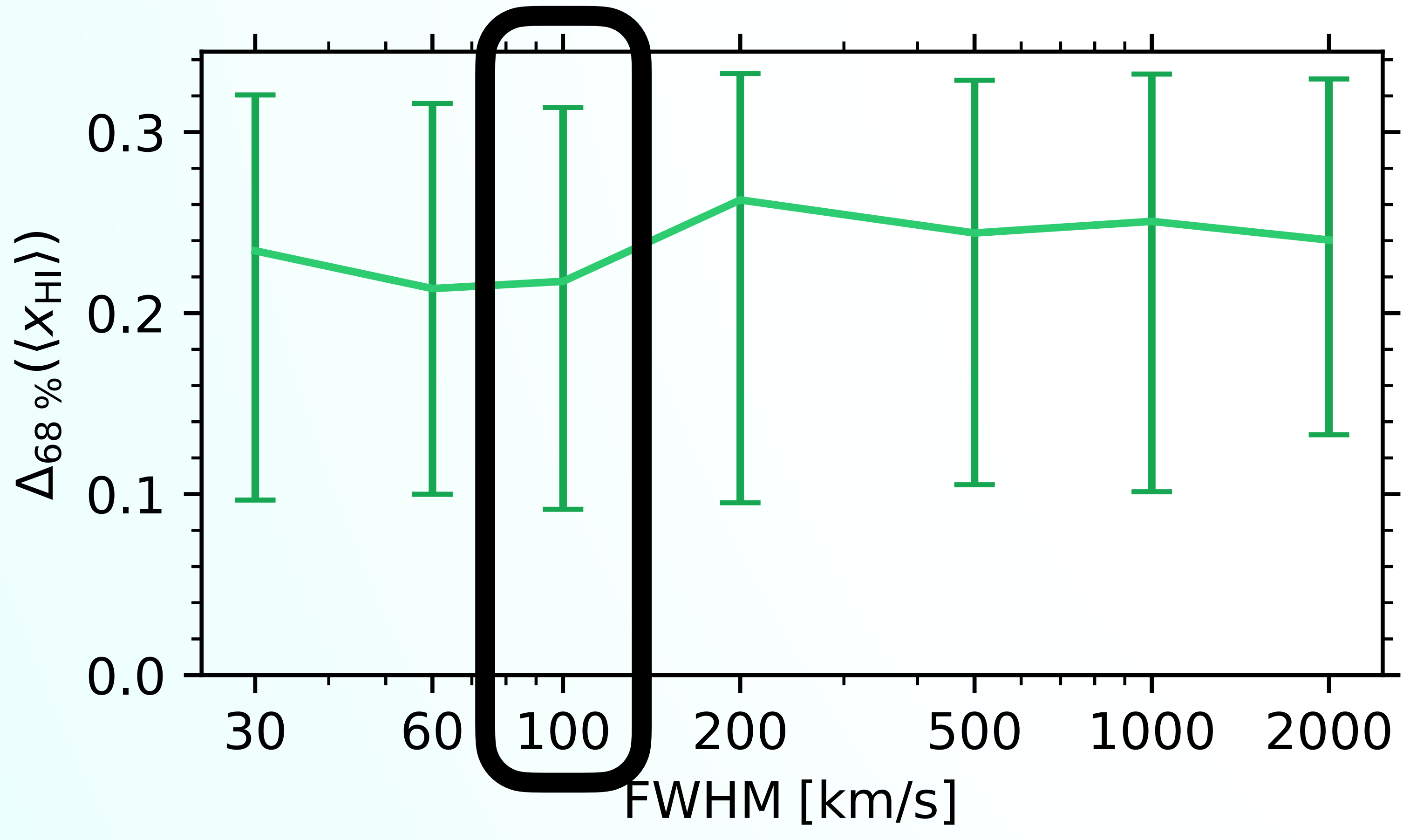

→ **Precision does not vary significantly with spectral resolution**

Red-side wavelength coverage

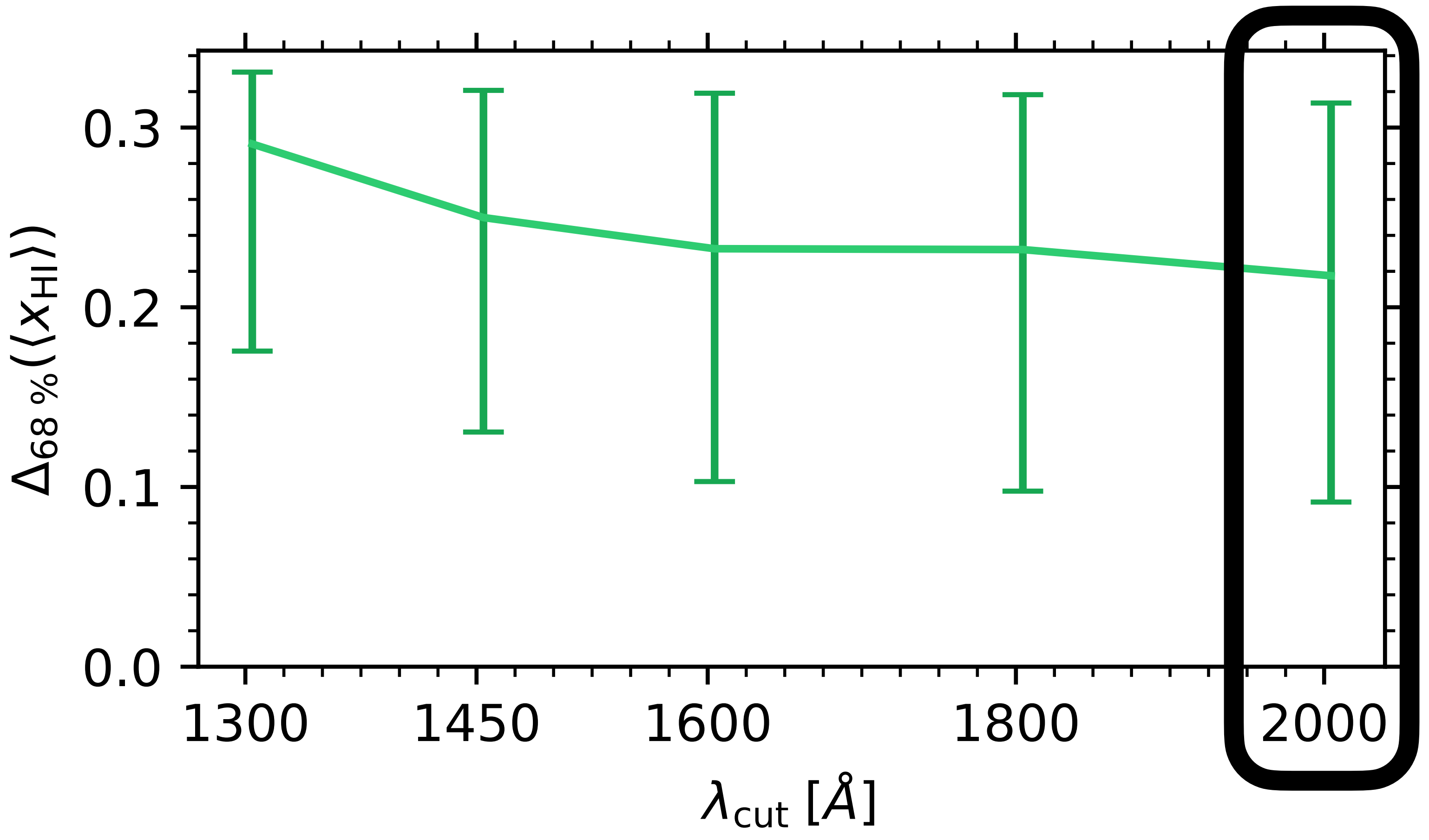

→ **Covering major emission lines is important**

S/N per 100 km/s velocity interval

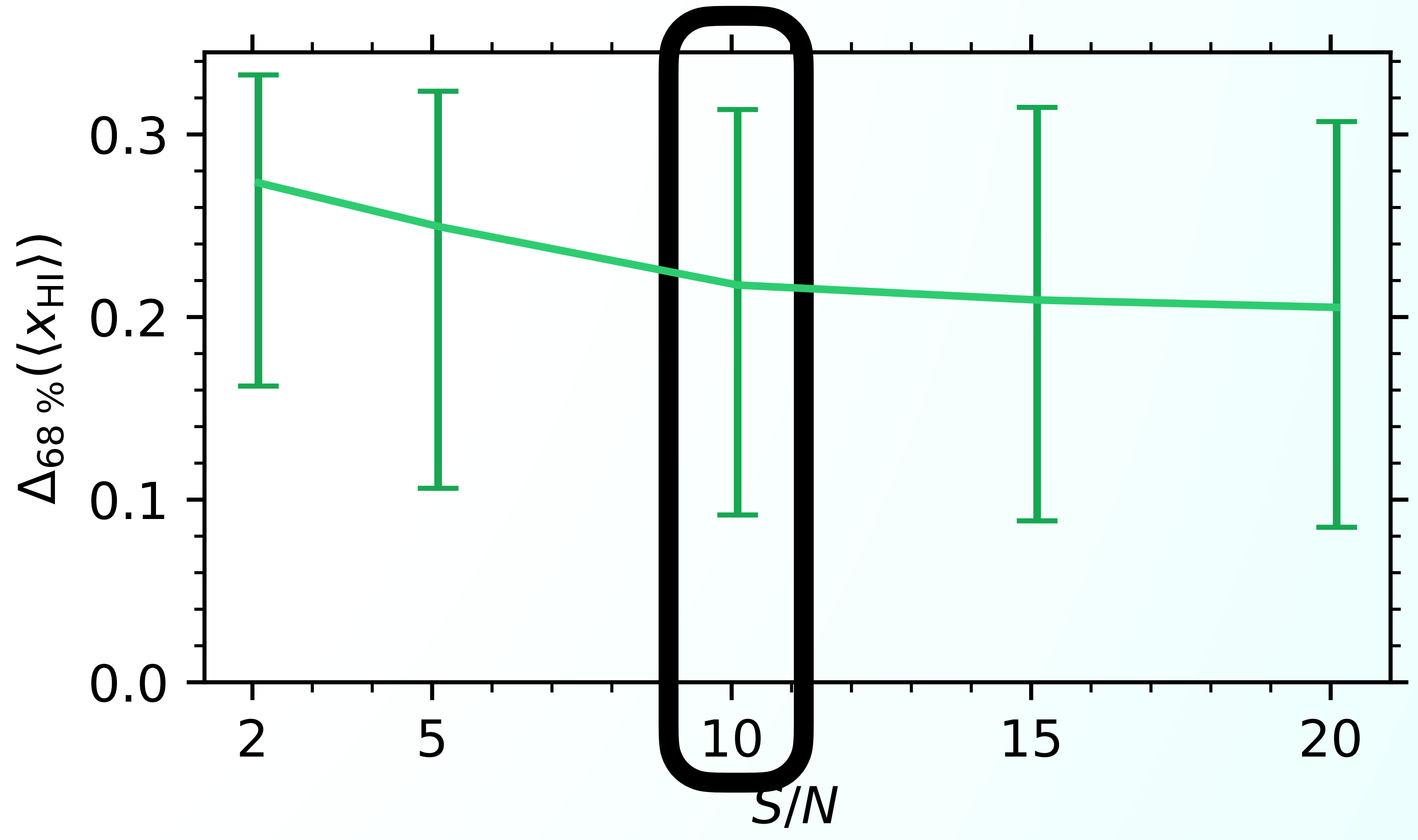

→ **Covering major emission lines is important**

Quantifying $\langle x_{\rm HI} \rangle$ Inference Precision

Variation across Model Components and Parameter Space

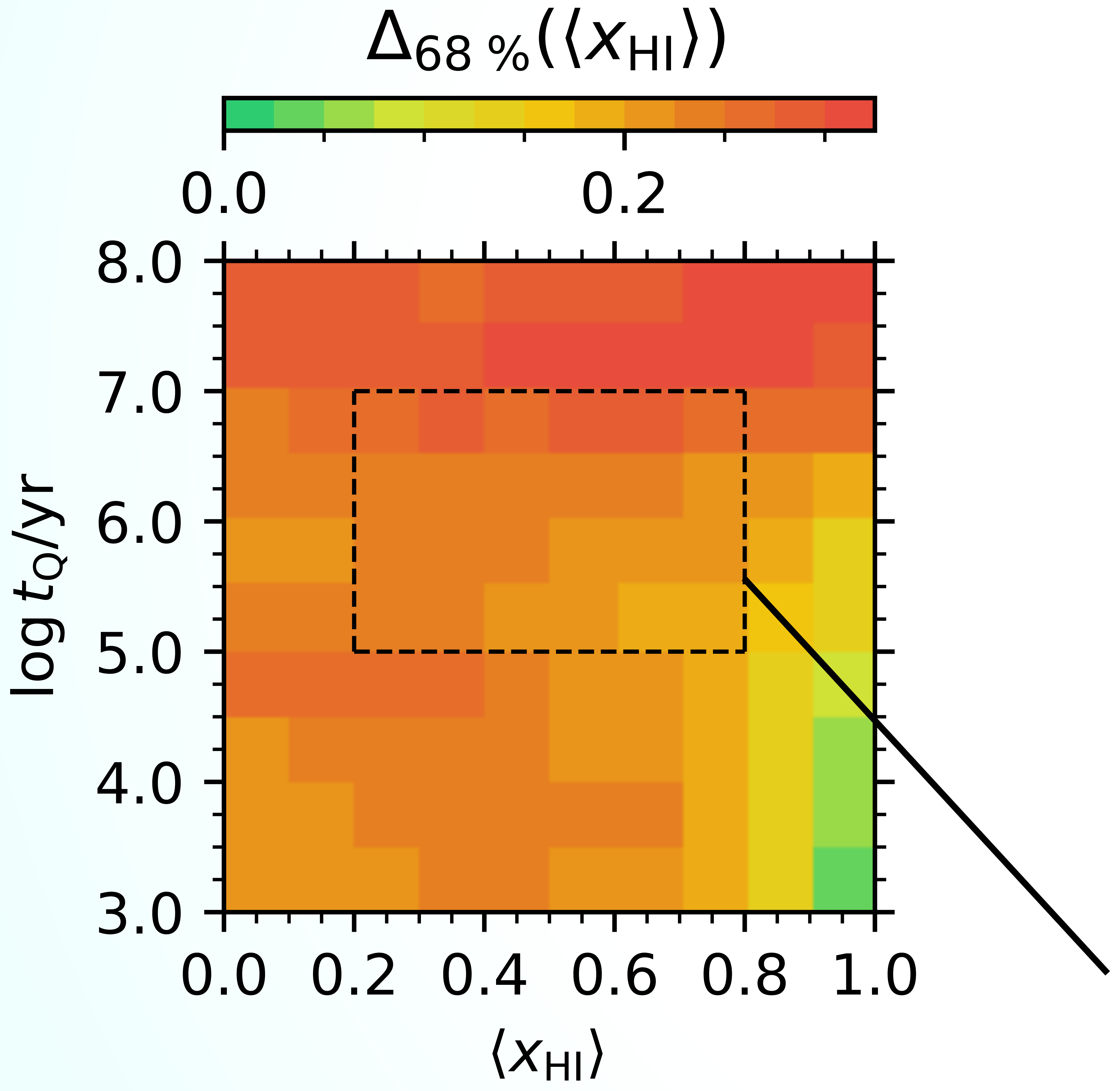

- Precision varies significantly across parameter space (between 2.6% and 39.3%)
- Median precision: 23.4%
- Stronger damping wing imprint (higher $\langle x_{\rm HI} \rangle$, lower $t_{\rm Q}$) improves precision

"Fiducial" region of parameter space

Kist, Hennawi, Davies+ 2023a (in prep.)

Quantifying $\langle x_{\rm HI} \rangle$ Inference Precision

Variation across Model Components and Parameter Space

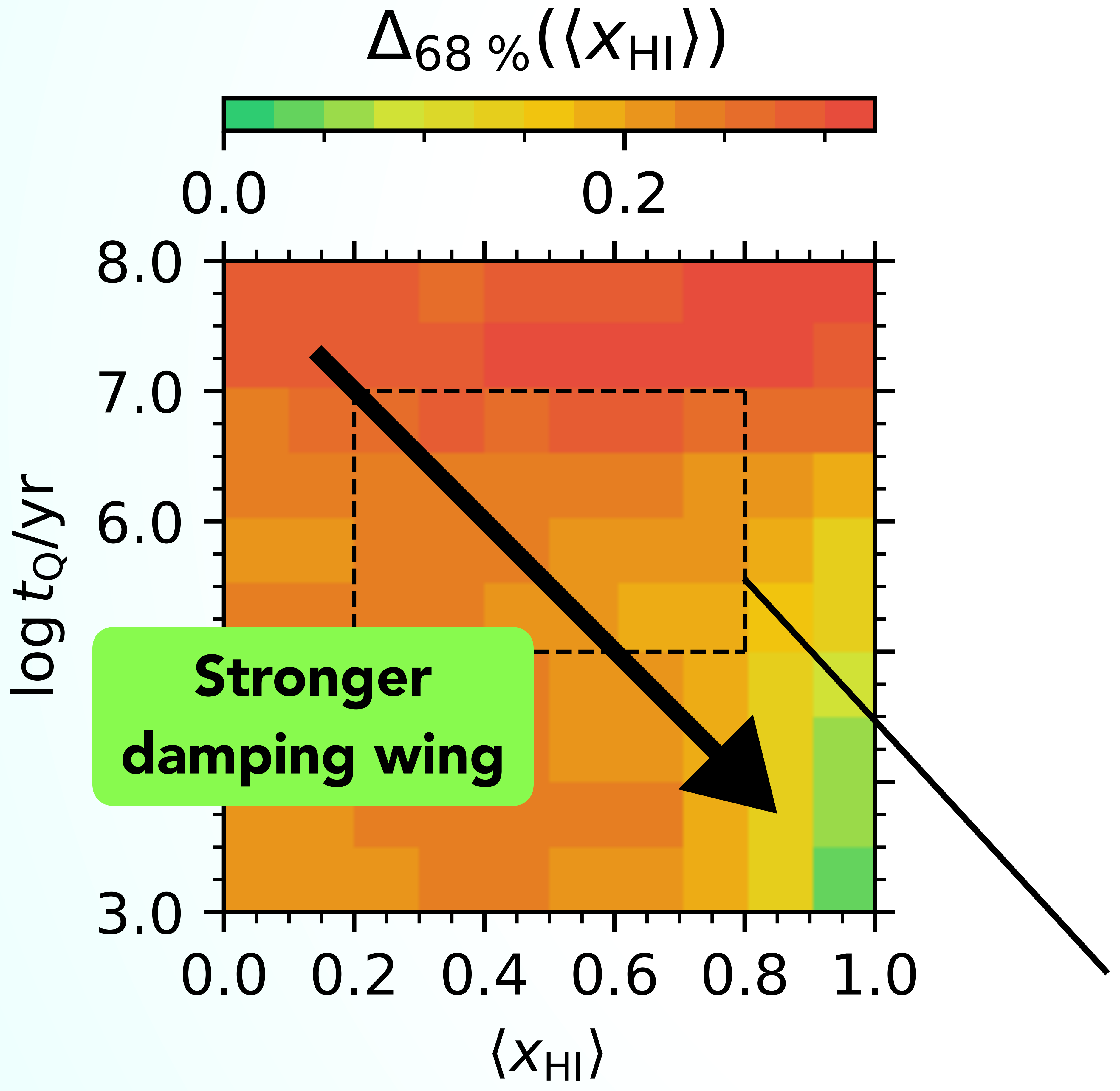

- Precision varies significantly across parameter space (between 2.6% and 39.3%)
- Median precision: 23.4%
- Stronger damping wing imprint (higher $\langle x_{\rm HI} \rangle$, lower $t_{\rm Q}$) improves precision

"Fiducial" region of parameter space

Kist, Hennawi, Davies+ 2023a (in prep.)

Quantifying $\langle x_{\mathrm{HI}} \rangle$ Inference Precision

Variation across Model Components and Parameter Space

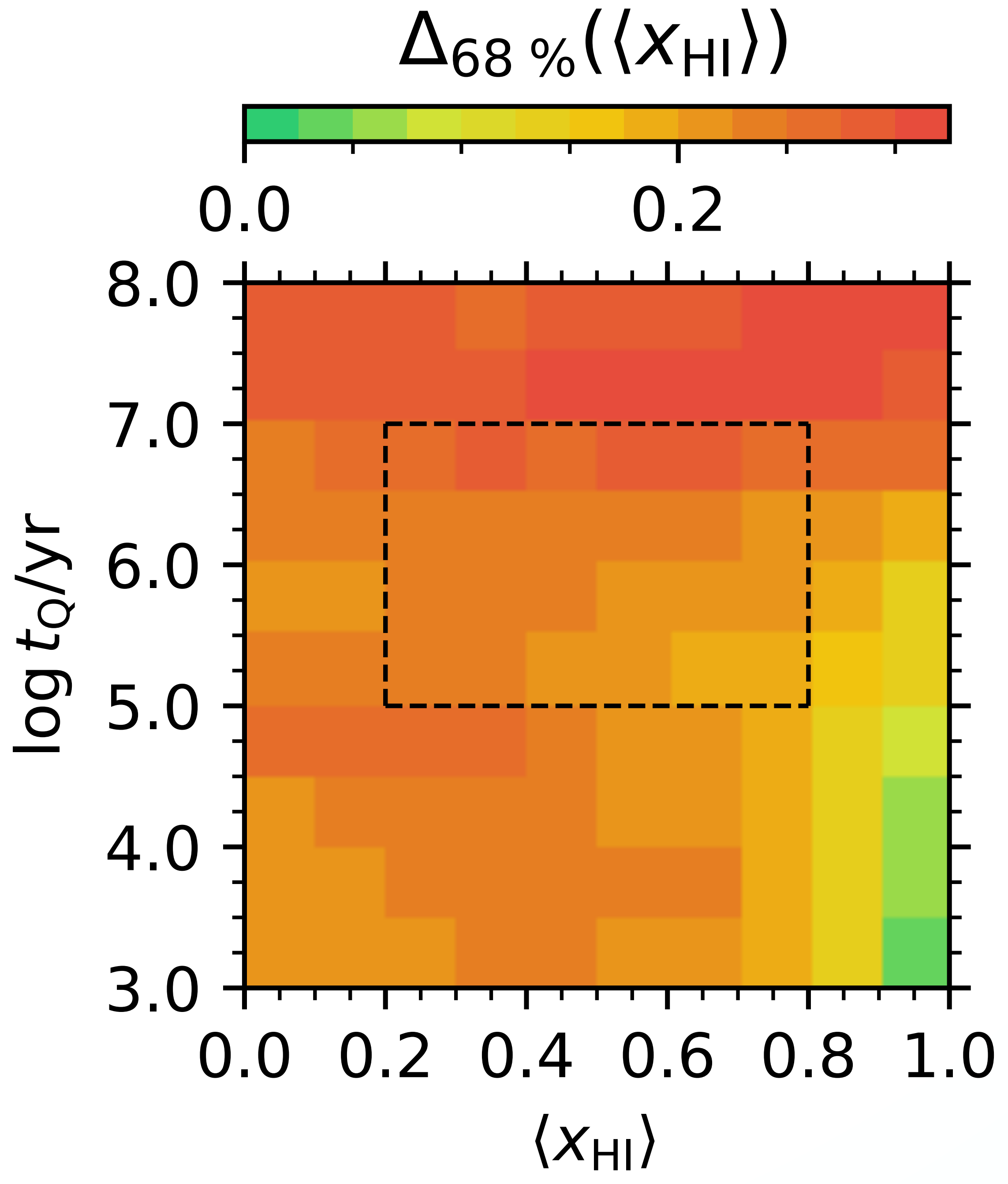

Quantifying $\langle x_{\rm HI} \rangle$ Inference Precision

Variation across Model Components and Parameter Space

Overall median: 2.2%
Fiducial median: 2.4%

Overall median: 14.9%
Fiducial median: 15.3%

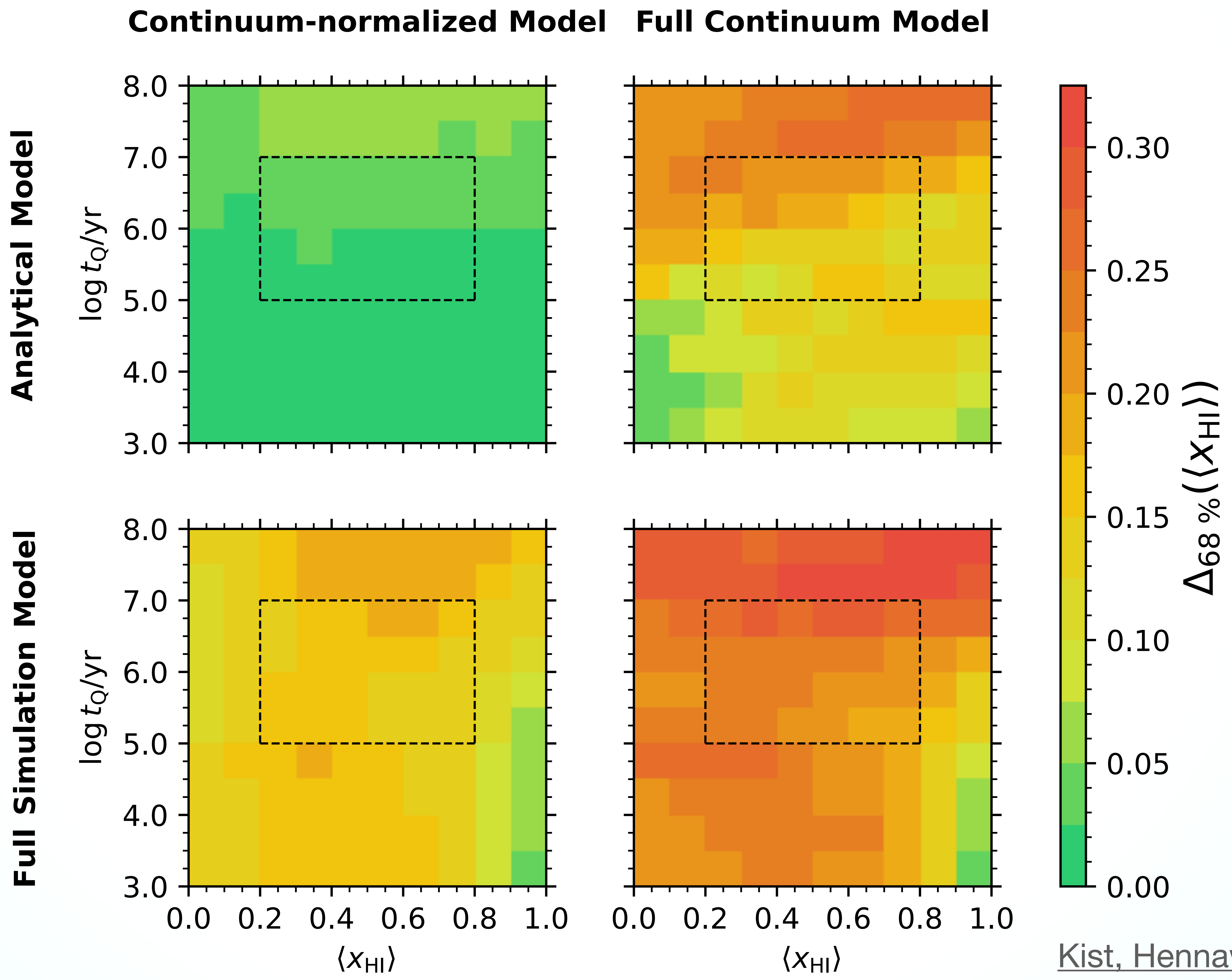

Overall median: 13.9%
Fiducial median: 15.8%

Overall median: 23.4%
Fiducial median: 23.4%

Kist, Hennawi, Davies+ 2023a (in prep.)

Quantifying $\langle x_{\mathrm{HI}} \rangle$ Inference Precision

Variation across Model Components and Parameter Space

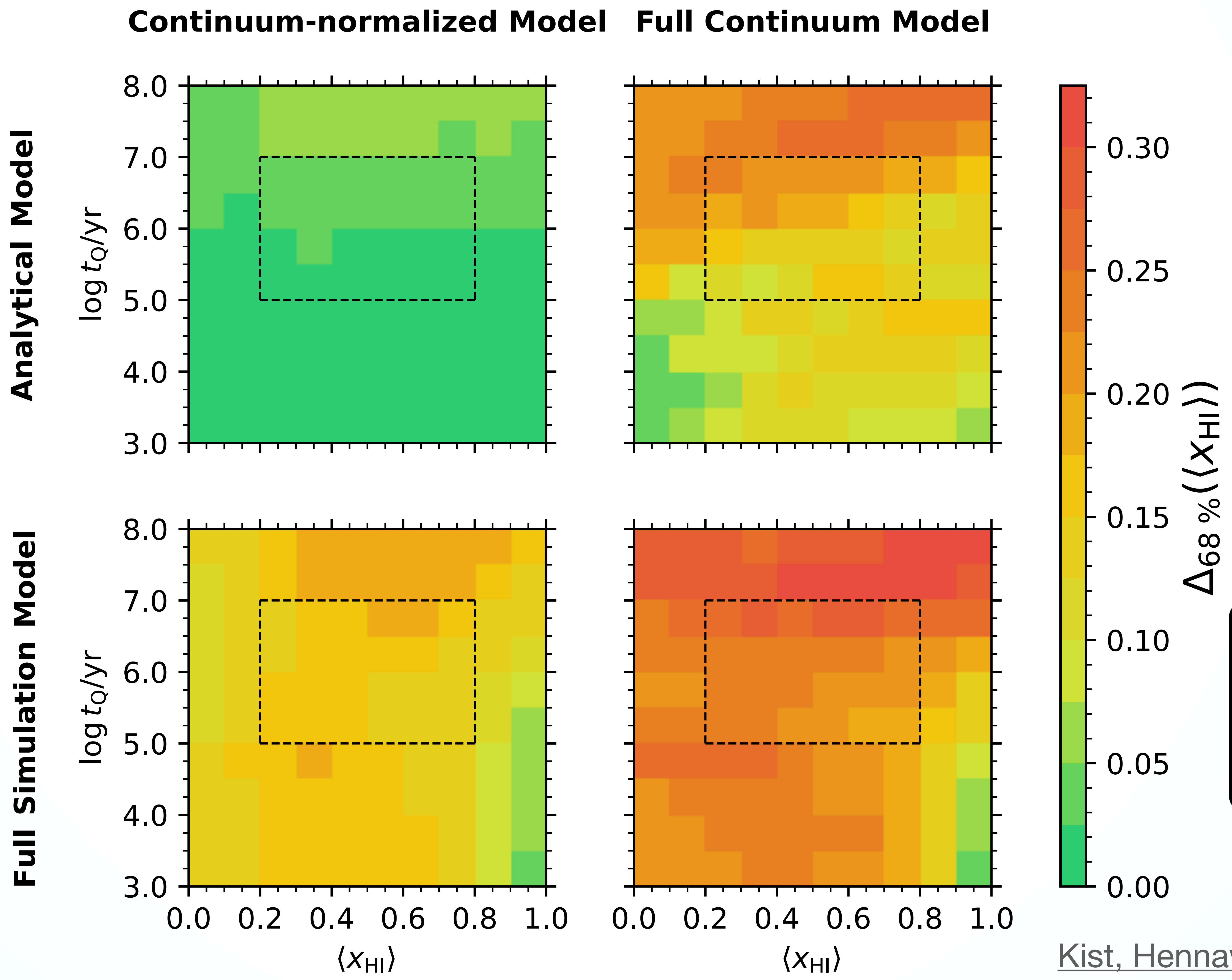

Overall median: 2.2%
Fiducial median: 2.4%

Overall median: 13.9%
Fiducial median: 15.8%

Overall median: 14.9%
Fiducial median: 15.3%

23.4% total
1σ-uncertainty

Kist, Hennawi, Davies+ 2023a (in prep.)

Quantifying $\langle x_{\rm HI} \rangle$ Inference Precision

Variation across Model Components and Parameter Space

Overall median: 2.2%
Fiducial median: 2.4%

Overall median: 14.9%
Fiducial median: 15.3%

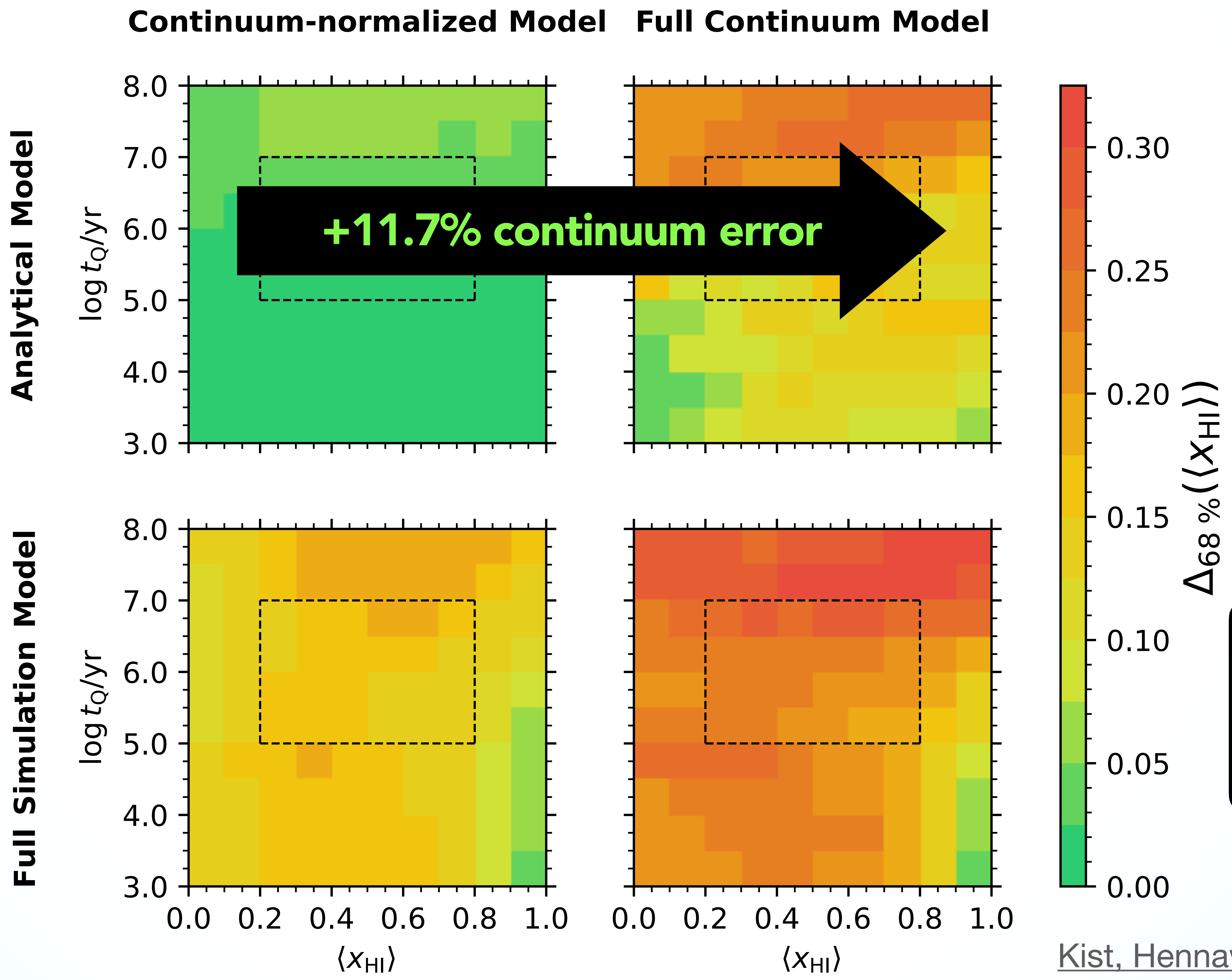

Overall median: 13.9%
Fiducial median: 15.8%

23.4% total 1σ-uncertainty

Kist, Hennawi, Davies+ 2023a (in prep.)

Quantifying $\langle x_{\rm HI} \rangle$ Inference Precision

Variation across Model Components and Parameter Space

Overall median: 2.2%
Fiducial median: 2.4%

Overall median: 14.9%
Fiducial median: 15.3%

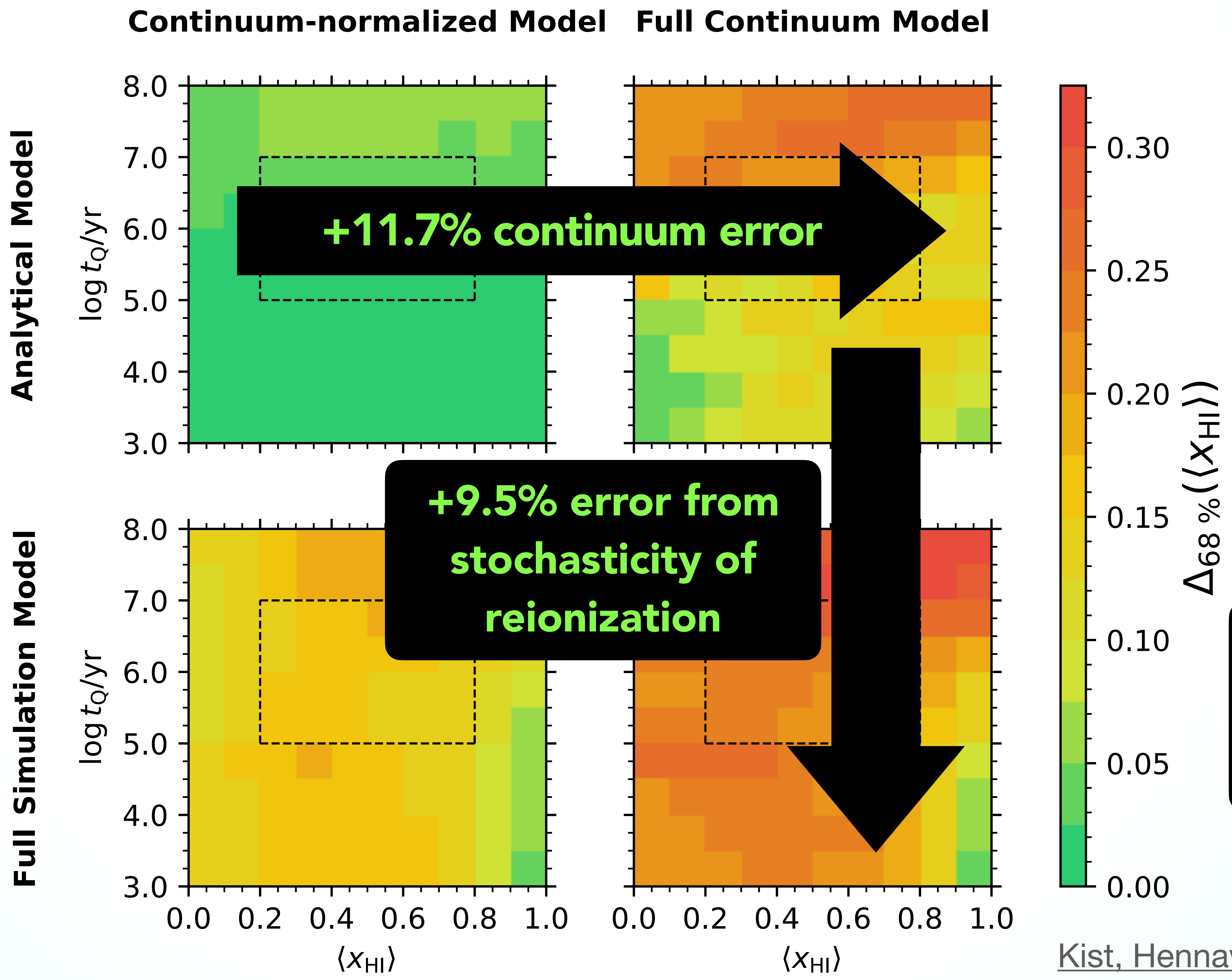

Overall median: 13.9%
Fiducial median: 15.8%

23.4% total 1σ-uncertainty

Kist, Hennawi, Davies+ 2023a (in prep.)

Quantifying t_Q Inference Precision

Variation across Model Components and Parameter Space

Overall median: 0.12 dex
Fiducial median: 0.08 dex

Overall median: 0.54 dex
Fiducial median: 0.71 dex

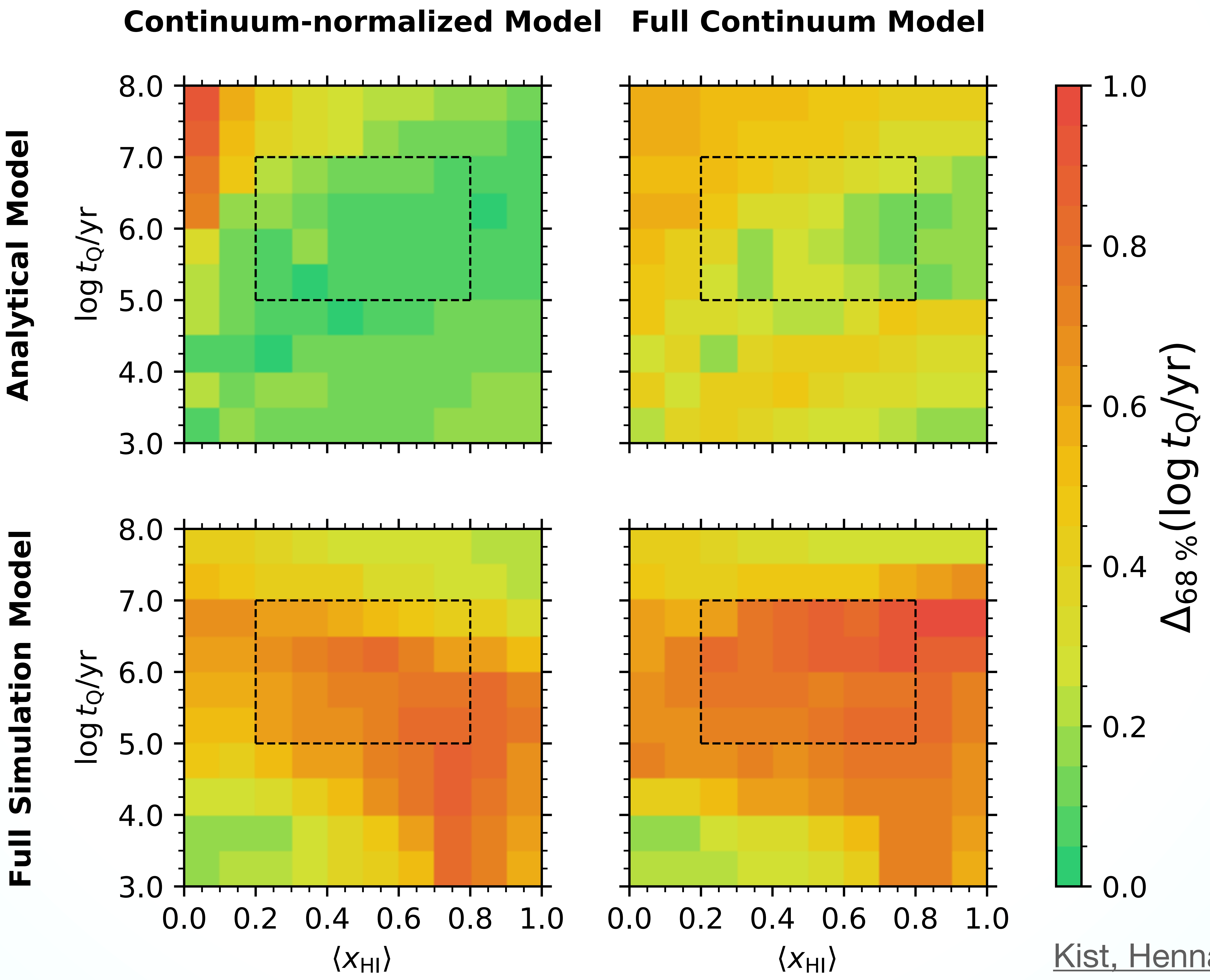

Overall median: 0.33 dex
Fiducial median: 0.26 dex

Overall median: 0.65 dex
Fiducial median: 0.86 dex

Kist, Hennawi, Davies+ 2023a (in prep.)

Timo Kist, Leiden Observatory, kist@strw.leidenuniv.nl

Inference Tests

Expected coverage probability

- testing if the inferred posterior represents the true distribution
- select the α-th credibility level of the inferred posterior
- compute the expected coverage probability C_α of the true distribution

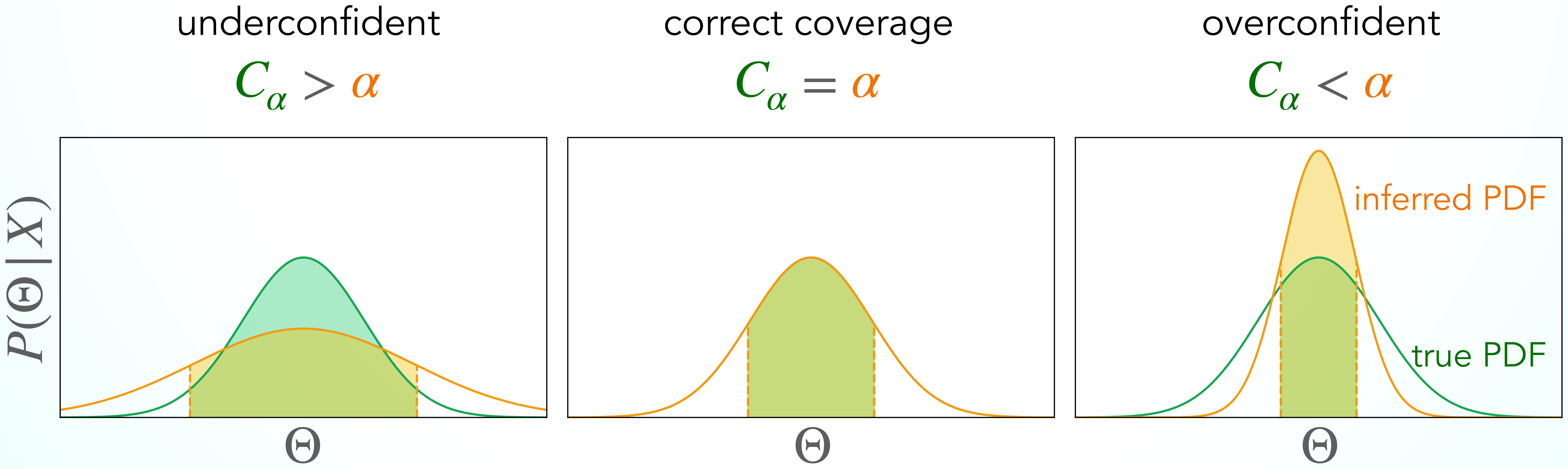

Timo Kist, Leiden Observatory, kist@strw.leidenuniv.nl

Coverage Tests

Practical computation

- for each quasar, order the MCMC samples by probability and choose the N highest ones, where $N = \alpha \cdot N_{\text{tot}}$
- test if the true probability is contained inside this region
- for each credibility level α determine the fraction of quasars C_α for which this is the case

Timo Kist, Leiden Observatory, kist@strw.leidenuniv.nl

Ensemble inference

Constraints on the Distribution of Quasar Lifetimes

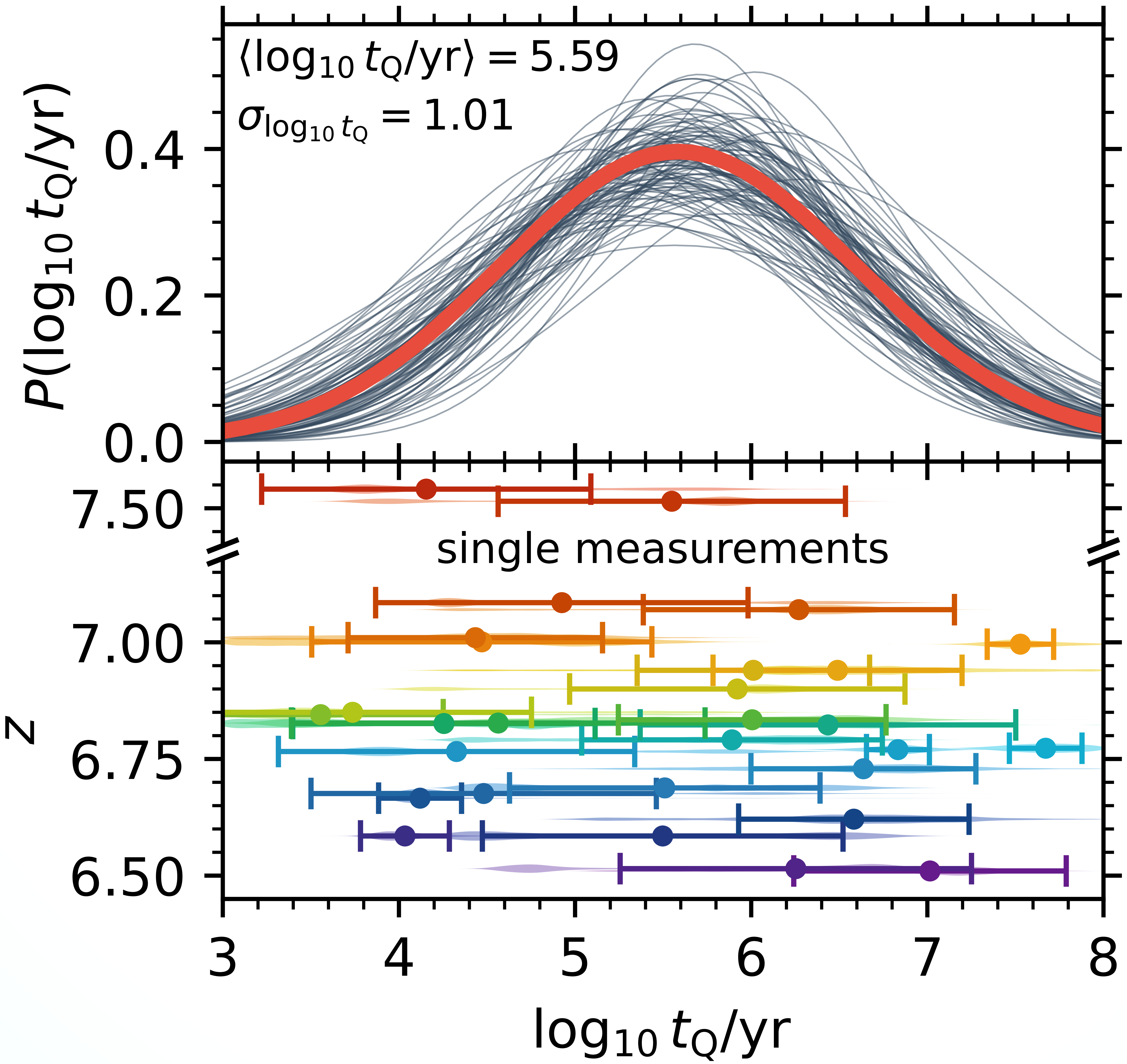

Kist, Hennawi+ 2023b (in prep.)

Timo Kist, Leiden Observatory, kist@strw.leidenuniv.nl

HI absorption cross section

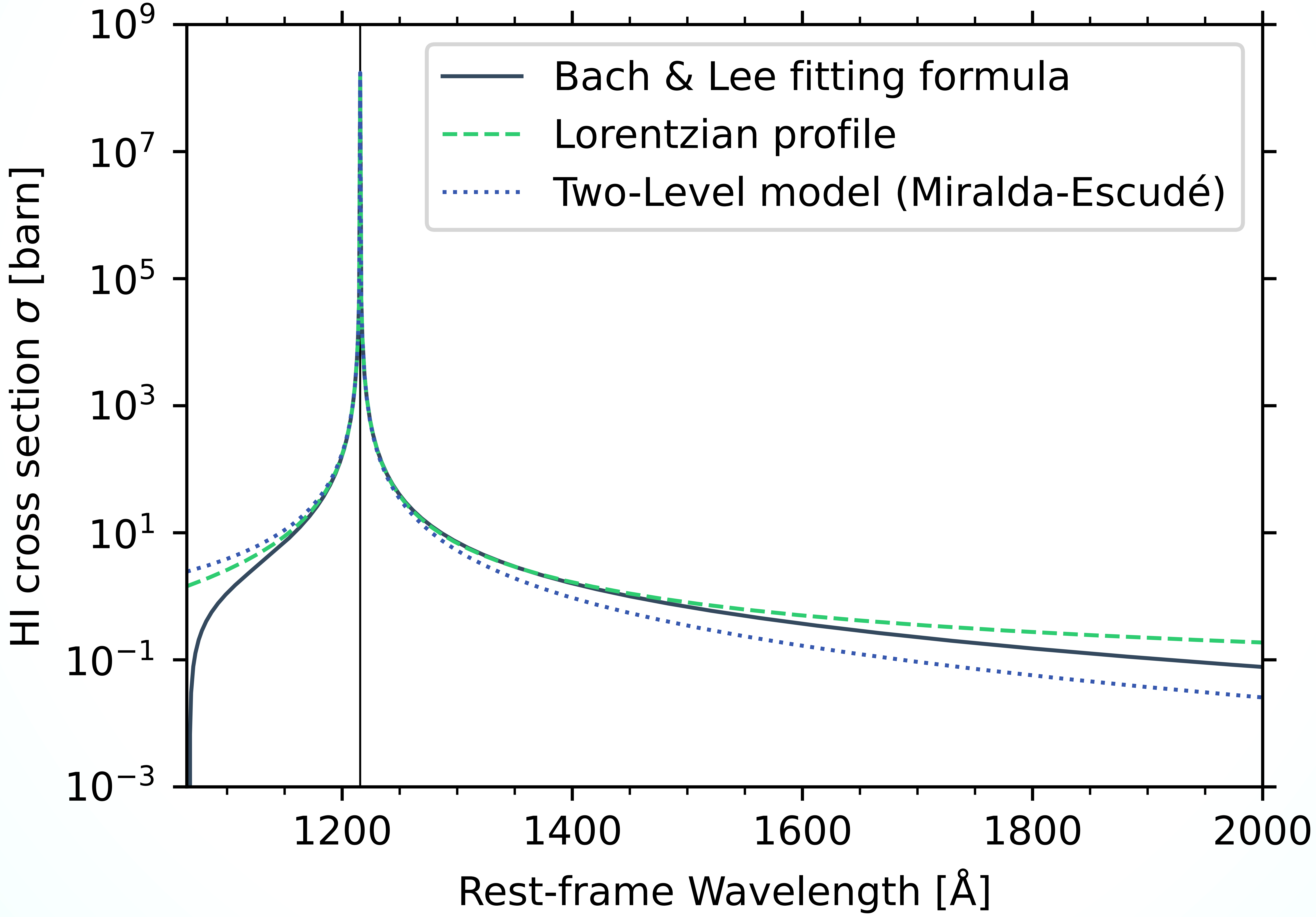

Kist, Hennawi+ 2023b (in prep.)

Constructing a new label that minimizes IGM transmission scatter

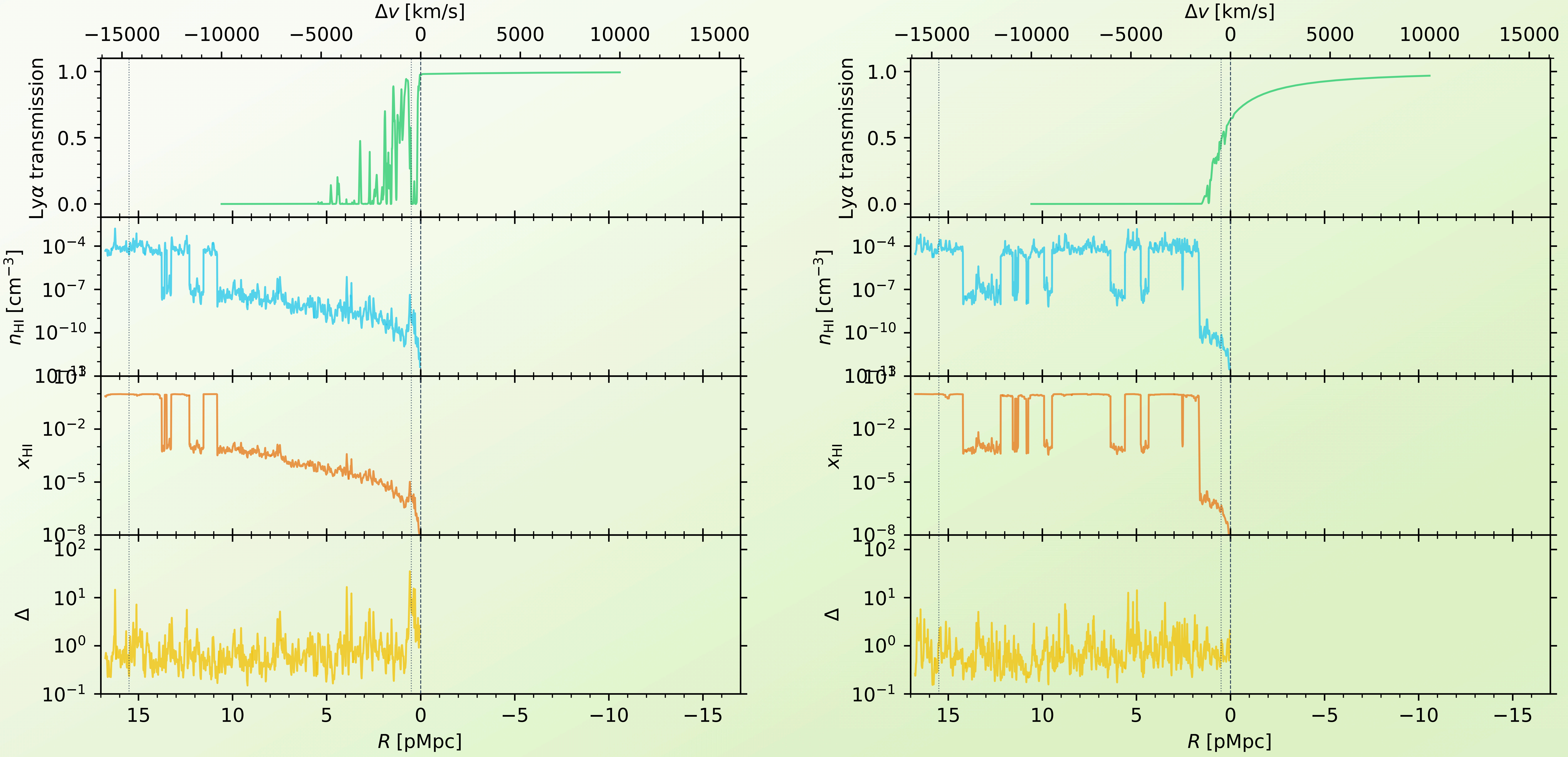

Constructing a new label that minimizes IGM transmission scatter

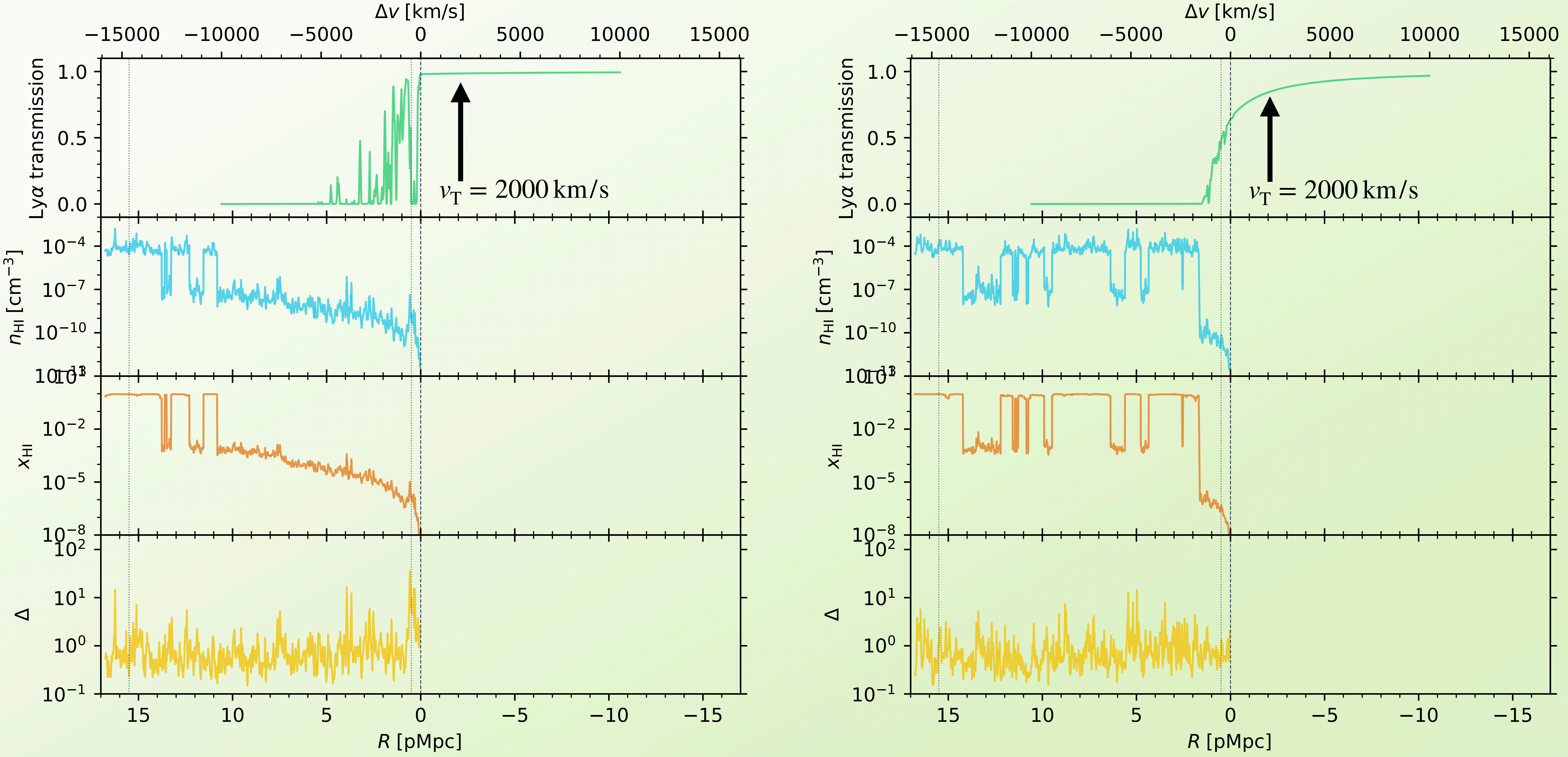

Constructing a new label that minimizes IGM transmission scatter

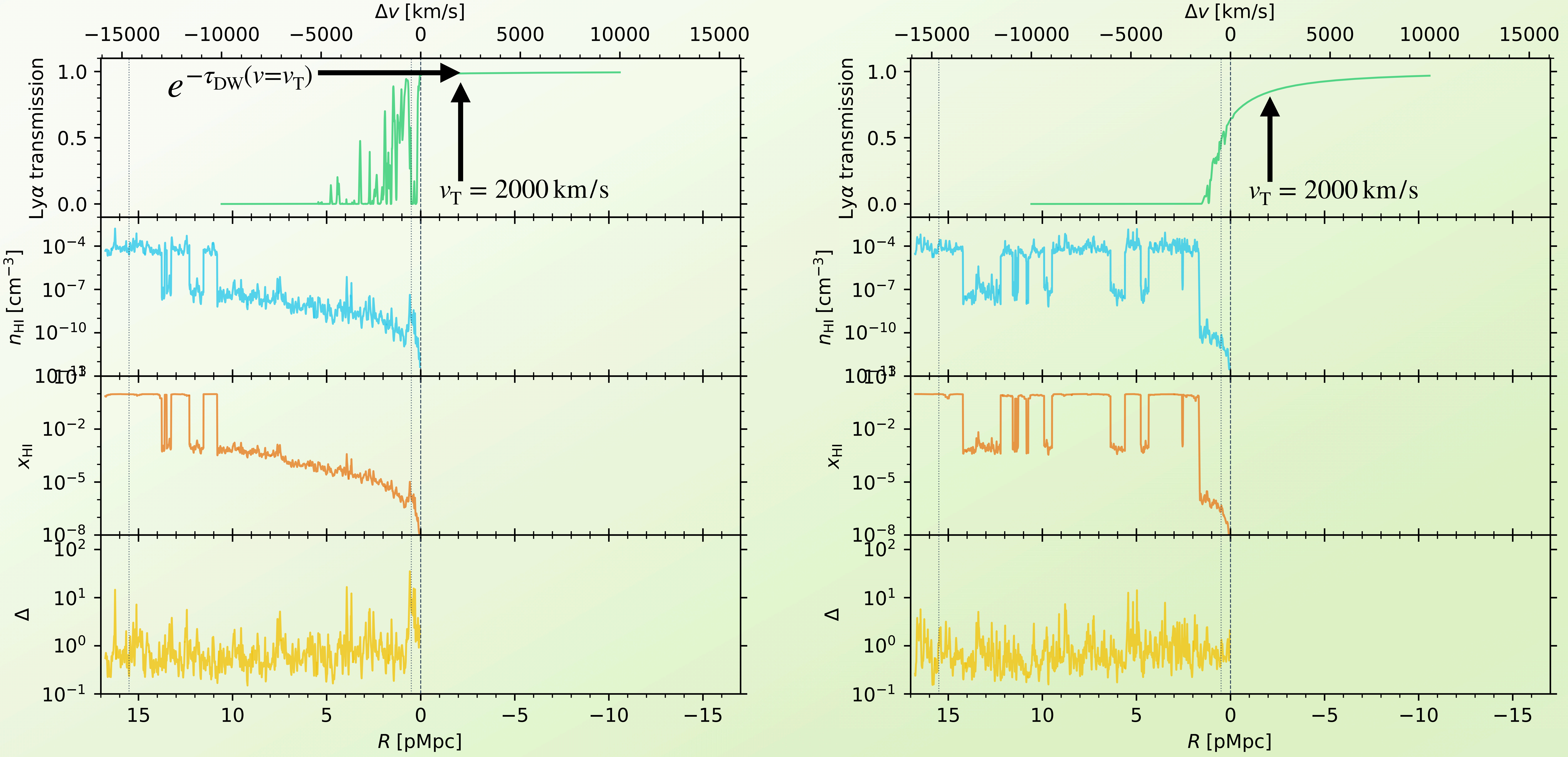

Constructing a new label that minimizes IGM transmission scatter

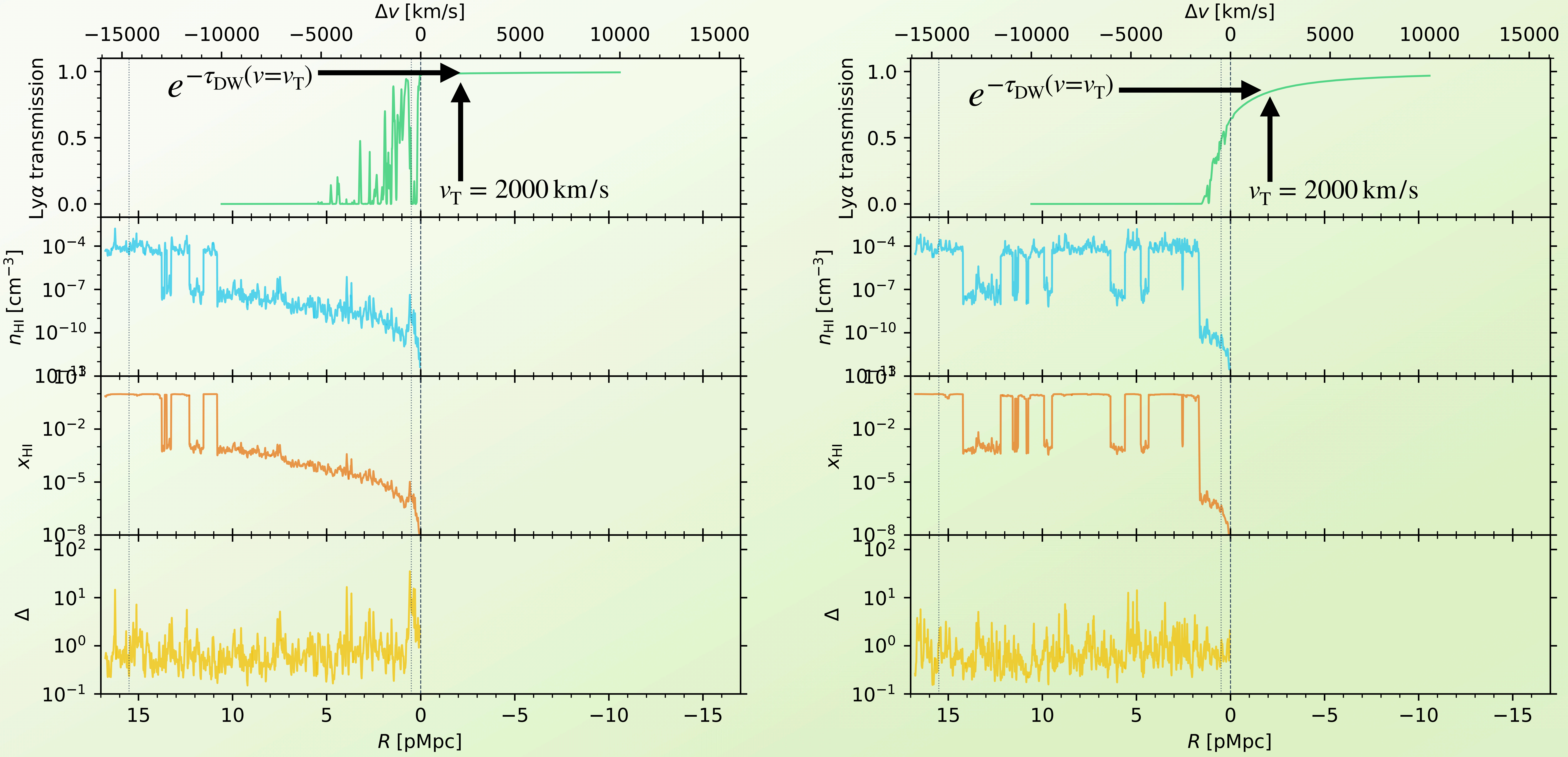

Constructing a new label that minimizes IGM transmission scatter

damping wing optical depth

$$\tau_{\rm DW}(\lambda_{\rm obs}) = \int_0^{R(z_{\rm QSO})} n_{\rm HI}^{\rm QSO}(R) \times \sigma_\alpha\left(\nu(R)\right)\, {\rm d}R$$

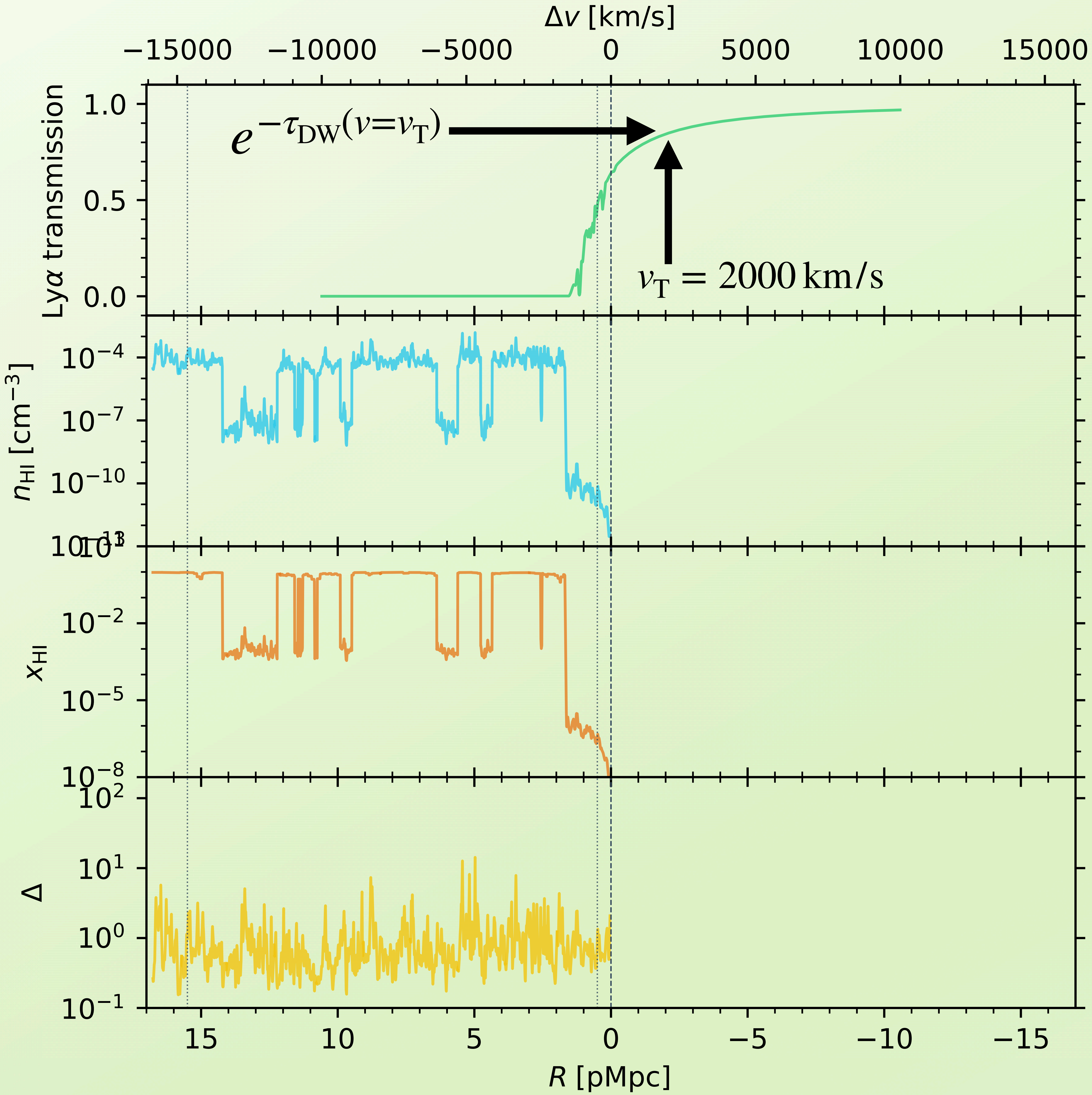

Constructing a new label that minimizes IGM transmission scatter

damping wing optical depth

$$\tau_{\mathrm{DW}}(\lambda_{\mathrm{obs}}) = \int_0^{R(z_{\mathrm{QSO}})} n_{\mathrm{HI}}^{\mathrm{QSO}}(R) \times \sigma_\alpha\left(\nu(R)\right)\, \mathrm{d}R$$

post-quasar HI density field

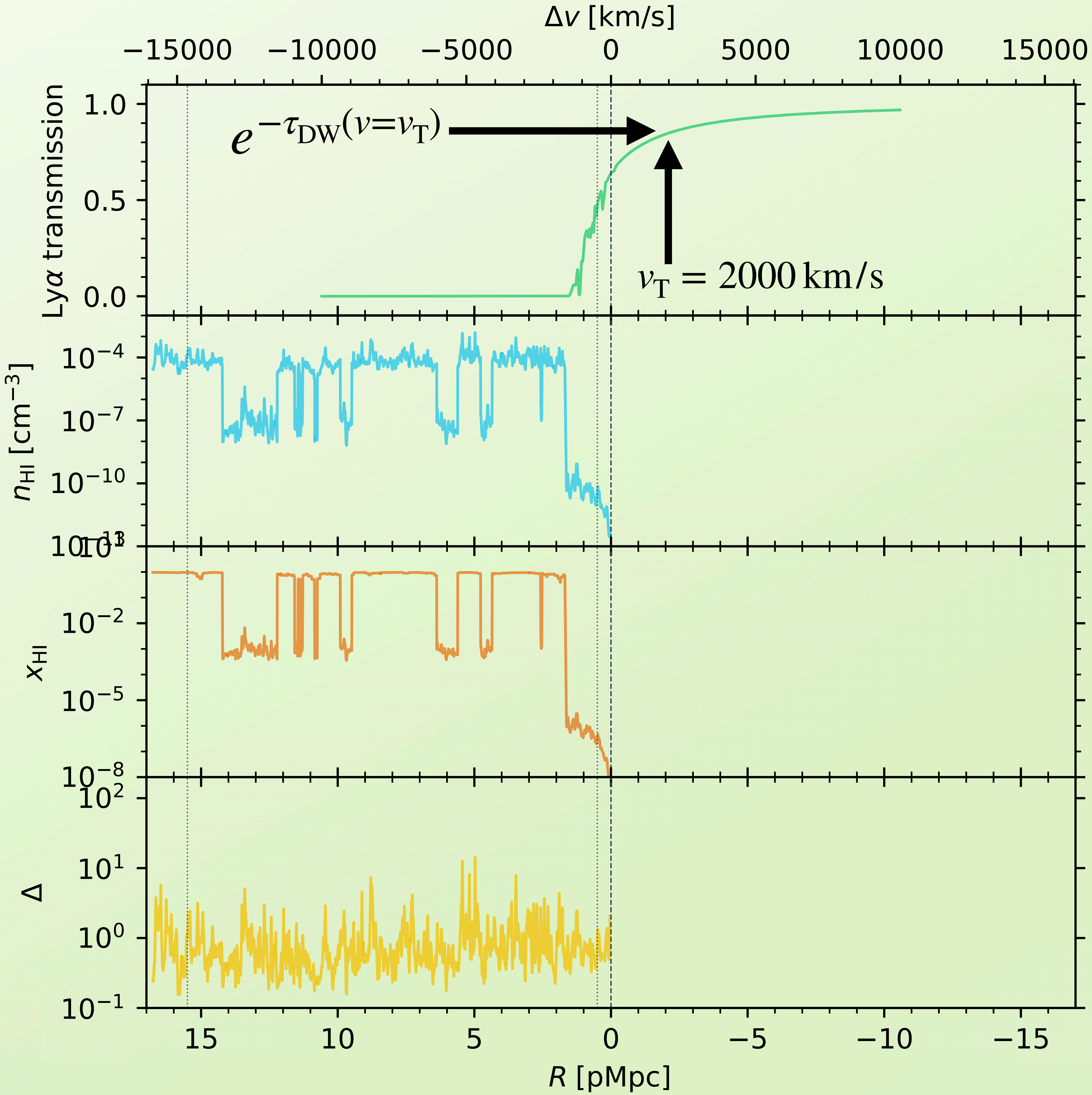

Constructing a new label that minimizes IGM transmission scatter

damping wing optical depth

$$\tau_{\rm DW}(\lambda_{\rm obs}) \;=\; \int_0^{R(z_{\rm QSO})} n_{\rm HI}^{\rm QSO}(R) \times \sigma_\alpha\left(\nu(R)\right)\; {\rm d}R$$

post-quasar HI density field

Lyα cross section

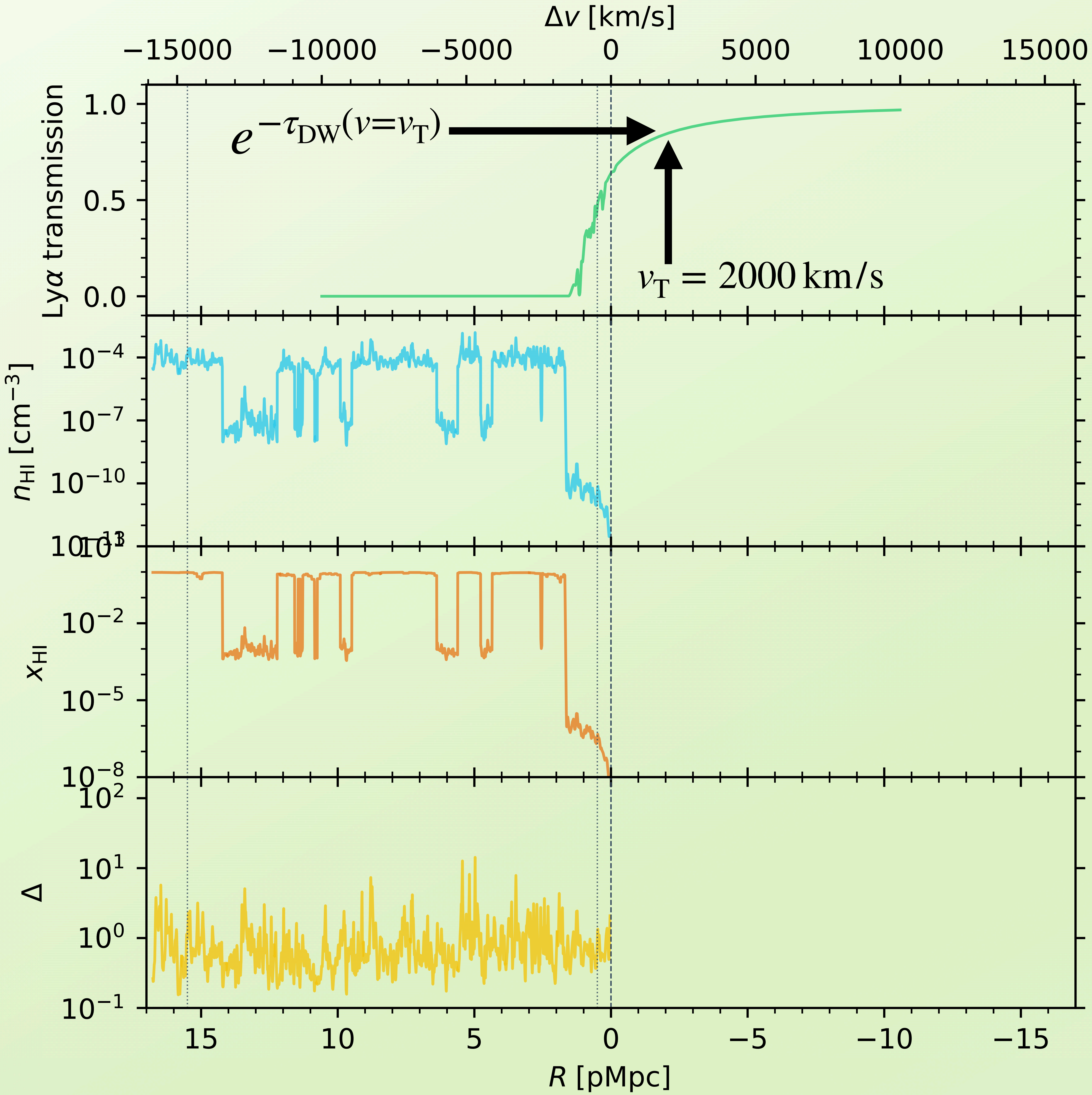

Constructing a new label that minimizes IGM transmission scatter

damping wing optical depth

$$\tau_{\rm DW}(\lambda_{\rm obs}) = \int_0^{R(z_{\rm QSO})} n_{\rm HI}^{\rm QSO}(R) \times \sigma_\alpha\left(\nu(R)\right) \, {\rm d}R$$

post-quasar HI density field

Lyα cross section

(velocity-weighted) HI column density

$$(N_{\rm HI})^w = \int_{R_{\rm min}}^{R_{\rm max}} n_{\rm HI}^{\rm gal}(R) \times w(R) \, {\rm d}R$$

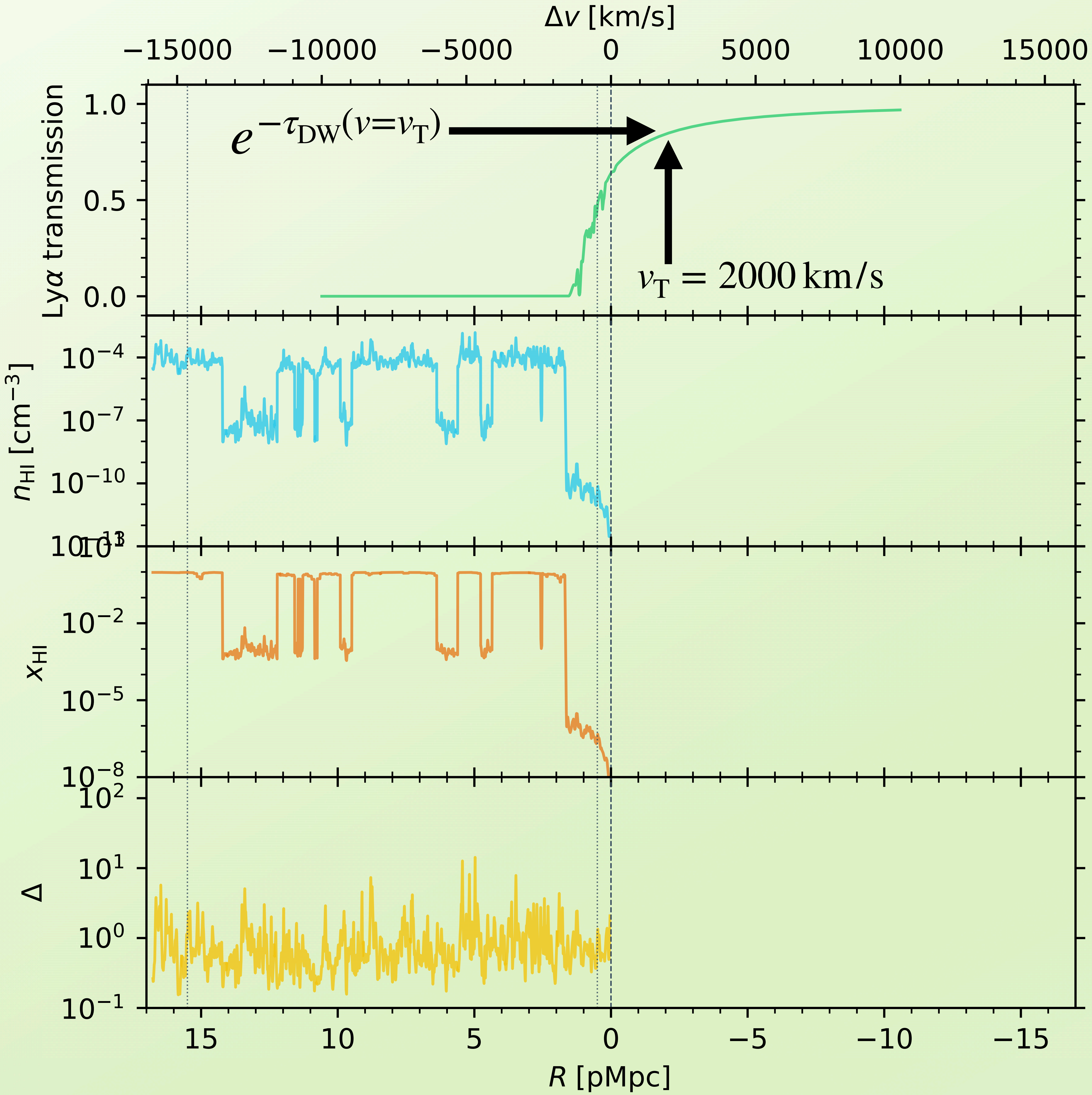

Constructing a new label that minimizes IGM transmission scatter

damping wing optical depth

$$\tau_{\rm DW}(\lambda_{\rm obs}) = \int_0^{R(z_{\rm QSO})} n_{\rm HI}^{\rm QSO}(R) \times \sigma_\alpha\left(\nu(R)\right) \, {\rm d}R$$

post-quasar HI density field

Lyα cross section $\simeq$ Lorentzian

(velocity-weighted) HI column density

$$(N_{\rm HI})^w = \int_{R_{\rm min}}^{R_{\rm max}} n_{\rm HI}^{\rm gal}(R) \times w(R) \, {\rm d}R$$

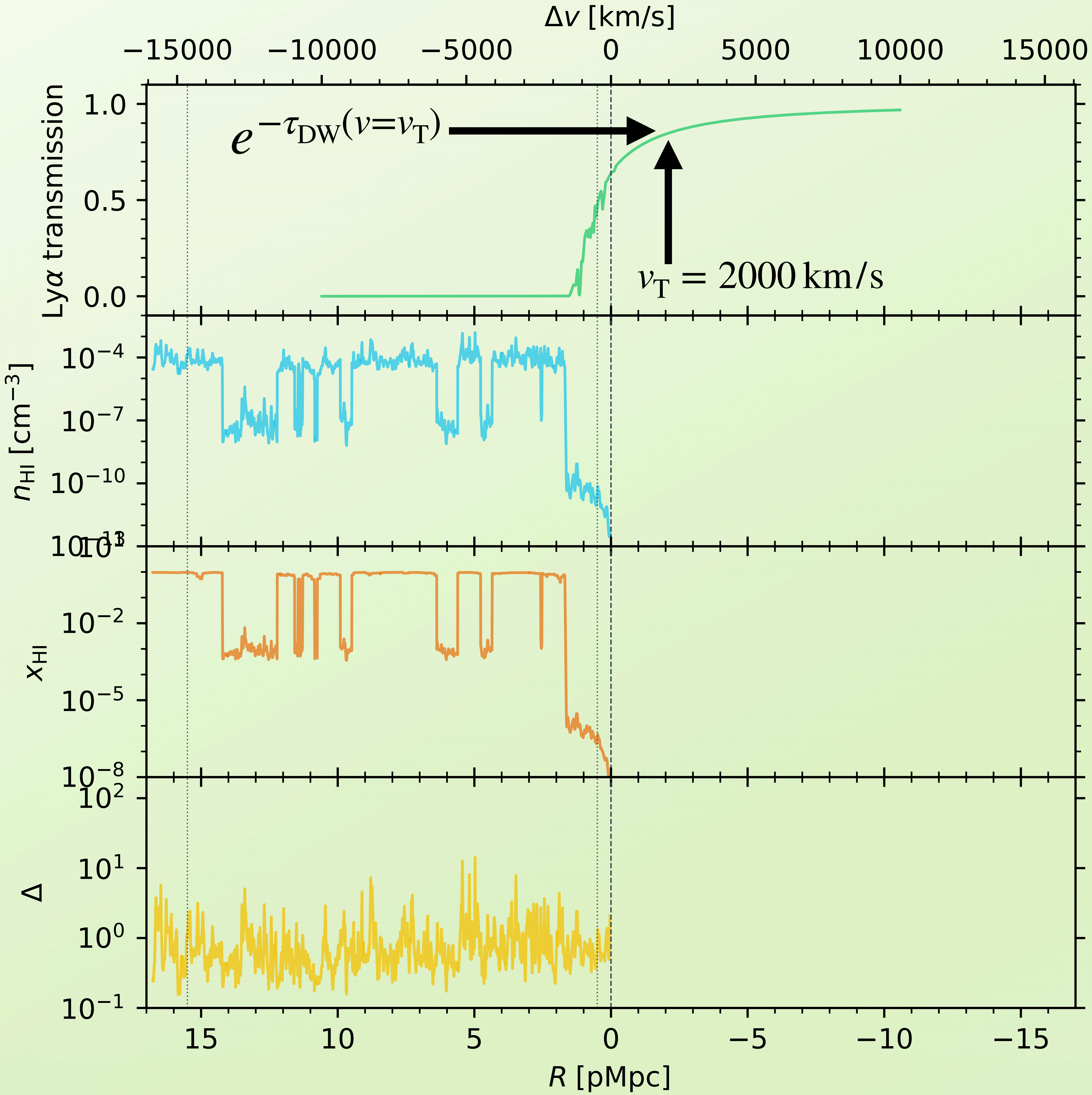

Constructing a new label that minimizes IGM transmission scatter

damping wing optical depth

$$\tau_{\rm DW}(\lambda_{\rm obs}) = \int_0^{R(z_{\rm QSO})} n_{\rm HI}^{\rm QSO}(R) \times \sigma_\alpha\left(\nu(R)\right) \, {\rm d}R$$

post-quasar HI density field

Lyα cross section $\simeq$ Lorentzian

(velocity-weighted) HI column density

$$(N_{\rm HI})^w = \int_{R_{\rm min}}^{R_{\rm max}} n_{\rm HI}^{\rm gal}(R) \times w(R) \, {\rm d}R$$

weighting function

$$w(R) \equiv \mathcal{N} \times (v - v_{\rm T})^{-2}$$

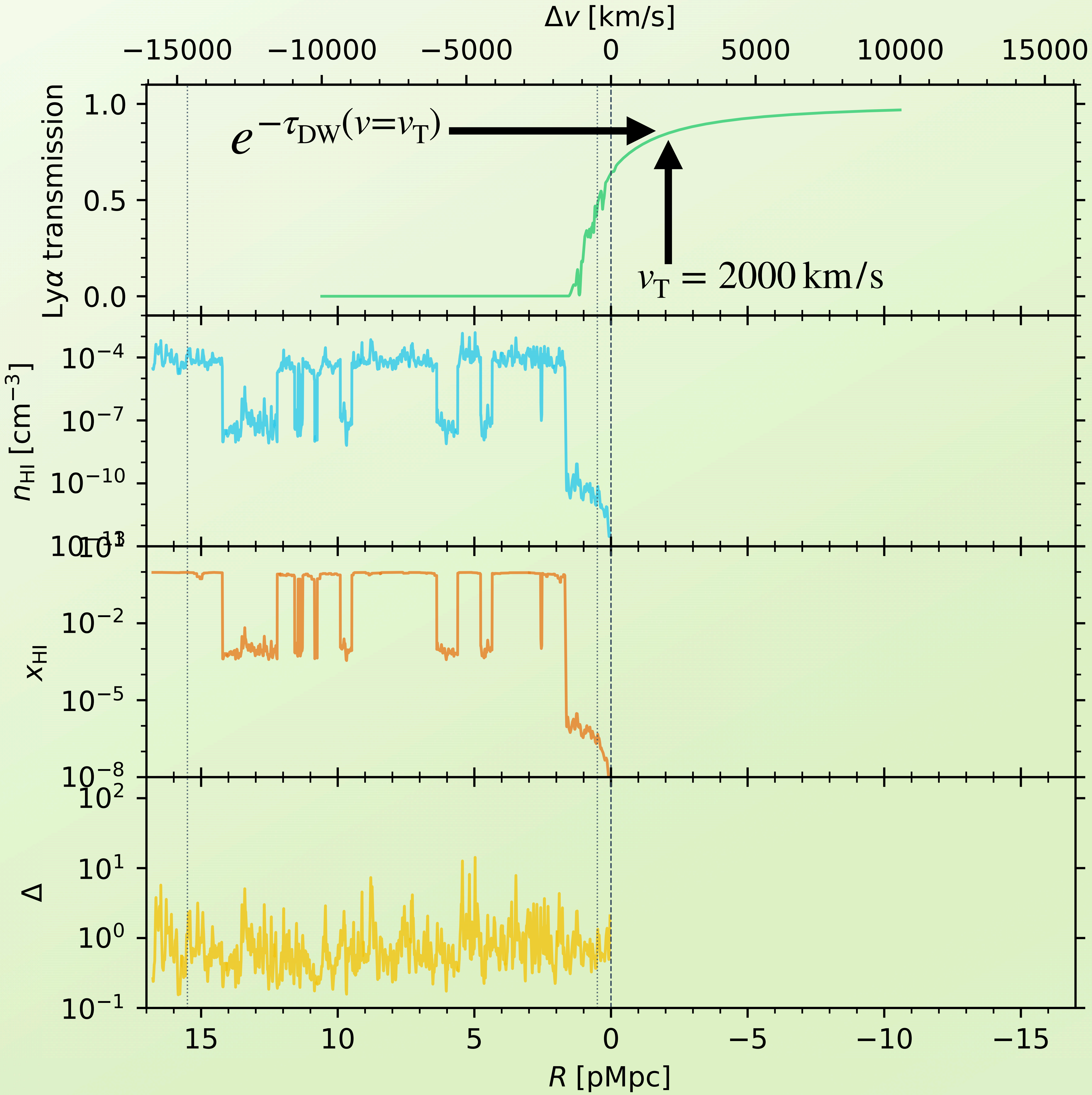

Constructing a new label that minimizes IGM transmission scatter

damping wing optical depth

$$\tau_{\rm DW}(\lambda_{\rm obs}) \;=\; \int_0^{R(z_{\rm QSO})} n_{\rm HI}^{\rm QSO}(R) \;\times\; \sigma_\alpha\left(\nu(R)\right)\; {\rm d}R$$

post-quasar HI density field

Lyα cross section $\simeq$ Lorentzian

(velocity-weighted) HI column density

15.5 pMpc

$$(N_{\rm HI})^w \;=\; \int_{R_{\rm min}}^{R_{\rm max}} n_{\rm HI}^{\rm gal}(R) \;\times\; w(R)\; {\rm d}R$$

0.5 pMpc

weighting function

$$w(R) \;\equiv\; \mathcal{N} \times (v - v_{\rm T})^{-2}$$

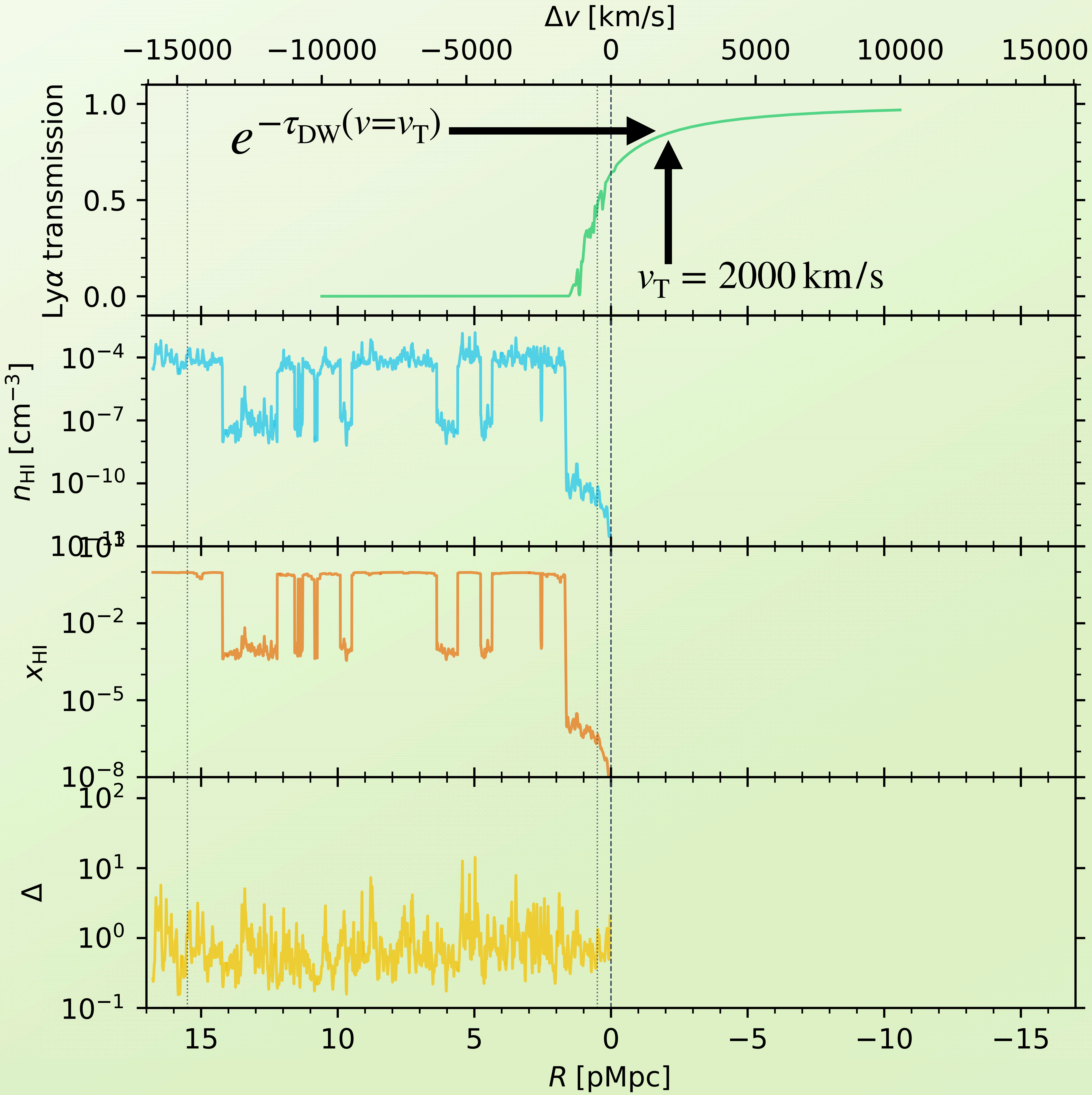

Constructing a new label that minimizes IGM transmission scatter

damping wing optical depth

$$\tau_{\rm DW}(\lambda_{\rm obs}) = \int_0^{R(z_{\rm QSO})} n_{\rm HI}^{\rm QSO}(R) \times \sigma_\alpha\left(\nu(R)\right)\, {\rm d}R$$

post-quasar HI density field
≃ pre-quasar HI density field

Lyα cross section
≃ Lorentzian

(velocity-weighted) HI column density

$$(N_{\rm HI})^w = \int_{R_{\rm min}}^{R_{\rm max}} n_{\rm HI}^{\rm gal}(R) \times w(R)\, {\rm d}R$$

$R_{\rm max}$: 15.5 pMpc

$R_{\rm min}$: 0.5 pMpc

weighting function

$$w(R) \equiv \mathcal{N} \times (v - v_{\rm T})^{-2}$$

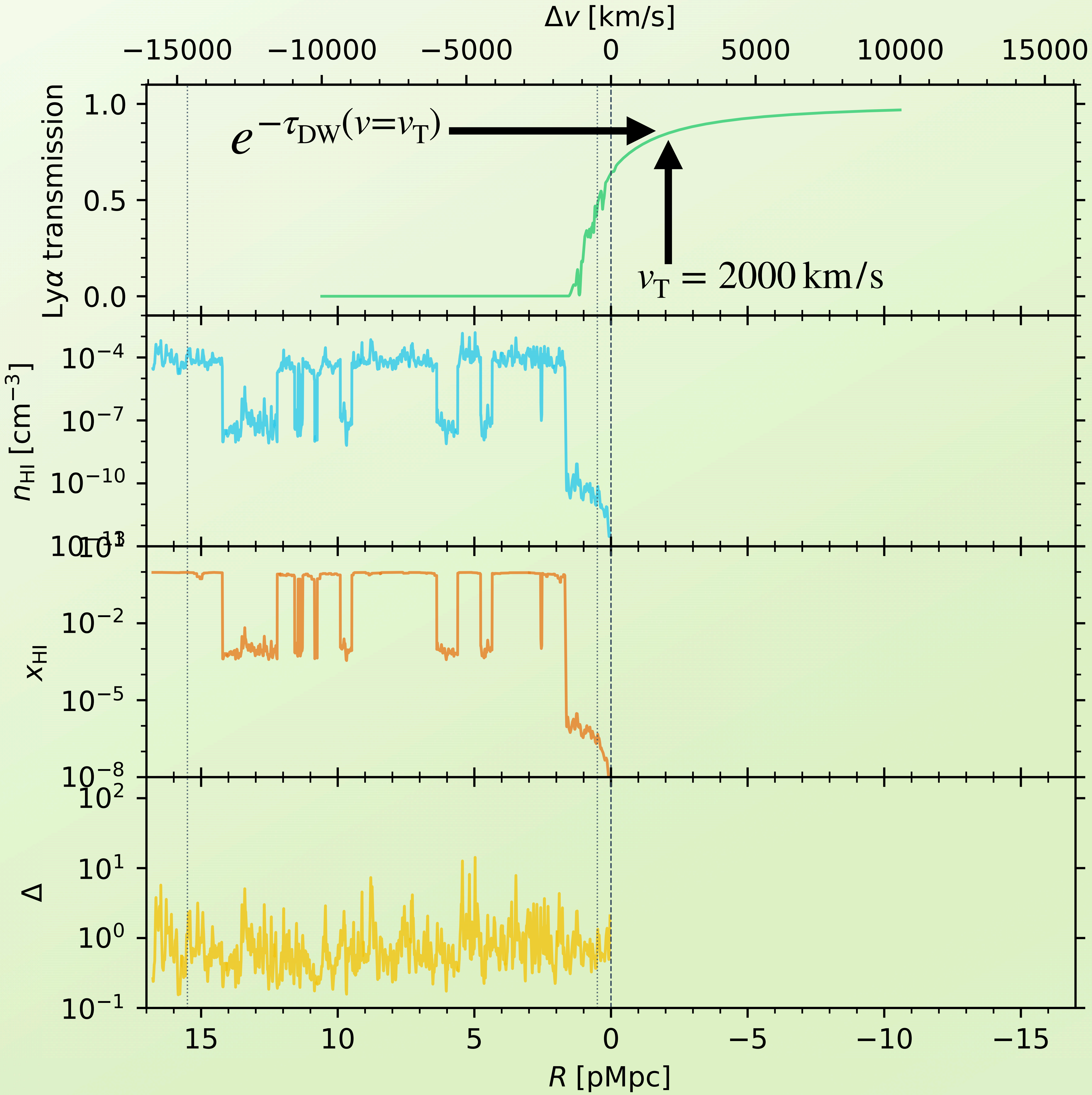

Constructing a new label that minimizes IGM transmission scatter

damping wing optical depth

$$\tau_{\rm DW}(\lambda_{\rm obs}) = \int_0^{R(z_{\rm QSO})} n_{\rm HI}^{\rm QSO}(R) \times \sigma_\alpha\left(\nu(R)\right)\, {\rm d}R$$

post-quasar HI density field $\simeq$ pre-quasar HI density field

Lyα cross section $\simeq$ Lorentzian

(velocity-weighted) HI column density

$$(N_{\rm HI})^w = \int_{R_{\rm min}}^{R_{\rm max}} n_{\rm HI}^{\rm gal}(R) \times w(R)\, {\rm d}R$$

$R_{\rm max}$: 15.5 pMpc

$R_{\rm min}$: 0.5 pMpc

weighting function

$$w(R) \equiv \mathcal{N} \times (v - v_{\rm T})^{-2}$$

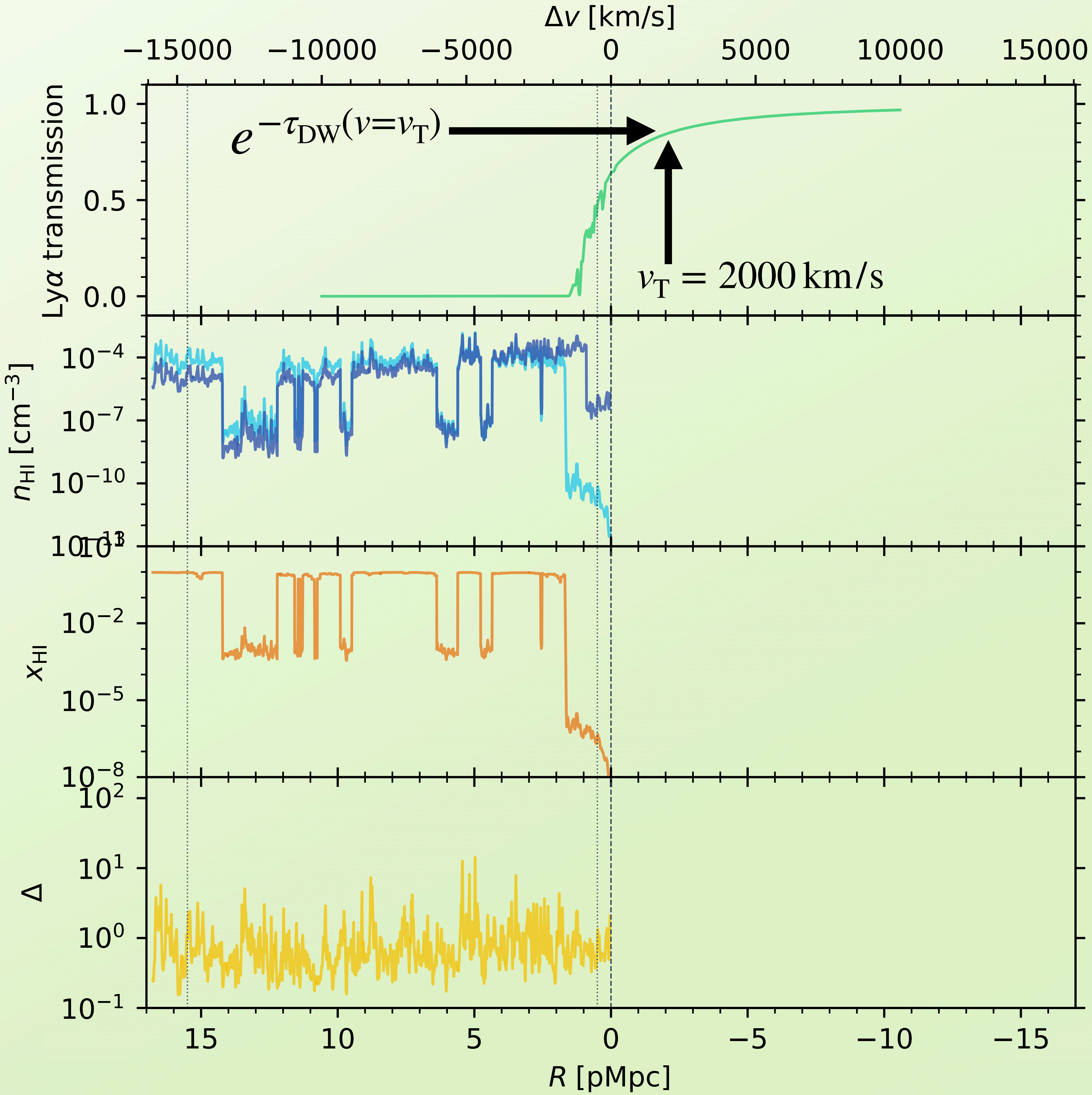

Constructing a new label that minimizes IGM transmission scatter

damping wing optical depth

$$\tau_{\rm DW}(\lambda_{\rm obs}) \;=\; \int_0^{R(z_{\rm QSO})} n_{\rm HI}^{\rm QSO}(R) \;\times\; \sigma_\alpha\left(\nu(R)\right)\; {\rm d}R$$

post-quasar HI density field
≃ pre-quasar HI density field

Lyα cross section
≃ Lorentzian

(velocity-weighted) HI column density

15.5 pMpc → $R_{\rm max}$

0.5 pMpc → $R_{\rm min}$

$$(N_{\rm HI})^w \;=\; \int_{R_{\rm min}}^{R_{\rm max}} n_{\rm HI}^{\rm gal}(R) \;\times\; w(R)\,{\rm d}R$$

weighting function

$$w(R) \;\equiv\; \mathcal{N} \times (v - v_{\rm T})^{-2}$$

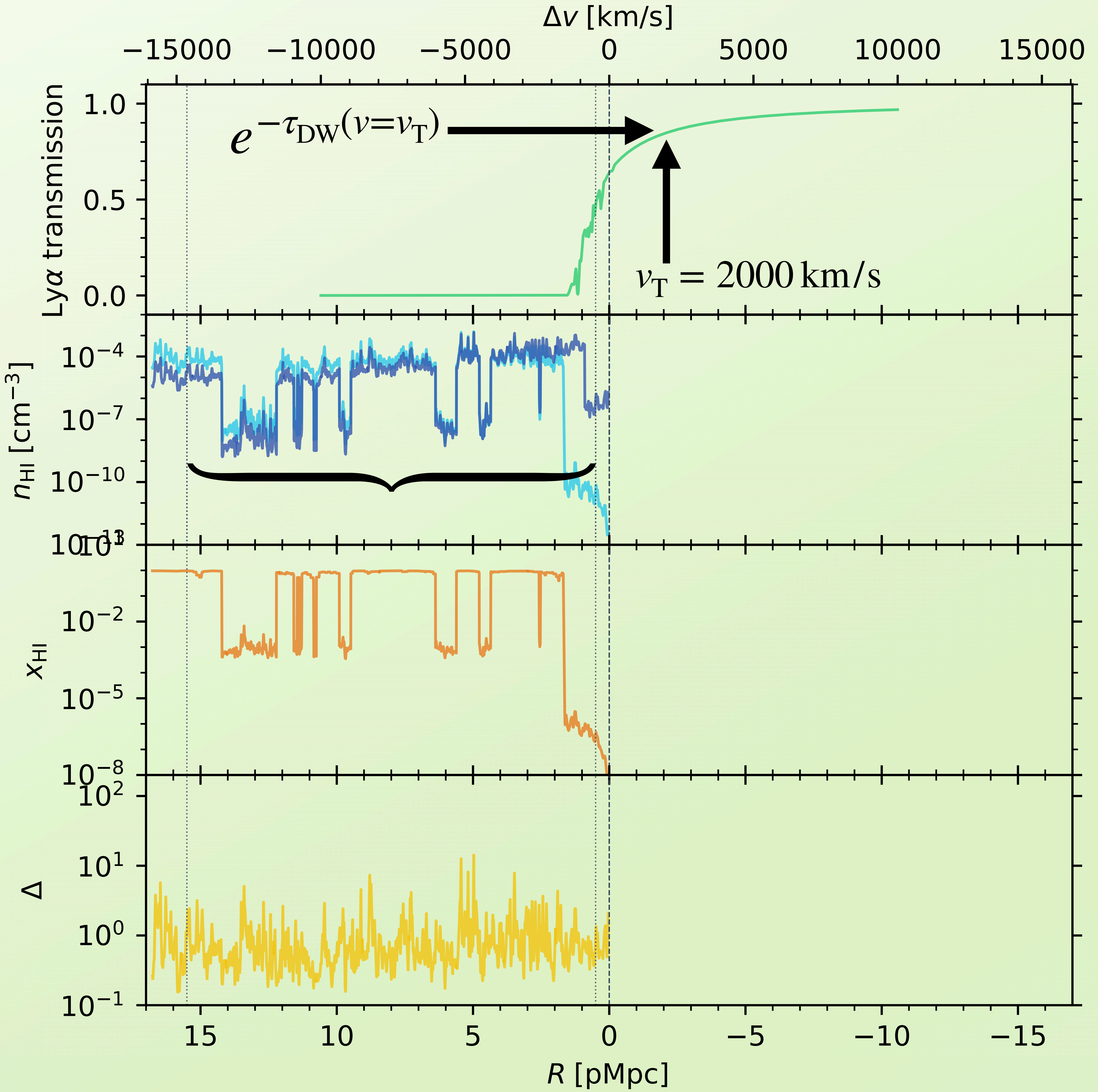

Constructing a new label that minimizes IGM transmission scatter

damping wing optical depth

$$\tau_{\rm DW}(\lambda_{\rm obs}) \;=\; \int_0^{R(z_{\rm QSO})} n_{\rm HI}^{\rm QSO}(R) \,\times\, \sigma_\alpha\left(\nu(R)\right)\; {\rm d}R$$

post-quasar HI density field
$\simeq$ pre-quasar HI density field

Lyα cross section
$\simeq$ Lorentzian

(velocity-weighted) HI column density

$$(N_{\rm HI})^w \;=\; \int_{R_{\rm min}}^{R_{\rm max}} n_{\rm HI}^{\rm gal}(R) \,\times\, w(R)\,{\rm d}R$$

$R_{\rm max}$ = 15.5 pMpc

$R_{\rm min}$ = 0.5 pMpc

weighting function

$$w(R) \equiv \mathcal{N} \times (v - v_{\rm T})^{-2}$$

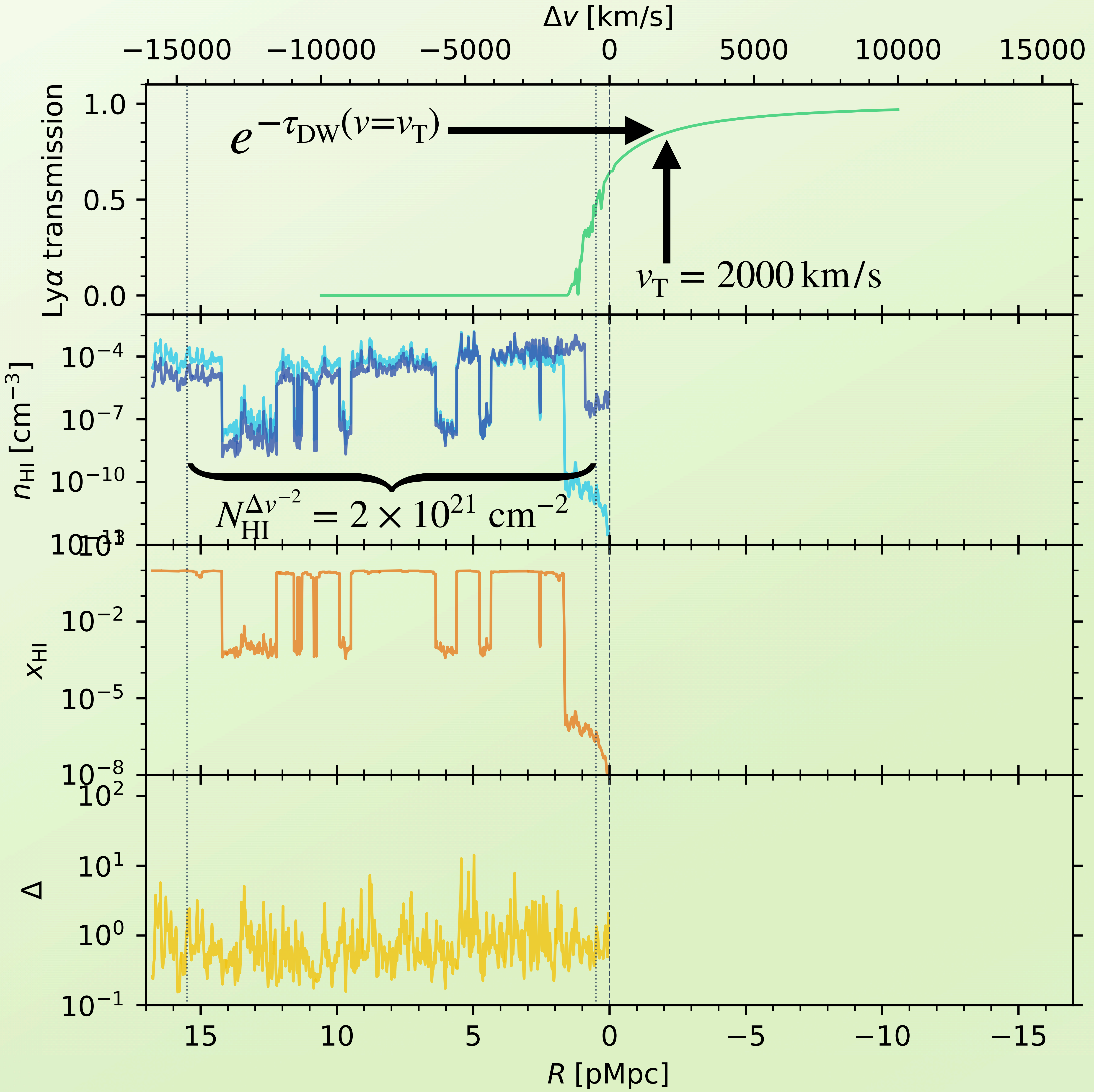

Constructing a new label that minimizes IGM transmission scatter

damping wing optical depth

$$\tau_{\mathrm{DW}}(\lambda_{\mathrm{obs}}) = \int_0^{R(z_{\mathrm{QSO}})} n_{\mathrm{HI}}^{\mathrm{QSO}}(R) \times \sigma_\alpha\big(\nu(R)\big)\ \mathrm{d}R$$

post-quasar HI density field
≃ pre-quasar HI density field

Lyα cross section
≃ Lorentzian

(velocity-weighted) HI column density

$$(N_{\mathrm{HI}})^w = \int_{R_{\mathrm{min}}}^{R_{\mathrm{max}}} n_{\mathrm{HI}}^{\mathrm{gal}}(R) \times w(R)\,\mathrm{d}R$$

R_{max}: 15.5 pMpc

R_{min}: 0.5 pMpc

weighting function

$$w(R) \equiv \mathcal{N} \times (v - v_{\mathrm{T}})^{-2}$$

$$\tau_{\mathrm{DW}}(v = v_{\mathrm{T}}) = \ldots \simeq \frac{e^2}{m_e c}\frac{f_\alpha \gamma_\alpha}{\nu_\alpha}\frac{(c/H(z_{\mathrm{QSO}}) - R_{\mathrm{T}})^2}{(R_{\mathrm{max}} + R_{\mathrm{T}})(R_{\mathrm{min}} + R_{\mathrm{T}})} \times N_{\mathrm{HI}}^{\Delta v^{-2}}$$

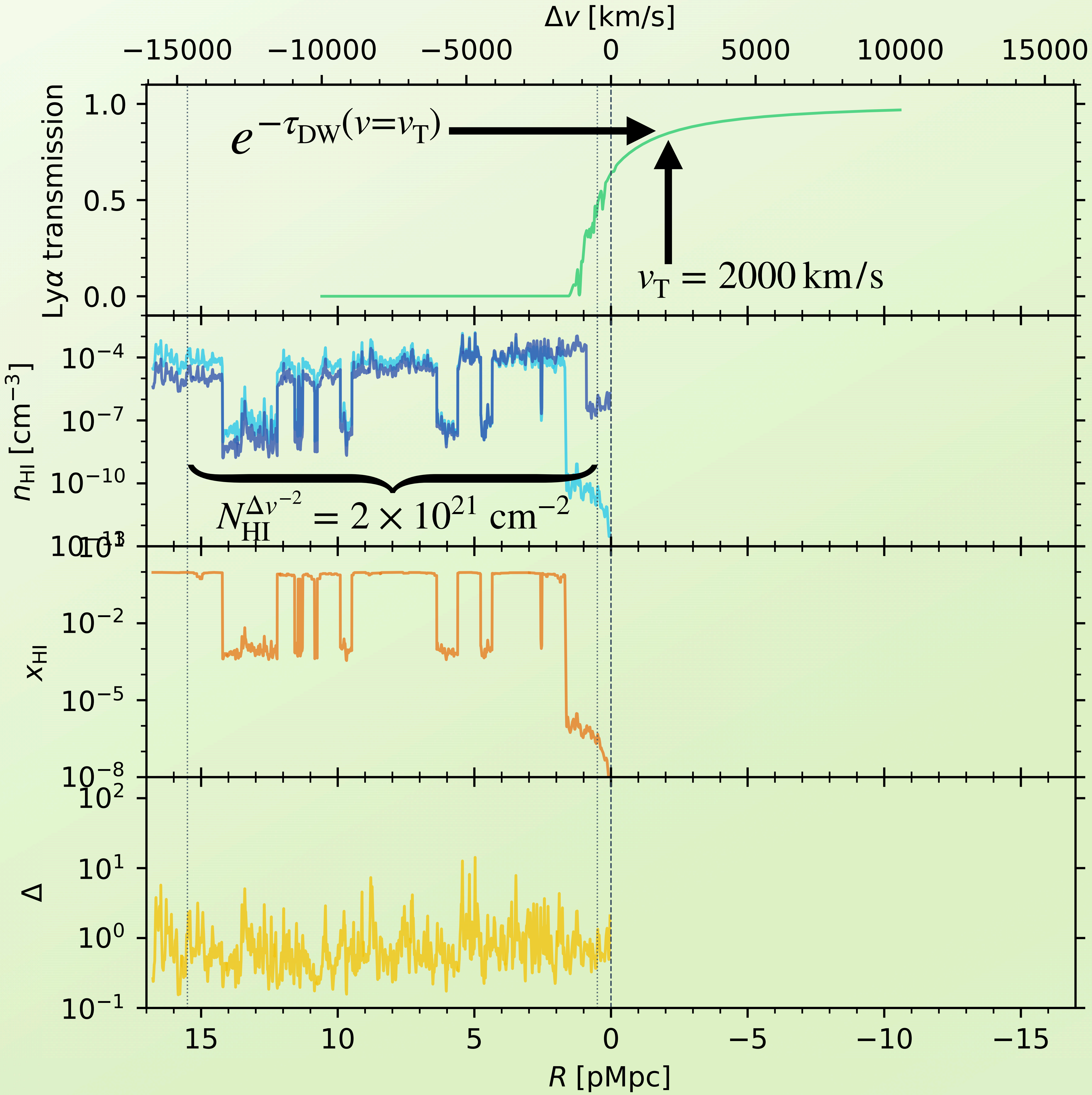

Comparing the old and new labels

Global IGM neutral fraction $\langle x_{\rm HI} \rangle$

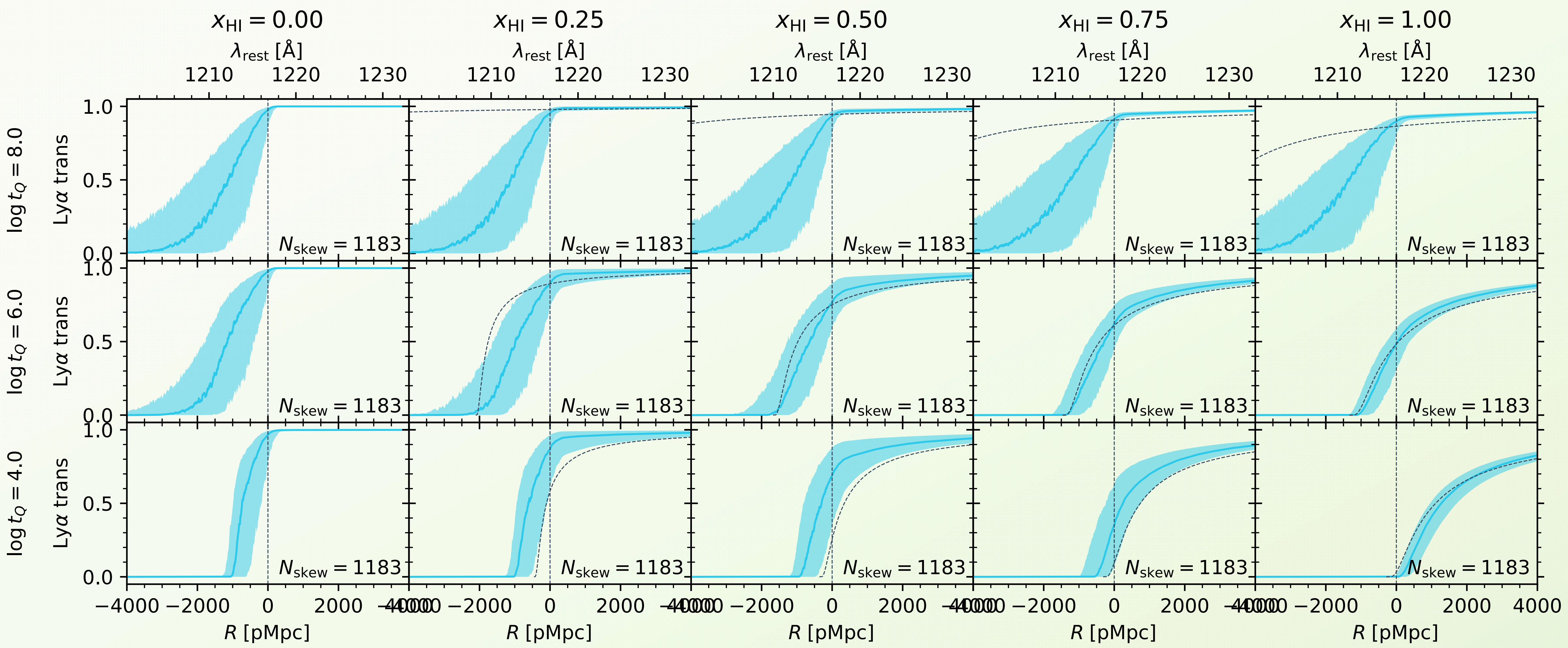

Local HI column density $N_{\rm HI}^{\Delta v^{-2}}$

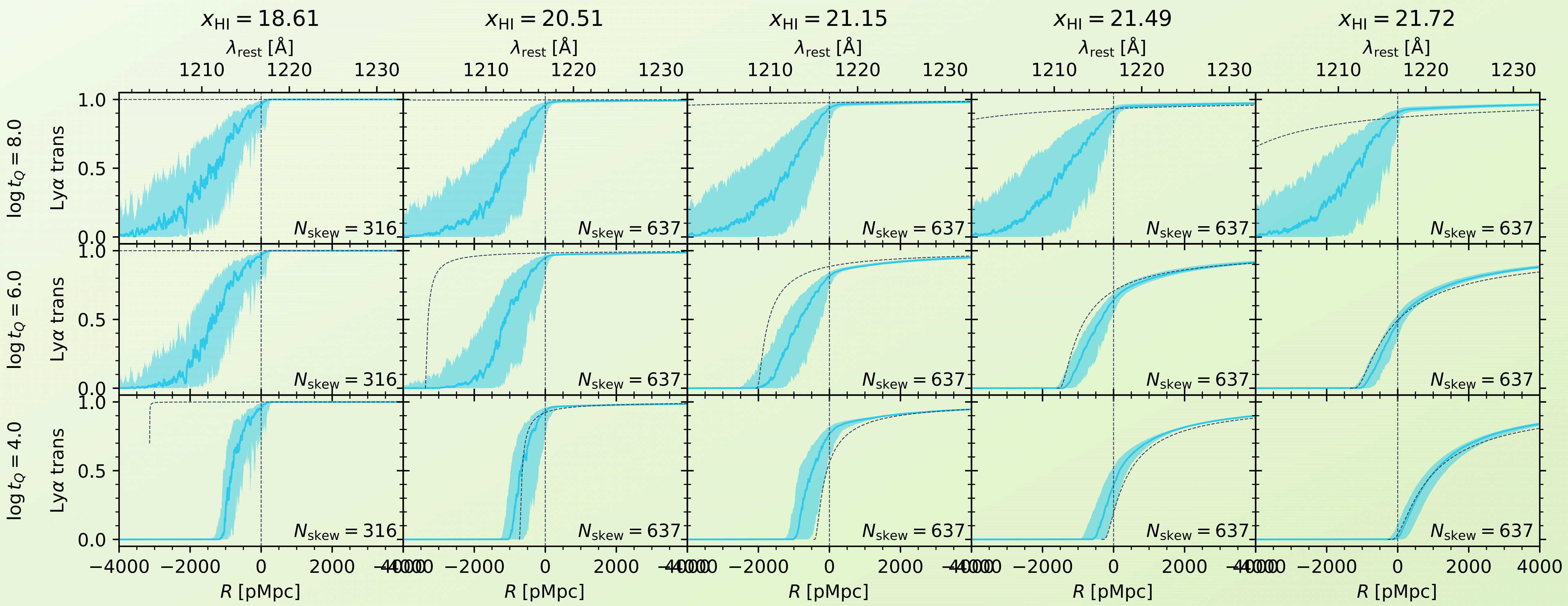

Comparing the old and new labels

Global IGM neutral fraction $\langle x_{\rm HI} \rangle$

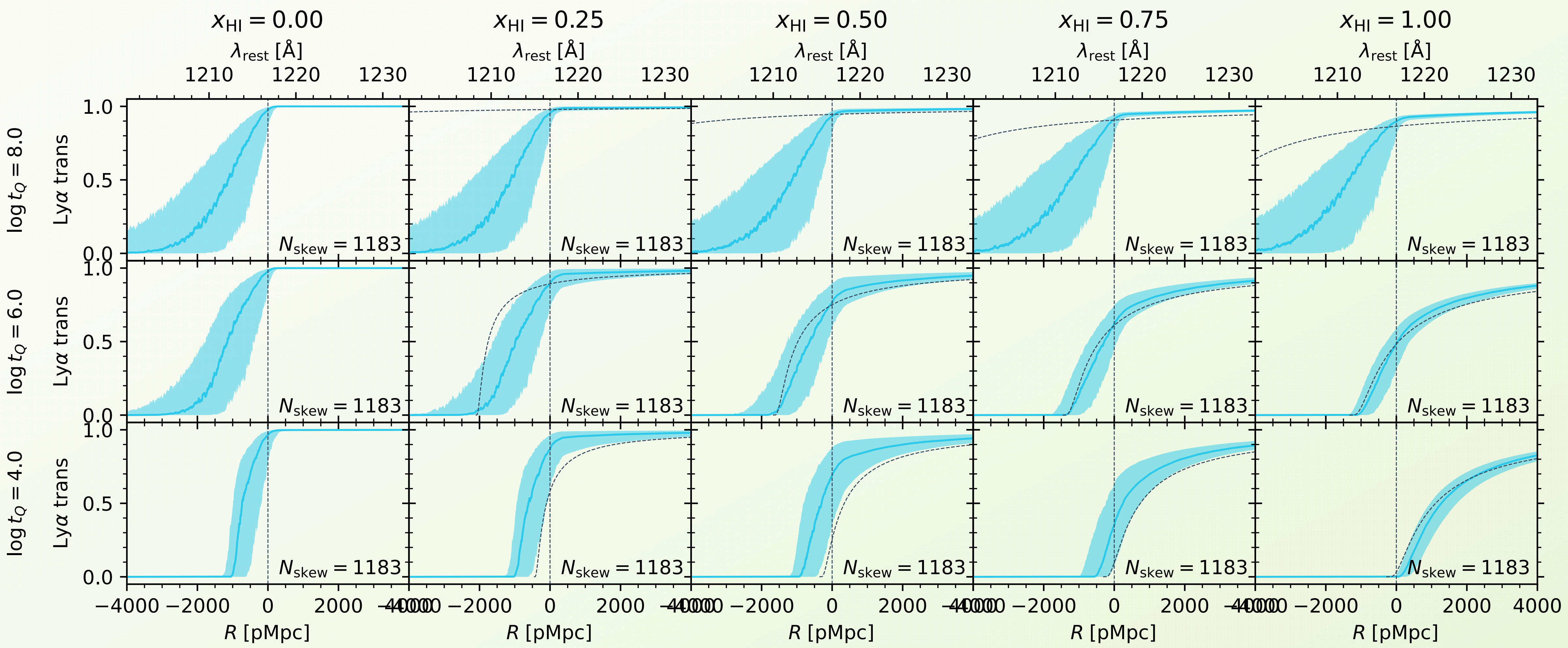

Local HI column density $N_{\rm HI}^{\Delta v^{-2}}$

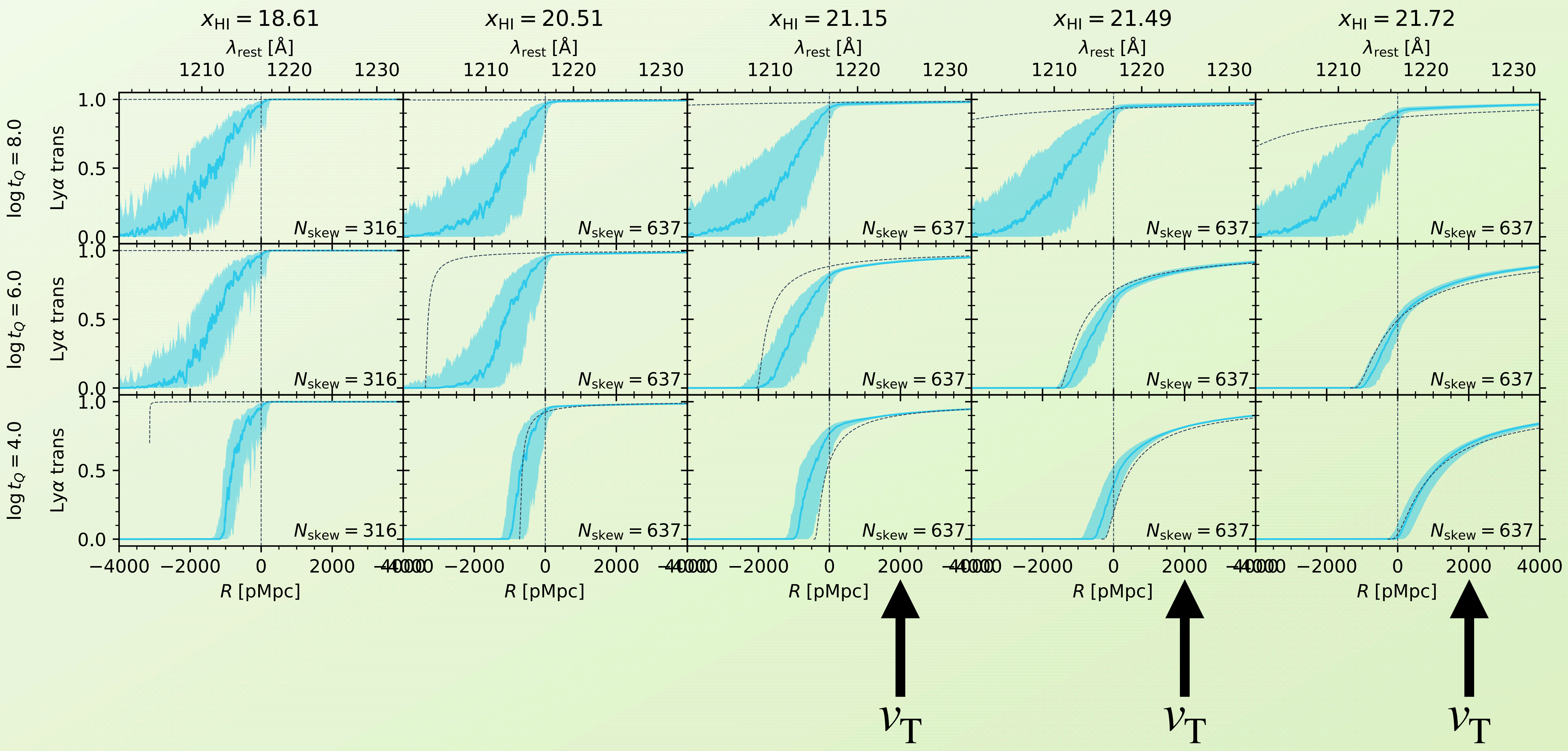

Comparing the old and new labels

Global IGM neutral fraction $\langle x_{\rm HI} \rangle$

Local HI column density $N_{\rm HI}^{\Delta v^{-2}}$

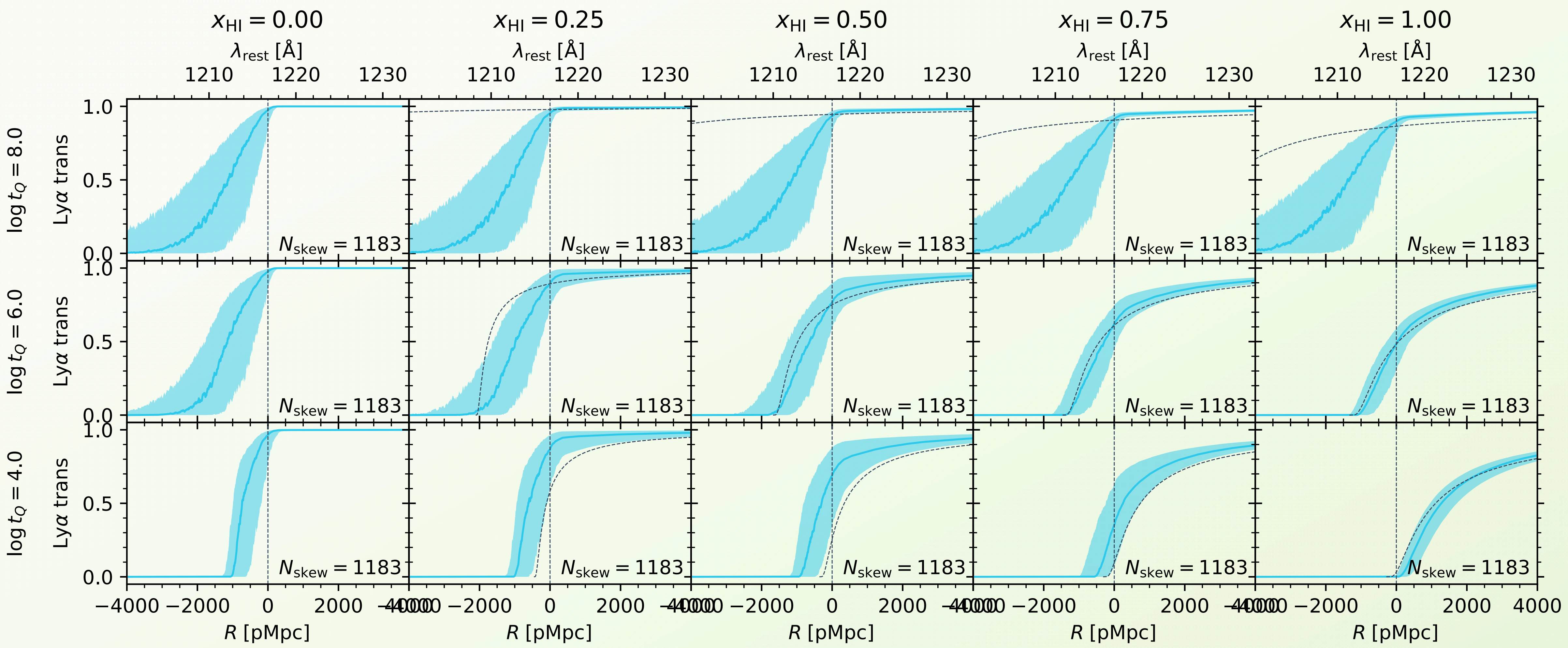

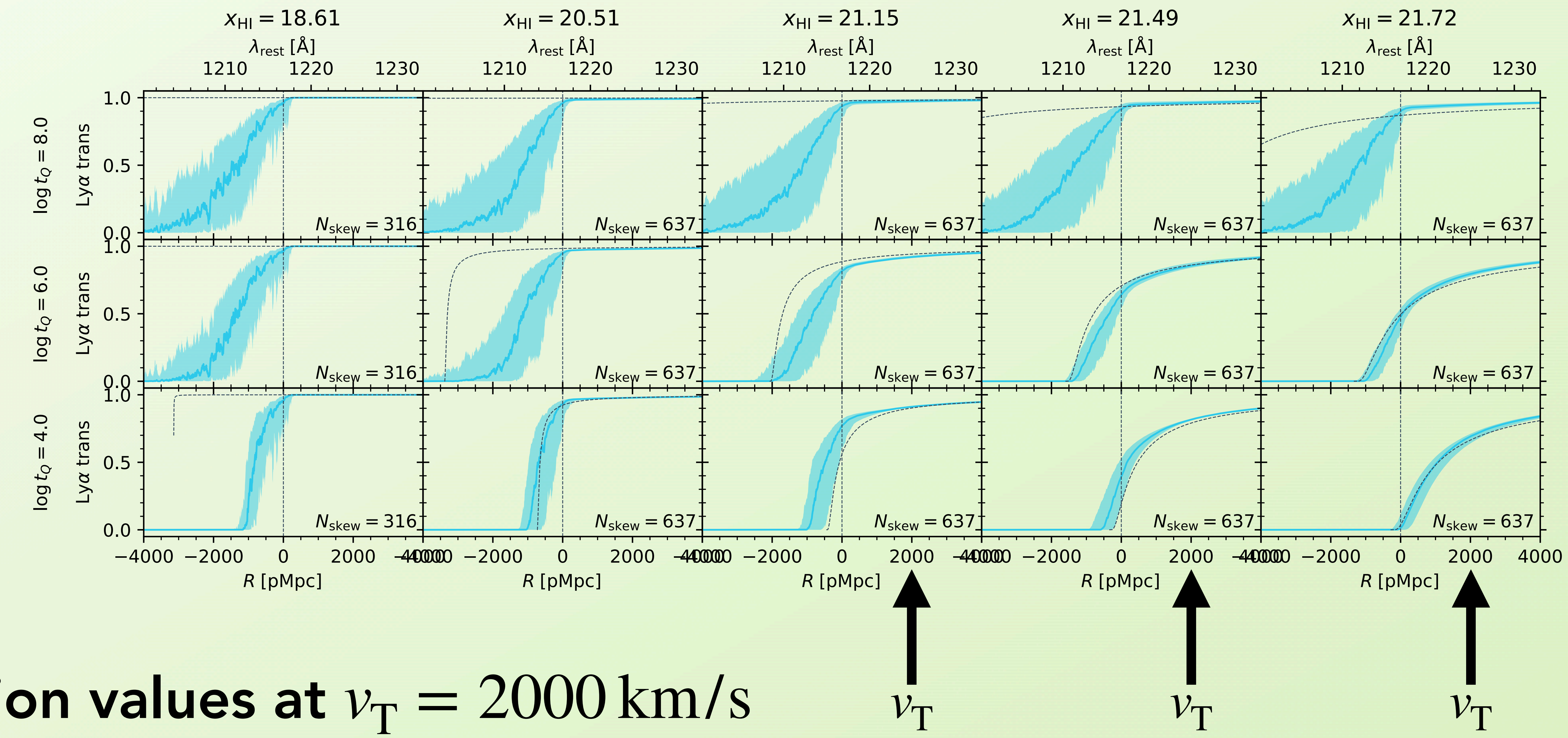

distribution of transmission values at $v_{\rm T} = 2000\,{\rm km/s}$

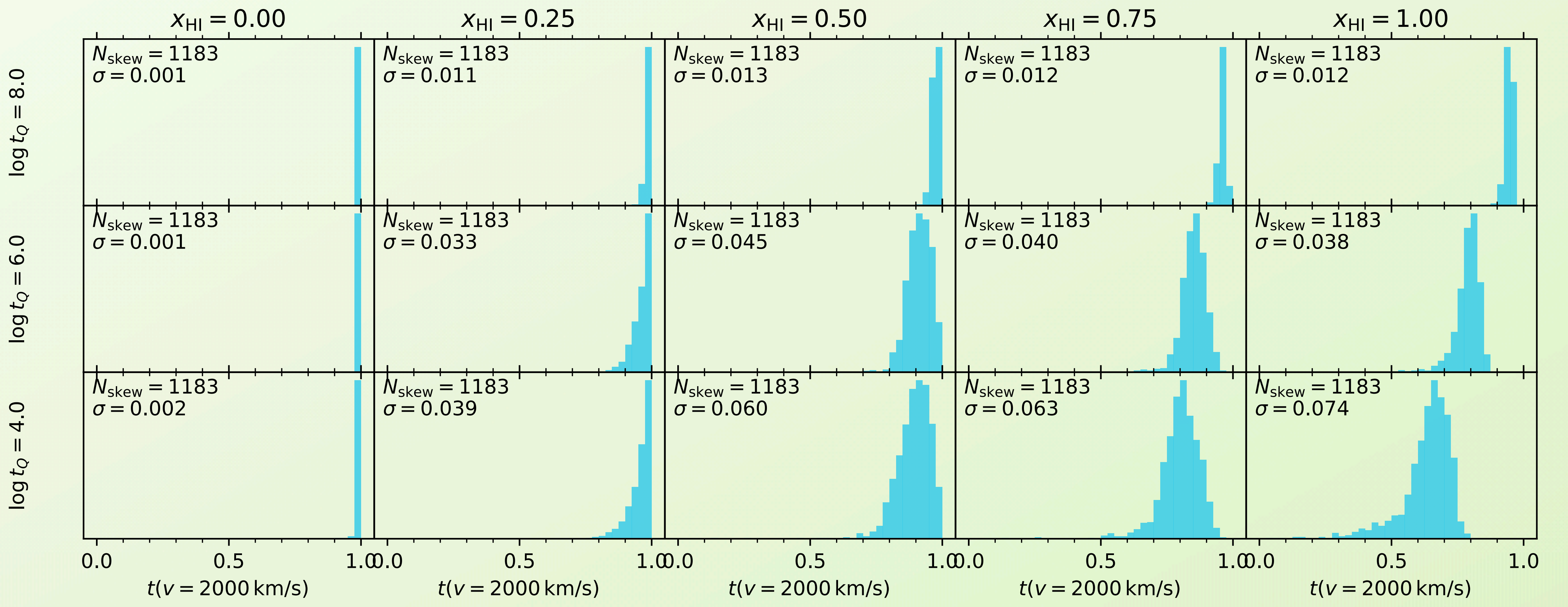

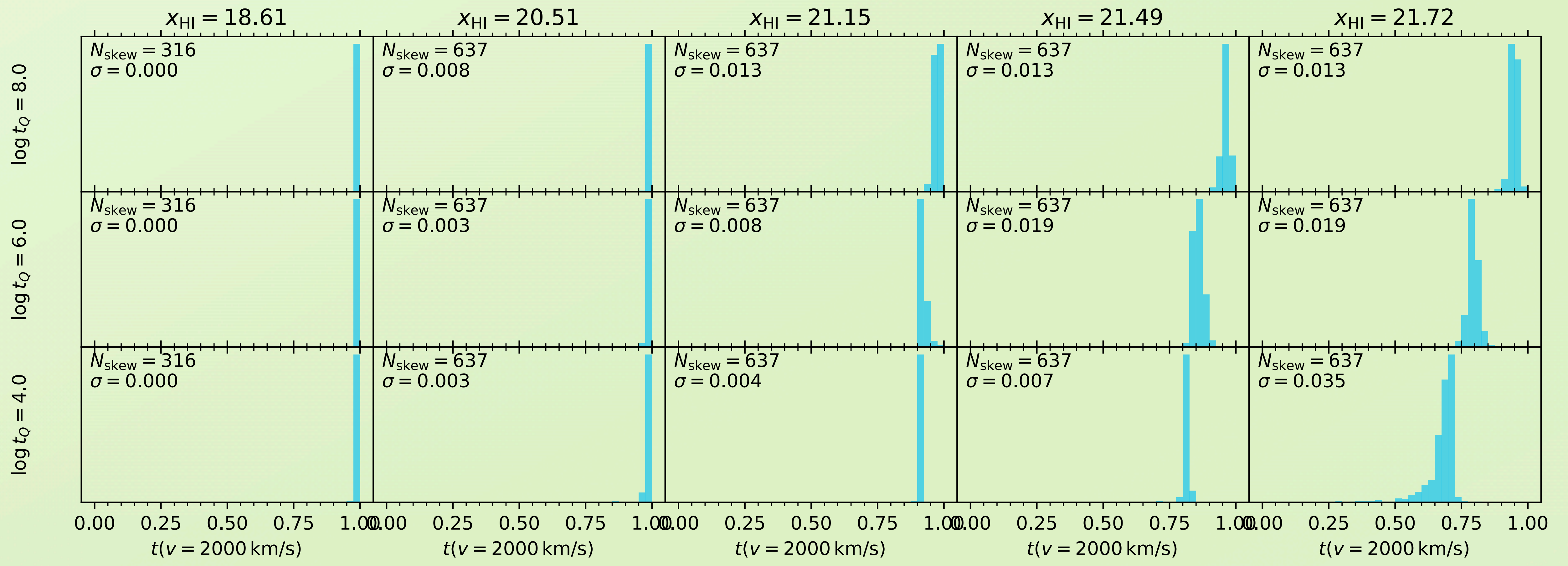

Comparing the old and new labels

Global IGM neutral fraction $\langle x_{\rm HI} \rangle$

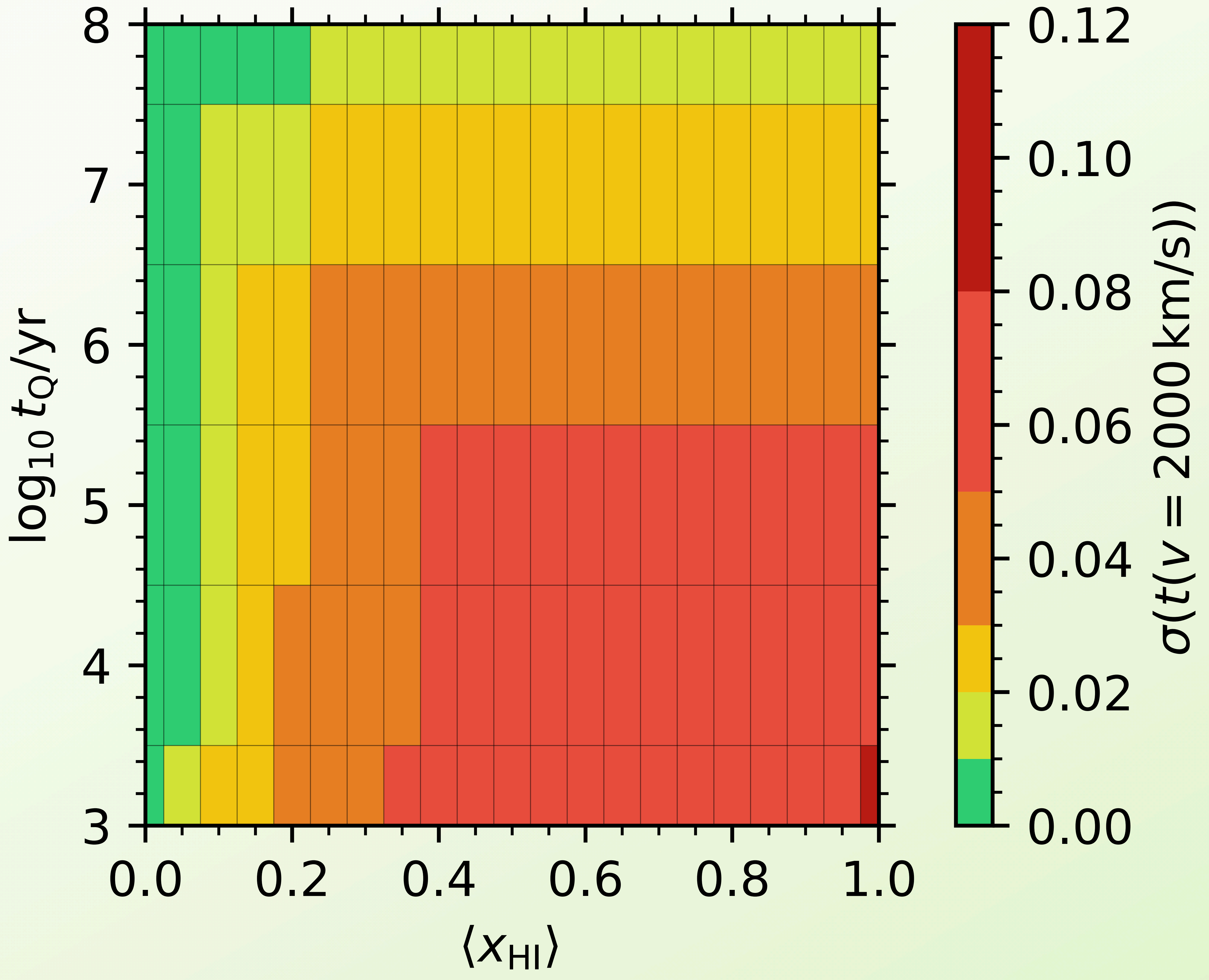

Local HI column density $N_{\rm HI}^{\Delta v^{-2}}$

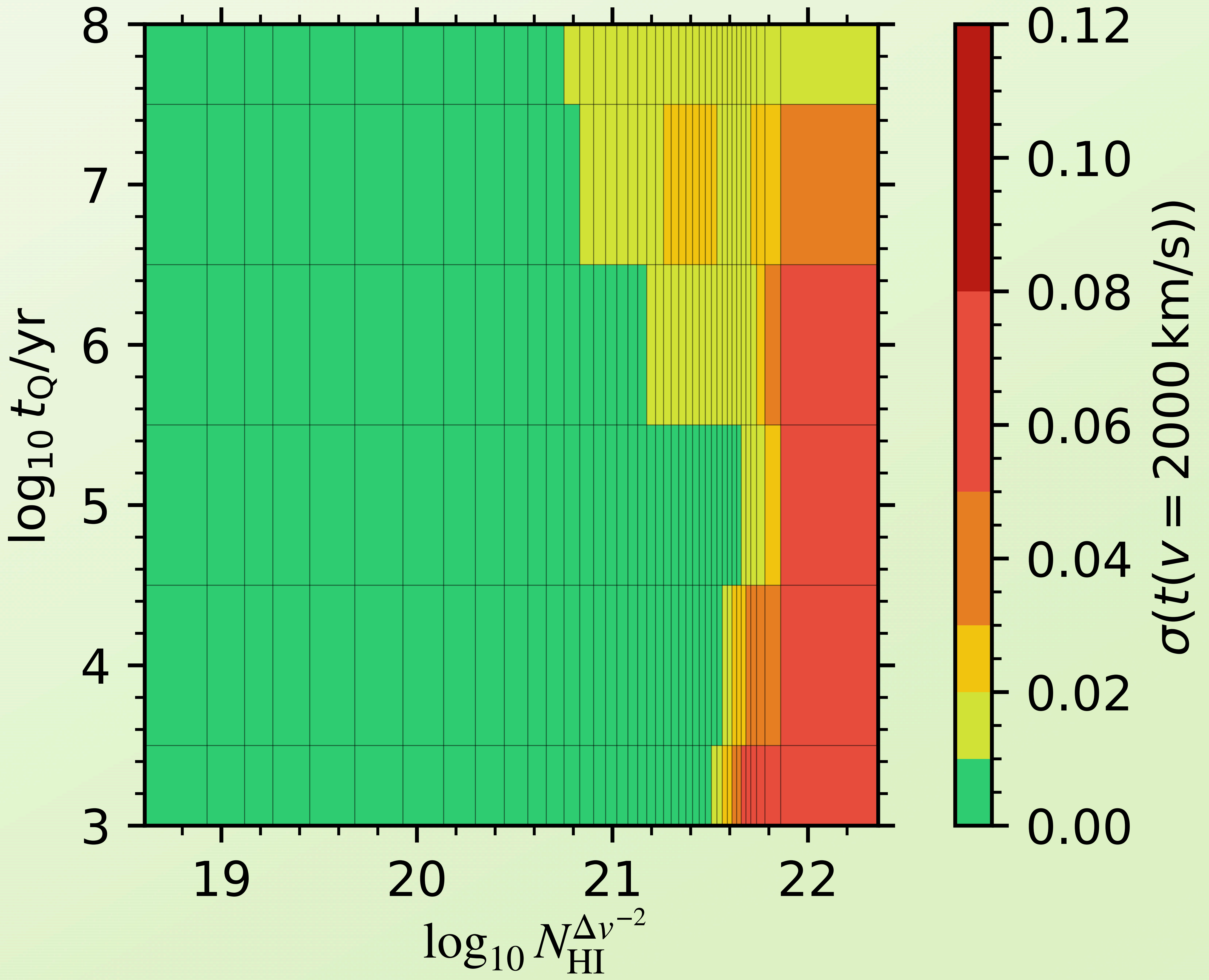

Comparing the old and new labels

Global IGM neutral fraction $\langle x_{\rm HI} \rangle$

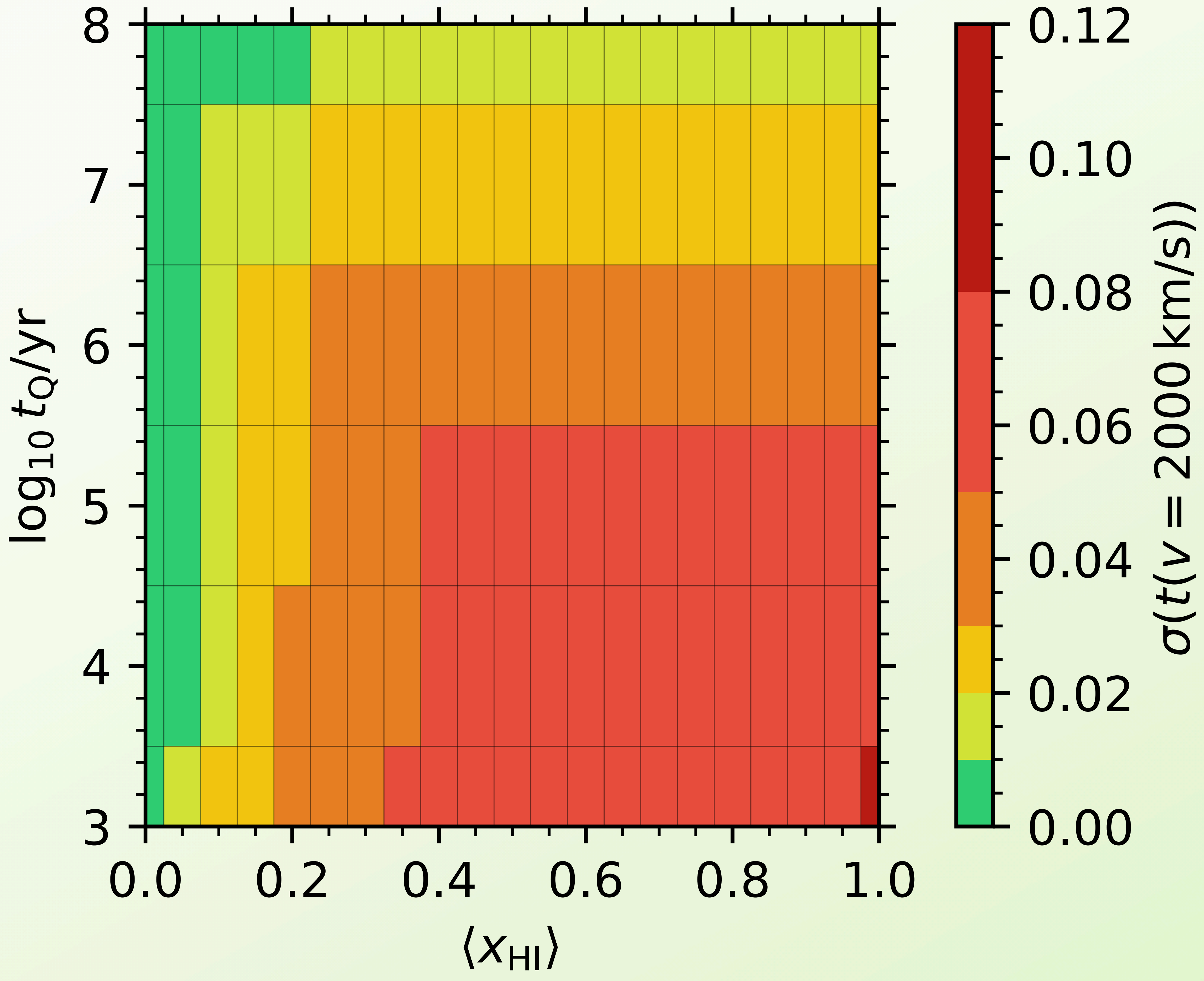

Local HI column density $N_{\rm HI}^{\Delta v^{-2}}$

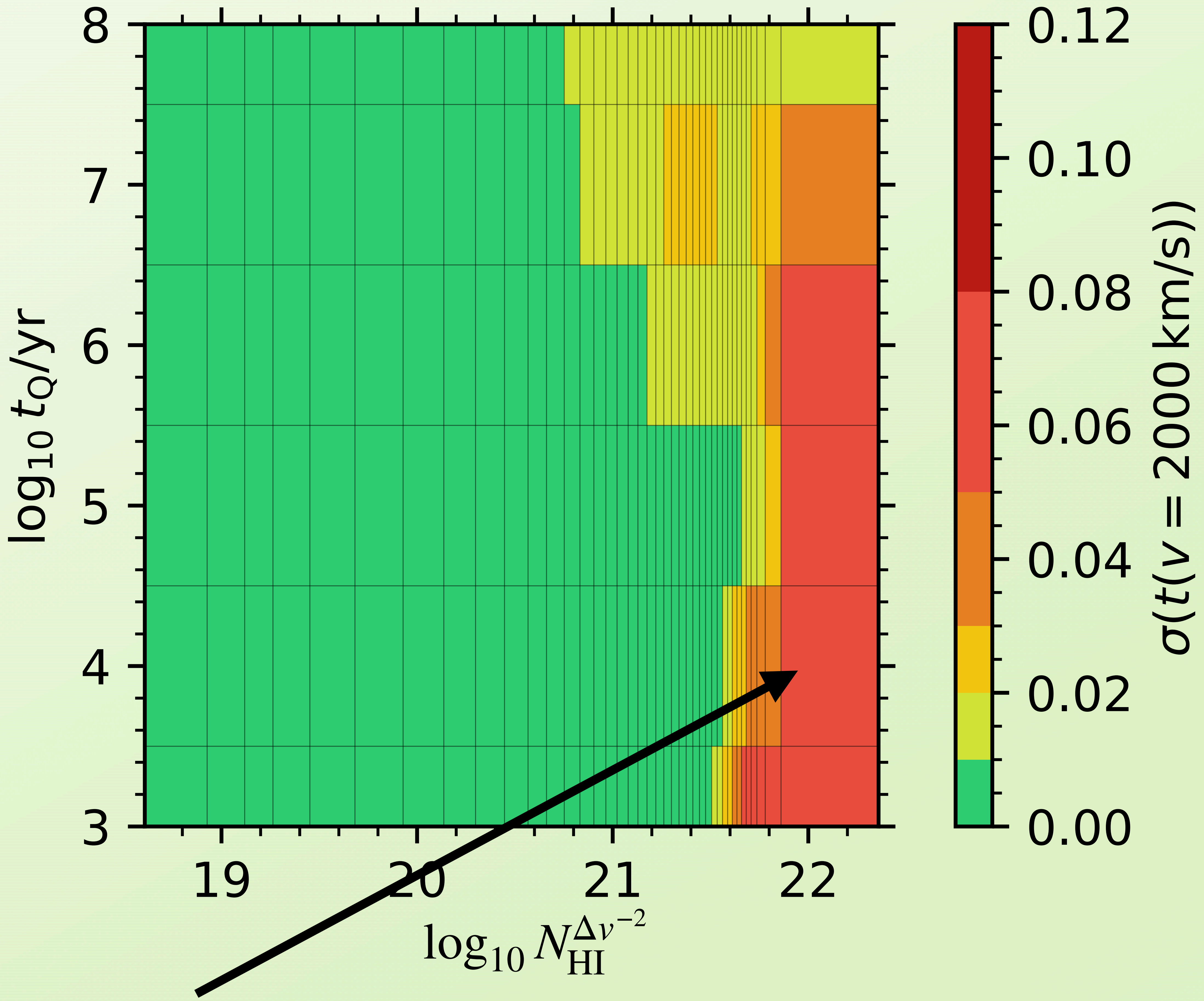

Comparing the old and new labels

Global IGM neutral fraction $\langle x_{\mathrm{HI}} \rangle$

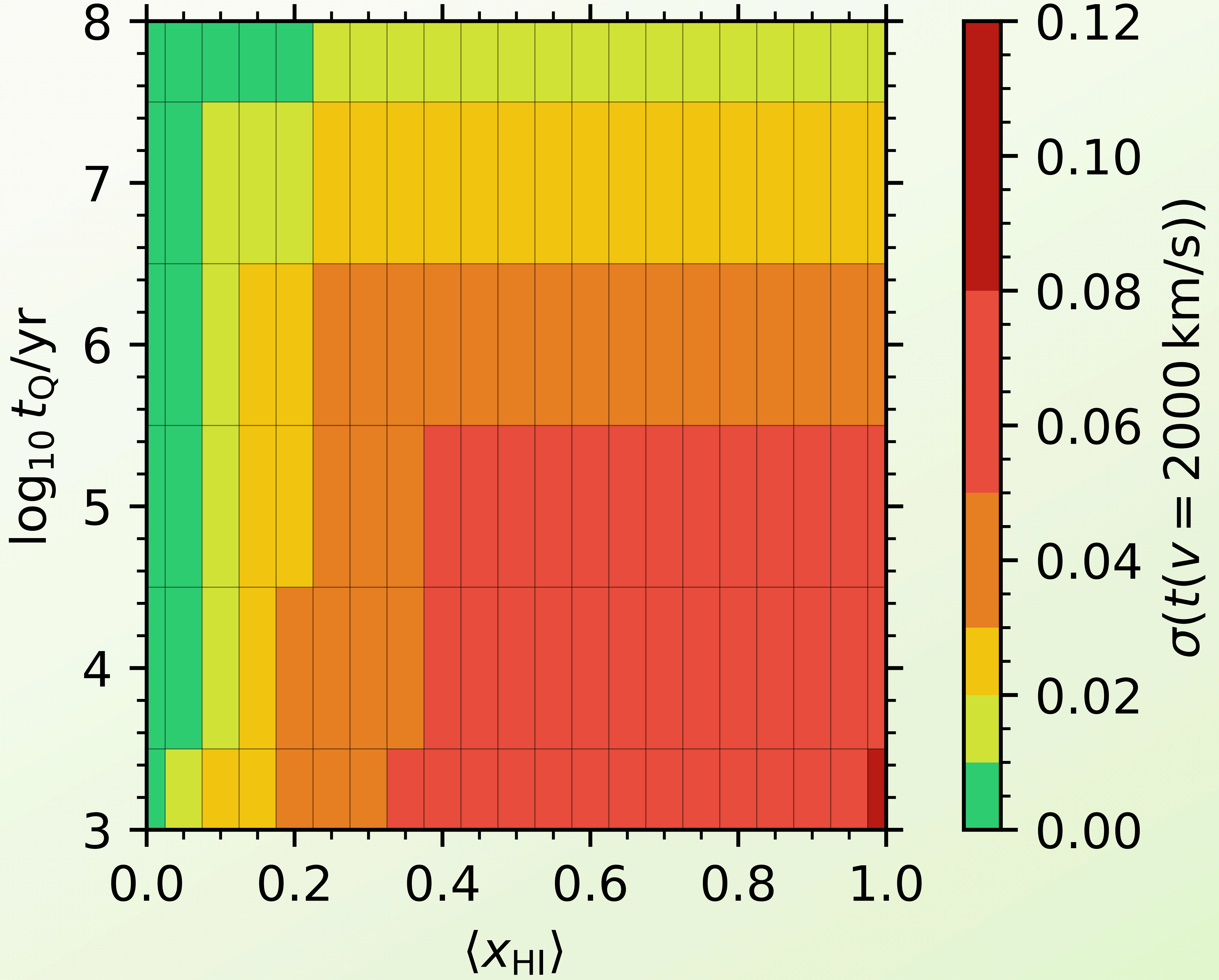

Local HI column density $N_{\mathrm{HI}}^{\Delta v^{-2}}$

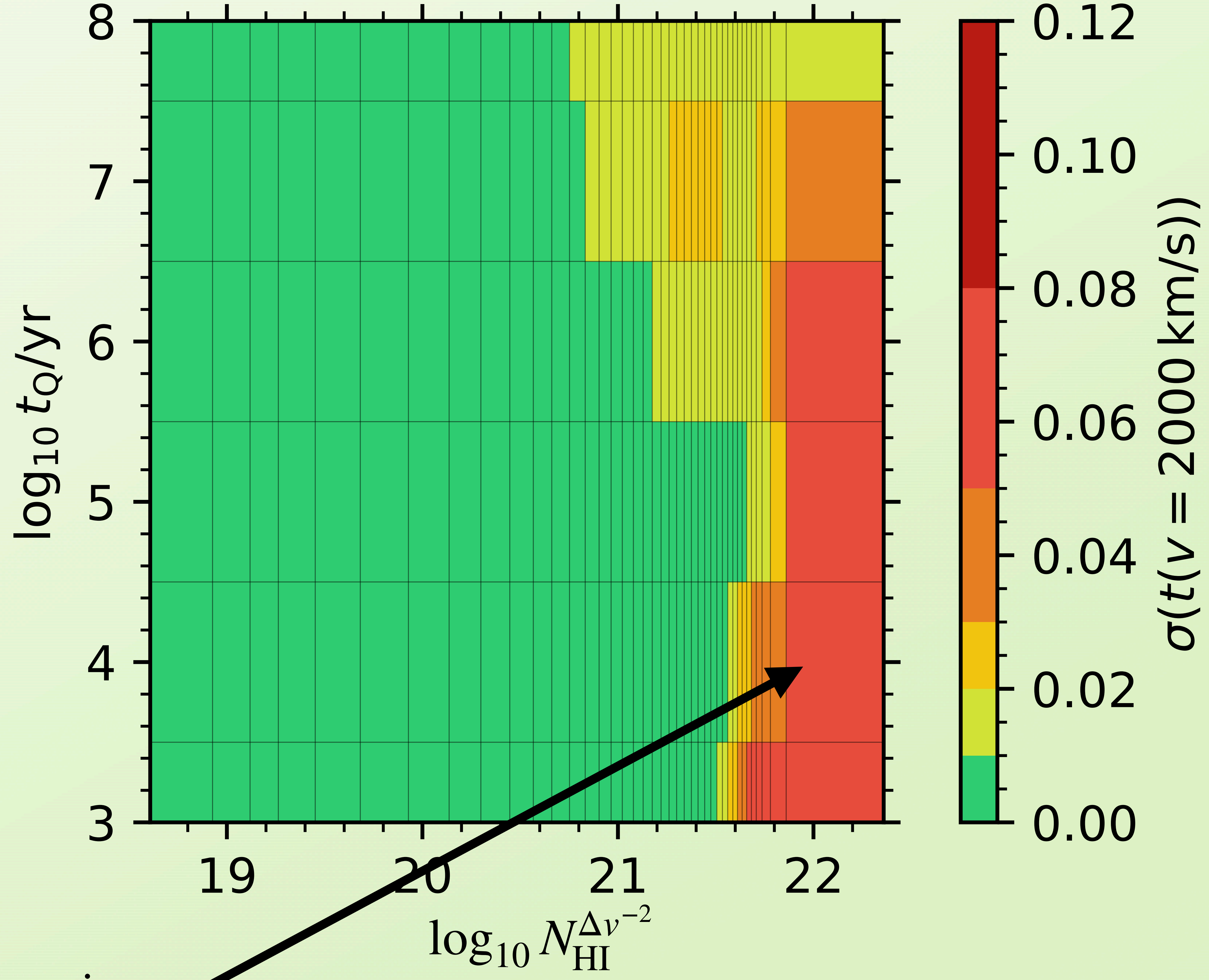

Strongest damping wings

→ impacted by structure at < 0.5 pMpc

Relating the old and new labels

$N_{\mathrm{HI}}^{\Delta v^{-2}}$ distribution based on skewers extracted from a uniform grid covering $0 \leq \langle x_{\mathrm{HI}} \rangle \leq 1$

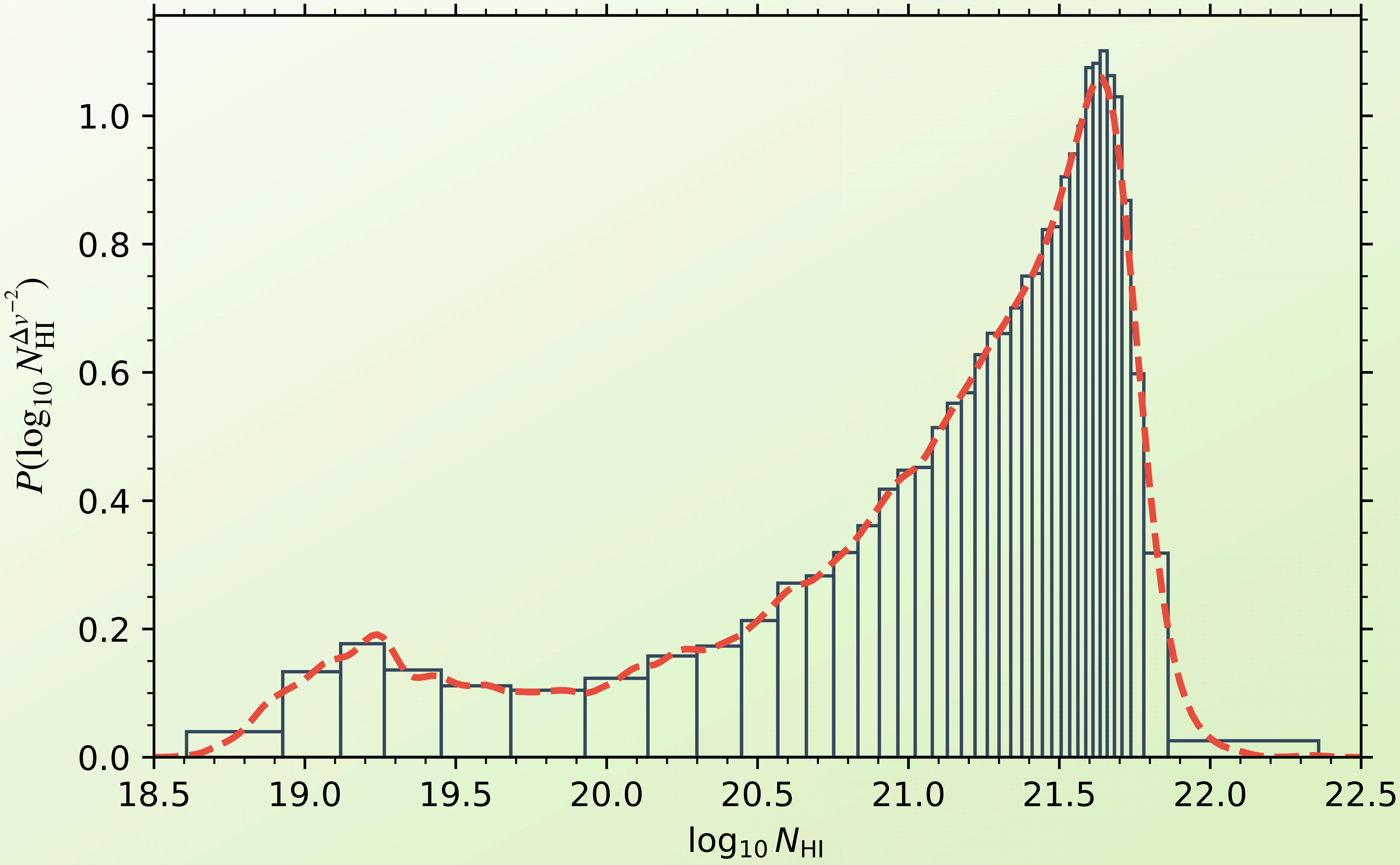

Relating the old and new labels

$N_{\mathrm{HI}}^{\Delta v^{-2}}$ **distribution at given** $\langle x_{\mathrm{HI}} \rangle$ **values**

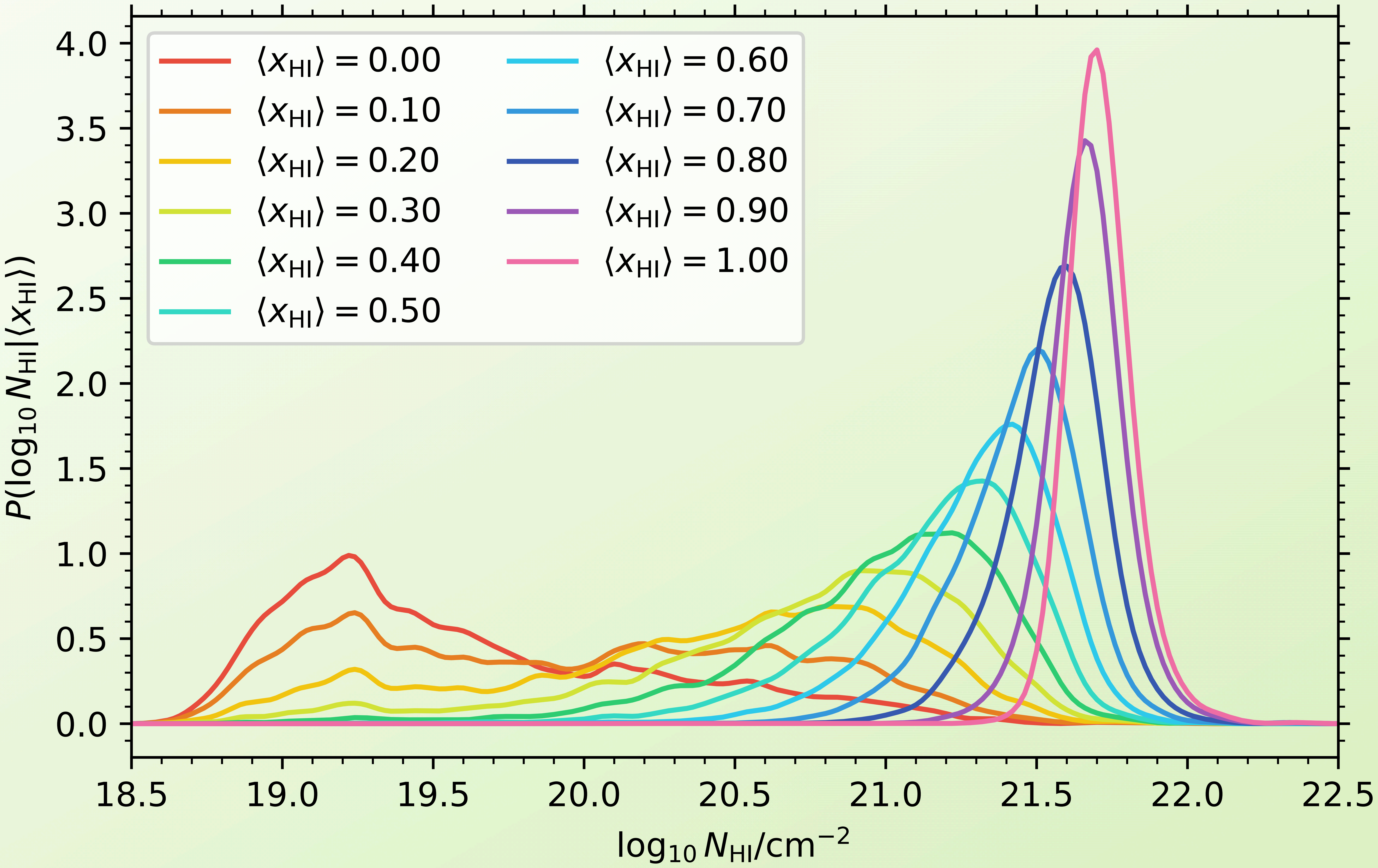

Relating the old and new labels

$$P\left(\langle x_{\mathrm{HI}}\rangle \,|\, N_{\mathrm{HI}}^{\Delta v^{-2}}\right)$$

$$P\left(N_{\mathrm{HI}}^{\Delta v^{-2}}, \langle x_{\mathrm{HI}}\rangle\right)$$

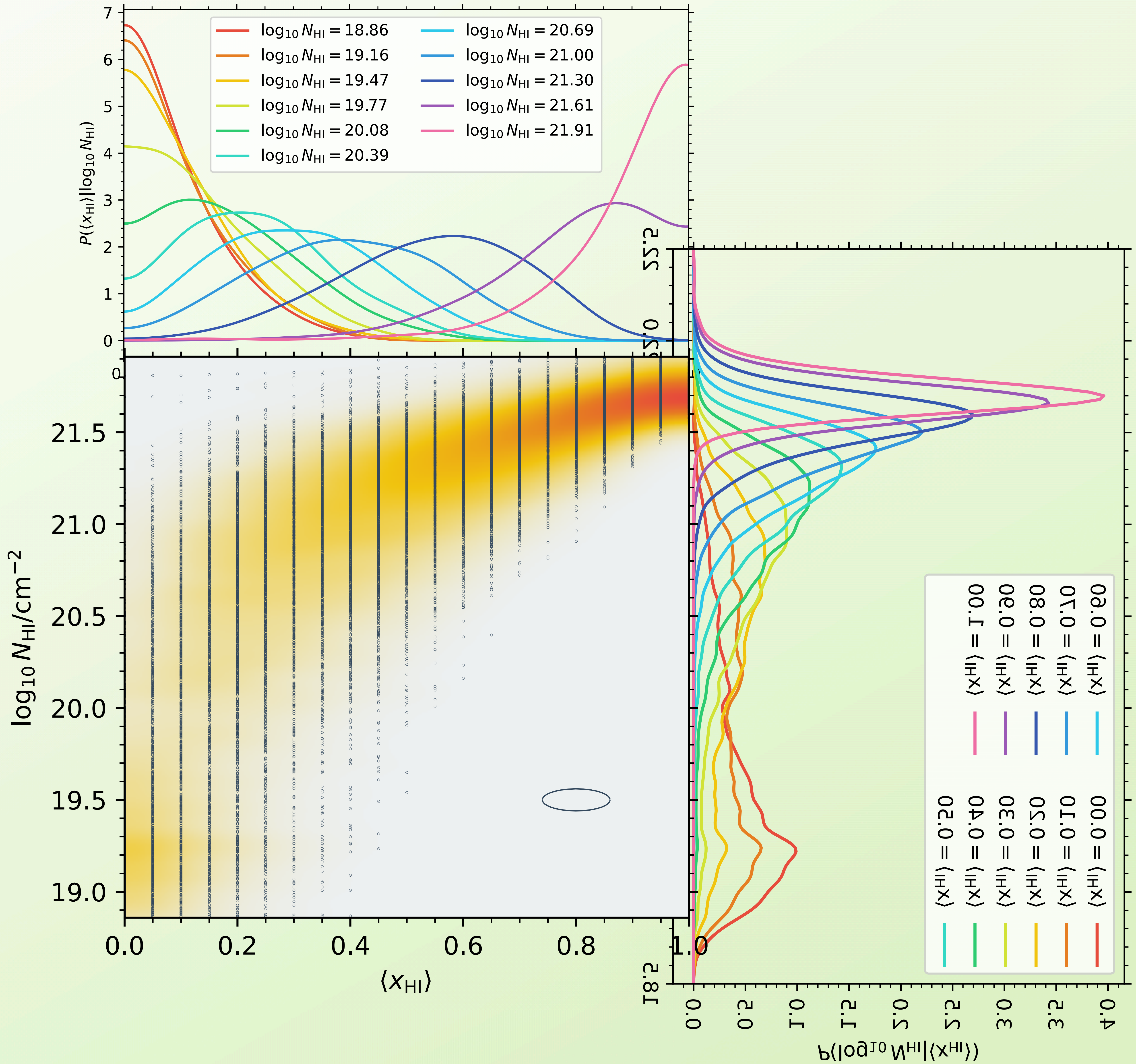

$$P\left(N_{\mathrm{HI}}^{\Delta v^{-2}} \,|\, \langle x_{\mathrm{HI}}\rangle\right)$$

Relating the old and new labels

$P\left(\langle x_{\mathrm{HI}}\rangle \,|\, N_{\mathrm{HI}}^{\Delta v^{-2}}\right)$

$P\left(N_{\mathrm{HI}}^{\Delta v^{-2}}, \langle x_{\mathrm{HI}}\rangle\right)$

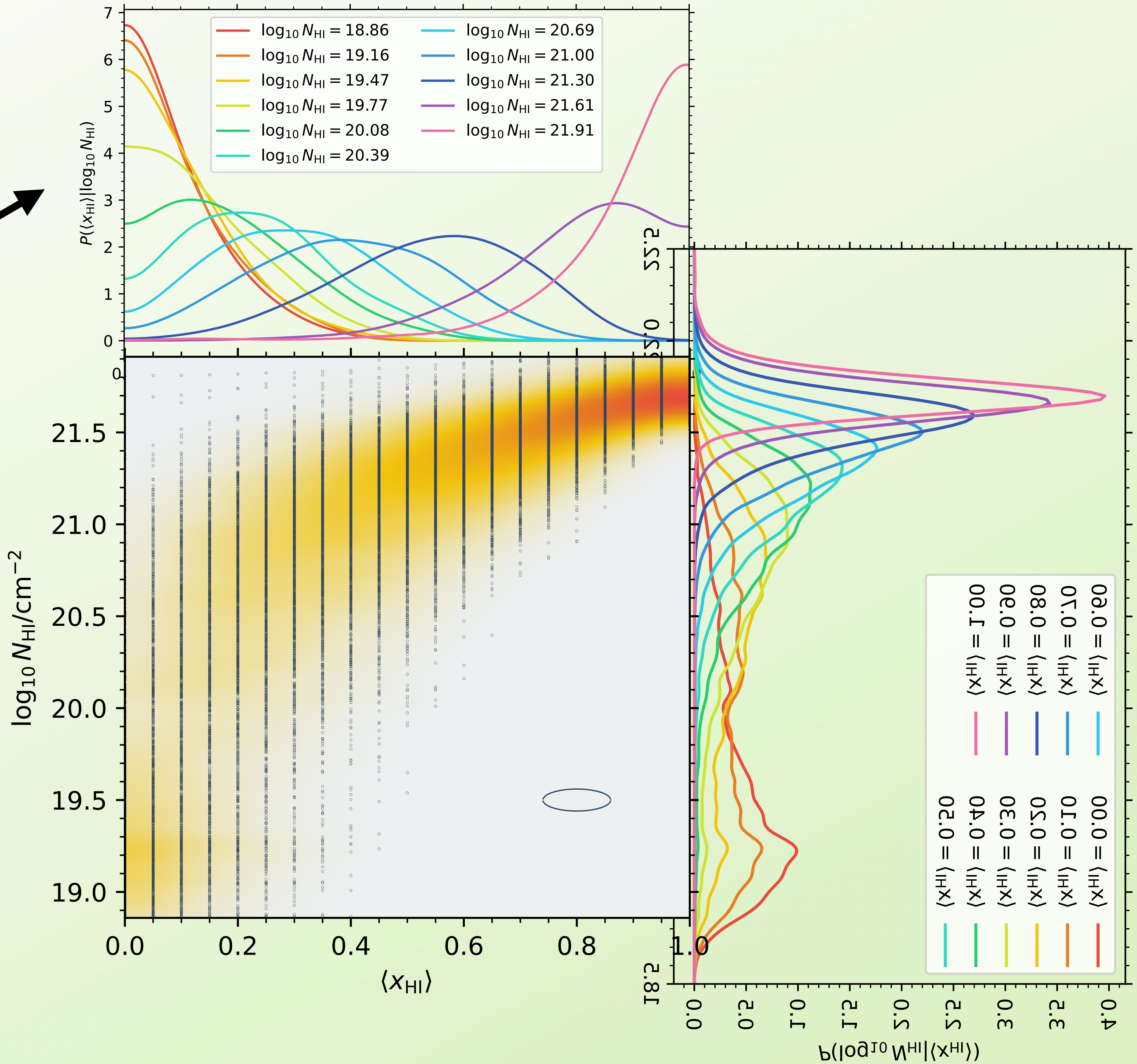

$P\left(N_{\mathrm{HI}}^{\Delta v^{-2}} \,|\, \langle x_{\mathrm{HI}}\rangle\right)$

Inference Tests

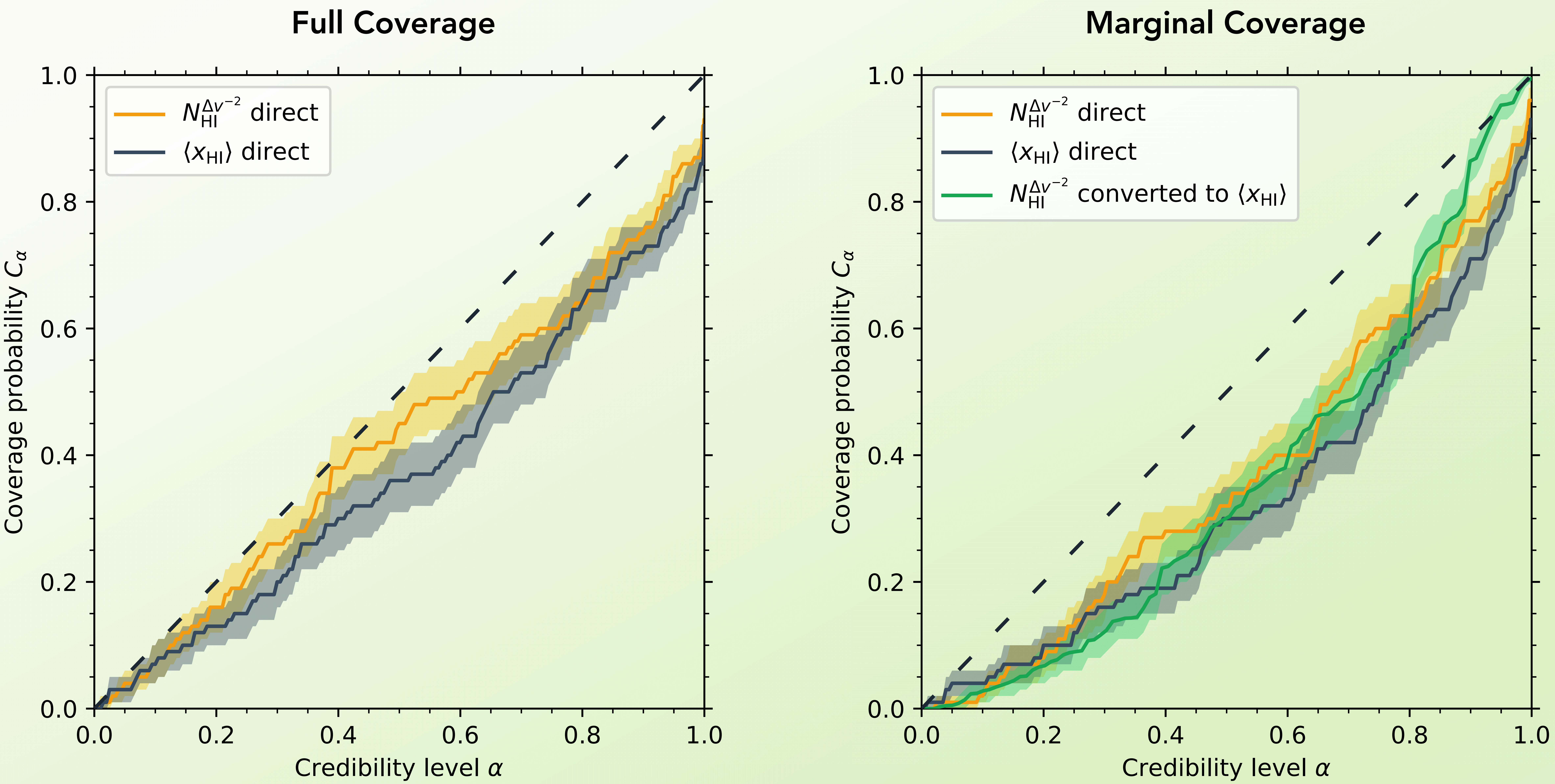

Comparing Inference Precision

Global IGM neutral fraction $\langle x_{\rm HI} \rangle$

Comparing Inference Precision

Global IGM neutral fraction $\langle x_{\mathrm{HI}} \rangle$

$28.0^{+8.2}_{-8.8}\,\%$

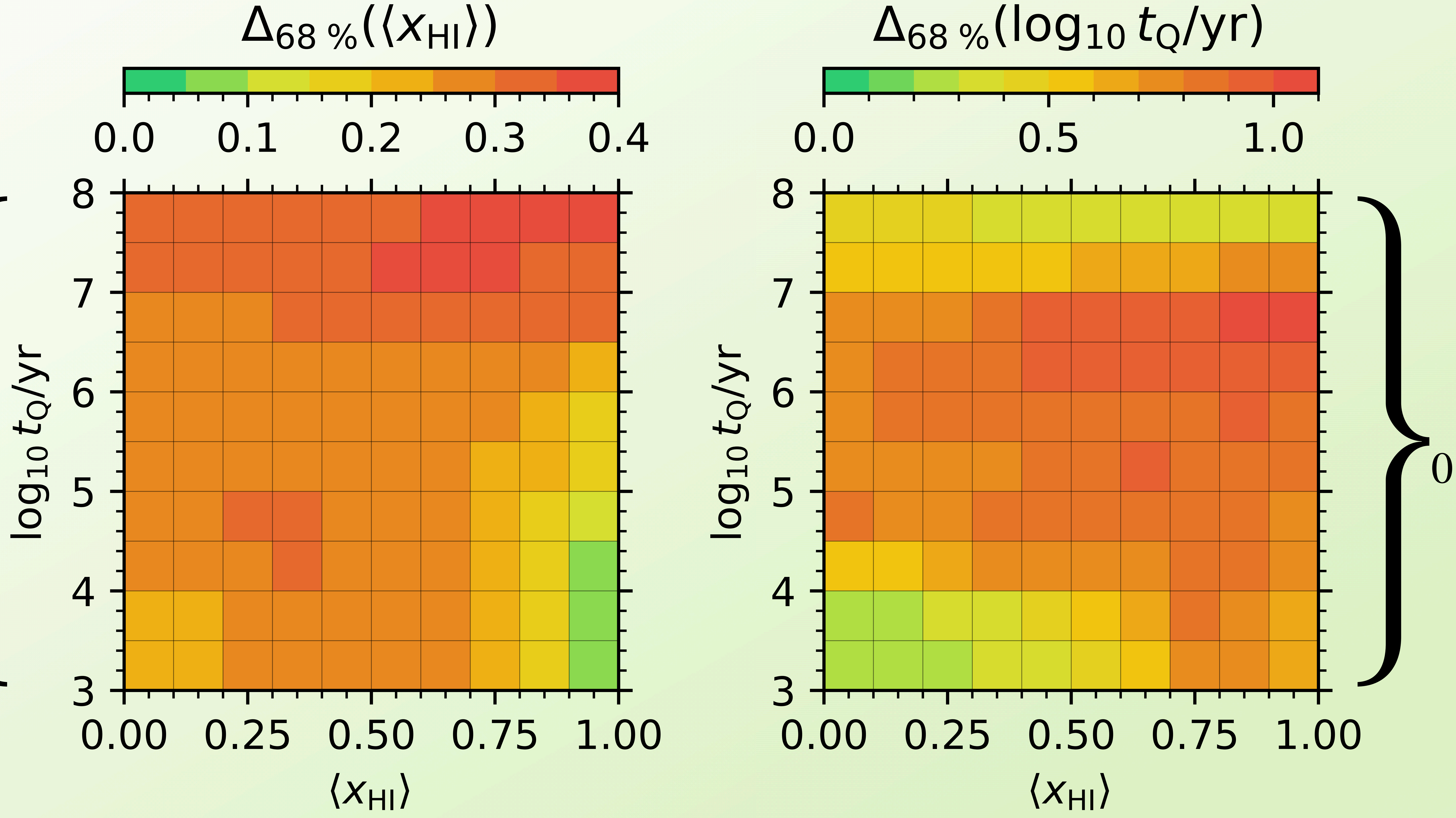

$0.80^{+0.22}_{-0.55}$ dex